April 7, 2019

Hydrogeologic Framework of Selected Areas in Butte and Glenn Counties, California

Prepared for the:

Butte County Department of Water and Resource Conservation
308 Nelson Ave
Oroville, California 9596 5

And

The Board of Trustees of the Leland Stanford Junior University
450 Serra Mall
Stanford, California 94305

Submitted by:

Aqua Geo Frameworks, LLC
130360 County Road D
Mitchell, NE 69357
Phone: (308) 641-2635

Theodore H. Asch, P.Gp. #1038
tasch@aquiageoframeworks.com

Jared D. Abraham, P.Gp. #1089
jabraham@aquageoframeworks.com

James C. Cannia, P.G.
jcannia@aquageoframeworks.com

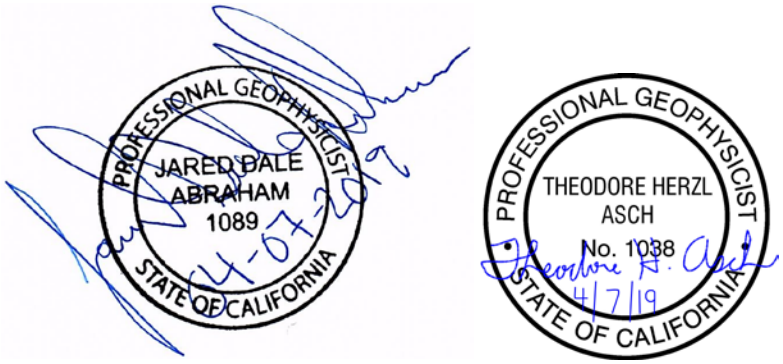

Executive Summary

Aqua Geo Frameworks, LLC. (AGF) is pleased to submit this report titled "*Hydrogeologic Framework of Selected Areas in Butte and Glenn Counties*". An understanding of the hydrogeological framework in the survey area is desired in order to assist in resource management. AGF entered into an agreement with the Butte County Department of Water and Resource Conservation (BCDWRC) and Leland Stanford Junior University (Stanford University or Stanford) to collect, process, and interpret airborne electromagnetic (AEM) data, in conjunction with other available background information, to develop a 3D hydrogeologic framework and to recommend future work to enhance groundwater management activities.

The scope of work for this project was as follows:

1. SCOPE OF WORK

1.1 Butte/Glenn Counties desire to obtain a hydrogeologic framework of selected areas of their jurisdiction. This work will be accomplished through use of Airborne Electromagnetic (AEM) surveys in conjunction with existing geologic and hydrogeologic information. There will be approximately 800 kilometers of AEM data collected and analyzed for the project. The AEM survey utilized the SkyTEM304M and SkyTEM312 systems. These flights have been provided as preliminary AEM inversions on December 5, 2018 and the final AEM data and inversions are included as a product attached to this data report.

1.2 The project goal was to acquire data using AEM to characterize the stratigraphy and aquifer architecture (hydrogeologic framework) and map out the distribution of clays, silts, sands, and gravels to a depth of approximately 1500 feet, with vertical resolution on the order of 3 feet near the surface to tens of feet at depth, utilizing existing well data for comparison.

1.2 AGF began project planning upon signing of the contract between the parties. This work included flight plans, database development, and review of hydrogeologic and geologic work for the area. The Butte/Glenn Counties assisted in providing information such as power line maps, a test hole database, and related aquifer characteristic studies to AGF. The fall 2017 water table elevation data from CA-DWR was selected for use because of its relationship to timing of the survey.

At the conclusion of the design process, the Butte AEM flight lines were divided into both block and reconnaissance flight lines. The reconnaissance flight lines were approximately 22 miles in length (36 km) at their longest and about 3.1 miles (5 km) at their shortest. The block flights had flight lines up to 12 miles in length (approximately 20 km) with tie lines approximately 8.6 miles in length (approximately 14 km) for the western block area. The eastern block flight lines were about 5.5 miles in length (approximately 9 km) with 4.9 miles long tie lines (about 8 km). Block flight lines were separated by about 1500 feet or so (about 450 m to 500 m).

1.4 Approximately 361 line-miles (585 line-kilometers) were acquired by the SkyTEM312 over the Butte-Glenn counties AEM survey area west of Chico on November 30 through December 2, 2018. Then on December 3, 2018, approximately 138 line-miles (224 line-kilometers) were acquired by the SkyTEM304M southeast of Chico. The Haigh Field at the Orland airport was used for landing and refueling between production flights. Status reports of the flying were provided to the Contract Representative of Butte County on a daily basis, including the areas flown,

production rates, and flight plan for the following day.

1.5 AGF processed and conducted quality assurance and quality control (QA/QC) procedures on all data collected from the acquisition system. AGF delivered preliminary data and inversions on December 5, 2018.

1.6 AGF inverted the AEM data. The inversion layer structure was finer in the near-surface for the SkyTEM304 data than for the SkyTEM312 data which had an emphasis on depth in the Valley. After inversion, AGF derived 2D sections, 3D electrical models, and interpreted geologic and hydrogeologic surfaces of the surveyed area. These final inverted georeferenced data are delivered to Butte County and Stanford University with this report.

1.7 AGF is providing a hydrogeologic framework report that includes maps of aquifer materials, maps of stratigraphic units, and maps of estimated potential recharge areas. This report, as mentioned above, also includes all data (acquired, processed, developed) files. The report is delivered in PDF digital format and the data in ASCII and native formats.

2. KEY FINDINGS

2.1 Boreholes - Information from boreholes was used to analyze the Butte AEM inversion results. A total of 362 holes contained lithology information and 183 holes contained geophysical information within the Butte AEM survey area. These boreholes were provided by Dr. Todd Greene, Associate Professor of Geological and Environmental Sciences at California State University, Chico under separate contract to Stanford University. The AEM inversion results matched up well with the majority of the geophysical logs and the lithological logs.

2.2 Digitizing Interpreted Geological Contacts - Characterization and interpretation of the subsurface was performed in cross-section and derived surface grid formats. Contacts between the geologic units were digitized in 2D including: Quaternary (***Q***), Tertiary Tehama FM (***Tte***), Tertiary Tuscan FM (***Tt***), Tertiary Upper Princeton Valley Fill (***Tupvf***), Tertiary Lovejoy Basalt (***Tl***), Tertiary Ione FM (***Ti***), and the Jurassic-Cretaceous Great Valley Sequence (***JKgvs***). However, because the ***Tupvf***, ***Ti***, and ***JKgvs*** are all electrically conductive, and could not be distinguished from each other at depth, they were grouped into one unit, ***JKTud*** – Undivided Upper Princeton/Ione/Great Valley Sequence. The interpretive process greatly benefited from the use of the borehole logs. Surface grids of the interpreted geologic formations were produced as well as interpretative profiles. Each flight line profile with interpretation is included in the appendices as well as the interpretative surface grids.

2.3 Comparing the AEM Results with the CA-DWR (2014) Cross-Sections - The stratigraphic interpretation of the Butte AEM inversion results compared well with cross-sections B-B', E-E', and F-F' from the CA-DWR (2014) report on the geology of the northern Sacramento Valley. There were two main differences between the AEM and the CA-DWR cross-sections. One was that the AEM shows the Tehama FM continuing further east than what is shown on cross-section B-B' before it thins out up against the foothills of the Sierra Nevada Mountains. The second difference was that the 312 did not image an extension of the Lovejoy Basalt because the flow was apparently too deep. Although it is also not clear if the Lovejoy actually extends out as far as the 312 AEM flight lines so that it could be imaged.

2.4 Comparing Results From the 304M and 312 Systems on the Overlap Line - Two airborne electromagnetic TEM systems were operated during the Butte AEM investigation. One was the SkyTEM304M (304M) and the other was the SkyTEM312 (312). In order to compare the systems, part of a traverse was flown twice, once by the 312 as part of flight line L710601 and a second time by the 304M as part of flight line L730300. While the 304M imaged the very near surface (<16 ft (<5 m)) better than the 312, below about 82 ft (25 m) depth, both systems imaged the subsurface equally well until an elevation of about -950 ft (-290 m). After that depth, the 312 system showed much better resolution than did the 304M at depth.

2.5 Resistivity/Lithology Relationship - An assessment of the lithologic character of the Tehama and Tuscan formations was conducted to determine the overall composition of the major categories used to define aquifer and aquitard material. The lithological log-AEM inversion match up information was used to develop the resistivity-lithology relationship. They are: Clay (<10 ohm-m), Sandy Clay (10-15 ohm-m), Sand and Gravel (15-34ohm-m) and Lahar/Coarse Sediments (>34 ohm-m). This allowed for the characterization of the ranges of resistivities present in the major geologic units described in this report which were then used in understanding the hydrogeological framework.

2.6 Hydrogeological Framework of the Butte AEM Survey Area - The Quaternary aquifer system was too thin and heterogeneous to subdivide into sediment packages. The water table is present in the Quaternary and is close to the land surface in most of the area. Thus, Quaternary alluvial material provides the pathway for recharge into the underlying Tertiary Tehama and Tuscan formations. The Tertiary Tehama FM is heterogeneous and in direct contact with the Quaternary across the AEM survey area providing a good hydrologic connection. The Tertiary Tuscan FM is in direct contact with the Tertiary Tehama FM across most of the AEM survey area and has a good hydrologic connection in many areas but is also limited in some areas due to thick clay zones above the Tuscan FM in the lower Tehama FM. The Great Valley Sequence Undivided formational package is considered the base of aquifer for this study. The Tertiary Lovejoy Basalt is considered a non-aquifer in this report. The lahar deposits are considered non-aquifers in this report as they are competent rock units, except where fractured. The eastern section of the survey area has near surface sub-crops and outcrops of the Tuscan FM and, in places, is nine miles wide providing an excellent recharge area for groundwater. Water quality at depth compared to some of the resistivity profiles shows that a potential change can be seen along the base of the Tuscan FM that possibly indicates an upwelling of poor-quality water in certain locations. A test-hole/water quality monitoring well installation would conclude whether the water quality is high in TDS and thus the contributes to the conductive signature in that area.

2.7 Estimation of Aquifer Volume and Water in Storage in the Butte AEM Survey Area - Estimation of aquifer volume and yield were not calculated for the Butte AEM survey area because the units are a complex mix of lahar, lava, sandstone, sand and gravel, sand, silty clay, and clay. The Tuscan FM, breaking down and discontinuous on its western extremum, is difficult to properly characterize without good aquifer production information such as porosity and specific yield to break down water availability in the different lithologies. If such information becomes available, an add-on project could be proposed to make the aquifer and volume estimations using the lithological-resistivity relationships developed during this investigation.

2.8 Potential Recharge Zones within the Butte AEM Survey Area - The Quaternary deposits are

hydrologically connected to the streams and rivers of the AEM survey area. This hydrologic connection can be strong in many areas due to the coarse nature of a large percentage of the sediments present. Where the Tehama FM, and underneath it, the Tuscan FM, are in direct contact with the Quaternary sediments, there is a direct hydrologic connection between them in many places. Recharge can be good between the surface, Quaternary sediments and Tehama and Tuscan formations along favorable sand and gravel sediments in contact with each other. Where there is subcrop and outcrop of the Tuscan FM along the east side of the 304M survey area, recharge can go directly from the surface to the groundwater system increasing the probability of a potentiometric surface downgradient from this area.

3. Recommendations

Recommendations provided to the Butte/Glenn Counties in this section are based on the interpretation and understanding gained from the addition of the AEM data to existing information and from discussions with the Butte/Glenn Counties about their management challenges. There are additional recommendations based on the results related to the pilot project experience.

3.1 **Additional AEM Mapping** - The aquifer maps provided in this report represent the detailed framework developed for the western and eastern block-flights and the reconnaissance level flight lines. The detail provided in the hydrogeological interpretations of the western and eastern block-flights allowed for confident development of hydrogeologic framework. The interpretations match well with the boreholes. No additional high resolution AEM information is needed within the Western and Eastern block-flights areas to resolve questions of resource management. Thus, it is recommended that additional areas of closely spaced lines or “block-flights” be collected to develop detailed frameworks in other areas. The 1640 ft (500 m) spacing between flight lines could be reduced to a 984 ft (300 m) spacing for greater detail and fidelity to the natural system.

Reconnaissance flight lines and the surrounding area should be mapped in detail by block flights to provide information on the hydrogeologic framework and the recharge areas. This would potentially be done in cooperation with the neighboring counties to get details to the continuous aquifer system that is shared in the area. The line spacing for the block flights should be on the order of 984 ft (300 m).

It is recommended that additional closely spaced block flight lines for collection of AEM data and interpretation be considered in critical areas of eastern Butte/Glenn Counties. This will supply the Butte/Glenn Counties with information at greater detail on groundwater flow, aquifer sustainability, and depletion to streams, well interference, groundwater withdrawal, and other management considerations.

3.2 **Update the Water Table map** - The groundwater data used in the analyses presented in this report used the Fall 2017 water table map. Additional water level measurement locations would improve the water table map. In particular, up in the foothills.

3.3 **Siting new test holes and production wells** – The AEM framework maps and profiles provided in this report provide insight in 3D on the relationship between current test holes and the local hydrogeology. At the time of this report, the currently available lithology and geophysical log data for the Butte/Glenn Counties area were used in building the framework maps and profiles. It is recommended that the results from this report be used to site new test holes and monitoring wells. Often test holes are sited based on previous work that is regional in nature or for local projects of small size. By utilizing the maps in this report new drilling locations can be sited in optimal locations. Consideration for the areas that have been identified as confined to semi-confined aquifers is a good place to start doing this work. These wells need to be screened in discreet zones in order to understand the potentiometric surfaces from each zone. These wells should also be spaced geographically for water level/potentiometric head measurements as well as water quality sampling. Small screened intervals would allow for age dating the water for improved understanding of recharge, time of travel along flow paths and groundwater-surface water interaction.

The location of new water supply wells for communities can also use the AEM results in this report to guide development of new water supply wells. Planners should locate wells in areas of greatest saturated thickness with the least potential for non-point source pollution.

3.4 **Aquifer testing and borehole logging** - Aquifer tests are recommended to improve estimates of aquifer characteristics. A robust aquifer characterization program is highly recommended at the state, county, and smaller municipal levels. Aquifer tests can be designed based on the results of AEM surveys and existing production wells could be used in conjunction with three or more installed water level observation wells (which can be used as monitoring wells for levels and water quality sampling after the test).

Additional test holes with detailed, functional, and well calibrated geophysical logging for aquifer characteristics are highly recommended. Most of the borehole geophysical logs provided for this investigation were well calibrated. However, there were also quite a few that demonstrate that additional calibrated and verified geophysical logs would be useful in the Butte/Glenn Counties.

Examples of additional logging would be flow meter logs and geophysical logs including gamma, neutron, electrical, and induction logs. Detailed aquifer characterization can be accomplished with nuclear magnetic resonance logging (NMR). This is a quick and effective way to characterize porosity and water content, estimates of permeability, mobile/bound water fraction, and pore-size distributions with depth. NMR logs compare well with the aquifer tests in our experience and are very cost effective when compared to traditional aquifer tests.

3.5 **Recharge Zones** - The Butte/Glenn Counties hydrogeologic framework in this report provides areas of recharge from the ground surface to the groundwater aquifers. The block flights of AEM data acquisition provide the most detailed information for understanding recharge throughout the block flight areas. It is recommended that additional AEM data be collected and interpreted

utilizing closely-spaced flight lines using an AEM system that has near-surface resolution in the reconnaissance line flight areas. It is further recommended that future work integrate new soils maps with the results of this study to provide details on soil permeability, slope, and water retention to provide a more complete understanding of the transport of water from the land surface to the groundwater aquifers.

3.6 **Managed Aquifer Recharge**- There are areas which may have potential for managed aquifer recharge (MAR) or aquifer storage and recovery (ASR) facilities. Detailed analysis for this purpose would need to be done to determine if this is a viable opportunity for the Butte/Glenn Counties. Additional AEM mapping along the streams in the Butte/Glenn Counties would also locate similar locations. A detailed plan for locating and developing Managed Aquifer Recharge sites would be beneficial to the Butte/Glenn Counties for providing storage and release of water for stream flow and other uses. During times of high surface water flow a prebuilt system of moving water from the rivers and streams to MAR or ASR facilities would be recommended to easily take advantage of this opportunity.

4. Deliverables

In summary, the following are included as deliverables:

- Raw EM Mag data as ASCII *.xyz
- SCI inversion as ASCII *.xyz
- Borehole databases as ASCII *.xyz
- Interpretations as ASCII *.xyz
- Raw Data Files - SkyTEM files *.geo, *skb, *.lin
- ESRI ArcView grid files – surface, topo, etc
- 3D fence diagrams of the Stratigraphic interpretation
- 3D voxel models as ASCII *.xyz for the Butte AEM data

KMZs for AsFlown, Retained, Recharge, and Interpretation results

Table of Contents

1 Introduction 1
1.1 Purpose of Current Project 1
1.2 Background 4
1.3 Description of the Butte AEM Project Area 4
2 Project Area Hydrogeology 6
2.1 Geologic Setting 6
2.1.1 Physiography and Regional Geologic Setting 6
2.1.2 Surficial Geology 8
2.1.3 Tertiary Geology 8
2.1.4 Cretaceous Geology 11
2.1.5 CA-DWR Interpretative Maps and Cross-Sections 11
2.2 Butte AEM Survey Area Hydrogeologic Characteristics 17
2.2.1 Aquifer Characteristics 20
2.2.2 Water Quality 22
3 Additional Background Information 24
3.1 Borehole Data 24
4 Geophysical Methodology, Acquisition and Processing 26
4.1 Geophysical Methodology 26
4.2 Flight Planning/Utility Mapping 27
4.3 AEM Survey Instrumentation 28
4.4 Data Acquisition 30
4.4.1 System Flight Parameters 32
4.4.2 Primary Field Compensation 42
4.4.3 Automatic Processing 42
4.4.4 Manual Processing and Laterally-Constrained Inversions 42
4.4.5 Power Line Noise Intensity (PLNI) 45
4.4.6 Magnetic Field Data 48
4.5 Spatially-Constrained Inversion 49
5 AEM Results and Interpretation 56
5.1 Interpretive Process – Merge AEM Flight Lines, Construct DEM 56
5.1.1 Merge AEM Flight Lines and Databases from Different Flights 56

5.1.2 Construct the Project Digital Elevation Model 57
5.2 Create Interpretative 2D Profiles 58
5.3 Comparison of Borehole Logs and the AEM Inversion Results 78
5.4 Comparison of CA-DWR (2014) Cross-Sections and the AEM Inversion Results 92
5.5 Comparison of 304M and 312 Systems 105
5.6 Create Interpretative Surface Grids 114
5.7 Resistivity-Lithology Relationship 125
5.8 Hydrogeological Framework of the Butte AEM Survey Area 132
5.9 Recharge Areas within the Butte AEM Survey Area 141
5.10 Key AEM Findings 149
5.10.1 Boreholes 149
5.10.2 Digitizing Interpreted Geological Contacts 149
5.10.3 Comparing the AEM Results with the CA-DWR (2014) Cross-Sections 149
5.10.4 Comparing Results From the 304M and 312 Systems on the Overlap Line 149
5.10.5 Resistivity/Lithology Relationship 150
5.10.6 Hydrogeological Framework of the Butte AEM Survey Area 150
5.10.7 Estimation of Aquifer Volume and Water in Storage in the Butte AEM Survey Area 150
5.10.8 Potential Recharge Zones within Butte AEM Survey Area 150
5.11 Recommendations 151
5.11.1 Additional AEM Mapping 151
5.11.2 Update the Water Table map 151
5.11.3 Siting new test holes and production wells 151
5.11.4 Aquifer testing and borehole logging 152
5.11.5 Recharge Zones 152
5.11.6 Managed Aquifer Recharge 153
6 Description of Data Delivered 154
6.1 Tables Describing Included Data Files 154
6.2 Description of Included Google Earth KMZ Data and Profiles 163
6.2.1 Included README for the Butte AEM Interpretation KMZ 163
7 References 166
Appendix 1. 2D Profiles and Surfaces
Appendix 2. 3D Images

List of Figures

Figure 1-1. Proposed AEM study area, showing water wells, reconnaissance flight lines (connecting points of good well control through regions that address one or more of the key issues), and dense flight blocks (core areas where better imaging will be obtained with closely-spaced flight lines).. 2

Figure 1-2. The Butte AEM survey area including county lines and major roads (99, 45, 32, 149). 3

Figure 1-3. Map of major river basins with streams within the Butte/Glenn counties AEM survey area 5

Figure 2-1. Hydrostratigraphic cross section developed by Blair et al. (1991) for the area in the vicinity of Oroville, California 7

Figure 2-2. Approximate Surface and Subsurface Extent of the Tehama and Tuscan Formations, and Surface Extent Only of the Laguna Formation. 12

Figure 2-3. Location of cross-sections B-B', E-E', and F-F' from Plate 2 and Plate 3 of CA-DWR (2014) ... 13

Figure 2-4. A portion of east-west cross-section B-B' from Plate 2 of CA-DWR (2014) 14

Figure 2-5. A portion of north-south cross-section E-E' from Plate 3 of CA-DWR (2014) 14

Figure 2-6. A portion of north-south cross-section F-F' from Plate 3 of CA-DWR (2014) 15

Figure 2-7. Geological units legend for cross-sections B-B', E-E', and F-F' 16

Figure 2-8. Map showing highly generalized regional groundwater flow paths around the project area 17

Figure 2-9. Map of Total Dissolved Solids (TDS) near the Butte AEM survey area 23

Figure 3-1. Locations of the boreholes near the Butte AEM survey area 24

Figure 4-1. Schematic of an airborne electromagnetic survey, modified from Carney et al. (2015a) 26

Figure 4-2. A) Example of a dB/dt sounding curve. B) Corresponding inverted model values. C) Corresponding resistivity earth model. 27

Figure 4-3. SkyTEM304M frame, including instrumentation locations and X and Y axes. Distances are in meters. Instrumentation locations listed in Table 4-1 28

Figure 4-4. Photo of the SkyTEM304M system in suspension beneath the helicopter 29

Figure 4-5. Butte AEM flight lines grouped by acquisition date 31

Figure 4-6. Map of the system height recorded during the Butte AEM survey 34

Figure 4-7. Map of the ground speed recorded during the Butte AEM survey 35

Figure 4-8. Map of the X-angle tilt recorded during the Butte AEM survey 36

Figure 4-9. Map of the Y-angle tilt recorded during the Butte AEM survey 37

Figure 4-10. Plot of the 210 Hz LM waveform for the SkyTEM312 system recorded during the Butte AEM survey 38

Figure 4-11. Plot of the 30 Hz HM waveform for the SkyTEM312 system recorded during the Butte AEM survey 39

Figure 4-12. Plot of the 210 Hz LM waveform for the SkyTEM304M system recorded during the Butte AEM survey 40

Figure 4-13. Plot of the 30 Hz HM waveform for the SkyTEM304M system recorded during the Butte AEM survey 41

Figure 4-14. Example locations of electromagnetic coupling with pipelines or power lines 43

Figure 4-15. A) Example of AEM data affected by electromagnetic coupling in the Aarhus Workbench editor. The top group of lines is the unedited data with the Low Moment on top and the High Moment on the bottom. The bottom group shows the same data after editing. 44

Figure 4-16. A) Laterally-Constrained inversion results where AEM data affected by coupling with pipelines and power lines were not removed. B) Inversion results where AEM data affected by coupling were removed. 45

Figure 4-17. Power Line Noise Intensity (PLNI) map of the Butte AEM project area. 46

Figure 4-18. Locations of inverted data (blue lines) along the AEM flight lines (red (304M) and orange (312) lines) in the Butte AEM survey area.. 47

Figure 4-19. Residual magnetic Total Field intensity data for the Butte AEM survey area corrected for diurnal drift, with the International Geomagnetic Reference Field (IGRF) removed 48

Figure 4-20. An example of an AEM profile illustrating increasing model layer thicknesses with depth. . 52

Figure 4-21. Data/model residual histogram for the Butte 304M SCI inversion results 53

Figure 4-22. Data/model residual histogram for the Butte 312 SCI inversion results 53

Figure 4-23. Map of data residuals for the Butte 304M SCI inversion results 54

Figure 4-24. Map of data residuals for the Butte 312 SCI inversion results 55

Figure 5-1. Map of the Digital Elevation Model for the Butte AEM survey area 57

Figure 5-2. 2D profile of resistivity data from Butte 304M flight line L730300 and the east end of cross-section B-B' 60

Figure 5-3. 2D profile of resistivity data from Butte 304M flight line L730300 with geophysical and lithological borehole data 61

Figure 5-4. Example digitization of stratigraphic contacts for AEM flight line L730300 63

Figure 5-5. Same digitization as in Figure 5-4, except all conductive stratigraphic units at depth below the Tuscan, which cannot be distinguished because of a lack of electrical resistivity contrast between them, are now grouped into one conductive basement stratigraphic unit 64

Figure 5-6. Lithology borehole color legend and grouped stratigraphic color scale 65

Figure 5-7. 304M AEM Reconnaissance flight line L730100 displaying the flight path on the USGS 100K topo map, the inverted resistivity section along the flight line, and interpreted stratigraphy 68

Figure 5-8. 312 AEM Reconnaissance flight line L710201 displaying the flight path on the USGS 100K topo map, the inverted resistivity section along the flight line, and interpreted stratigraphy 69

Figure 5-9. 312 AEM Reconnaissance flight line L710201, the same as in Figure 5-8, except that the resistivity color scale now ranges from 9 ohm-m to 50 ohm-m 70

Figure 5-10. 304M AEM Block flight line L300801 displaying the flight path on the USGS 100K topo map, the inverted resistivity section along the flight line, and interpreted stratigraphy 71

Figure 5-11. 304M AEM Block flight line L400401 displaying the flight path on the USGS 100K topo map, the inverted resistivity section along the flight line, and interpreted stratigraphy. 72

Figure 5-12. 312 AEM Block flight line L100700 displaying the flight path on the USGS 100K topo map, the inverted resistivity section along the flight line, and interpreted stratigraphy 74

Figure 5-13. 312 AEM Block flight line L100700, the same as in Figure 5-12, except that the resistivity color scale now ranges from 9 - 50 ohm-m 75

Figure 5-14. 312 AEM Block flight line L200501 displaying the flight path on the USGS 100K topo map, the inverted resistivity section along the flight line, and interpreted stratigraphy 76

Figure 5-15. 312 AEM Block flight line L100700, the same as in Figure 5-13, with the addition of a line at Easting 579400, the location at which L200501 crosses L100700 77

Figure 5-16. Comparison of borehole resistivity and lithology logs and AEM flight line L200401 80

Figure 5-17. Comparison of borehole resistivity and lithology logs and AEM flight line L101201 81

Figure 5-18. This is the same interpreted profile as in Figure 5-17 for L101201 except that the resistivity scale has been changed from 7 – 50 ohm-m to 9 – 50 ohm-m 82

Figure 5-19. This is the next line to the northeast from L101201 in Figure 5-18, L101301 83

Figure 5-20. This is the same profile, L101301, as in Figure 5-19 except that the resistivity scale has changed from 7 – 50 ohm-m to 9 – 50 ohm-m 84

Figure 5-21. Comparison of borehole resistivity and lithology logs and AEM flight line L101501 85

Figure 5-22. Comparison of borehole resistivity and lithology logs with AEM flight line L101700 86

Figure 5-23. Both lithology and resistivity logs match the AEM inversion results for L200301 very well except on the very far left 87

Figure 5-24. AEM flight line L300301 in the 304M AEM flight area. Note the very good match between lithology log *e0160820* on the right side of the profile and the AEM inversion results 88

Figure 5-25. AEM flight line L300801 in the 304M AEM flight area. Note the very good match between lithology log *e062957* and the very poor match with log 21N02E26E003M. 89

Figure 5-26. AEM Reconnaissance flight line L710101 in the 312 AEM flight area. There is a very good match with the resistivity logs along this profile 90

Figure 5-27. AEM Reconnaissance flight line L730201 in the 304 AEM flight area. Note the very good match between resistivity logs MW-CSU1 in the center of the profile with the AEM inversion results and resistivity log VMW-36F located across the Tuscan, Upper Princeton Valley Fill, and Lovejoy Basalt contacts 91

Figure 5-28. 3D fence diagram of the stratigraphic interpretation of the Butte AEM flight lines, including both Reconnaissance and Block flight lines, looking to the north 94

Figure 5-29. 3D fence diagram of the stratigraphic interpretation of the Butte AEM Block flight lines, looking to the north-northeast 95

Figure 5-30. 3D fence diagram of the stratigraphic interpretation of the Butte AEM Block flight lines, looking to the southwest 96

Figure 5-31. 3D fence diagram of the stratigraphic interpretation of the Butte AEM Reconnaissance flight lines looking to the northeast 97

Figure 5-32. 3D fence diagram of the stratigraphic interpretation of the Butte AEM Reconnaissance flight lines looking to the southwest 98

Figure 5-33. 3D fence diagram of the stratigraphically-interpreted Butte AEM Reconnaissance flight lines with CA-DWR (2014) cross-sections B-B' and E-E' 99

Figure 5-34. 3D fence diagram of the stratigraphically-interpreted Butte AEM Reconnaissance flight lines with CA-DWR (2014) cross-sections B-B' and E-E' 100

Figure 5-35. 3D fence diagram of the stratigraphically-interpreted Butte AEM Reconnaissance flight lines with CA-DWR (2014) cross-sections B-B' and E-E' 101

Figure 5-36. An alternate view of the Lovejoy Basalt being "too deep" out in the Valley and below the Depth of Investigation of the SkyTEM304M. 102

Figure 5-37. A third view of the "too deep" Lovejoy Basalt below the Depth of Investigation (DOI) of the SkyTEM304M 103

Figure 5-38. View of the Lovejoy Basalt not quite extending to a location beneath the SkyTEM312 AEM flight lines 104

Figure 5-39. AEM flight line over part of which both the 304M and the 312 acquired data 106

Figure 5-40. Inversion results for 304M AEM flight line L730300 107

Figure 5-41. Inversion results for 312 AEM flight line L710601 108

Figure 5-42. Zone of overlap of inversion results for 304M flight line L730300 and 312 flight line L710601 109

Figure 5-43. 3D fence diagram of stratigraphic interpretation for 304 AEM flight line L730300 inversion results 110

Figure 5-44. 3D fence diagram of stratigraphic interpretation for 304 AEM flight line L730300 inversion results with overlay of overlap area with 312 AEM flight line L710601 111

Figure 5-45. 3D fence diagram of stratigraphic interpretation for 304 AEM flight line L730300 inversion results 112

Figure 5-46. 3D fence diagram of stratigraphic interpretation for 304 AEM flight line L730300 inversion results with overlay of overlap area with 312 AEM flight line L710601 113

Figure 5-47. Map of the water table elevation during the fall of 2017 within and surrounding the Butte AEM survey area 115

Figure 5-48. Map of the elevation of the top of the Tehama FM within the Butte AEM survey area 116

Figure 5-49. Map of the elevation of the top of the Tuscan FM within the Butte AEM survey area 117

Figure 5-50. Map of the elevation of the top of the Lovejoy Basalt within the Butte AEM survey area . 118

Figure 5-51. Map of the elevation of the top of the Upper Princeton Valley Fill within the Butte AEM survey area 119

Figure 5-52. Map of the total thickness of Quaternary deposits within the Butte survey area 120

Figure 5-53. Map of the total thickness of the Tehama FM within the Butte AEM survey area 121

Figure 5-54. Map of the total thickness of the Tuscan FM within the Butte AEM survey area 122

Figure 5-55. Map of the total thickness of the Lovejoy Basalt within the Butte survey area 123

Figure 5-56. Map of the thickness of sand and gravel within the Tehama FM within the Butte AEM survey area 124

Figure 5-57. Plot displaying the resistivities by major lithological material color categories (green – clay, yellowish green – sandy clay, orange – sand and gravel, pink – lahar/coarse sediments) 125

Figure 5-58. Lithological interpretation of AEM Reconnaissance flight line L730300 in the bottom profile 127

Figure 5-59. Lithological interpretation of AEM Reconnaissance flight line L710701 in the bottom profile 128

Figure 5-60. Lithological interpretation of AEM Reconnaissance flight line L710501 in the bottom profile 129

Figure 5-61. Lithological interpretation of AEM Reconnaissance flight line L710301 in the bottom profile 130

Figure 5-62. Lithological interpretation of AEM Reconnaissance flight line L710101 in the bottom profile 131

Figure 5-63. 3D fence diagram, looking north, of the interpreted geologic formations within the AEM survey area 133

Figure 5-64. 3D fence diagram, looking south, of the interpreted geologic formations within the AEM survey area 134

Figure 5-65. Interpreted AEM profile L730300 which is a west to east flight line 135

Figure 5-66. Interpreted AEM profile L101501 which is a northwest to southeast flight line 138

Figure 5-67. Interpreted AEM profile L200701 which is a southwest to northeast flight line 139

Figure 5-68. Map of the total thickness of the Tuscan FM within the Butte AEM survey area showing areas of thick sand and gravel deposits as well as lahar in some places 140

Figure 5-69. Map of the inverted AEM resistivities (>20 ohm-m) related to the geologic materials from 0' to 3' below the ground surface within the 2018 Butte AEM survey area 142

Figure 5-70. Map of the inverted AEM resistivities (>20 ohm-m) related to the geologic materials from 3' to 7' below the ground surface within the 2018 Butte AEM survey area 143

Figure 5-71. Map of the inverted AEM resistivities (>20 ohm-m) related to the geologic materials from 7' to 11' below the ground surface within the 2018 Butte AEM survey area 144

Figure 5-72. Profile L710201 provides interpretation of the geologic materials along a flight path paralleling the Sacramento River from south to north..... 146

Figure 5-73. Profile L200801 provides interpretation of the geologic materials along a flight path perpendicular to the Sacramento River from west to east 147

Figure 5-74. A cut voxel model showing the resistivity of the geologic materials greater than 15 ohm-m from the ground surface to the top of the undivided Upper Princeton Valley Fill/Ione FM/Great Valley Sequence..... 148

Figure 6-1. Example Google Earth image for the Butte Interpretation kmz..... 165

List of Tables

Table 2-1. Quaternary and Tertiary geology of the Butte AEM survey area, northern Sacramento Valley, California. 9

Table 2-2. Aquifers in Quaternary and Tertiary Age stratigraphic units..... 19

Table 2-3. Generalized aquifer-test data. 21

Table 2-4. TDS Ranges of Ca-Mg HCO3 and Mg-Ca HCO3 types..... 22

Table 4-1. Positions of instruments on the SkyTEM304M frame, using the center of the frame as the origin, in meters 30

Table 4-2. Positions of corners of the SkyTEM304M transmitter coil, using the center of the frame as the origin in meters 30

Table 4-3. Location of DGPS and magnetic field base station instruments at the Orland, CA airport 30

Table 4-4. Butte AEM flight line production by flight 32

Table 4-5. Thickness and depth to bottom for each layer in the Spatially Constrained inversion (SCI) AEM earth models for the SkyTEM304M 49

Table 4-6. Thickness and depth to bottom for each layer in the Spatially Constrained inversion (SCI) AEM earth models for the SkyTEM312 50

Table 5-1. Combination of 304M and 312 flight lines within the Butte AEM survey area 56

Table 6-1. Raw SkyTEM data files 156

Table 6-2. Channel name, description, and units for Butte_EM304_MAG.xyz and Butte_EM312_MAG.xyz with EM, magnetic, DGPS, Inclinometer, altitude, and associated data 156

Table 6-3. Channel name, description, and units for Butte_304_312_AEM_SCI_Inv_v1.xyz with EM inversion results. 157

Table 6-4. Files containing borehole information 158

Table 6-5. Channel name, description, and units for borehole collar files 158

Table 6-6. Channel name description and units for Lithology borehole data 158

Table 6-7. Channel name description and units for E-Logs borehole data 159

Table 6-8. Channel name, description, and units for the interpretation results file Butte_InterpSurfaces_v1.xyz 160

Table 6-9. Files containing ESRI ArcView Binary Grids *.flt (NAD 83 UTM 10 North, meters) 161

Table 6-10. Channel name, description, and units for Butte_AEM_gt15_voxel.xyz and Butte_AEM_ALLRho_voxel.xyz 162

List of Abbreviations

1D	One-dimensional
2D	Two-dimensional
3D	Three-dimensional
$A*m^2$	Ampere meter squared
AEM	Airborne Electromagnetic
AGF	Aqua Geo Frameworks, LLC
BCDWRC	Butte County Department of Water and Resource Conservation
Bgl/Bgs	Below Ground Level/Below Ground Surface
Ca	Calcium
CA-DWR	California Department of Water Resources
CV	Central Valley of California
CVA	Central Valley Aquifer
dB/dt	Change in amplitude of magnetic field with time
DEM	Digital Elevation Model
DOI	Depth of Investigation
DGPS	Differential global positioning system
em, EM	Electromagnetic
ft	Feet
Fm, FM	Formation
GIS	Geographic Information System
gpm	Gallons per minute
HCO3	Bicarbonate
HEM	Helicopter Electromagnetic
Hz	Hertz (cycles per second)
IGRF	International Geomagnetic Reference Field
ID	Intermediate Deep

IS	Intermediate Shallow
JKgvs	Jurassic-Cretaceous Great Valley Sequence
JKTud	Jurassic-Cretaceous-Tertiary Undivided stratigraphic unit
Kc	Cretaceous Chico Formation
Km/km	Kilometers
KMZ/kmz	Keyhole Markup language Zipped file
$\mathbf{K_r}$	Horizontal hydraulic conductivity
LTA	Lower Tuscan Aquifer
m	Meters
MAG	Magnetic (data); Magnetometer (instrument)
MCG	Minimum curvature gridding
md	Meters per day
m^2d^{-1}	Meters squared per day
Mg	Magnesium
mg/L	Milligrams per liter
MPv	Miocene-Pliocene volcanic rocks
NAD83	North American Datum of 1983
NAVD88	North American Vertical Datum of 1988
NMR	Nuclear Magnetic Resonance
OM	Geosoft Oasis montaj
pKmi	pre-Cretaceous metamorphic igneous rocks
PFC	Primary Field Compensation
PLNI	Power Line Noise Intensity
PLSS	Public Land Survey System
Q	Quaternary
Qa	Quaternary alluvium
Qb	Quaternary Basin fill
Qls	Holocene landside depoists
Qm	Quaternary Modesto Formation
QPto	Plio-Pleistocene Tuffs of Oroville
Qr	Pleistocene Riverbank Formation
Qrb	Pleistocene Red Bluff Formation
Pv	Pliocene volcanic rocks
Rx	Receiver
S	Storativity
Sy	Specific yield
SCI	Spatially-Constrained Inversion
STD	Standard Deviation
TEM	Transient Electromagnetic
TDEM	Time-Domain Electromagnetic
TDS	Total dissolved solids
Tg	Eocene “auriferous” gravels
Ti	Tertiary Ione Formation
Tl	Tertiary Lovejoy Basalt
Tlpvf	Tertiary Lower Princeton Valley Fill
Tt	Tertiary Tuscan Formation
Tte	Tertiary Tehama Formation
TteLow	Tertiary Tuscan bottom contact over the Tehama Formation

Tupvf	Tertiary Upper Princeton Valley Fill
Tx	Transmitter
USGS	United States Geological Survey
UTM	Universal Transverse Mercator
V/m^2	Volts per meter squared

1 Introduction

1.1 Purpose of Current Project

The Butte County's Department of Water and Resource Conservation desires an improved understanding of the hydrogeologic framework in their management area (Figure 1-1). In the western area, there is interest in defining a transition zone between the Tertiary Tehama (***Tte***) and Tertiary Tuscan (***Tt***) formations which has potential for the lower Tehama/Tuscan to act as a confined to semi-confined system. In the eastern area there is interest in potential recharge areas along the eastern edge of the of the alluvial basin providing information on the movement and restrictions of groundwater into and through the area. Groundwater and surface water sustainability, groundwater recharge including storage facilities, water quality and surface water supply are some of the top reasons for using the information from the AEM survey. Characterization of the bedrock and its topography including any geologic structural control are of interest as well including mapping any saltwater at depth.

An airborne electromagnetic (AEM) survey was selected, and designed (Figure 1-2), to assist in the development of a 3D hydrogeologic framework of the project areas and to suggest future work to enhance groundwater management activities. It was decided that two versions of available AEM systems, the SkyTEM304M and SkyTEM312, would be utilized to conduct this investigation (Figure 1-2). The SkyTEM312 would provide higher resolution at depth in the northern Sacramento Valley and the SkyTEM304M would provide higher resolution of the near-surface near the foothills of the Sierra Nevada mountains. As a quality control measure and to provide the clients with greater understanding of the use of AEM, part of one flight line was to be flown with each system and the results compared.

The survey design involves flying a total of approximately 800-line kilometers. In the areas of dense coverage (block flights) the lines have ~500 m spacing with ~3 km spacing between cross lines. The specific design of this survey seeks to address the Project Goals with a layout of AEM lines that strikes a balance between line density, cost efficiency, logistical constraints, and geologic control. The survey design has two main areas of focus: 1) a "western" area, west of the City of Chico, which crosses the Sacramento River, and 2) an "eastern" area, south and southeast of the City of Chico. The proposed survey areas, including water wells considered "active" by the California Department of Water Resources (CA-DWR), dedicated groundwater monitoring wells, and "Reconnaissance Flight Lines", which represent transects that connect points of good well control through regions that address one or more of the key issues.

Maps, 2D profiles, and other 3D images of the aquifer materials, their relationship to current test holes and production groundwater wells, and of estimated potential recharge areas are desired.

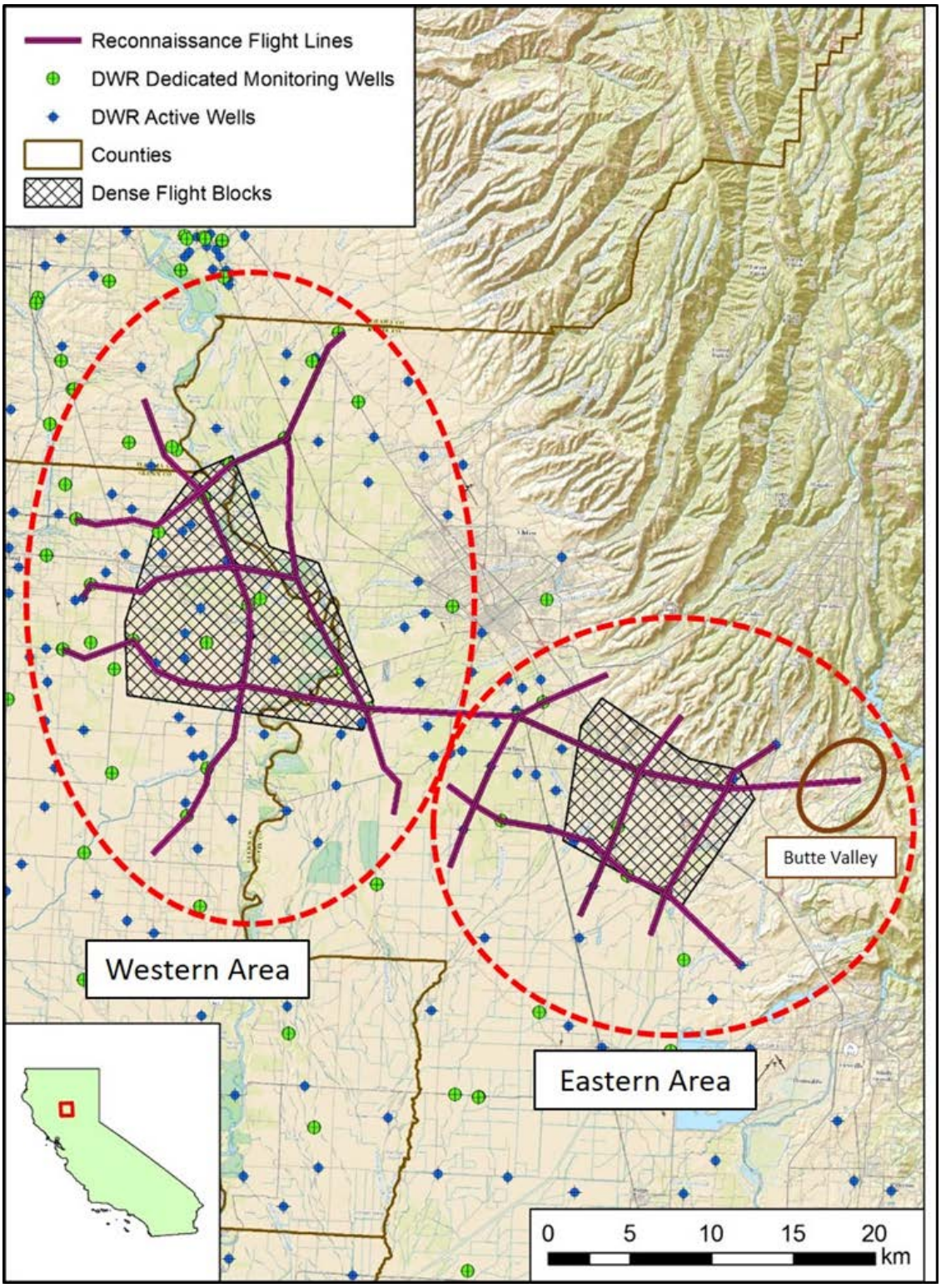

Figure 1-1. Proposed AEM study area, showing water wells, reconnaissance flight lines (connecting points of good well control through regions that address one or more of the key issues), and dense flight blocks (core areas where better imaging will be obtained with closely-spaced flight lines). Total line kilometers to be acquired: approximately 800. (modified from Butte County-AGF AEM contract).

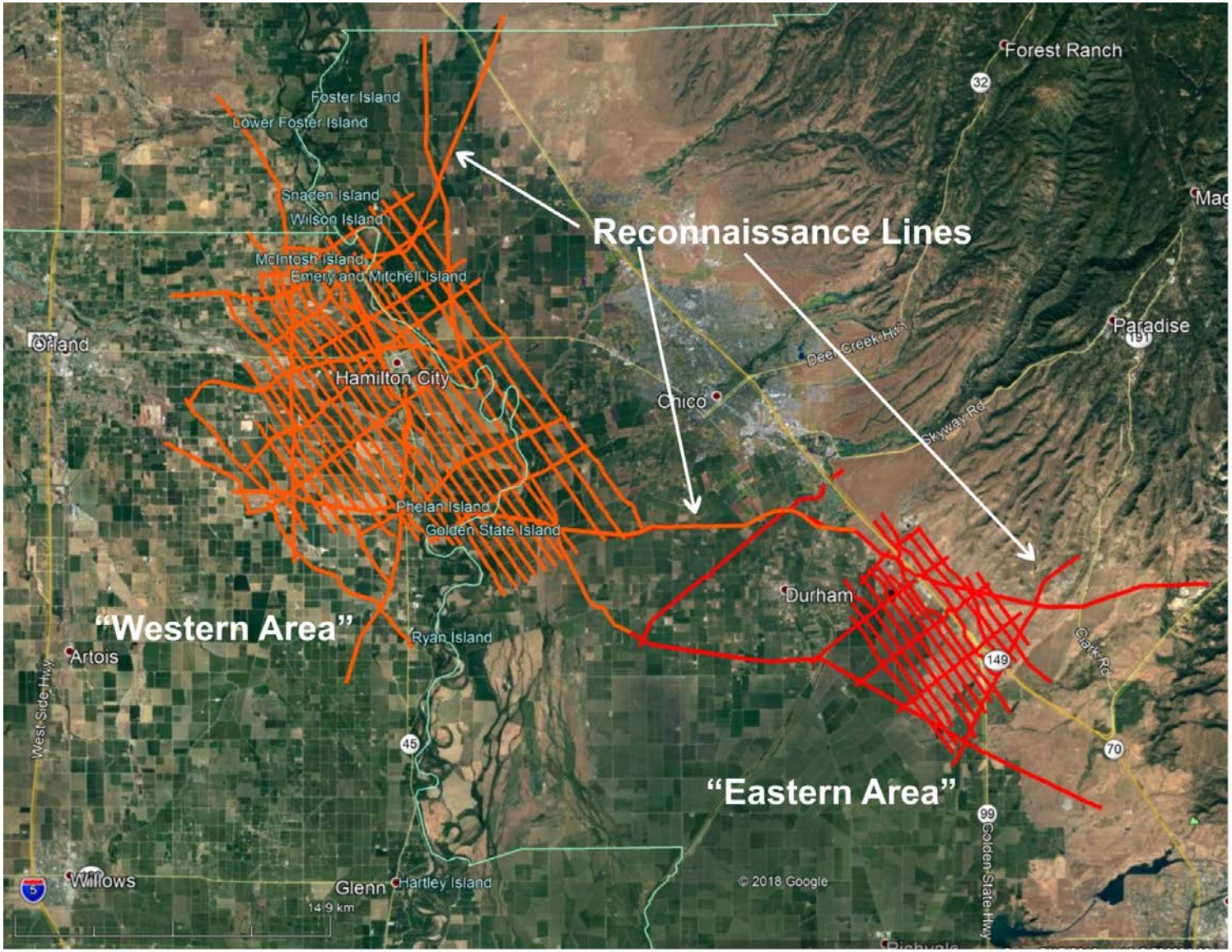

Figure 1-2. The Butte AEM survey area including county lines and major roads (99, 45, 32, 149). The orange lines are SkyTEM312 flight lines and the red lines are SkyTEM304 flight lines.

1.2 Background

Use of AEM technology to map and evaluate groundwater resources has gained momentum over the last 20 years in the United States and abroad. The State of California has been implementing AEM for water resources management over the last few years with projects across the state in a variety of geologic settings (Knight et al., 2018; Asch et al., 2017; Asch et al., 2018). In recent years, Stanford University has coordinated efforts between various local and state agencies and Aqua Geo Frameworks, LLC (AGF) in support of several projects designed to characterize the hydrogeology at various locations across the state. For purposes of this pilot project, Butte/Glenn Counties, Stanford University, and California State University at Chico (CSU-Chico) are cooperating with AGF to complete this AEM investigation. This pilot project will not only provide information on the hydrogeologic framework of the Butte/Glenn county area but will also provide experience for all partners in design and application of AEM surveys as well as educate the partners on the expectations on the nature of the results from these types of surveys. Butte County is the managing agency for this work and entered into contract with AGF on September 25, 2018.

1.3 Description of the Butte AEM Project Area

The two areas of interest, the eastern area and the western area, in Butte/Glenn Counties AEM survey area, are located in the northern Sacramento Valley in California and encompass approximately 669 square miles (Figure 1-2). These areas lie within parts of two counties: Butte and Glenn. Precipitation and irrigation runoff within the survey area feed into Sacramento River basin through many tributaries with the most prominent being Pine Creek, Burch Creek, Rock Creek, Big Chico Creek, Little Chico Creek, Butte Creek and Little Dry Creek (Figure 1-3). The area has a groundwater supply within the sands and gravels of the Tehama, Tuscan, Laguna formations and the unconsolidated alluvial materials that cover the area. Groundwater flow is towards the Sacramento River from both sides of the valley. The land use is a combination of irrigated agriculture, pasture, forest and municipal. Irrigation comes from groundwater wells and surface water supplies.

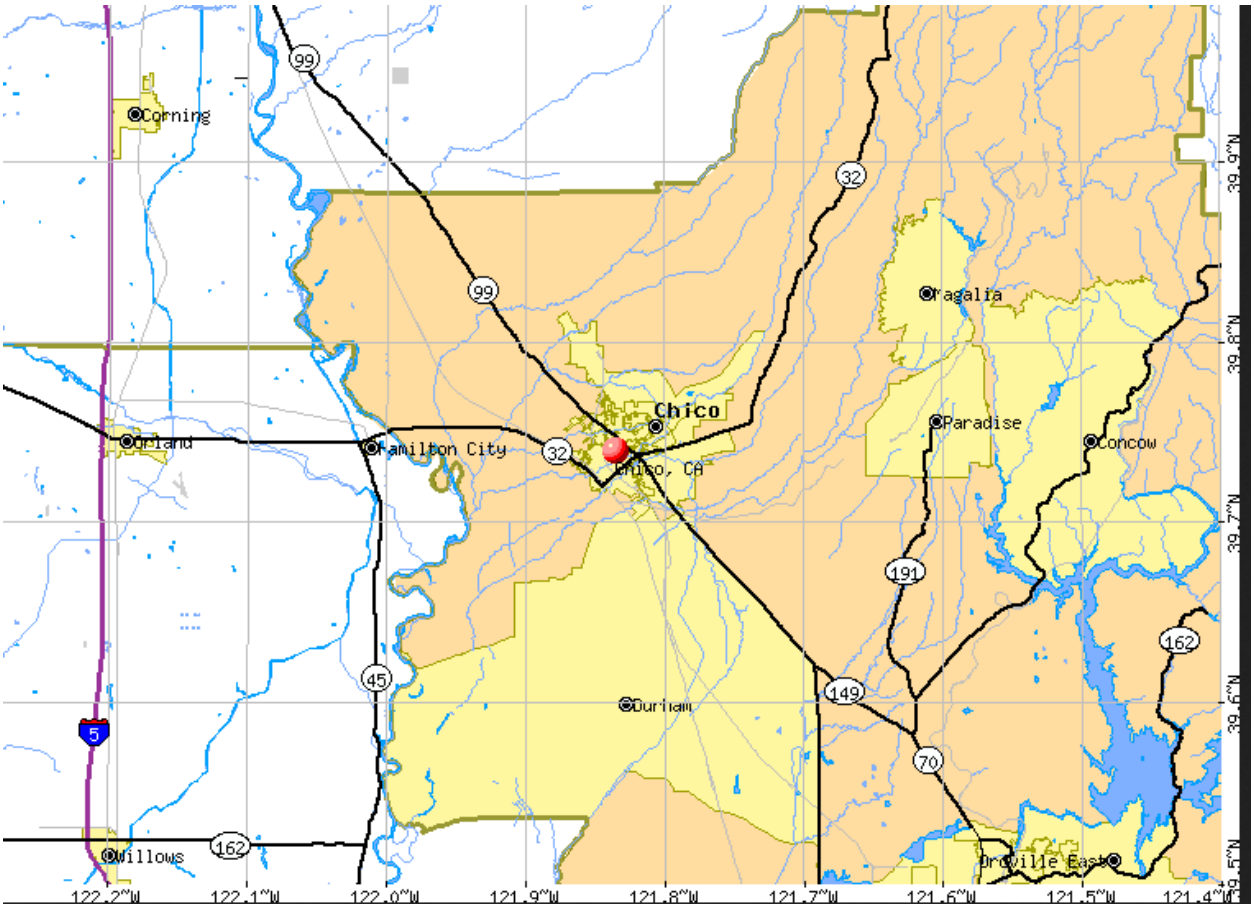

Figure 1-3. Map of major river basins with streams within the Butte/Glenn counties AEM survey area (from http://www.city-data.com/city/Chico-California.html)

2 Project Area Hydrogeology

The AEM survey's objective is to map the geology and related hydrogeology of Quaternary and Tertiary deposits that serve as either groundwater aquifers or confining units. Background geology and hydrogeology for the project area is discussed in more detail in Steele (1980), Page (1986), Blair et al. (1991), Planert and Williams (1995), California Department of Water Resources (2014), and Greene and Hoover (2014). The following narrative is based primarily on the findings from these reports.

2.1 Geologic Setting

The geology of the project area is largely volcanic with a heterogeneous mix of alluvial and fluvial fan units, including silt, sand, and gravel, with beds of claystone, siltstone, sandstone, and conglomerate (Page, 1986). Undifferentiated alluvium and colluvium deposits occupy much of the incised valleys of the uplands.

2.1.1 Physiography and Regional Geologic Setting

As mentioned in the Section 1, AEM data were collected over a survey area in Butte and Glenn counties. The Butte AEM survey areas, over 669 square miles (1733 km^2), lies in the northern part of California's Central Valley (CV). The survey primarily lies in the northwestern part of Butte and the northeastern part of Glenn Counties, California. The largest populated cities in the study area (U.S. Census Bureau, 2018) are Chico (86,187), Orland (7,291), and Durham (5,518; not a city but a census designated place). The cities of Oroville (15,546), Corning (7,663), and Willows (6,166) lie within 16 km of the study area.

The generalized geology in the AEM survey area varies considerably. A large paleo-valley (Figure 2-1) makes up most of the CV. This paleo-valley is composed mostly of unconsolidated Quaternary alluvium to marine deposits. Miocene and Pliocene volcanics and tuffs, as well as Cretaceous and Jurassic rocks make up much of the uplands and Cascade Range and Sierra Nevada to the east (Blake et al., 1992; Saucedo and Wagner, 1992). Major Quaternary units are unconsolidated to coarse-detrital alluvial, lake, playa, and terrace deposits (CA-DWR, 2014). The northeast corner of the basin is the southern terminus of the lava plateaus and volcanos of the Cascade Range (Planert and Williams, 1995).

Multiple stream terraces, ranging in age from about 10,000 to 1.25M years old were mapped in the CV (Steele, 1980). Most precipitation that falls in the CV evaporates before becoming recharge to the Central Valley Aquifer (CVA) system. Runoff from mountain streams provide nearly all the average recharge (584 mm) to the CVA (Planert and Williams, 1995).

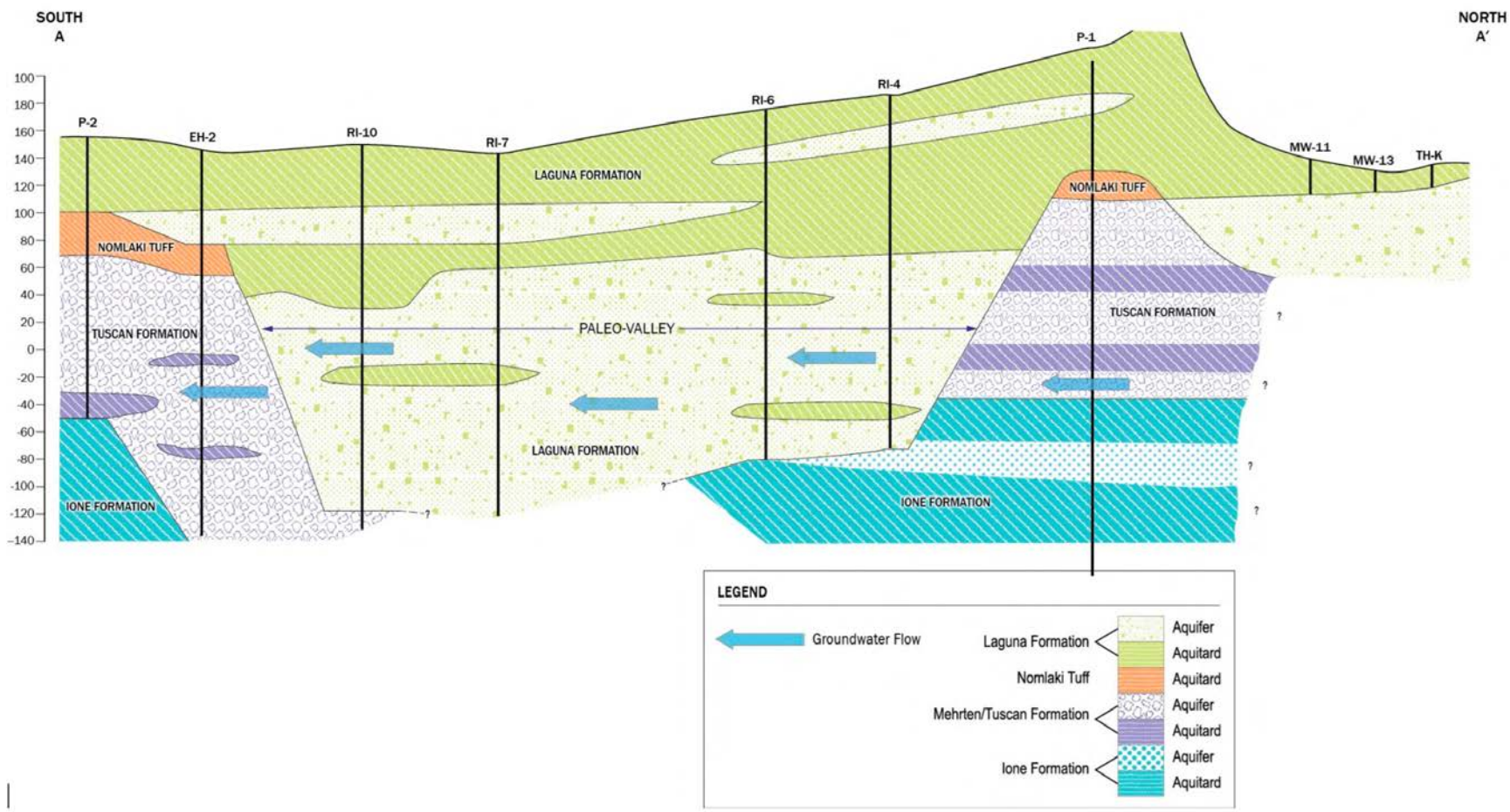

Figure 2-1. Hydrostratigraphic cross section developed by Blair et al. (1991) for the area in the vicinity of Oroville, California. Cross section shows development of paleo-valley formed by younger Laguna Formation resulting in aquifers of this formation being placed adjacent to other aquifers including the Lower Tuscan Aquifer.

2.1.2 Surficial Geology

The surficial geology of the project area is a complex assortment of volcanic and undifferentiated alluvial and colluvial deposits. The CVA is a large basin-fill aquifer system that mostly contains fresh water at depths less than 2,493 ft (760 m) (Planert and Williams, 1995) and is the largest groundwater system in the project area. Depending on depth of the groundwater, the system is confined or unconfined, though most of the shallow groundwater is unconfined. Most sediments in the northern Sacramento Valley section of the CVA average between about 984 ft and 1,968 ft (300 m and 600 m) in depth (Planert and Williams, 1995).

Burnett et al. (1969), Blake et al. (1992), and Saucedo and Wagner (1992) report that Quaternary deposits are predominantly alluvium of the Modesto Formation (***Qm***), and basin (***Qb***) and channel deposits (***Qa***). The Pleistocene Red Bluff Formation (***Qrb***) and Riverbank Formation (***Qr***) along with the Pliocene Tuscan Formation (***Tt***) and minor amounts of the Plio-Pleistocene Tuffs of Oroville (***QPto***) and Pliocene volcanic rocks (***Pv***) crop out in the eastern uplands. Holocene landslide deposits (***Qls***) also are present locally as are deposits of Miocene-Pliocene volcanic rocks (***MPv***) and the Miocene Lovejoy Basalt (***Tl***), and the Eocene "auriferous" gravels (***Tg***), and the Cretaceous Chico Formation (***Kc***) (Blake et al., 1992; Saucedo and Wagner, 1992).

2.1.3 Tertiary Geology

Tertiary geology within and adjacent to the study area is a complex sequence of marine to non-marine sediments. The Tertiary sediments are aerially extensive sandstones, siltstones, and mudstones interbedded with silty shale, conglomerates, and/or volcanic lahars and basalts. Table 2-1 describes the primary Tertiary sediments in the study area.

The Tehama FM (***Tte***) is an aerially extensive massive formation, that thins eastward. Primarily comprised of alluvial and fluvially derived deposits out of the coastal mountains. Contains pale green, gray and tan sandstone and siltstone with lenses of pebble and cobble conglomerate. Interfingers with the Tuscan Formation in the middle of the Sacramento Valley basin. Maximum thickness is about 2000 ft (610 m).

The ***Tt*** largely is identified as four separate, but lithologically identical, units. The first two units are identified by some researchers as Pleistocene (CA-WDR, 2014). The ***Tt*** is aerially extensive interbedded lahars, volcanic conglomerates, volcanic sandstone, siltstone, and pumiceous tuff. The ***Tt*** interfingers with the ***Tte*** in the basin and thins to the west. Unit D, the youngest unit, of the ***Tt*** is largely fragmental flow deposits characterized by monolithic masses containing gray hornblende and basaltic andesites and black pumice. Maximum thickness about 164 ft (50 m). Unit C of the ***Tt*** is volcanic lahars with some interbedded volcanic conglomerate and sandstone, and reworked sediments. Maximum thickness about 590 ft (180 m).

Table 2-1. Quaternary and Tertiary geology of the Butte AEM survey area, northern Sacramento Valley, California

Cenozoic	Unit/Formation	Division	Description[1]
Holocene	Stream channel and basin deposits		Unconsolidated deposits of gravel, sand, silt, and clay. Deposits derived from erosion and reworking of Tehama Formation and Quaternary stream terrace deposits. Units typically represent the upper part of the unconfined zone where saturated. Thickness can be up to 79 ft (24 m). Basin deposits result from sediment laden floodwaters and consist primarily of silts and clays. May be interbedded with some stream channel deposits. Generally, contains low permeabilities with maximum thickness of 151 ft (46 m).
Pleistocene	Modesto Formation[2]		Terrace deposits consisting of poorly indurated sand, silt and clay in gravels and cobbles. Deposits derived by reworking and intermixing Tehama and Riverbank formations. Maximum thickness nearly 200 ft (61 m).
	Riverbank Formation[2]		Terrace deposits that underlies the Modesto Fm and overlies Tuscan Fm. Consists of poorly-to-highly permeable pebble and small cobble gravels intermixed with clays, silts, and sands. Maximum thickness over 200 ft (61 m).
Plio-Pleistocene	Tehama Formation[3]		Aerially extensive, eastward thinning. Alluvial and fluvially-derived deposits derived from coastal mountains. Pale green, gray, and tan sandstone and siltstone with lenses of pebble and cobble conglomerate. Interfingers with the Tuscan Formation in the middle of the Sacramento Valley basin. Maximum thickness about 2000 ft (610 m).
	Tuscan Formation[3]		Aerially extensive interbedded lahars, volcanic conglomerates, volcanic sandstone, siltstone, and pumiceous tuff. Interfingers with the Tehama Formation in the middle of the basin. Thins westerly.
		Tuscan Unit D	Fragmental flow deposits characterized by monolithic masses containing gray hornblende and basaltic andesites

			and black pumice. Maximum thickness about 164 ft (50 m).
		Tuscan Unit C	Volcanic lahars with some interbedded volcanic conglomerate and sandstone, and reworked sediments. Maximum thickness about 590 ft (180 m).
Pliocene		Tuscan Unit B	Layered, interbedded lahars, volcanic conglomerate volcanic sandstone, and siltstone. Coarser boulder breccia than Unit A. Maximum thickness about 590 ft (180 m).
		Tuscan Unit A	Interbedded lahars, volcanic conglomerate, volcanic sandstone, and siltstone containing rock fragments. Maximum thickness about 394 ft (120 m).
Miocene	Upper Princeton Valley Fill		Aerially extensive non-marine sediments composed of sandstone with interbeds of mudstone, occasional conglomerate, and conglomerate sandstone. Maximum thickness about 1,394 ft (425 m).
	Lovejoy Basalt		Aerially extensive to the north and east. Black, dense, hard microcrystalline basalt, in the study area this formation thins to the south and the west. Maximum thickness about 66 ft (20 m).
Eocene	Ione Formation		Aerially extensive marine to non-marine deltaic sediments, light colored, commonly white conglomerate, sandstone and siltstone, soft and easily eroded. Maximum thickness about 656 ft (200 m).
	Lower Princeton Valley Fill		Aerially extensive marine sandstone, conglomerate, and interbedded silty shale. Maximum thickness about 2,394 ft (730 m).

[1]Modified from Blake et al. (1992), Saucedo and Wagner (1992); California Department of Water Resources (2014).

[2] CA-DWR (2003a, 2003b, 2003c)

[3] Saucedo and Wagner (1992) and CA-DWR (2003a, 2003b, 2003c) date as Pliocene

2.1.4 Cretaceous Geology

The primary Cretaceous sediments in the study area is the Great Valley Sequence which formed throughout the Late Jurassic and Cretaceous Periods. CA-DWR (2014) reports the eastern and western edge of the Great Valley Sequence were folded upward forming "a widely spread trough" (CA-DWR, 2014, p. 51). The lower Princeton Submarine Valley fill (Lower Princeton Valley fill in Table 2-1) unconformably overlies this trough. The sequence is characterized by deep-marine turbidites formed from eroded sediments from nearby mountains. The turbidites consist of varying compositions of interbedded marine sandstone, siltstone, and conglomerates with a maximum thickness of 45,000 ft (13,700 m) (CA-DWR, 2014; Ingersoll and Dickenson, 1981). Saline groundwater occurs throughout these sediments. Along the margins of the Great Valley Sequence, local areas of fresh water that flushed saline groundwater can be found (CA-DWR, 2014).

2.1.5 CA-DWR Interpretative Maps and Cross-Sections

The CA-DWR (2014) report also provides interpretative maps and cross-sections of the geology of the northern Sacramento Valley which have been quite useful in the analysis of the AEM inversion results (Discussed in Section 5 below). One interesting geological map is presented in Figure 2-2. As indicated in Figure 1-2, the AEM survey area is comprised of a 'western' area just west of Chico, CA and an 'eastern' area just southeast of Chico. The geological map in Figure 2-2 indicates that in the area around Chico the surface expression of the Tuscan FM (***Tt***) stops just east of Chico and then continues through the subsurface under Chico with an 'uncertain extent' (from the legend in Figure 2-2). Similarly, the Tehama FM (***Tte***) is also in the subsurface in this area with an 'uncertain extent'.

CA-DWR (2014) also provides interpretative cross-sections in Plate 2 (B-B') and Plate 3 (E-E', F-F'). The locations of these cross-sections are presented in Figure 2-3. Cross-section B-B' runs east-west and begins in the foothills and proceeds out into the valley through the center of the SkyTEM312 flight lines. Cross-section B-B' intersects cross-section E-E' (which runs north-south) at the edge of the foothills, just east of Chico and then intersects cross-section F-F' just east of the SkyTEM312 AEM survey area. A portion of cross-section B-B' which is in the vicinity of the AEM survey area is presented in Figure 2-4. Similarly, portions of cross-sections E-E' and F-F' in the vicinity of the AEM survey area are presented in Figure 2-5 and Figure 2-6, respectively. For convenience, a legend for the geological units depicted in the cross-sections is presented in Figure 2-7.

On cross-section B-B' in Figure 2-4 there are four key observations. The first is the steeply dipping nature of the units on the far right as they come off the foothills. The second is the relation of the different units to each other, i.e. the order of deposition. The third is the interthreaded nature of the ***Tt*** and ***Tte*** formations on the far left. The fourth item is to note the thinning nature of the ***Tte*** near the surface proceeding from west to east. And the fifth element to note are the "?" on most of the contacts indicating their actual position, depth, and thickness are unknown or, at least, uncertain. This includes that thinning ***Tte*** tongue just mentioned.

On cross-section E-E' in Figure 2-5 there are two elements to note. The first is again the relationship between the different units and the second is the depth to the top of the Lovejoy Basalt near its termination, about an elevation of -1400 ft.

On the F-F' cross-section in Figure 2-6 the main element to note is the discontinuous nature of the ***Tt*** in this area. This suggests either erosion or fracturing of the ***Tt*** has occurred as one proceeds into the CV.

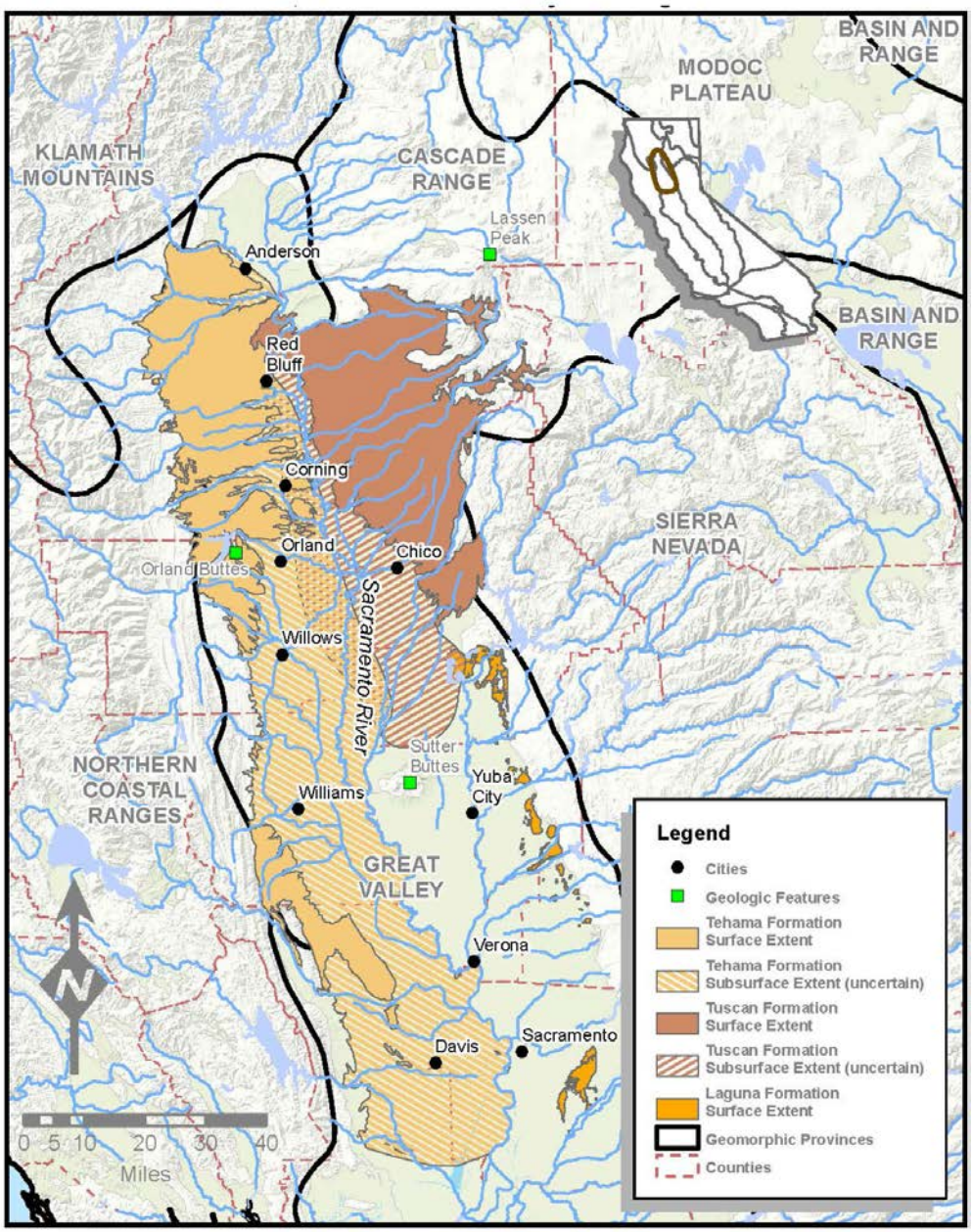

Figure 2-2. Approximate Surface and Subsurface Extent of the Tehama and Tuscan Formations, and Surface Extent Only of the Laguna Formation (Figure 5 in CA-DWR, 2014. Source: California Department of Conservation, Division of Mines and Geology. 1960-1962. "Geologic Map of California." (Redding, Ukiah, Westwood, and Chico sheets)).

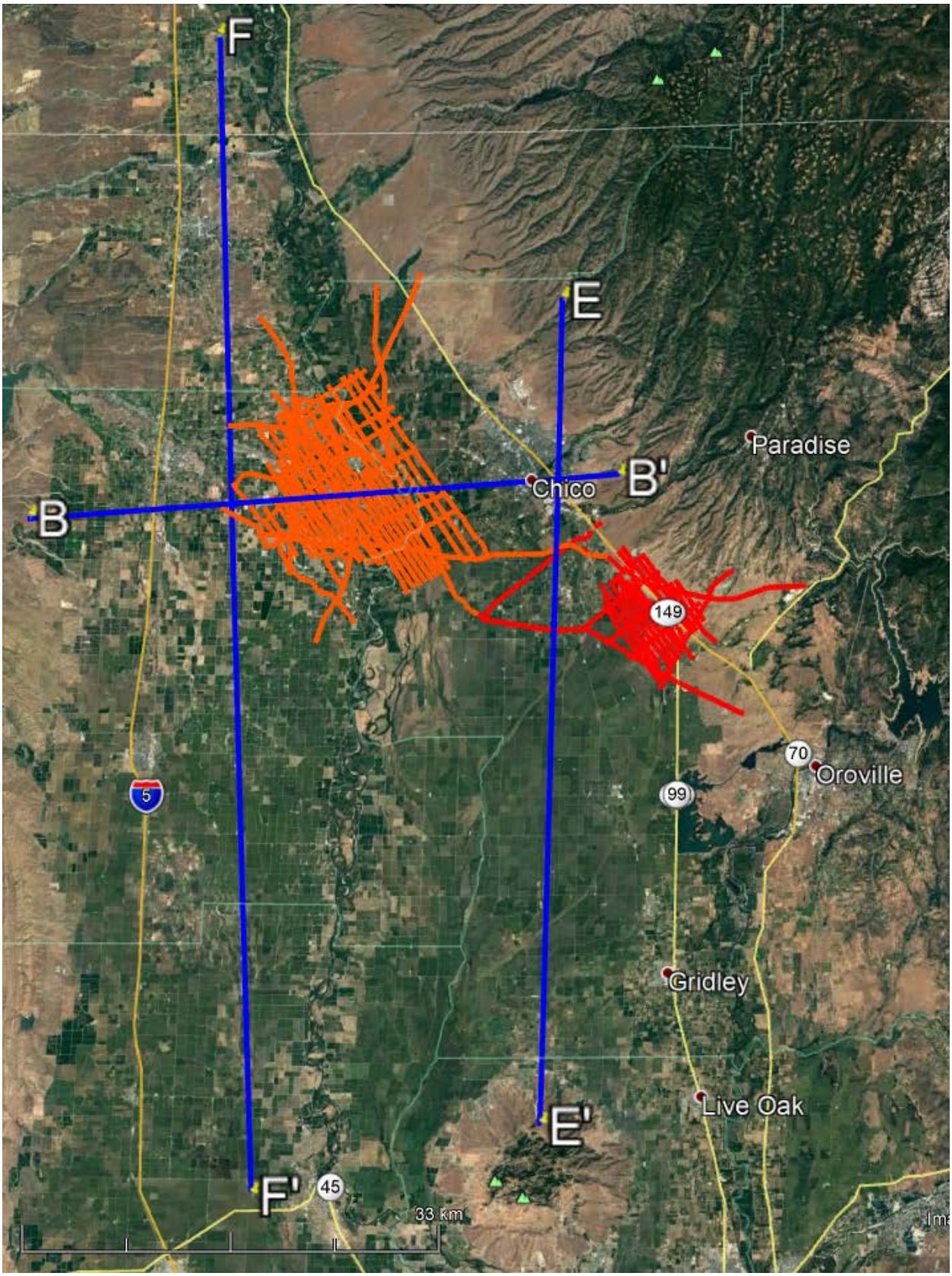

Figure 2-3. Location of cross-sections B-B', E-E', and F-F' from Plate 2 and Plate 3 of CA-DWR (2014).

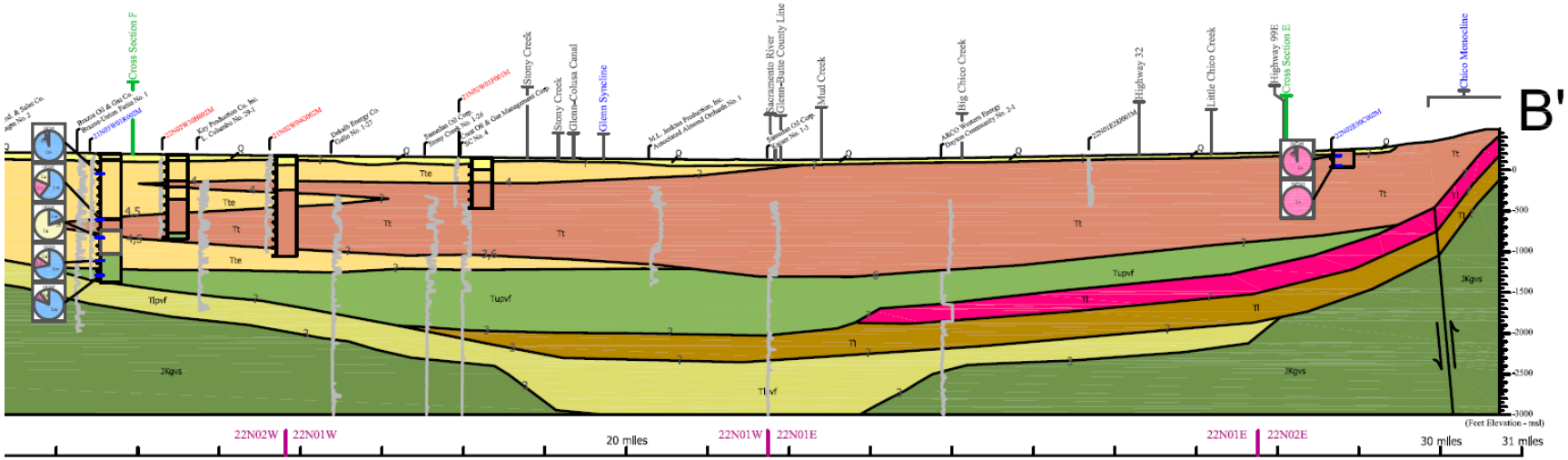

Figure 2-4. A portion of east-west cross-section B-B' from Plate 2 of CA-DWR (2014).

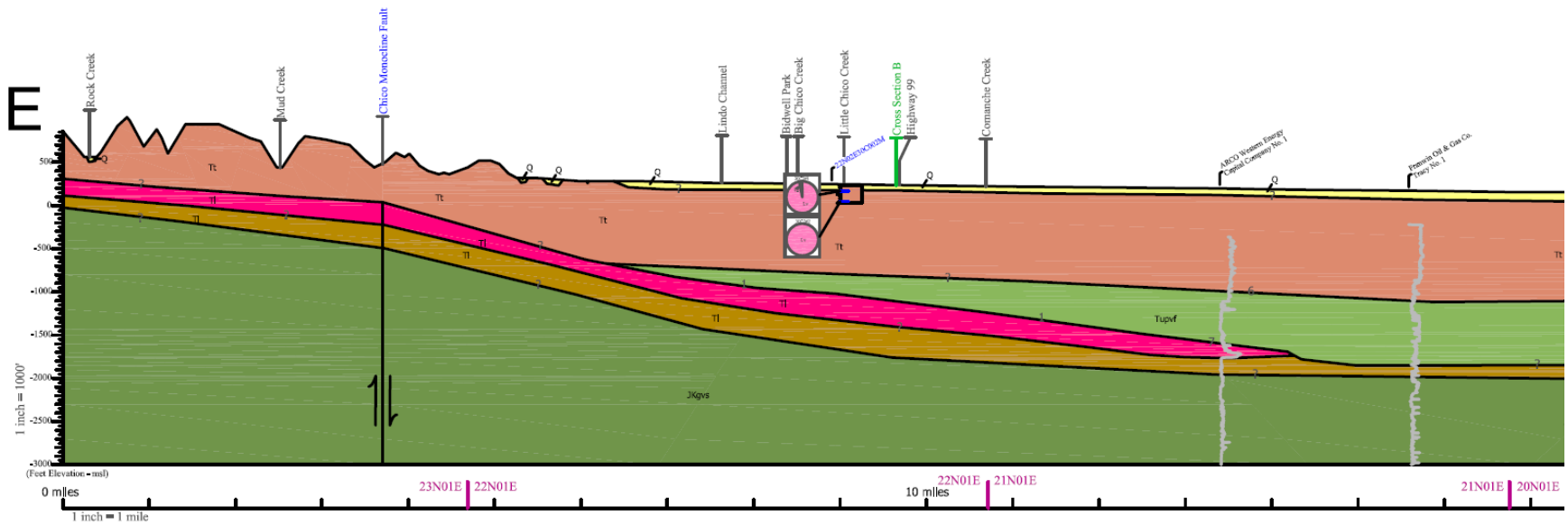

Figure 2-5. A portion of north-south cross-section E-E' from Plate 3 of CA-DWR (2014).

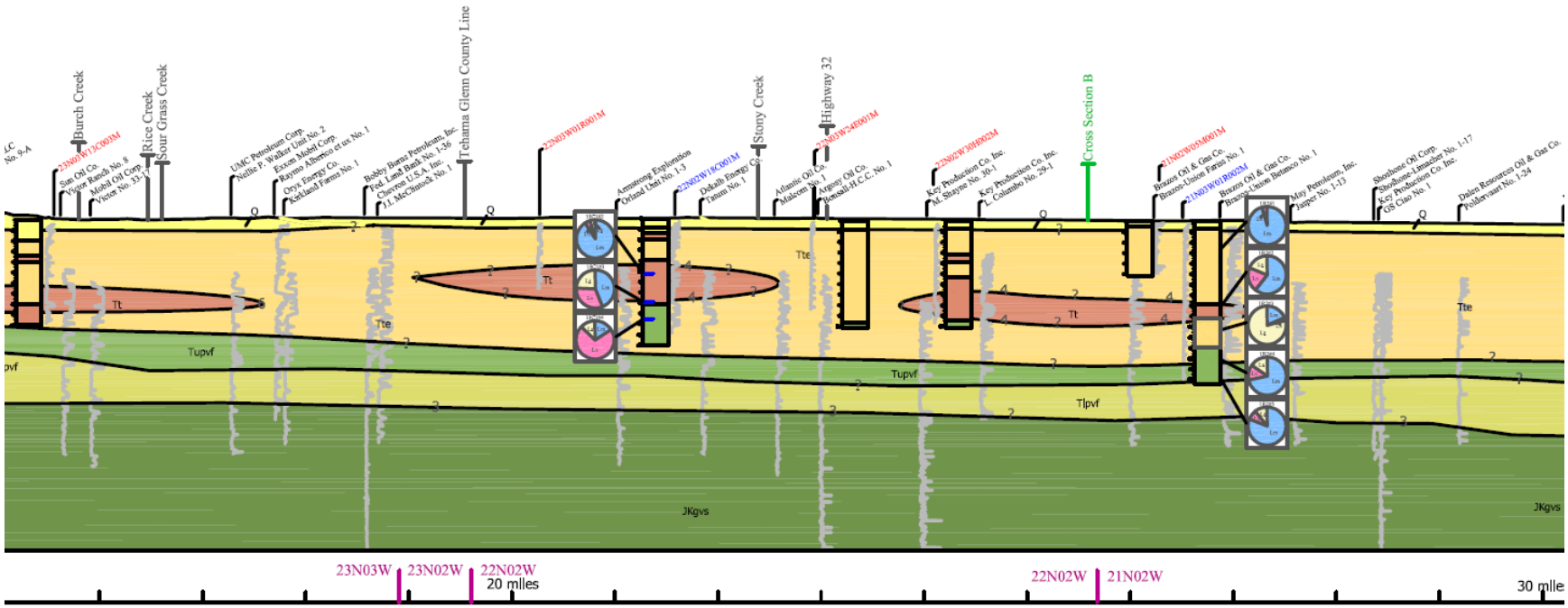

Figure 2-6. A portion of north-south cross-section F-F' from Plate 3 of CA-DWR (2014).

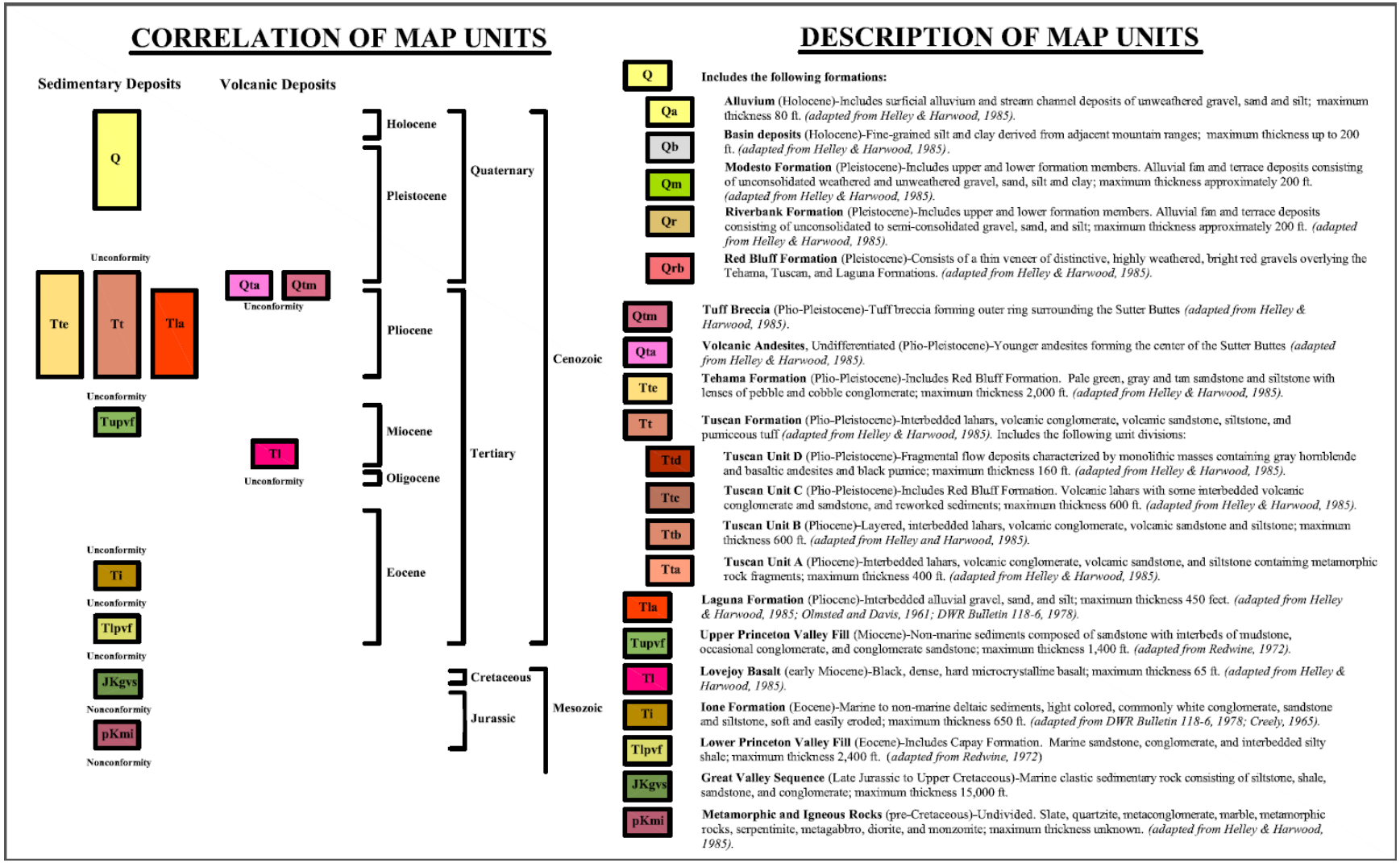

Figure 2-7. Geological units legend for cross-sections B-B', E-E', and F-F' above in Figure 2-4, Figure 2-5, and Figure 2-6, respectively (modified from CA-DWR, 2014)

2.2 Butte AEM Survey Area Hydrogeologic Characteristics

The primary hydraulic features in the project area are related to the perennial streams—the Sacramento River and the Big Chico and Butte Creeks—and several large surface-water canals/reservoirs, such as the Glenn-Colusa Canal and Lake Oroville. The Sacramento River is the primary stream of the project area and runs through the area covered by the AEM flights. Annual daily-mean discharge for the Sacramento River from USGS streamgage 11377100 Sacramento River above Bend Bridge near Red Bluff, California (about 45 km north of the project area) to USGS streamgage at 11389500 at Calusa, California (about 45 km south of the project area) for water year 2017 was 560.1 to 515.1 m^3/s (USGS, 2018a). Therefore, annual daily-mean streamflow during water year 2017 decreased downstream. The cause or causes of the decrease in streamflow is not discussed in this report; however, it likely is, in part due to recharge into the CVA and diversions into canals prevalent throughout the area. Groundwater connectivity to surface-water systems in the project area is complex due to the numerous surface-water features that recharge the groundwater system.

Spring 2018 groundwater levels indicate generalized southerly flow with groundwater discharging into the Sacramento River (Figure 2-8; CA-DWR, 2018).

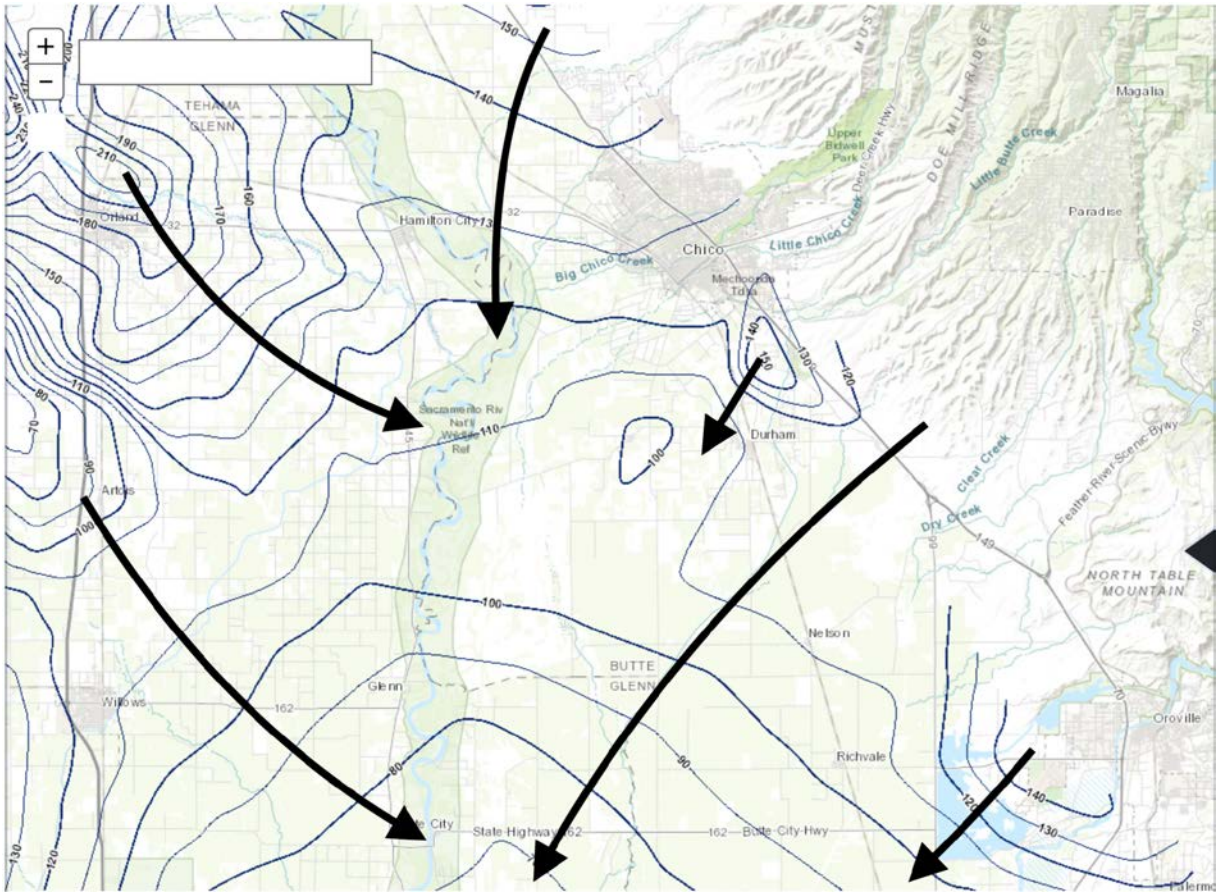

Figure 2-8. Map showing highly generalized regional groundwater flow paths around the project area (Modified from CA-DWR, 2018). Arrows indicate general groundwater flow directions. Contour interval 10 ft. (https://gis.water.ca.gov/app/gicima/).

Groundwater-level data from the U.S. Geological Survey's (USGS) National Water Information System (NWIS) (USGS, 2018b) indicate the shallowest (<3 m below land surface (bls)) groundwater typically were found south of the study area near the Sacramento River or largely adjacent to or downgradient of the Thermalito Afterbay (about 4 km south of the flight area). Moderately-shallow groundwater levels (10 ft to 50 ft or 3 m to 15 m bls) generally were found along the Sacramento River and its tributaries, or similar to shallow water levels near Thermalito Afterbay. These moderately-shallow water levels appear more regional than shallow water levels. Most moderately-deep (50 ft to 98 ft or 15 m to 30 m) water levels were located near the foothills of the Cascade Range/Sierra Nevada Mountains. The deepest (>98 ft or >30 m) groundwater levels all were located within mountain ranges. Most groundwater levels less than 11.5 ft or 3.5 m bls were (1) found in the central or eastern side of the valley and (2) largely found in two larger clusters. Groundwater-levels between 50 ft to 98 ft (15 m and 30 m) generally were located on the west to northwestern side of the valley Groundwater levels between 11.5 ft to 50 ft bls (3.5 m and 15 m) are generally distributed throughout the valley., whereas those greater than 30 m bls were distributed throughout the Valley.

Planert and Williams (1995) report the volcanic and metamorphic rocks that surround and underlie the CV are consolidated and almost impermeable. Consequently, little water flows through these deposits. However, the CVA is formed primarily of sand and gravel deposits with silt and clay, all of which have been eroded from the mountains that surround the valley. These deposits, together with deposits from lacustrine beds, volcanic rocks, and dune deposits are all part of the CVA (Planert and Williams, 1995). Lens-shaped clay beds help make up a heterogeneous aquifer system that is under unconfined conditions in the upper hundred meters, but under confined conditions with depth.

Table 2-2 summarizes information for Quaternary and Tertiary aquifer units within the area. Included in this table are the geologic system hosting the aquifer, generalized aquifer thickness, and a general discussion regarding the aquifer framework, groundwater flow system characteristics, and aquifer parameters.

Table 2-2. Aquifers in Quaternary and Tertiary Age stratigraphic units (modified from CA-DWR, 2003a, 2003b, 2003c). CA-DWR gives age of Tehama and Tuscan as Pliocene)

System	Series	Hydrologic unit	Maximum thickness, ft.
Quaternary	Holocene	Aquifer in undifferentiated Central Valley stream channel and basin deposits	Generally, less than 150 ft (46 m)
Undifferentiated sand and gravel units in stream-valley and paleo-valley systems. Sacramento River stream-aquifer systems can be intermixed with paleo-valley sand and gravel deposits making the Holocene deposits difficult to distinguish from older Pliocene deposits. Hydraulic head is typically unconfined. Locally or regionally hydraulically connected to underlying Pleistocene, Plio-Pleistocene and Tertiary deposits. Recharge is principally from leakage from surface-water canals, and influx from adjacent near mountain boundaries, with some influx from local precipitation. Surface-water canal leakage can be rapid if the source area is primarily sand and gravel. Thickness and aerial extent of deposits limit water carrying capability. Wells capable of yielding up to several thousand liters per minute.			
Quaternary	Pleistocene	Aquifer in Modesto Formation	About 200 ft (61 m)
Poorly indurated sand, silt and clay in gravels and cobbles. Deposits derived by reworking and intermixing Tehama and Riverbank formations. Yields moderate amounts of water to domestic and shallow irrigation wells and to deeper irrigation wells that have multiple screened intervals.			
Quaternary	Pleistocene	Aquifer in Riverbank Formation	About 200 ft (61 m)
Underlies Modesto Formation and overlies Tuscan Formation. Consists of poorly-to-highly permeable pebble and small cobble gravels intermixed with clays, silts, and sands. Yields moderate amounts of water to domestic and shallow irrigation wells and to deeper irrigation wells that have multiple screened intervals.			
Quaternary	Pliocene/Plio-Pliestocene	Aquifer in Tehama Formation	About 2,000 ft (610 m)
Primary or predominant water-bearing unit in CDWR groundwater sub-basins 5-21-51 and 5-21-52 (CA-DWR 2003a and 2003b). Moderately compacted silt and clay layers enclosing			

lenses of sand and gravel, and cemented conglomerate. Occasional deep sands and thin gravel lenses present. These occasional lenses create poor to moderate, deep production zones.			
Tertiary	**Pliocene**	**Aquifer in Tuscan Formation deposits**	**Can exceed 1,312 ft (400 m)**
Present throughout most of the project area. Date could be Plio-Pleistocene. Four separate, but lithologically similar units. Locally or regionally interfingers with and is hydraulically connected to overlying Tehama Formation. Composed of a series of volcanic mudflows, breccias, sandstones, and siltstones. Unit A (Table 2-1) considered oldest water-bearing unit of the formation. Saturated thickness varies by location. Can exceed 1,312 ft (400 m) and thins westerly. Recharge mostly from mountain boundaries, canal and reservoir leakage, precipitation, and inflow from hydraulically connected aquifers. Presence of lahars can form thick confining layers for groundwater contained in more permeable deposits.			

2.2.1 Aquifer Characteristics

Aquifer characteristics of the project area were concatenated from localized or large regional studies. Aquifer tests (constant discharge, slug, or permeameter) performed in or near (within 30 miles) of the project area help characterize the aquifer(s). However, discussion on aquifer tests are point source tests and should not be construed as representing an aquifer as a whole. Point-source tests can be qualitatively used to represent regional systems when viewed with certain caveats (e.g., difference in scale—local vs. regional, difference in sediment, and difference in aquifer thickness). Keeping the scale in mind, all discussion of aquifer tests herein are local tests used to represent a regional system. Consequently, these values are reported as regional generalities and not meant to qualitatively represent any place other than where the aquifer tests were performed.

Table 2-3 summarizes generalized aquifer-test data in or near the project area. $\mathbf{K_r}$ is horizontal hydraulic conductivity; $\mathbf{md^{-1}}$ is meters per day; **T** is transmissivity; $\mathbf{m^2d^{-1}}$ is meters squared per day; **S** is storativity; **LTA** is Lower Tuscan Aquifer; "**—**" is not reported or not applicable; **IS** - Intermediate Shallow; and **ID** - Intermediate Deep.

Transmissivity values depend on $\mathbf{K_r}$ and saturated thickness. The volume of water that moves through an aquifer would depend on the groundwater gradient at the site. Specific yield (***Sy***) or storativity **S** can be related closely to, but is less than an aquifers total porosity Bear (1979). Specific Yield is an estimate of the percentage of water in an aquifer that will drain under gravity (Heath, 1983). Recharge rates vary with location, soil type, depth to water, and irrigated vs. dryland.

Table 2-3. Generalized aquifer-test data.

Researcher(s)	Year	Location	Aquifer (if listed)	K_r (md^{-1})	T (m^2d^{-1})	S
Greene and Hoover	2014	Near Hamilton City, CA	LTA	--	186 to 604	$1x10^{-3}$ to $1x10^{-4}$
Dames and Moore[1]	1993	South of Oroville, CA	LTA		1,870	$2.8x10^{-4}$
California DWR[1]	1995	Chico Ranch Deeper	LTA		856	$2.7x10^{-5}$
	1996	Chico Ranch Intermediate	LTA		1,960	$1x10^{-5}$
Crystal Geyser[1]	2009	Crystal Geyser Water Co.	Tehama Formation	22 to 40	286 to 484	$1x10^{-3}$ to $1x10^{-4}$
California DWR	2009	Glenn-Colusa Irrigation District	LTA	3.1 to 3.5	370 to 459	$4x10^{-4}$ to $7x10^{-5}$
Brown and Caldwell	2013	Esquon Ranch IS Test 1	LTA	4.0	373	$4x10^{-5}$
		Esquon Ranch ID Test 1	LTA	2.6	234	$4x10^{-6}$
		Esquon Ranch IS Test 2	LTA	24	2,200	$3x10^{-4}$
		Esquon Ranch ID Test 2	LTA	18	1,600	$9.6x10^{-4}$
French et al.[2]	1983	Butte City, CA (493 ft)		$3.0x10^{-3}$	--	--
		Butte City, CA (957 ft)		$4.0x10^{-1}$	--	--
		Butte City, CA (1066 ft)		$8.8x10^{-1}$	--	--
		Butte City, CA (1182 ft)		$6.1x10^{-2}$	--	--
		Butte City, CA (1414 ft)		$6.1x10^{-4}$	--	--

[1] Reported in Brown and Caldwell, 2013

[2] Laboratory sidewall core tests for horizontal hydraulic conductivity

2.2.2 Water Quality

Concentrations of total dissolved solids (TDS) above 1,500 milligrams per liter (mg/L) can affect the bulk resistivity values impacting the interpretations of the geological materials. Therefore, TDS data from 36 wells in the USGS NWIS (USGS, 2018b) were used to determine TDS concentrations in the Butte project area. Thirty-four of the 36 wells contained water samples with TDS concentrations less than the 500 mg/L. The other two wells had water samples with TDS concentrations of 503 and 550 mg/L and neither of these two wells were located in the flight line area (Figure 2-9). Most wells that had TDS concentrations were located south of the flight lines. As a result, groundwater samples collected from wells throughout the project area show all TDS concentrations were far less than the 1,500 mg/L threshold and; therefore, water quality in the project area likely did not affect interpretation of bulk resistivity values.

CA-DWR (2003a, 2003b, and 2003c) reported TDS in groundwater samples from wells in subbasins the project area lies within. The TDS from these samples range from 48 in the Vina Subbasin to 1,220 mg/L in the Colusa Subbasin. CDWR did not report any samples exceeding 1,500 mg/L.

Table 2-4. TDS Ranges of Ca-Mg HCO3 and Mg-Ca HCO3 types

Site	Range (mg/L)	Average (mg/L)
Corning Subbasin (5-21.51)	**130 to 490**	**286**
Colusa Subbasin (5-21.52)	**120 to 1,220**	**391**
Vina Subbasin (5-21.51)	**48 to 543**	**285**

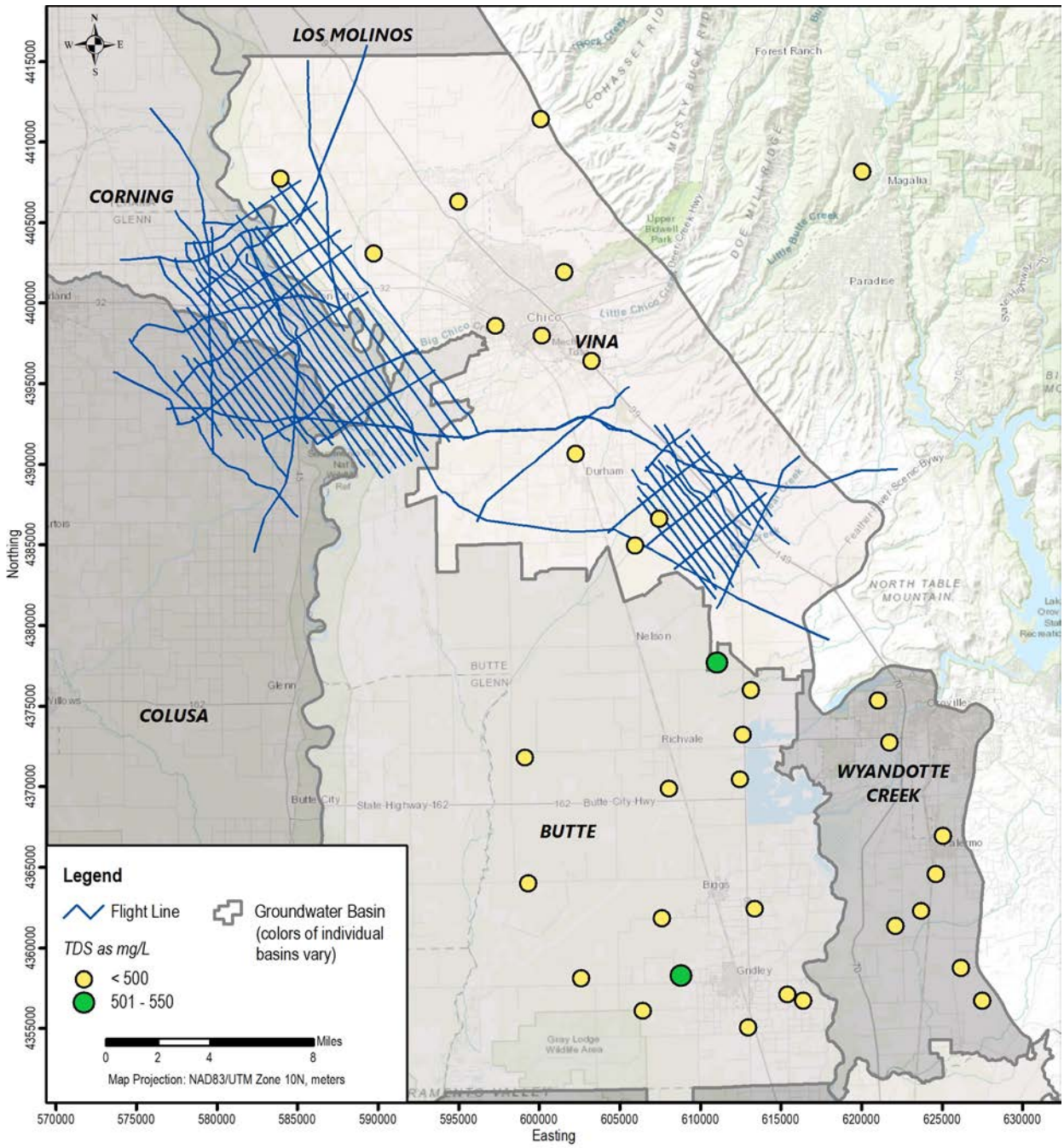

Figure 2-9. Map of Total Dissolved Solids (TDS) near the Butte AEM survey area.

3 Additional Background Information

Various sources of background information were used to interpret the AEM data, which is discussed in Section 5.

3.1 Borehole Data

Borehole data for this project consisted of a combination of lithologic and downhole geophysical logs. The borehole information was gathered by Todd Greene, Associate Professor of Geological and Environmental Sciences at California State University, Chico. The geophysical logs were first provided on October 19, 2018 and the lithological logs on October 18, 2018 with additions on November 2, 2018.

The locations of the boreholes utilized in the Butte AEM survey analysis are indicated in Figure 3-1. A total of 362 holes contained lithology information and 183 holes contained geophysical information within the Butte AEM survey area.

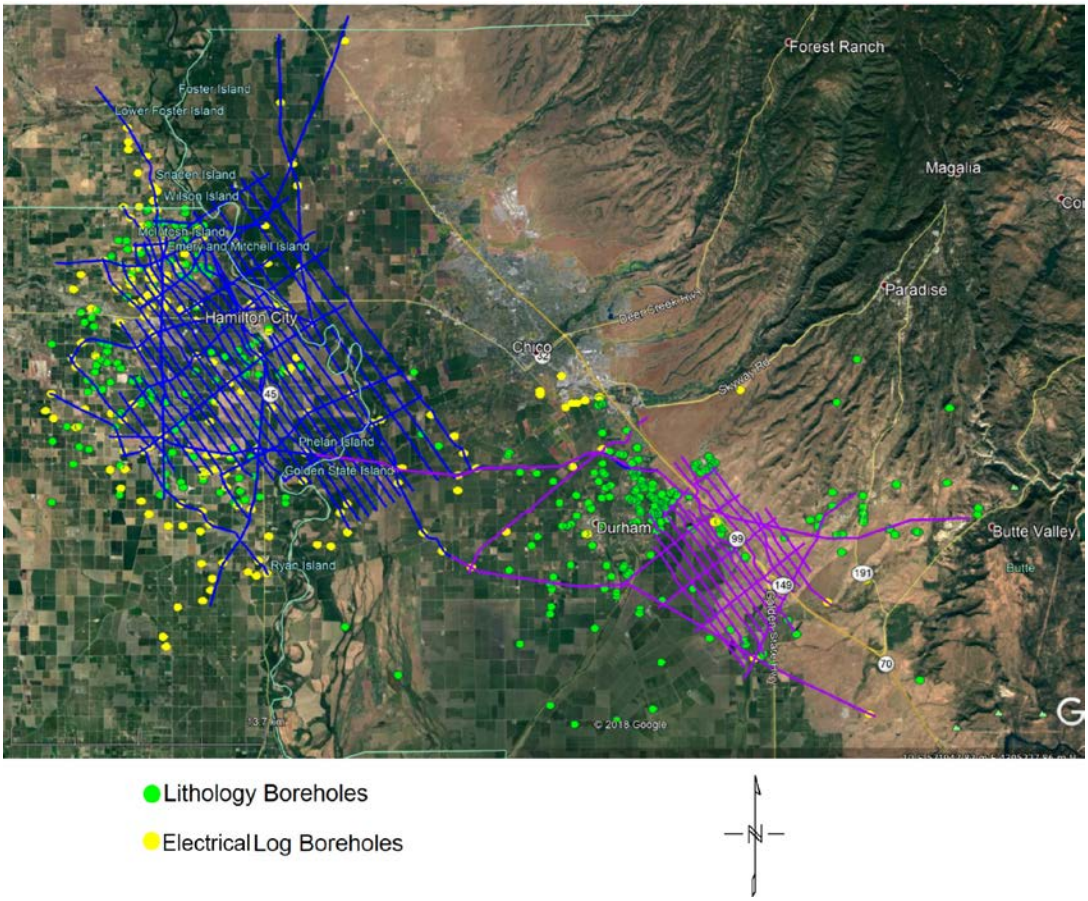

Figure 3-1. Locations of the boreholes near the Butte AEM survey area. Green circles represent boreholes with lithology information and yellow circles are borehole locations with geophysical information. 312 flight lines in blue, 304 flight lines in purple.

Since, typically, resistivity logs are of various vintages and conducted by various staff with differing equipment, a critical examination of the absolute values of the resistivity needs to include an awareness of errors in calibration and in the proper operation of the equipment. There is a long-standing issue with using geophysical logs as ground truths when comparing to AEM inversions that are well calibrated using modern techniques. Throughout much of the geophysical logging world at the time it was acquired, the relative deflections of the resistivity measurements were all that was required or expected from a geophysical log. Operators were seldom trained in the proper operation of a calibrated sonde or in the ability to recognize high contact resistance of a cable head. This has led to many geophysical logs that are potentially uncalibrated. Note that these logs still have scientific merit in their ability to relatively indicate an increase or a decrease in the formation resistivity. The logs used herein are for qualitative comparison to the AEM because detailed calibration and corrections would need to be carried out for the resistivity values in some of the logs to be directly used as numerical constraints in the inversion of the AEM data (Ley-Cooper and Davis, 2010).

4 Geophysical Methodology, Acquisition and Processing

4.1 Geophysical Methodology

Airborne Transient Electromagnetic (TEM) or airborne Time-Domain Electromagnetic (TDEM), or generally AEM, investigations provide characterization of electrical properties of earth materials from the land surface downward using electromagnetic induction. Figure 4-1 gives a conceptual illustration of the airborne TEM method.

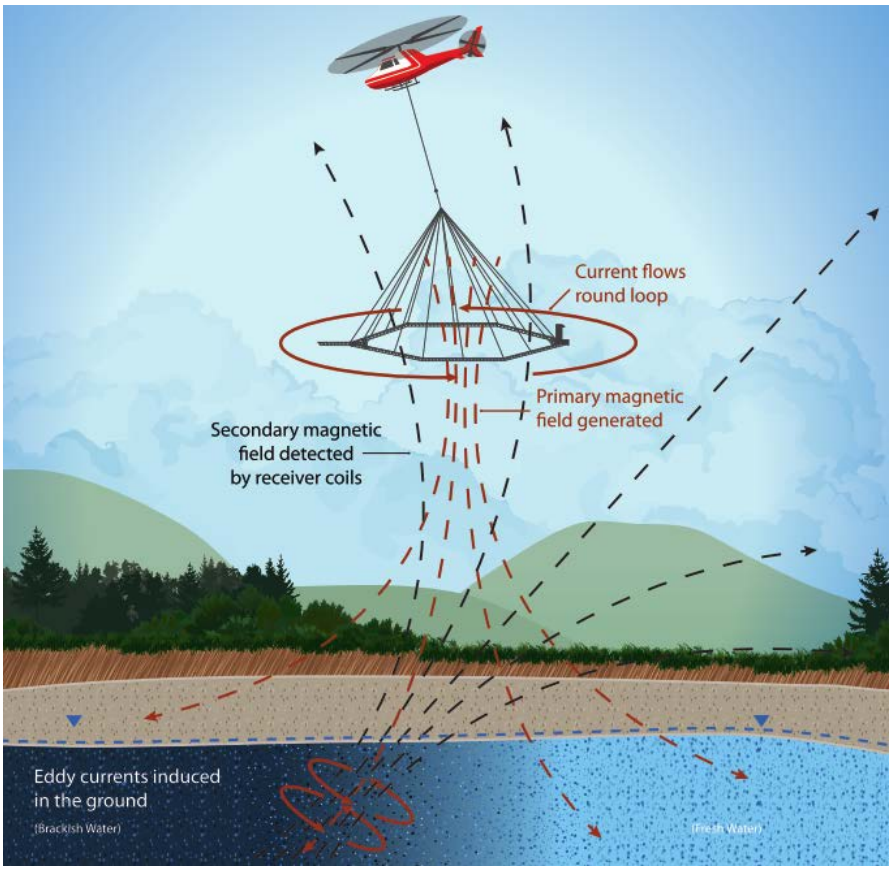

Figure 4-1: Schematic of an airborne electromagnetic survey, modified from Carney et al. (2015).

To collect TEM data, an electrical current is sent through a large loop of wire consisting of multiple turns which generates an electromagnetic (EM) field. This is called the transmitter (Tx) coil. After the EM field produced by the Tx coil is stable, it is switched off as abruptly as possible. The EM field dissipates and decays with time, traveling deeper and spreading wider into the subsurface. The rate of dissipation is dependent on the electrical properties of the subsurface (controlled by the material composition of the geology including the amount of mineralogical clay, the water content, the presence of dissolved solids, the metallic mineralization, and the percentage of void space). At the moment of turnoff, a secondary EM field, which also begins to decay, is generated within the subsurface. The decaying secondary EM field generates a current in a receiver (Rx) coil, per Ampere's Law. This current is measured at several different moments in time (each moment being within a time band called a "gate"). From the induced current, the time rate of decay of the magnetic field, B, is determined (dB/dt). When compiled in time,

these measurements constitute a “sounding” at that location. Each TEM measurement produces an EM sounding at one point on the surface.

The sounding curves are numerically inverted to produce a model of subsurface resistivity as a function of depth. Inversion relates the measured geophysical data to probable physical earth properties. Figure 4-2 shows an example of a dual-moment TEM dB/dt sounding curve and the corresponding inverted electrical resistivity model.

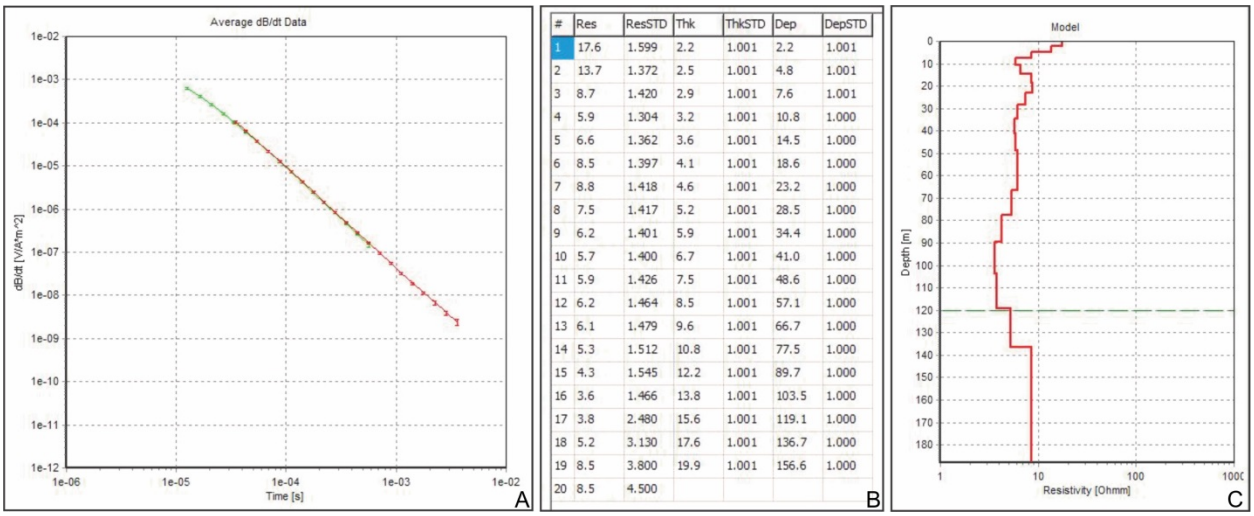

#	Res	ResSTD	Thk	ThkSTD	Dep	DepSTD
1	17.6	1.599	2.2	1.001	2.2	1.001
2	13.7	1.372	2.5	1.001	4.8	1.001
3	8.7	1.420	2.9	1.001	7.6	1.001
4	5.9	1.304	3.2	1.001	10.8	1.000
5	6.6	1.362	3.6	1.001	14.5	1.000
6	8.5	1.397	4.1	1.001	18.6	1.000
7	8.8	1.418	4.6	1.001	23.2	1.000
8	7.5	1.417	5.2	1.001	28.5	1.000
9	6.2	1.401	5.9	1.001	34.4	1.000
10	5.7	1.400	6.7	1.001	41.0	1.000
11	5.9	1.426	7.5	1.001	48.6	1.000
12	6.2	1.464	8.5	1.001	57.1	1.000
13	6.1	1.479	9.6	1.001	66.7	1.000
14	5.3	1.512	10.8	1.001	77.5	1.000
15	4.3	1.545	12.2	1.001	89.7	1.000
16	3.6	1.466	13.8	1.001	103.5	1.000
17	3.8	2.480	15.6	1.001	119.1	1.000
18	5.2	3.130	17.6	1.001	136.7	1.000
19	8.5	3.800	19.9	1.001	156.6	1.000
20	8.5	4.500				

Figure 4-2: A) Example of a dB/dt sounding curve. B) Corresponding inverted model values. C) Corresponding resistivity earth model.

4.2 Flight Planning/Utility Mapping

The primary source of noise in geophysical electromagnetic surveys are other electromagnetic devices that are part of typical municipal utility infrastructure. These include, for example, power lines, railroads, pipelines, and water pumps. Prior to AEM data acquisition in Butte and Glenn counties, three types of utilities (pipelines, railroads, and power lines) were located.

The locations of the flight lines were converted from a regularly spaced grid to one with flight lines optimized in order to avoid electromagnetic coupling with the previously mentioned utilities. This was done by moving along each flight line in Google Earth to inspect the path for visible power lines, radio towers, railroads, highways and roads, confined feeding operations and buildings, and any other obstructions that needed to be avoided during flight. The paths of the flight lines were also modified so as to fly closer to known borehole locations.

At the conclusion of the design process, the Butte AEM flight lines were divided into both block and reconnaissance flight lines. The reconnaissance flight lines were approximately 22 miles in length (36 km) at their longest and about 3.1 miles (5 km) at their shortest. The block flights had flight lines up to 12 miles in length (approximately 20 km) with tie lines approximately 8.6 miles in length (approximately 14 km) for the western block area. The eastern block flight lines were about 5.5 miles in length

(approximately 9 km) with 4.9 miles long tie lines (about 8 km). Block flight lines were separated by about 1500 feet or so (about 450 m to 500 m) (Figure 1-2 and Figure 4-5).

4.3 AEM Survey Instrumentation

AEM data were acquired using both the SkyTEM304M (304M) and the SkyTEM312 (312) airborne electromagnetic systems (SkyTem Airborne Surveys Worldwide, 2018). The 304M is a rigid frame, dual-magnetic moment (Low and High) TEM system. The area of the 304M Tx coil is 342 m^2 and the coil contains four (4) turns of wire. A peak current of nine (9) amps is passed through one turn of wire in the Tx for Low Moment measurements and a peak current of 110 amps is passed through the four turns of wire for High Moment measurements. This results in peak Tx Low and High magnetic moments of ~3,000 Ampere-meter-squared ($A*m^2$) and ~150,000 $A*m^2$, respectively.

The SkyTEM312 uses the same frame as the 304M but different electronics and transmitter wiring. A peak current of six (6) amps is passed through two (2) turns of wire in the Tx for Low Moment measurements and a peak current of 110 amps is passed through the twelve (12) turns of wire for High Moment measurements. This results in peak Tx Low and High magnetic moments of ~4,100 Ampere-meter-squared ($A*m^2$) and ~450,000 $A*m^2$, respectively.

The SkyTEM304M and 312 systems utilize an offset Rx positioned slightly behind the Tx resulting in a 'null' position which is a location where the intensity of the primary field from the system transmitter is minimized. This is desirable as to minimize the amplitude of the primary field at the Rx to maximize the sensitivity of the Rx to the secondary fields. The 304M and 312 multi-turn Rx vertical (Z) coil has an effective area of 105 m^2. In addition to the Tx and Rx that constitute the TEM instrument, the 304M and 312 are also equipped with a Total Field magnetometer (MAG) and data acquisition systems for both instruments. The 304M and 312 also include two each of laser altimeters, inclinometers/tilt meters, and differential global positioning system (DGPS) receivers. Positional data from the frame mounted DGPS receivers are recorded by the AEM data acquisition system. The magnetometer includes a third DGPS receiver whose positional data is recorded by the magnetometer data acquisition system. Figure 4-3 gives a simple illustration of the 304M and 312 frame and instrument locations. The image is viewed along the +z axis looking at the horizontal x-y plane. The axes for the image are labeled with distance in meters. The magnetometer is located on a boom off the front of the frame (right side of image). The Tx coil is located around the octagonal frame and the Rx Coil is located at the back of the frame (left side of image).

The coordinate system used by the 304M and 312 defines the +x direction as the direction of flight, the +y direction is defined 90 degrees to the right and the +z direction is downward. The center of the transmitter loop, mounted to the octagonal SkyTEM frame is used as the origin in reference to instrumentation positions. Table 4-1 lists the positions of the instruments and Table 4-2 lists the corners of the transmitter loop.

The DGPS and magnetometer mounted on the frame of the 304M and 312 require the use of base stations, which are located on the ground and are positioned in an area with low cultural noise. In this case these instruments were located at the airport near Orland, California. Data from the magnetometer

and DGPS base stations were downloaded each day after the end of the day's AEM flights. The DGPS and magnetometer base stations were placed at the Universal Transverse Mercator (UTM) coordinate system location listed in Table 4-3. The horizontal geodetic reference used is North American Datum of 1983 (NAD83 in feet). All elevations are from USGS's National Elevation Dataset, referenced to the North American Vertical Datum of 1988; with feet as the unit of measurement.

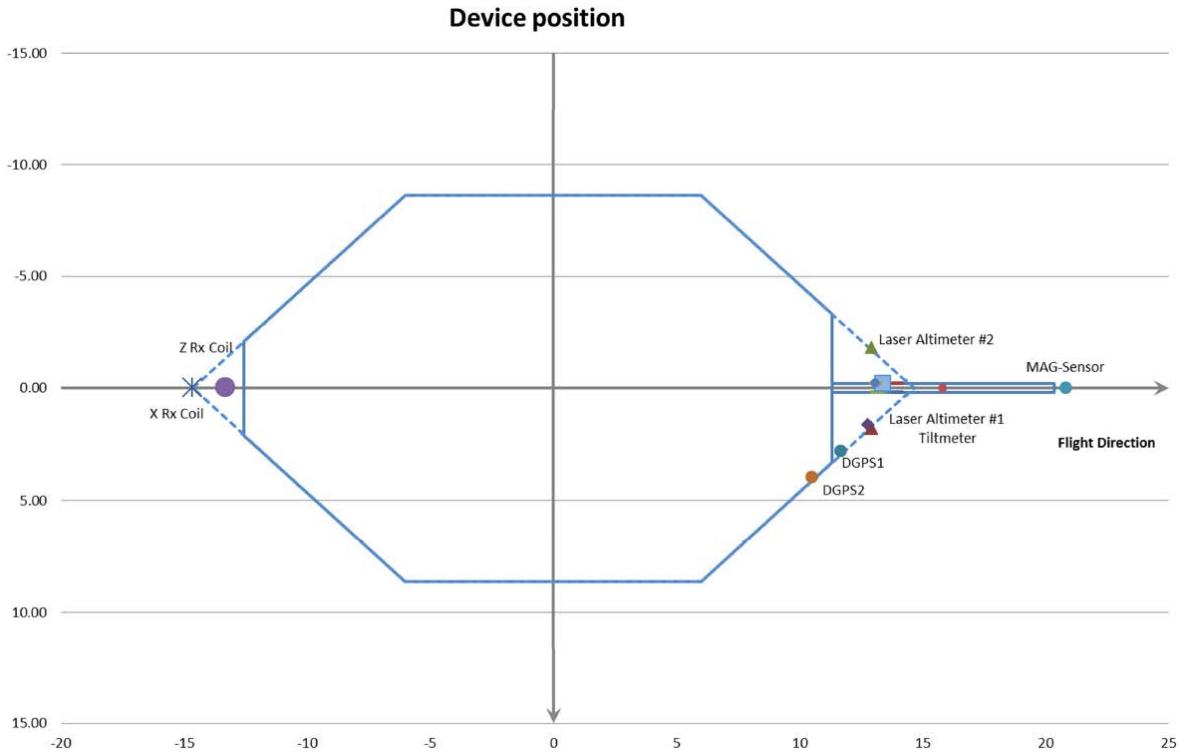

Figure 4-3: SkyTEM304M/312 frame, including instrumentation locations and X and Y axes. Distances are in meters. Instrumentation locations listed in Table 4-1.

Figure 4-4: Photos of the SkyTEM304M/312 system in suspension beneath the helicopter.

For this project, the 304M was flown at an average speed of 56 mi/hr (90.8 kilometers/hr) at an average flight height of 44.5 m above land surface, using the sling-load cargo system of a Eurocopter AS350 helicopter. Figure 4-4 displays a couple of images of the 304M in operation.

Table 4-1: Positions of instruments on the SkyTEM304M/312 frame, using the center of the frame as the origin, in meters.

	DGPS 1	DGPS 2	Inclinometer 1	Inclinometer 2	Altimeter 1	Altimeter 2	Magnetic Sensor	Rx Coil
X	11.68	10.51	12.79	12.79	12.94	12.94	20.50	-13.25
Y	2.79	3.95	1.64	1.64	1.79	-1.79	0.00	0.00
Z	-0.16	-0.16	-0.12	-0.12	-0.12	-0.12	-.56	-2.00

Table 4-2: Positions of corners of the SkyTEM304M/312 transmitter coil, using the center of the frame as the origin, in meters.

Tx Corners	1	2	3	4	5	6	7	8
X	-12.55	-6.03	6.03	11.34	11.34	6.03	-6.03	-12.55
Y	-2.10	-8.63	-8.63	-3.31	3.31	8.63	8.63	2.10

Table 4-3: Location of DGPS and magnetic field base station instruments at the Orland, CA airport.

Instrument	Easting (m)	Northing (m)	UTM Zone
Magnetometer Base Station	573399	4396864	10 N
DGPS Base Station	573367	4396876	10 N

4.4 Data Acquisition

All SkyTEM systems are calibrated to a ground test site in Lyngby, Denmark prior to being used for production work (HydroGeophysics Group Aarhus University, 2010; HydroGeophysics Group Aarhus University, 2011; Foged et al., 2013). The calibration process involves acquiring data with the system hovering at different altitudes, from 16 ft to 164 ft (5 m to 50 m), over the Lyngby site. Acquired data are processed and a scale factor (time and amplitude) is applied so that the inversion process produces the model that approximates the known geology at Lyngby.

For these surveys, installation of the navigational instruments in the helicopter and assembly of the SkyTEM312 system (which was flown first) commenced prior to the beginning of the project in the San Joaquin Valley. The helicopter and the SkyTEM312 system were located at the Haigh Field at the Orland airport. Calibration test flights were flown to ensure that the equipment was operating within technical specifications. Survey set-up procedures included measurement of the transmitter waveforms, verification that the receiver was properly located in a null position, and verification that all positioning instruments were functioning properly. A high-altitude test, used to verify system performance, was flown prior to the beginning of the survey's production flights. In the field, quality control of the operational parameters for the EM and magnetic field sensors including current levels, positioning sensor dropouts, acquisition speed, and system orientation were conducted with proprietary SkyTEM software following each flight. After the 312 flights were completed, the SkyTEM crew disassembled the 312 and installed and set up the 304M instrumentation and performed similar system checks prior to conducting data acquisition

Approximately 361 line-miles (585 line-kilometers) were acquired by the SkyTEM312 over the Butte-Glenn counties AEM survey area west of Chico on November 30 through December 2, 2018. Then on December 3, 2018, approximately 138 line-miles (224 line-kilometers) were acquired by the SkyTEM304M southeast of Chico. The Haigh Field at the Orland airport was used for landing and refueling between production flights. A data acquisition map is presented in Figure 4-5 with the flight lines grouped by acquisition date and Table 4-4 lists the acquisition dates, flights, and amount acquired on each day.

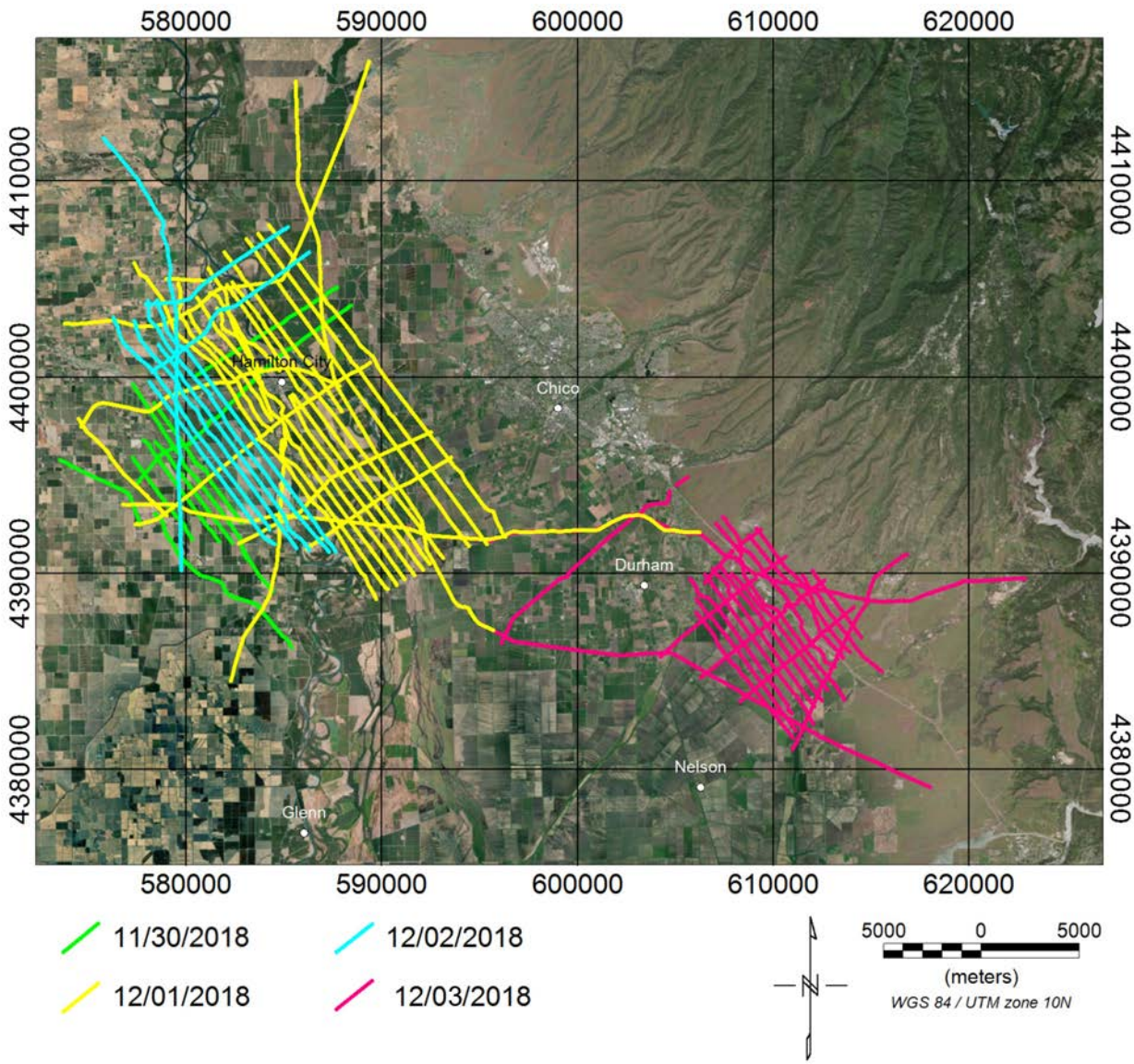

Figure 4-5: Butte AEM flight lines grouped by acquisition date.

Table 4-4. Butte AEM flight line production by flight.

Date	Flight	System	Distance (km)
30-November-18	1	312	26.7
30-November-18	4	312	53.2
1-December-18	1	312	199.9
1-December -18	2	312	179.2
2-December -18	1	312	125.5
3-December -18	2	304M	158.3
3-December-18	3	304M	65.9
Total	**7**		**808.7**

4.4.1 System Flight Parameters

4.4.1.1 Flight Height

The system height was specified at 30-35 meters AGL; however, due to safety and other judgments by the pilot the flight heights will deviate. The goal is to maintain a height as low as possible in the window from 25 to 50 m AGL. In the Butte AEM data set the average height was 44.5 m AGL with a minimum of 22.3 m AGL and a maximum of 236.4 m AGL. The maximum flight heights were encountered over large powerlines. Those data contaminated by the power lines will be removed from the dataset before inversion due to EM coupling and will not impact the final product. A map of the flight height throughout the survey area is presented in Figure 4-6.

4.4.1.2 Flight Speed

Speed determines the distance between ground samples. However, there is a tradeoff between the cost of the survey and the speed of the system related to the foot print of the system. In many surveys, the specified speed is 100 km/hr. The critical factor in the flight speed is to maintain a speed where the system is as level as possible. This may require that the pilot speed up in the downwind direction or slowdown in the up-wind direction. The pilot uses the readout display of the system tilt angles to help maintain this speed. A map of the flight speeds of the Butte AEM survey is presented in Figure 4-7. The average ground speed of the survey was 90.8 km/hr with a minimum ground speed of 0.3 km/hr and a maximum ground speed of 115.3 km/hr.

4.4.1.3 System Angles

System angles are critical to ensure that quality data are submitted to the inversion. The system's Tx initial current at time-off of 0.0 sec is the image of the size of the loop on the surface. If the system is tilted, that image will be less than the original size of the TX. Inversion algorithms can account for ±10 degrees of angle in calculating the effective Tx size. To this end, it is important to keep the Tx frame within ±10 degrees. The position of the Rx is also impacted by the angle of the system and any deviation from perpendicular has an impact by including off perpendicular components. As noted, algorithms can account for ±10 degrees in the Rx angle. Both the X-Angle (in the direction of flight) and the Y-Angle (perpendicular to the direction of flight) were checked during the Butte AEM survey. When the system is

flown over obstacles or while turning around at the end of a line, the angles can be higher than the ±10 degrees. These flight line edges are typically cut out of the survey data set prior to inversion. Figure 4-8 and Figure 4-9 are plots of the X-angle and the Y-angle tilts, respectively. During the Butte AEM survey, both angles were within acceptable ranges. The X-angle averaged approximately -1.5 degrees with a minimum of -29.8 degrees and a maximum of 29.40 degrees. The Y-angle tilt averaged about 0.63 degrees with a minimum of –18.9 degrees and a maximum of 25.9 degrees. Maximum and minimum tilts occurred around infrastructure and will not impact the data as much of that area will be removed during the decoupling processing

4.4.1.4 Transmitter Current

The SkyTEM system utilizes a dual-moment system (High (HM) and Low (LM)) and two different Tx currents and waveforms. These waveforms are recorded before and after the survey to ensure that no changes have occurred during the survey. Figure 4-10 and Figure 4-11 are plots of the recorded low moment (LM) and the high moment (HM) Tx waveforms for the SkyTEM312 system, respectively. Figure 4-12 and Figure 4-13 are plots of the recorded low moment (LM) and the high moment (HM) Tx waveforms for the SkyTEM304M system, respectively. The LM Tx source is used to highlight the very near surface geology and the HM current source is used to get more electromagnetic power at depth to characterize the deeper geologic units

The current should be stable throughout the survey, but changes in the temperature can impact the resistance of the Tx wire and circuit by either increasing or lowering the peak current output. The peak current is recorded during acquisition of each sounding and is used to adjust the Tx waveform in the inversion. For the Butte AEM survey the 304M LM mean current was 9.07 amp with a minimum current of 9.06 amp and a maximum current of 9.08 amp. For the 304M HM, the mean current was 111.79 amp with a minimum current of 111.19 amp and a maximum current of 112.86 amp. For the Butte AEM survey with the 312 system, the LM mean current was 5.95 amp with a minimum current of 5.94 amp and a maximum current of 5.97 amp. For the 304M HM, the mean current was 111.01 amp with a minimum current of 108.38 amp and a maximum current of 113.52 amp. All system moments show stability in the current and provided no problems in the inversions.

Note the difference in timing between the 304M and the 312. These differences affect the way in which the electromagnetic signal is transmitted into the subsurface by the different systems.

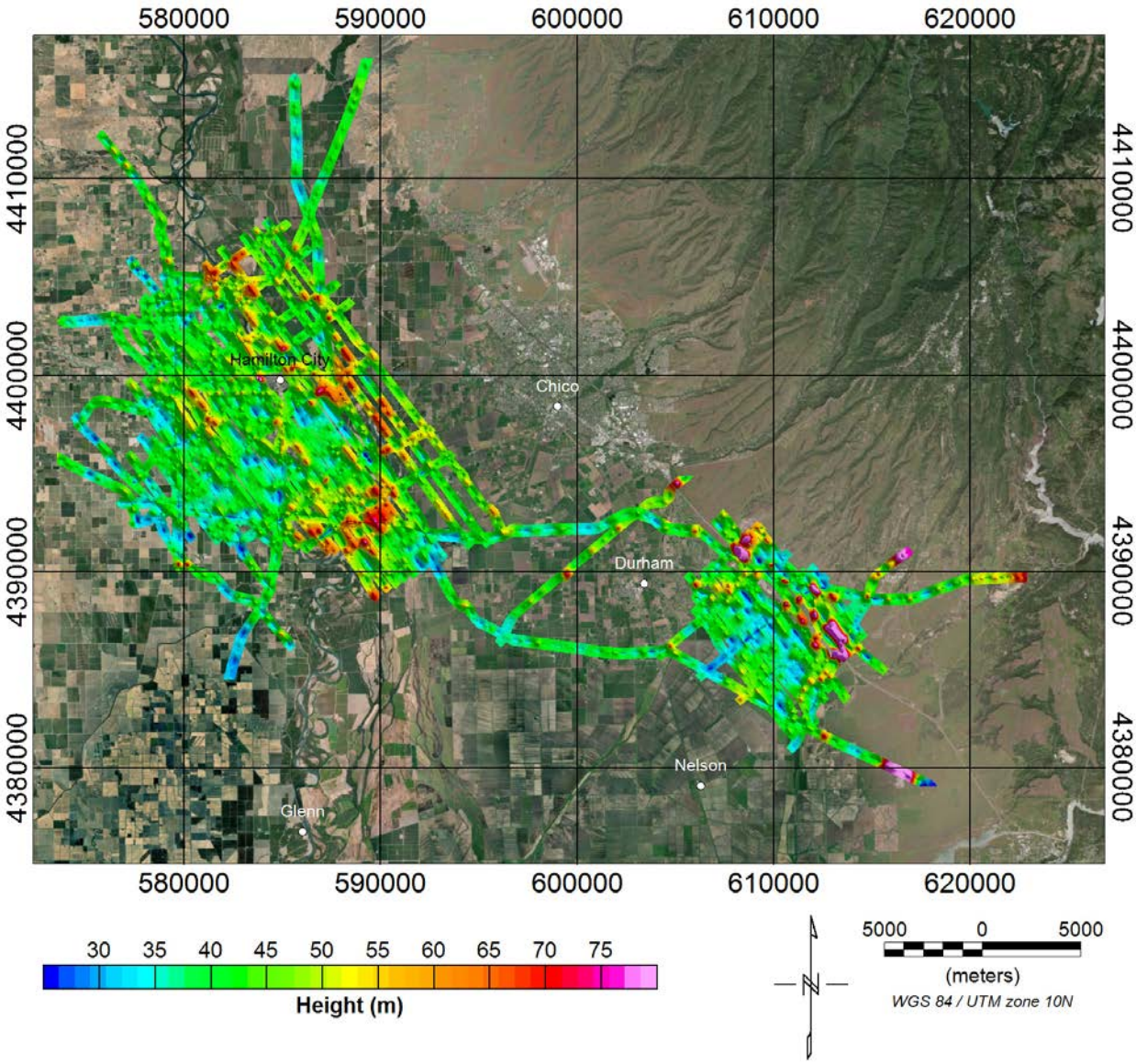

Figure 4-6. Map of the system height recorded during the Butte AEM survey.

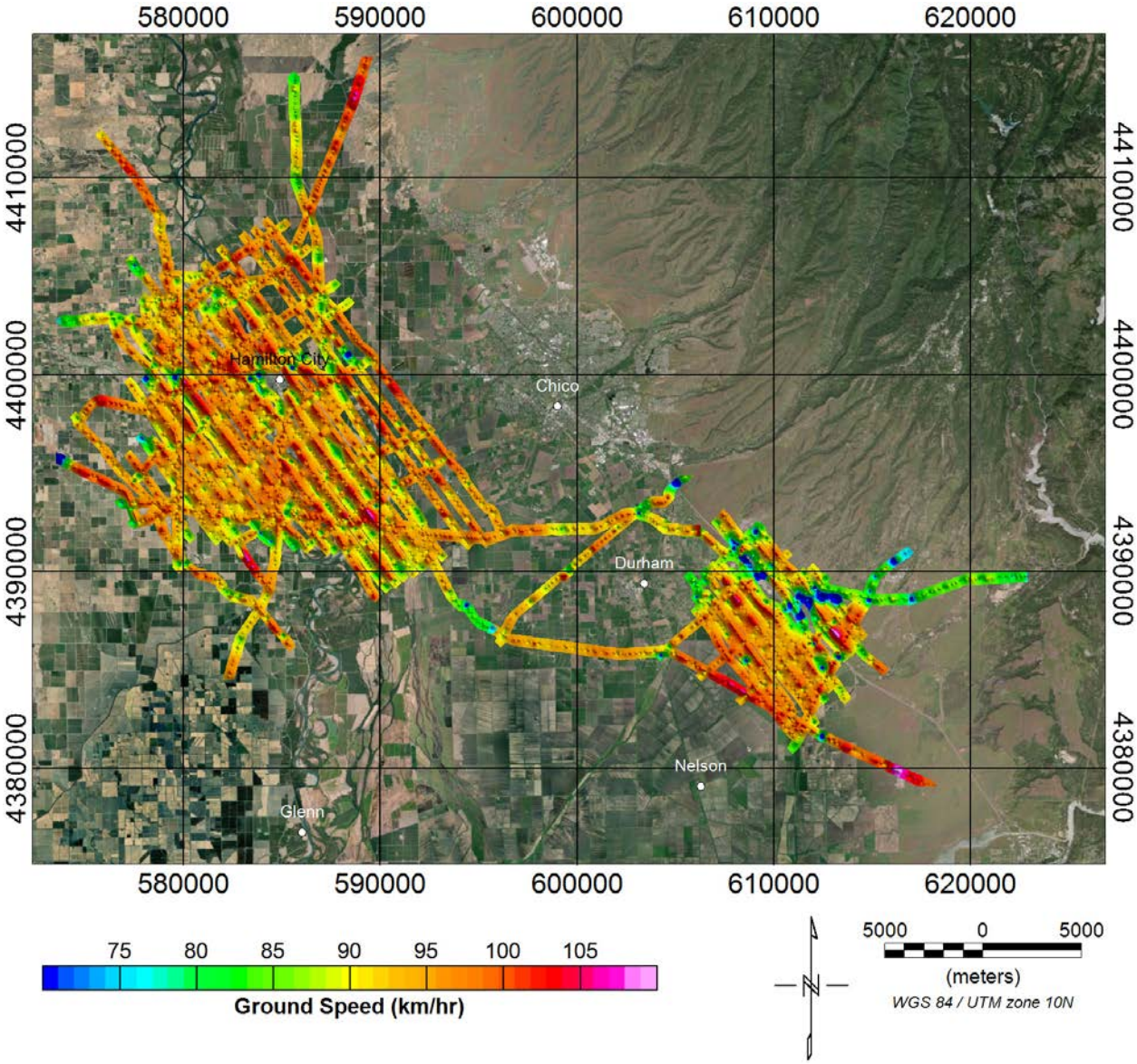

Figure 4-7. Map of the ground speed recorded during the Butte AEM survey.

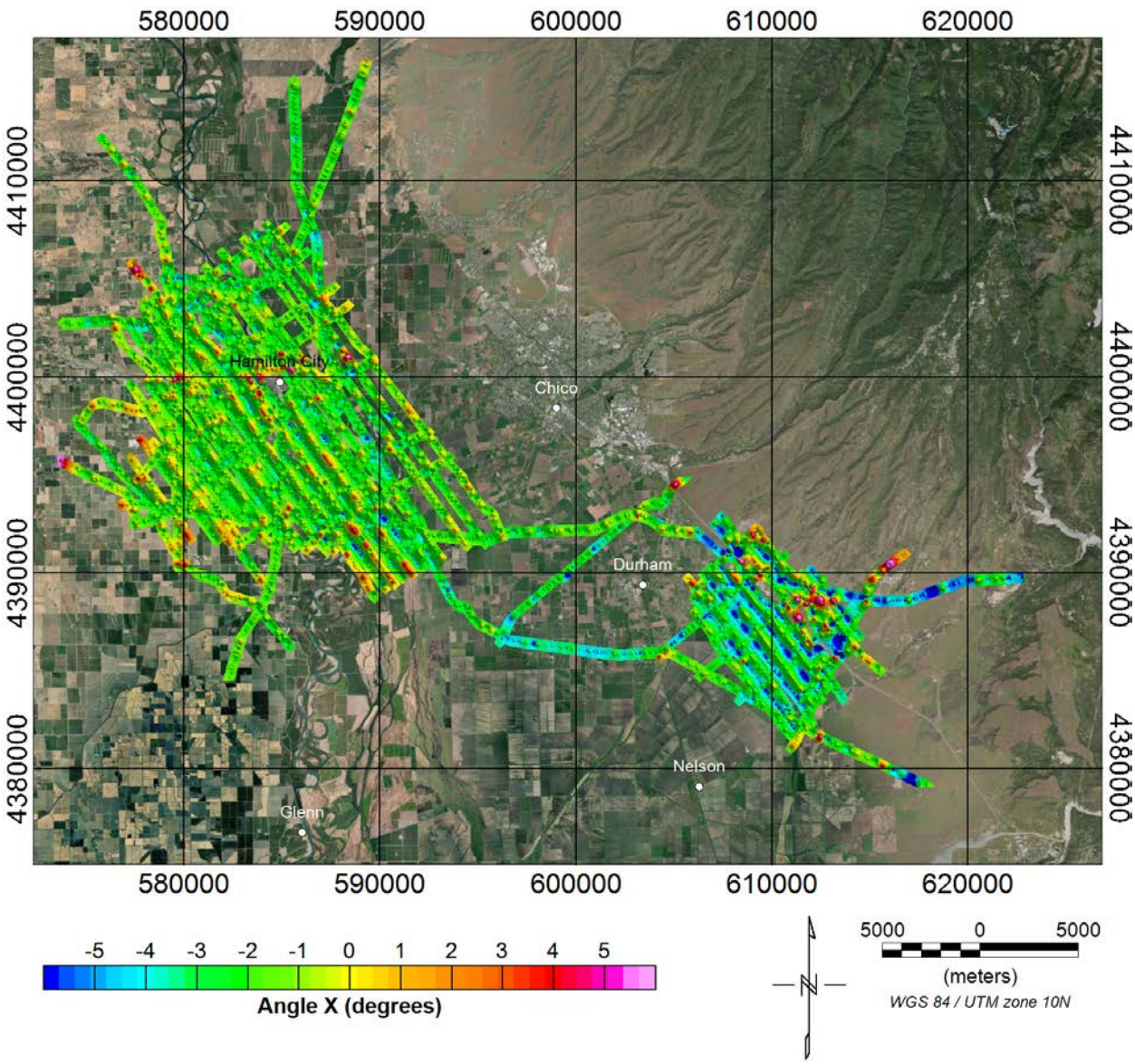

Figure 4-8. Map of the X-angle tilt recorded during the Butte AEM survey.

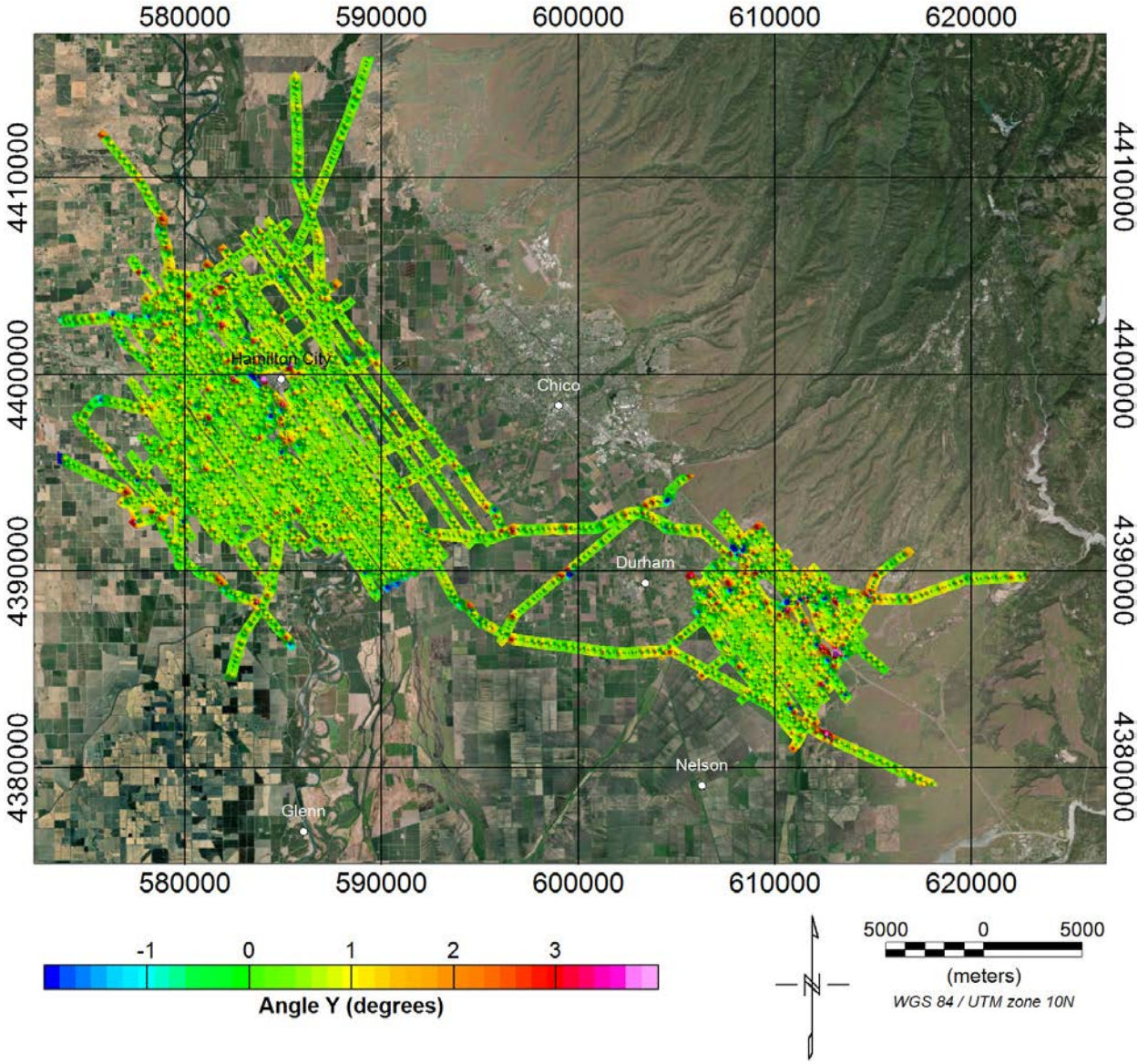

Figure 4-9. Map of the Y-angle tilt recorded during the Butte AEM survey.

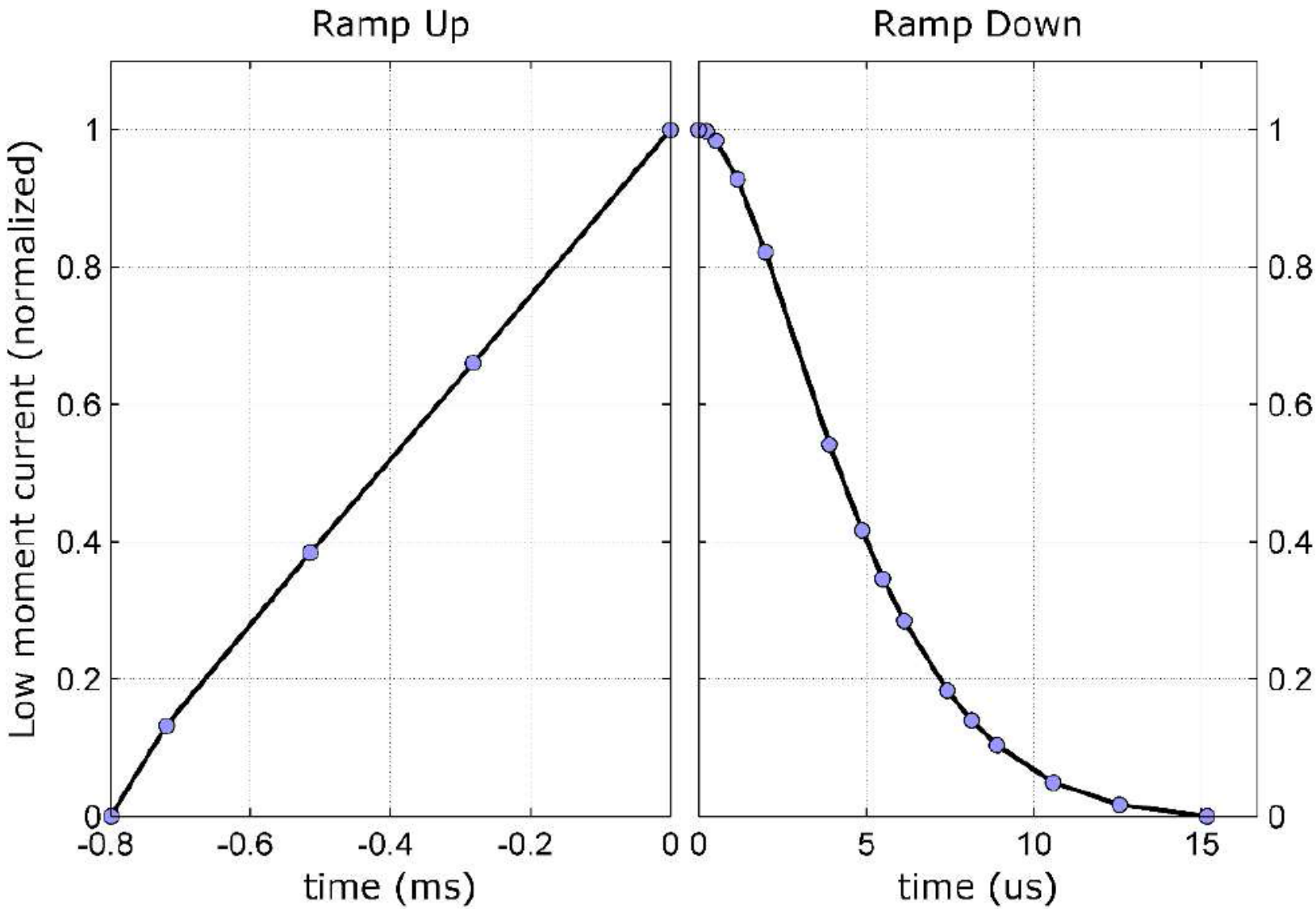

Figure 4-10. Plot of the 210 Hz LM waveform for the SkyTEM312 system recorded during the Butte AEM survey. Current ramp up is on the left and the ramp down to turn off is on the right. The current is normalized. Note the different x-axis scales between the left and right sides of the figure.

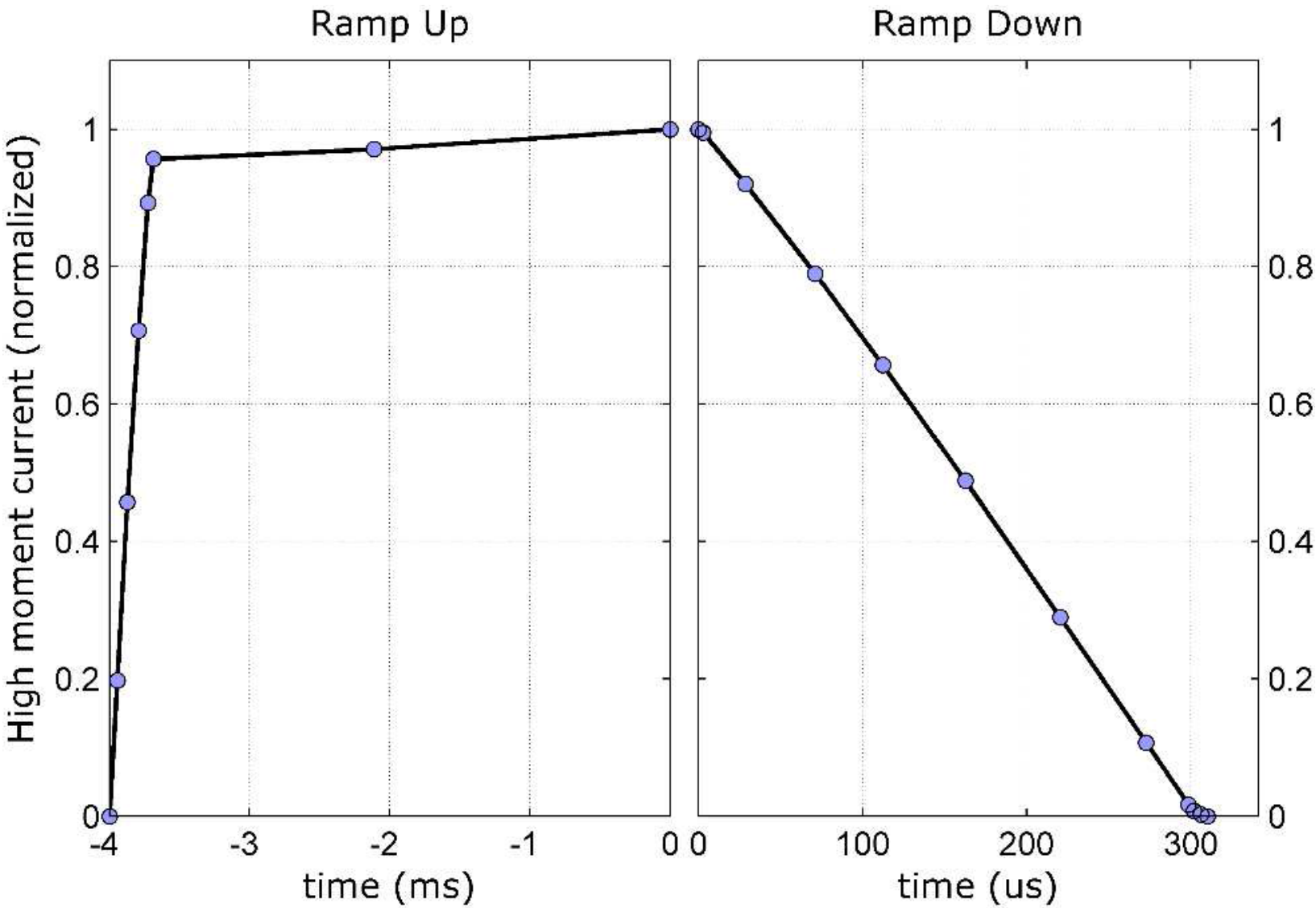

Figure 4-11. Plot of the 30 Hz HM waveform for the SkyTEM312 system recorded during the Butte AEM survey. Current ramp up is on the left and the ramp down to turn off is on the right. The current is normalized. Note the different x-axis scales between the left and right sides of the figure.

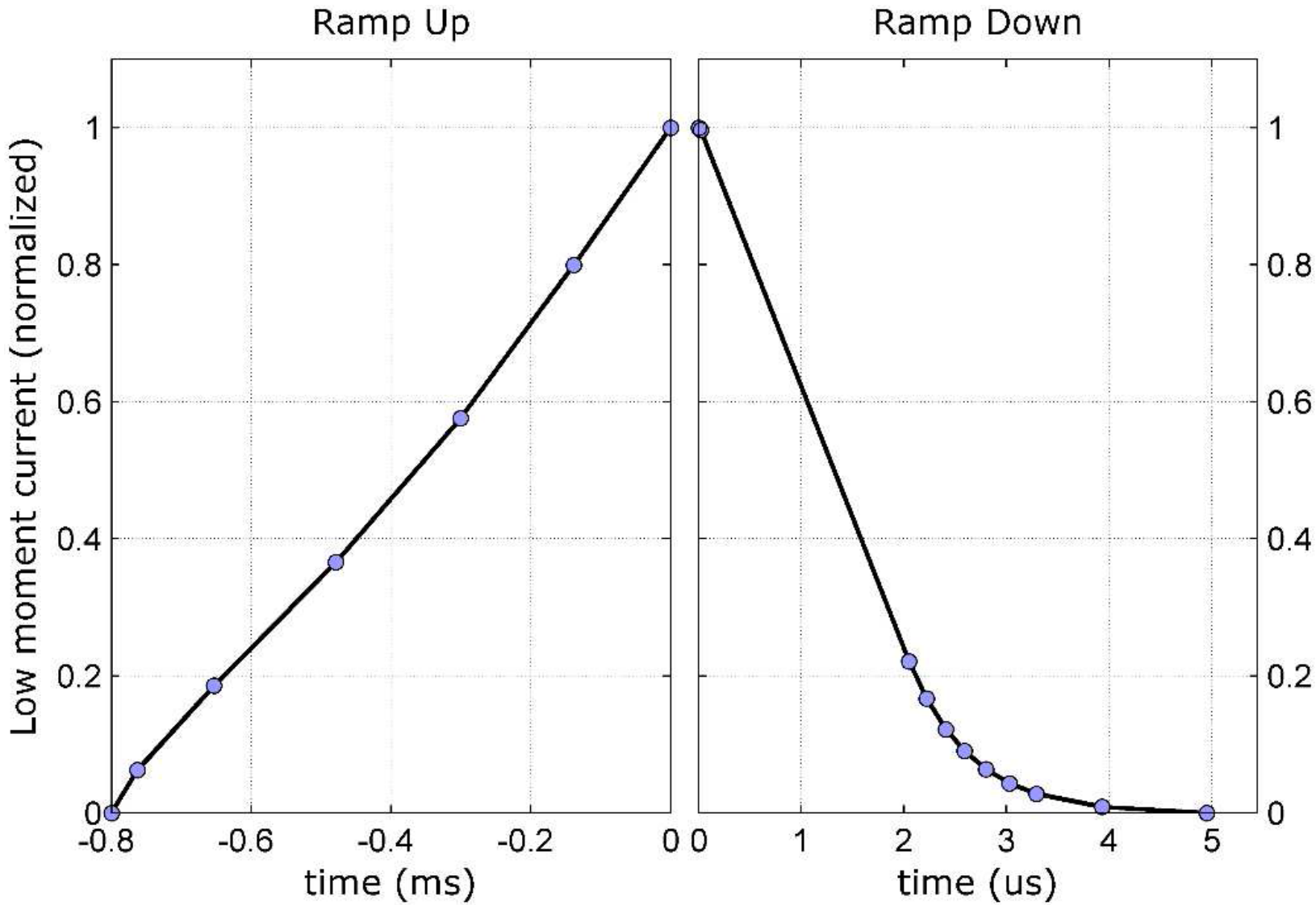

Figure 4-12. Plot of the 210 Hz LM waveform for the SkyTEM304M system recorded during the Butte AEM survey. Current ramp up is on the left and the ramp down to turn off is on the right. The current is normalized. Note the different x-axis scales between the left and right sides of the figure.

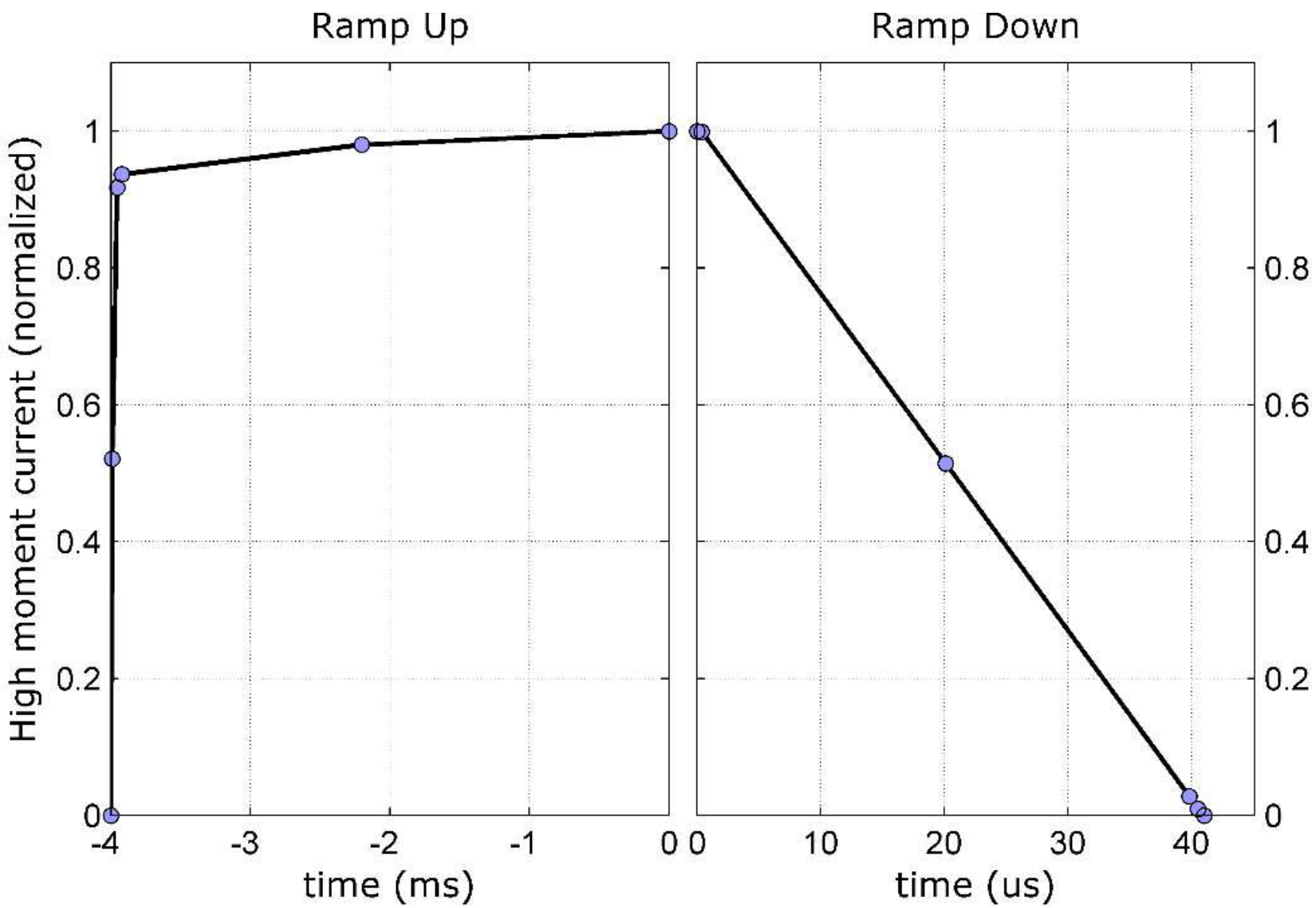

Figure 4-13. Plot of the 30 Hz HM waveform for the SkyTEM304M system recorded during the Butte AEM survey. Current ramp up is on the left and the ramp down to turn off is on the right. The current is normalized. Note the different x-axis scales between the left and right sides of the figure.

4.4.2 Primary Field Compensation

A standard SkyTEM data acquisition procedure involves review of acquired raw data by SkyTEM in Denmark for Primary Field Compensation (PFC) prior to continued data processing by AGF (Schamper et al., 2014). The primary field of the transmitter affects the recorded early time gates, which in the case of the Low Moment, are helpful in resolving the near surface resistivity structure of the ground. The Low Moment uses a saw tooth waveform which is calculated and then used in the PFC correction to correct the early time gates.

4.4.3 Automatic Processing

The AEM data collected by the 304M were processed using Aarhus Workbench version 5.8.3 (at Aarhus Geosoftware (https://www.aarhusgeosoftware.dk/workbench-overview)) described in HydroGeophysics Group, Aarhus University (2011).

Automatic processing algorithms provided within the Workbench program are initially applied to the AEM data. DGPS locations were filtered using a stepwise, second-order polynomial filter of nine seconds with a beat time of 0.5 seconds, based on flight acquisition parameters. The AEM data are corrected for tilt deviations from level and so filters were also applied to both of the tilt meter readings with a median filter of three seconds and an average filter of two seconds. The altitude data were corrected using a series of two polynomial filters. The lengths of both eighth-order polynomial filters were set to 15 seconds with shift lengths of six (6) seconds. The lower and upper thresholds were 1 and 100 meters, respectively.

Trapezoidal spatial averaging filters were next applied to the AEM data. The times used to define the trapezoidal filters for the Low Moment were $1.0x10^{-5}$ sec, $1.0x10^{-4}$ sec, and $1.0x10^{-3}$ sec with widths of 4, 7, and 18 seconds. The times used to define the trapezoid for the High Moment were $1.0x10^{-4}$ sec, $1.0x10^{-3}$ sec, and $1.0x10^{-2}$ sec with widths of 10, 20, and 36 seconds. The trapezoid sounding distance was set to 1.0 seconds and the left/right setting, which requires the trapezoid to be complete on both sides, was turned on. The spike factor and minimum number of gates were both set to 25 percent for both soundings. Lastly, the locations of the averaged soundings were synchronized between the two moments.

4.4.4 Manual Processing and Laterally-Constrained Inversions

After the implementation of the automatic filtering, the AEM data were manually examined using a sliding two-minute time window. The data were examined for possible electromagnetic coupling with surface and buried utilities and metal, as well as for late time-gate noise. Data affected by these were removed. Examples of locating areas of EM coupling with pipelines or power lines and recognizing and removing coupled AEM data in Aarhus Workbench are shown in Figure 4-14 and Figure 4-15, respectively. Examples of two inversions, one without EM coupling and the other with EM coupling, are shown in Figure 4-16. Areas were also cut out where the system height was flown greater than 200 feet above the ground surface which caused a decrease in the signal level.

The AEM data were then inverted using a Laterally-Constrained Inversion (LCI) algorithm (HydroGeophysics Group Aarhus University, 2011). The profile and depth slices were examined, and any remaining electromagnetic couplings were masked out of the data set.

After final processing, 109.3 line-miles (177 line-km) of 304M data were retained and 303 lines-miles (491 line-kilometers) of 312 data were retained for the final inversions for the Butte AEM survey area. Each set was inverted separately. This amounts to a data retention of 79% for the 304 and 84% for the 312 data sets. These high rates are the result of careful flight line planning and design.

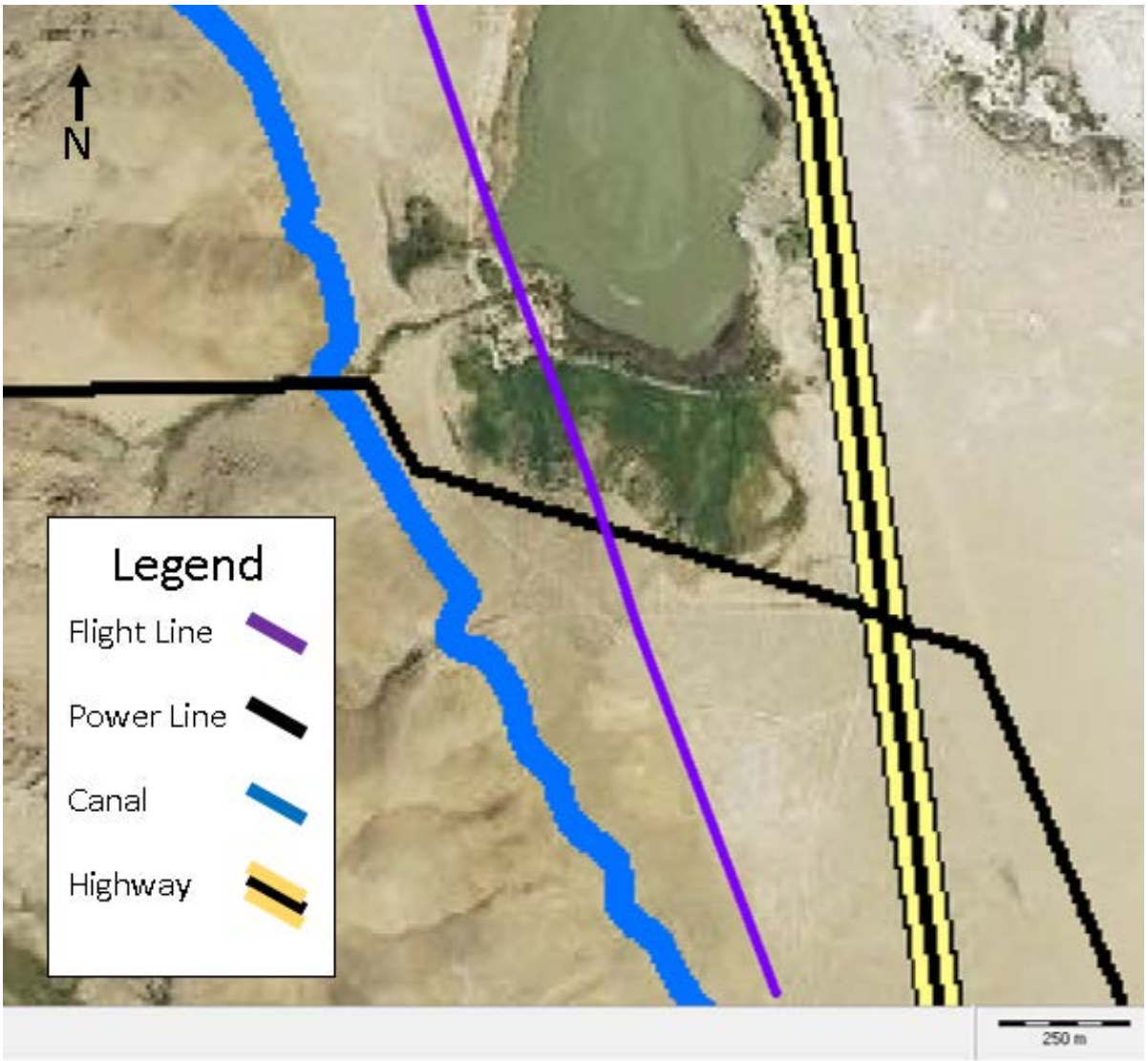

Figure 4-14. Example locations of electromagnetic coupling with pipelines or power lines.

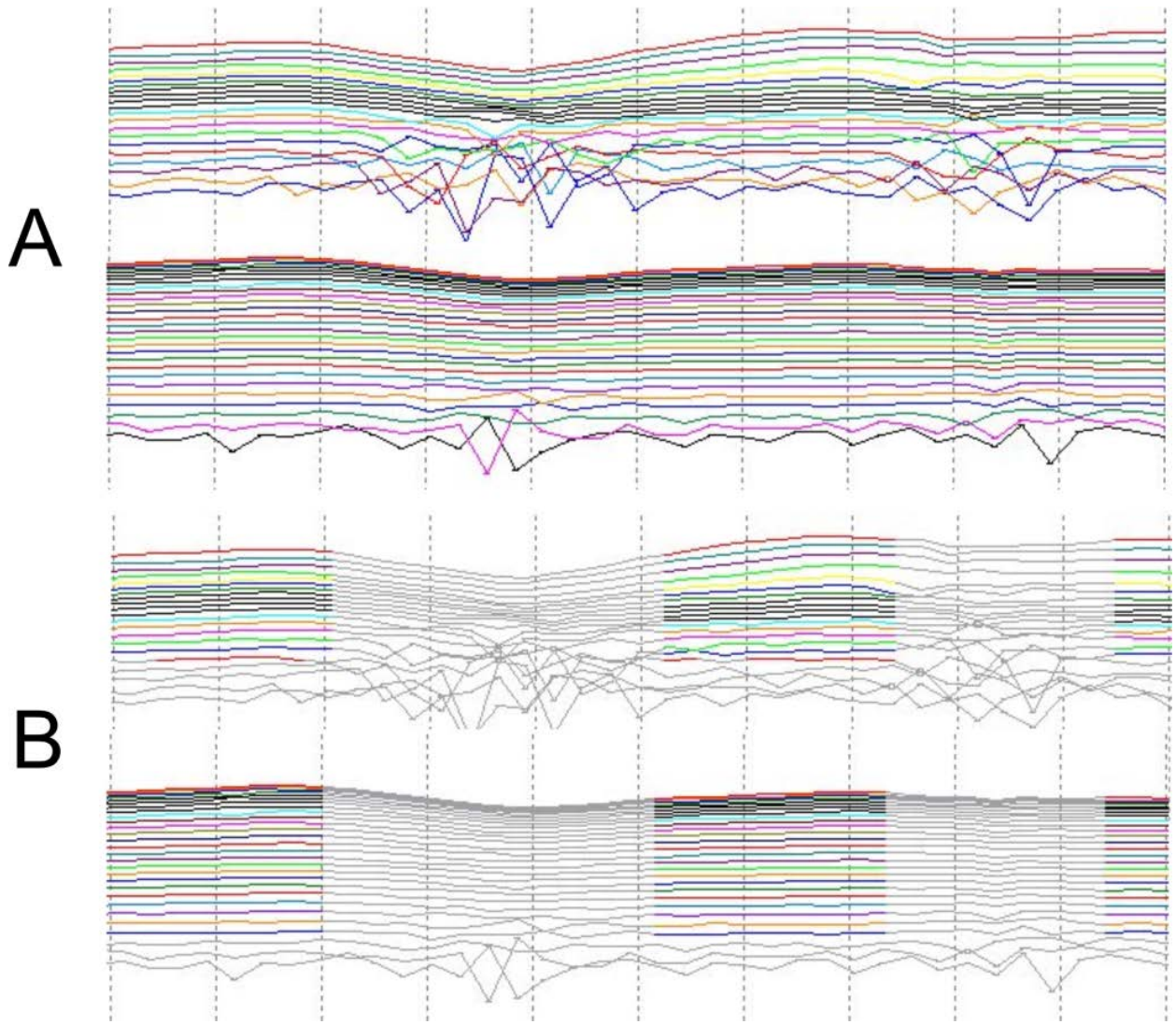

Figure 4-15. A) Example of AEM data affected by electromagnetic coupling in the Aarhus Workbench editor. The top group of lines is the unedited data with the Low Moment on top and the High Moment on the bottom. The bottom group shows the same data after editing.

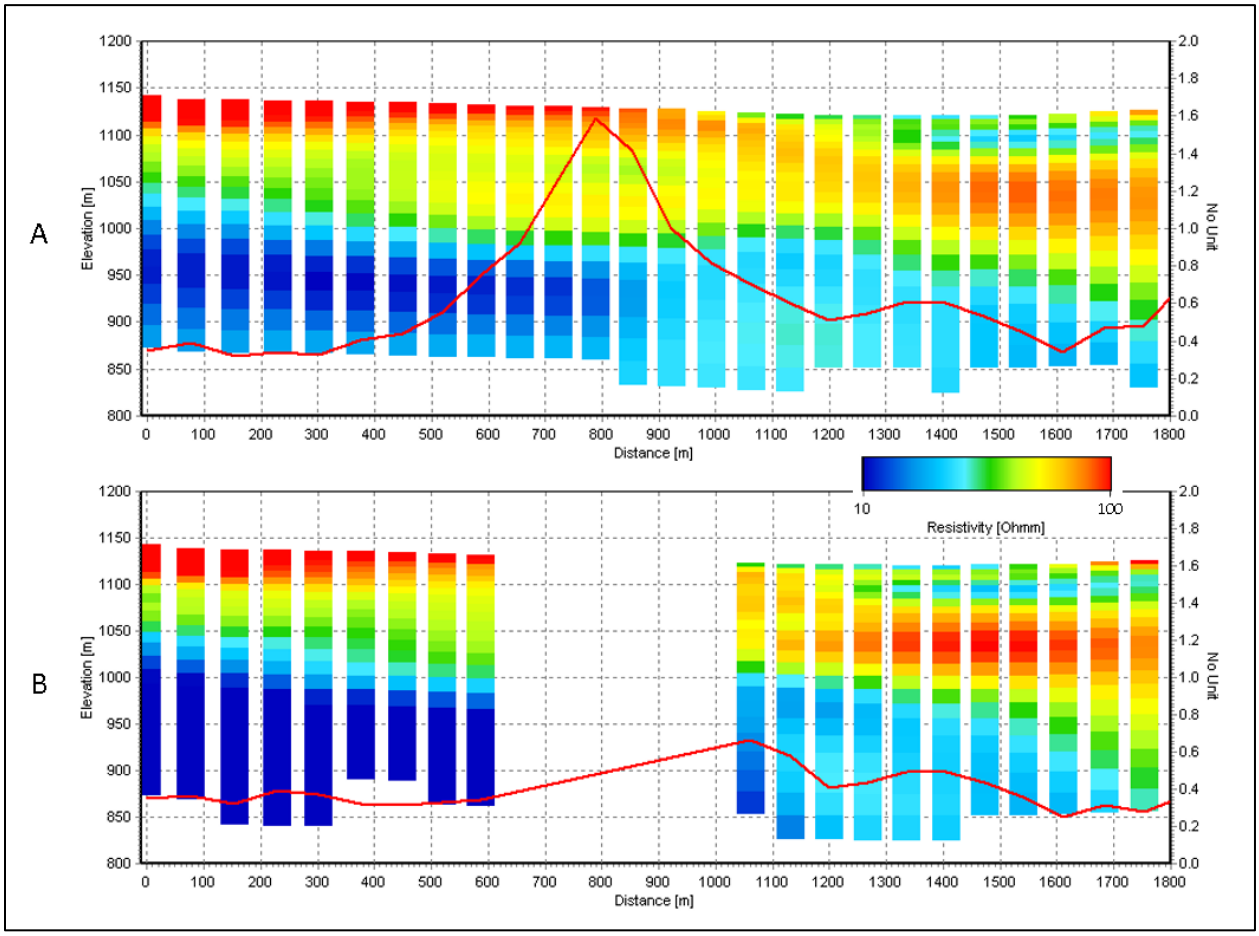

Figure 4-16. A) Example of Laterally-Constrained inversion results where AEM data affected by coupling with pipelines and power lines were not removed. B) Inversion results where AEM data affected by coupling were removed.

4.4.5 Power Line Noise Intensity (PLNI)

The Power Line Noise Intensity (PLNI) channel assists in identifying possible sources of noise from power lines. Pipelines, unless they are cathodically-protected, are not mapped by the PLNI. The PLNI is produced by performing a spectral frequency content analysis on the raw received Z-component SkyTEM data. For every Low Moment data block, a Fourier Transform (FT) is performed on the latest usable time gate data. The FT is evaluated at the local power line transmission frequency (60 Hz) yielding the amplitude spectral density of the local power line noise. The PLNI data for the Butte AEM survey are presented in Figure 4-17. The Butte AEM-flight lines with blue colors representing data retained for inversion and red lines representing 304M data removed and orange lines representing 312 data remove due to infrastructure and late time noise are presented in Figure 4-18.

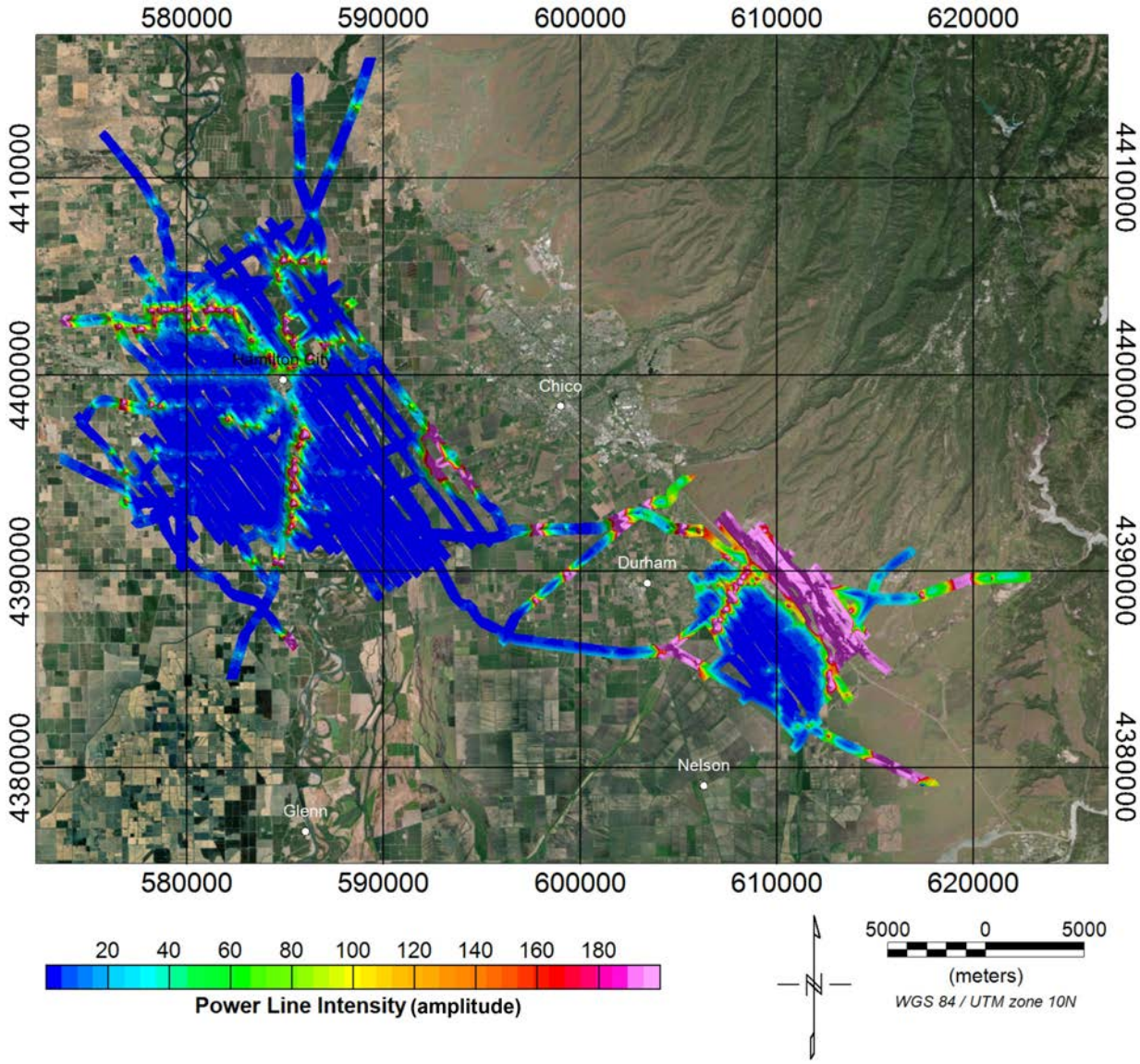

Figure 4-17. Power Line Noise Intensity (PLNI) map of the Butte AEM project area.

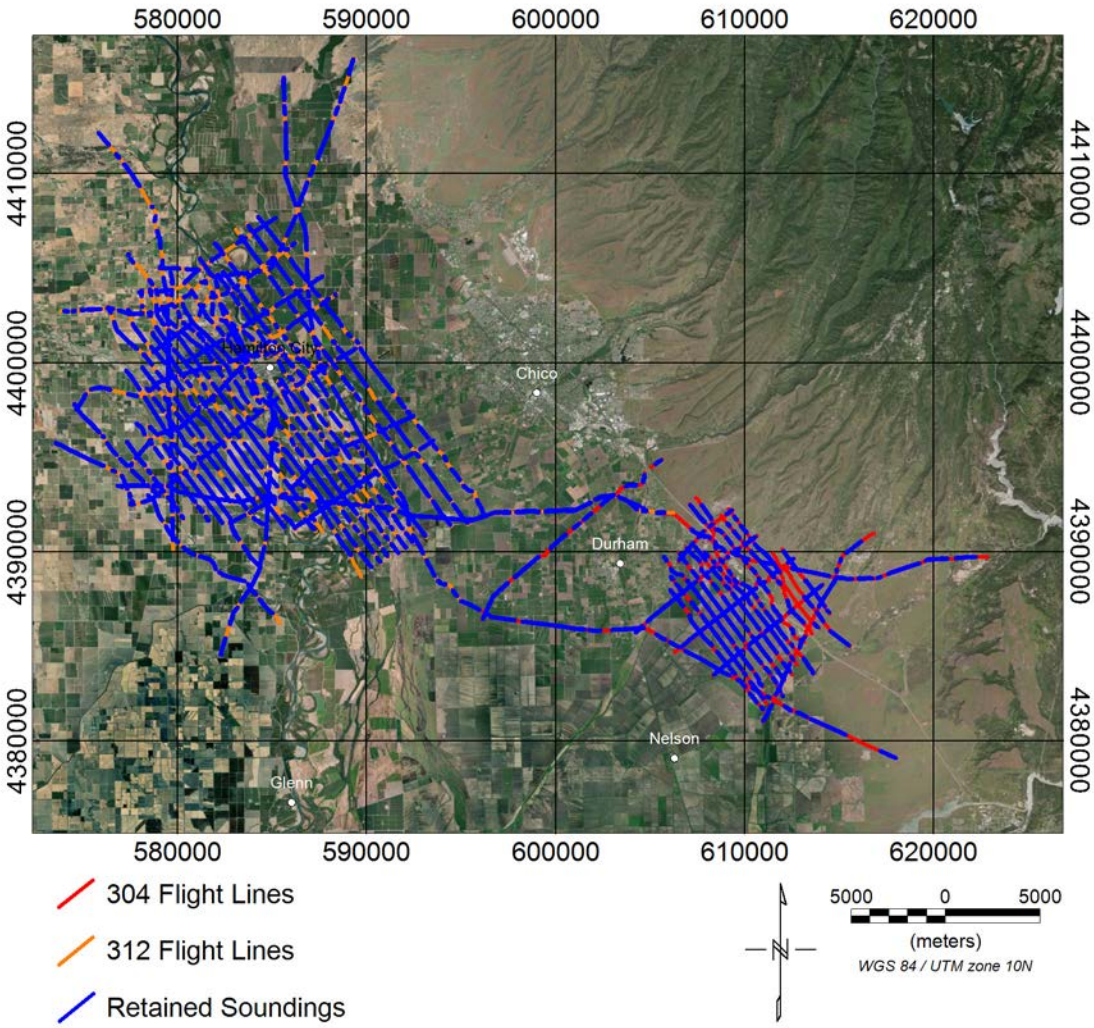

Figure 4-18. Locations of inverted data (blue lines) along the AEM flight lines (red (304M) and orange (312) lines) in the Butte AEM survey area. Where blue lines are not present indicates decoupled (removed) data. Google Earth kmz's of the inverted data locations as well as the flight lines are included in Appendix 3\KMZ.

4.4.6 Magnetic Field Data

As discussed above, the SkyTEM 304M and 312 systems include a Total Field magnetometer whose location is listed in Table 4-1. The magnetic Total Field data can yield information about infrastructure as well as geology. Figure 4-19 shows the residual magnetic Total Field intensity data for the Butte AEM survey area after correcting for diurnal drift and removing the International Geomagnetic Reference Field (IGRF). This data is also used in decoupling efforts.

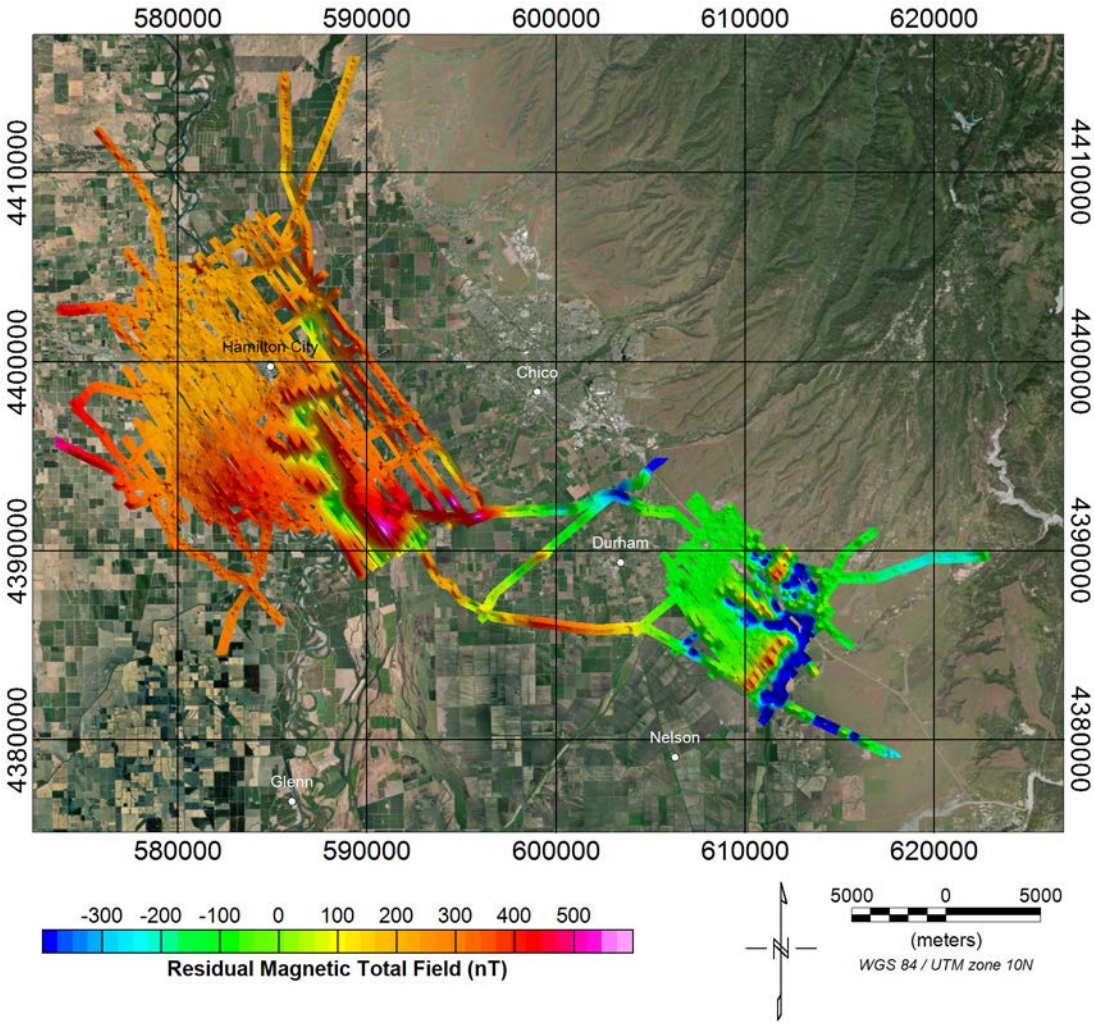

Figure 4-19. Residual magnetic Total Field intensity data for the Butte AEM survey area corrected for diurnal drift, with the International Geomagnetic Reference Field (IGRF) removed.

4.5 Spatially-Constrained Inversion

Following the initial decoupling and LCI analysis, Spatially-Constrained Inversions (SCI) were performed. SCI's use EM data along, and across, flight lines within a user-specified distance criteria (Viezzoli et al., 2008).

The Butte AEM data were inverted using SCI smooth models with 40 layers, each with a starting resistivity of 10 Ohm-m (equivalent to a 10 ohm-m halfspace). The thicknesses of the inversion models for the 304M and the 312 were different because of the different sensing character of the two systems. While the 312 images deeper than the 304 (and needs deeper and thicker layers), the 304M is more sensitive to the near-surface (and so needs finer layering at the surface). Also, the thicknesses of the layers increase with depth as the resolution of the technique decreases (an example of a 30-layer model is presented in Figure 4-20). The thicknesses of the first layer of the 304M models were about 3 ft (1 m) (Table 4-5) with the thicknesses of the consecutive layers increasing by a factor of about 1.1. The thicknesses of the first layer of the 312 models (Table 4-6) were about 10 ft (3 m) with the thicknesses of the consecutive layers increasing by a factor of about 1.07. The depths to the bottoms of the 39th layers for the 304M were set to 1,229 ft, with maximum thicknesses up to about 112 ft. The depths to the bottoms of the 39th layers for the 312 were set to 1,804 ft, with maximum thicknesses up to about 126 ft. The spatial reference distance, ***s***, for the constraints were set to 328 ft (100 m) with a power law fall-off of 0.75. The vertical and lateral constraints, ***ResVerSTD*** and ***ResLatStD***, were set to 2.4 and 1.4, respectively, for all layers.

It is important to note that the SCI's for the 304M used much earlier LM vertical (Z) receiver time gates than for the 312. The 304M used LM Z-time gates 3,4,6-26 and the 312 HM used LM time gates of 9-26. The 304M LM used the system response analysis for the three earliest time gates (3, 4, and 6). 304M LM Z-receiver gate 5 was deemed to be too noisy and adversely affected the inversion response in preliminary SCI's.

In addition to the recovered resistivity models, the SCI's also produce data-model residual error values (single sounding error residuals) and Depth of Investigation (DOI) estimates. The data residuals compare the measured data with the response of the individual inverted models (Christensen et al., 2009; SkyTEM Airborne Surveys Worldwide, 2012). The DOI provides a general estimate of the depth to which the AEM data are sensitive to changes in the resistivity distribution at depth (Christiansen and Auken, 2012). Two DOI's are calculated: an "Upper" DOI at a cumulative sensitivity of 1.2 and a "Lower" DOI set at a cumulative sensitivity of 0.6. Examination of the SCI results indicated that a much lower cumulative sensitivity, maybe 0.1 to 0.2, would still be sufficient to delineate the Butte AEM DOI. A more detailed discussion on the DOI can be found in Asch et al. (2015).

Table 4-5: Thickness and depth to bottom for each layer in the Spatially Constrained Inversion (SCI) AEM earth models for the SkyTEM304M. The thickness of the model layers increase with depth as the resolution of the AEM technique decreases.

Layer	Depth to Bottom (ft)	Thickness (ft)	Layer	Depth to Bottom (ft)	Thickness (ft)
1	3.3	3.3	21	203.1	21.0
2	6.9	3.6	22	226.0	23.0
3	10.8	3.9	23	251.3	25.3
4	15.1	4.3	24	279.1	27.9
5	20.0	4.9	25	309.7	30.5
6	25.3	5.2	26	343.1	33.5
7	30.9	5.6	27	379.8	36.7
8	37.1	6.2	28	420.2	40.3
9	44.0	6.9	29	464.5	44.3
10	51.5	7.5	30	513.0	48.5
11	59.7	8.2	31	566.5	53.5
12	68.9	9.2	32	624.9	58.4
13	79.1	10.2	33	689.1	64.3
14	89.9	10.8	34	759.7	70.5
15	102.0	12.1	35	837.1	77.4
16	115.1	13.1	36	922.0	85.0
17	129.6	14.4	37	1015.2	93.2
18	145.7	16.1	38	1117.5	102.3
19	163.0	17.4	39	1229.7	112.2
20	182.1	19.0			

Table 4-6: Thickness and depth to bottom for each layer in the Spatially Constrained Inversion (SCI) AEM earth models for the SkyTEM312. The thickness of the model layers increase with depth as the resolution of the AEM technique decreases.

Layer	Depth to Bottom (ft)	Thickness (ft)	Layer	Depth to Bottom (ft)	Thickness (ft)
1	9.8	9.8	21	439.2	37.7
2	20.3	10.5	22	479.5	40.3
3	31.4	11.2	23	522.8	43.3
4	43.6	12.1	24	569.0	46.2
5	56.4	12.8	25	618.2	49.2
6	70.2	13.8	26	671.0	52.8
7	84.9	14.8	27	727.5	56.4
8	100.7	15.7	28	787.8	60.4
9	117.4	16.7	29	852.4	64.6
10	135.4	18.0	30	921.6	69.2
11	154.8	19.4	31	995.4	73.8
12	175.4	20.7	32	1074.5	79.0
13	197.4	22.0	33	1159.1	84.6
14	221.0	23.6	34	1249.3	90.2
15	246.3	25.3	35	1346.1	96.8
16	273.2	26.9	36	1449.4	103.3
17	302.0	28.9	37	1559.9	110.5
18	332.9	30.8	38	1678.0	118.1
19	366.0	33.1	39	1804.3	126.3
20	401.4	35.4			

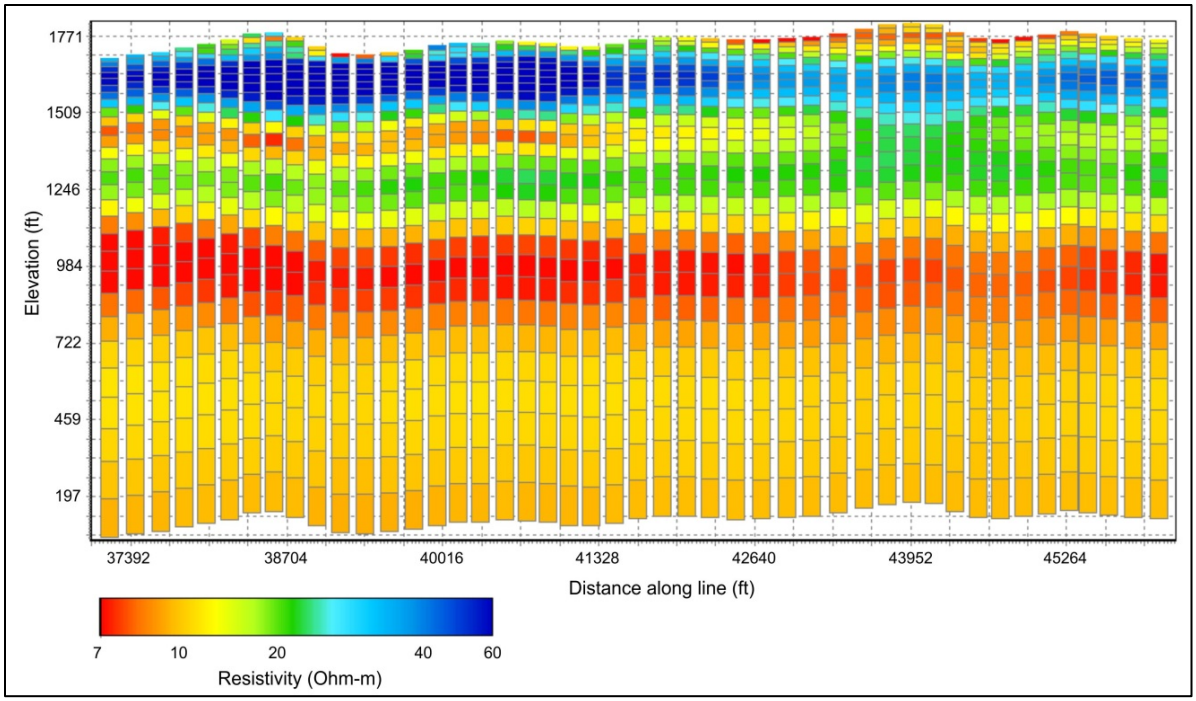

Figure 4-20. An example of an AEM profile illustrating increasing model layer thicknesses with depth. This is a 30-layer model.

Figure 4-21 presents a histogram of the Butte 304M SCI inversion data/model residuals and Figure 4-22 presents the histogram of the Butte 312 SCI inversion data/model residuals. A map of data residuals for the Butte AEM study area is presented for the 304M in Figure 4-23 and in Figure 4-24 for the 312 SCI inversion results.

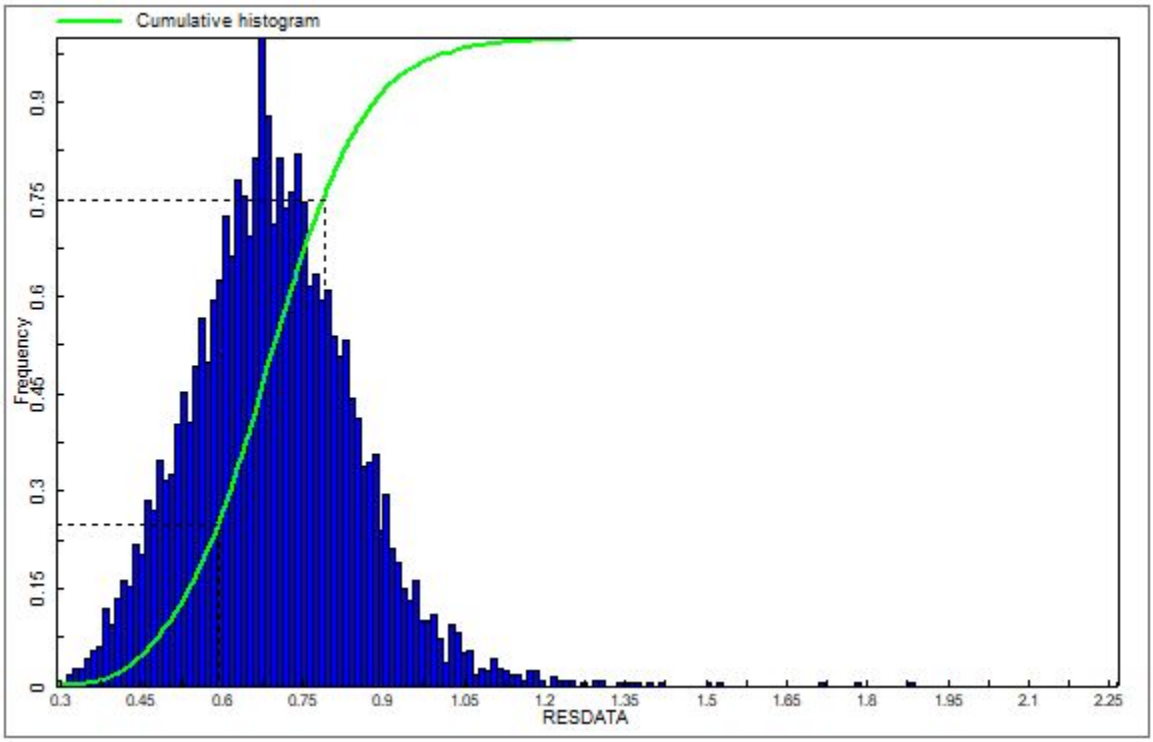

Figure 4-21. Data/model residual histogram for the Butte 304M SCI inversion results.

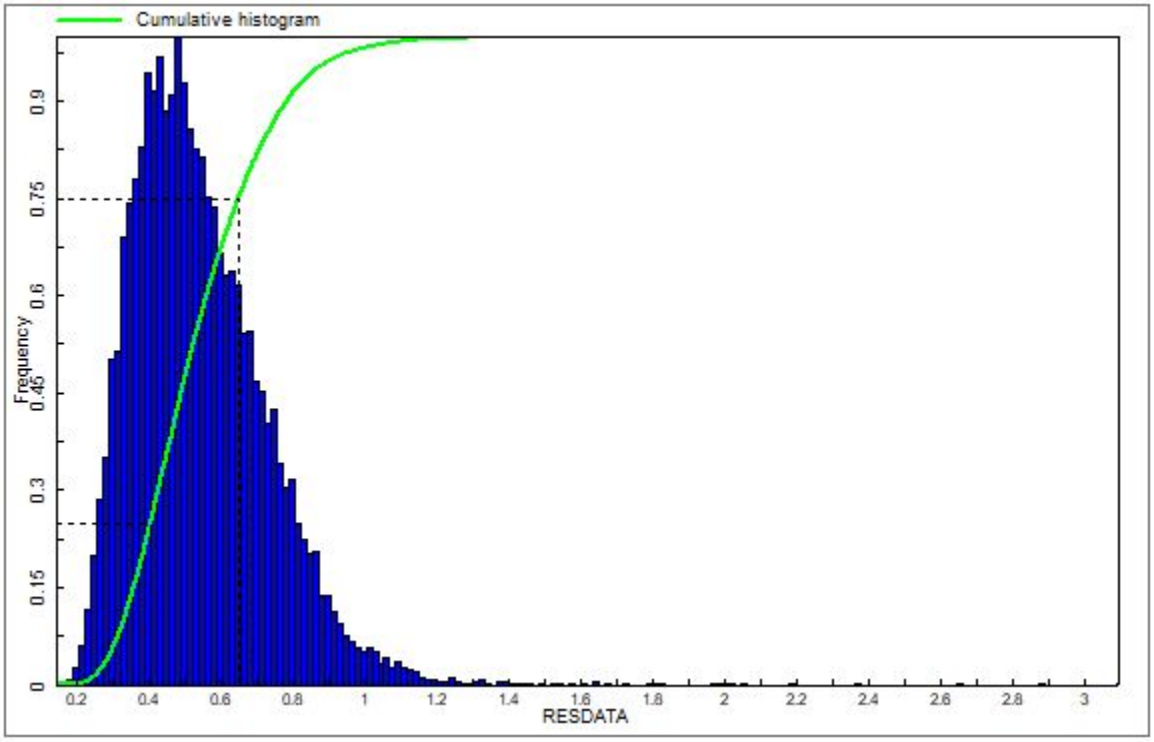

Figure 4-22. Data/model residual histogram for the Butte 312 SCI inversion results.

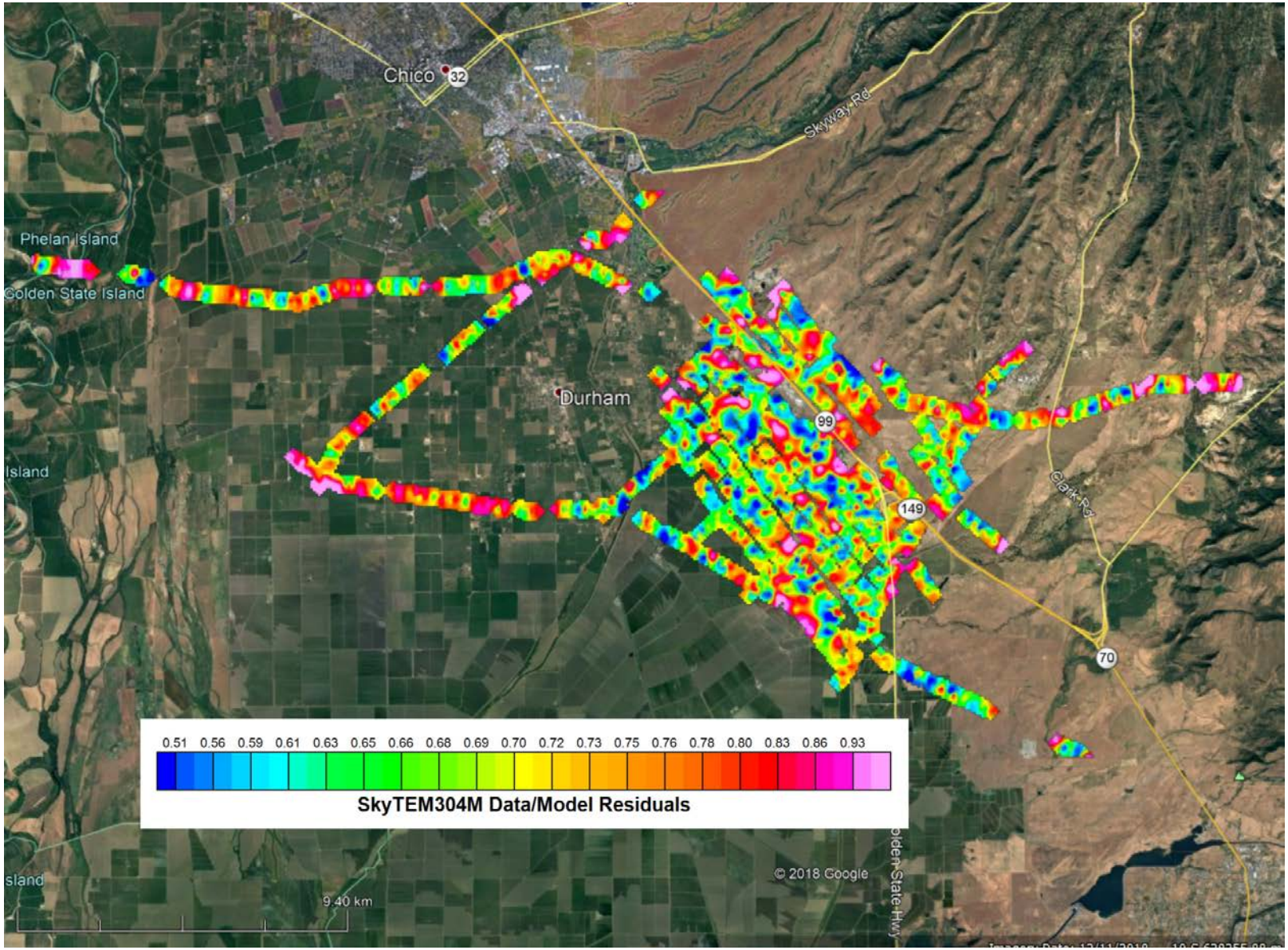

Figure 4-23. Map of data residuals for the Butte 304M SCI inversion results.

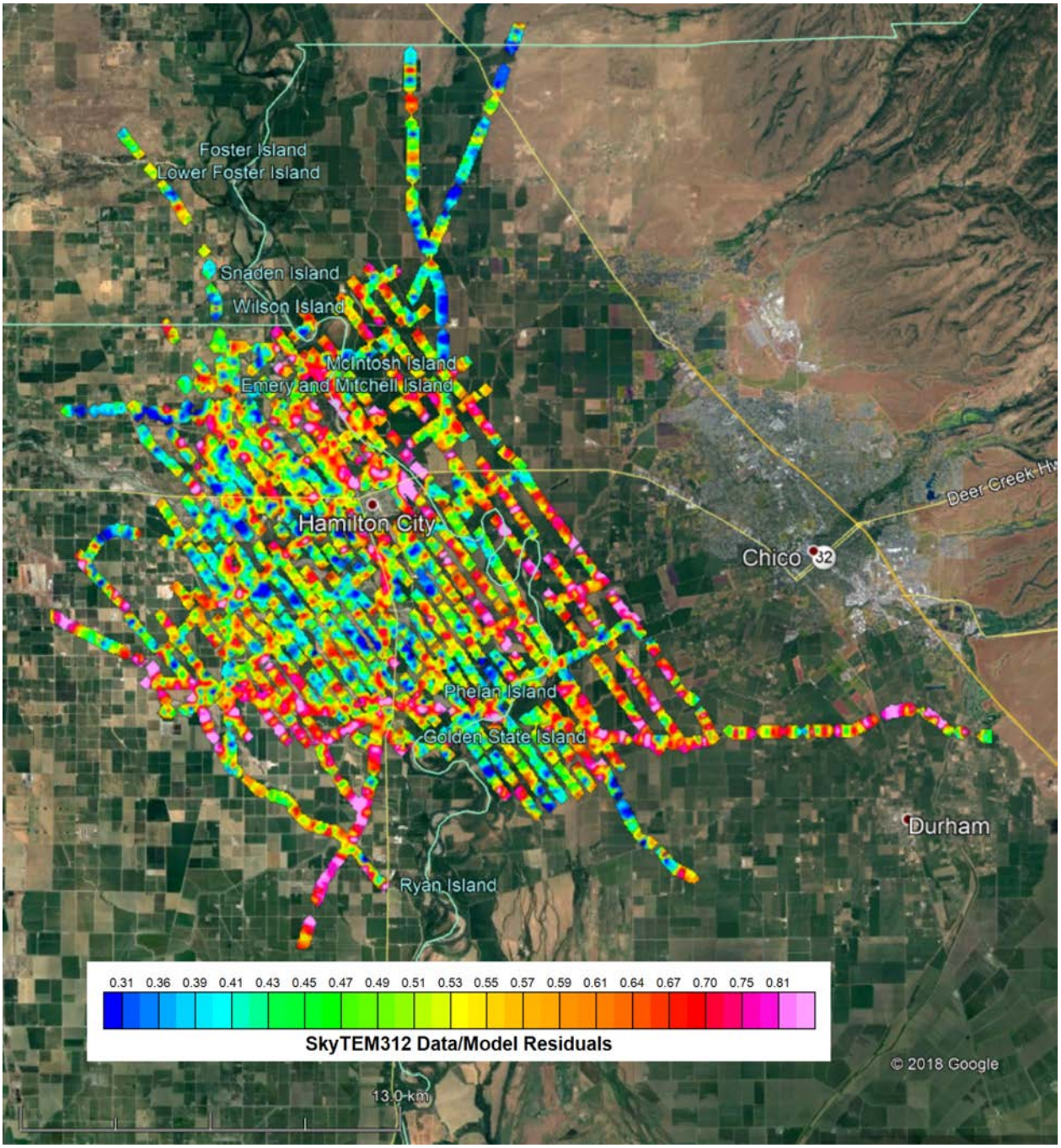

Figure 4-24. Map of data residuals for the Butte 312 SCI inversion results.

5 AEM Results and Interpretation

This section provides the details on the process involved in the interpretation of the Butte AEM data and inversion results.

5.1 Interpretive Process – Merge AEM Flight Lines, Construct DEM

5.1.1 Merge AEM Flight Lines and Databases from Different Flights

After the inversion process several short lines were combined to form continuous lines within the survey area. These included lines in both the 304M and 312 flight areas. These continuous lines allow for improved viewing and interpretation of the AEM inversions results. Table 5-1 lists the original flown lines and the new combined lines for the 304M and the 312.

Table 5-1. Combination of 304M and 312 flight lines within the Butte AEM survey area.

System	Original Line	Original Line	Merged Line
304	L400101	L400102	L400100
	L400201	L400202	L400200
	L730101	L730102	L730100
	L730301	L730302	L730300
	L730401	L730402	L730400
312	L100201	L100202	L100200
	L100701	L100702	L100700
	L100801	L100802	L100800
	L101601	L101602	L101600
	L101701	L101702	L101700
	L101901	L101902	L101900
	L102001	L102002	L102000

5.1.2 Construct the Project Digital Elevation Model

To ensure that the elevation used in the project is constant for all the data sources (i.e. boreholes and AEM data), a Digital Elevation Model (DEM) was constructed for the Butte AEM survey. The data was downloaded from the National Elevation Dataset (NED) located at the National Map Website (U.S. Geological Survey, 2018a) at a resolution of 1 arc-second or approximately 100 ft. The geographic coordinates are North American Datum of 1983 (NAD 83) and the elevation values are referenced to the North American Vertical Datum of 1988 (NAVD 88). The 100 ft grid cell size was used throughout the project and resulting products. Figure 5-1 is a map of the DEM. This DEM was used to reference all elevations within the AEM datasets.

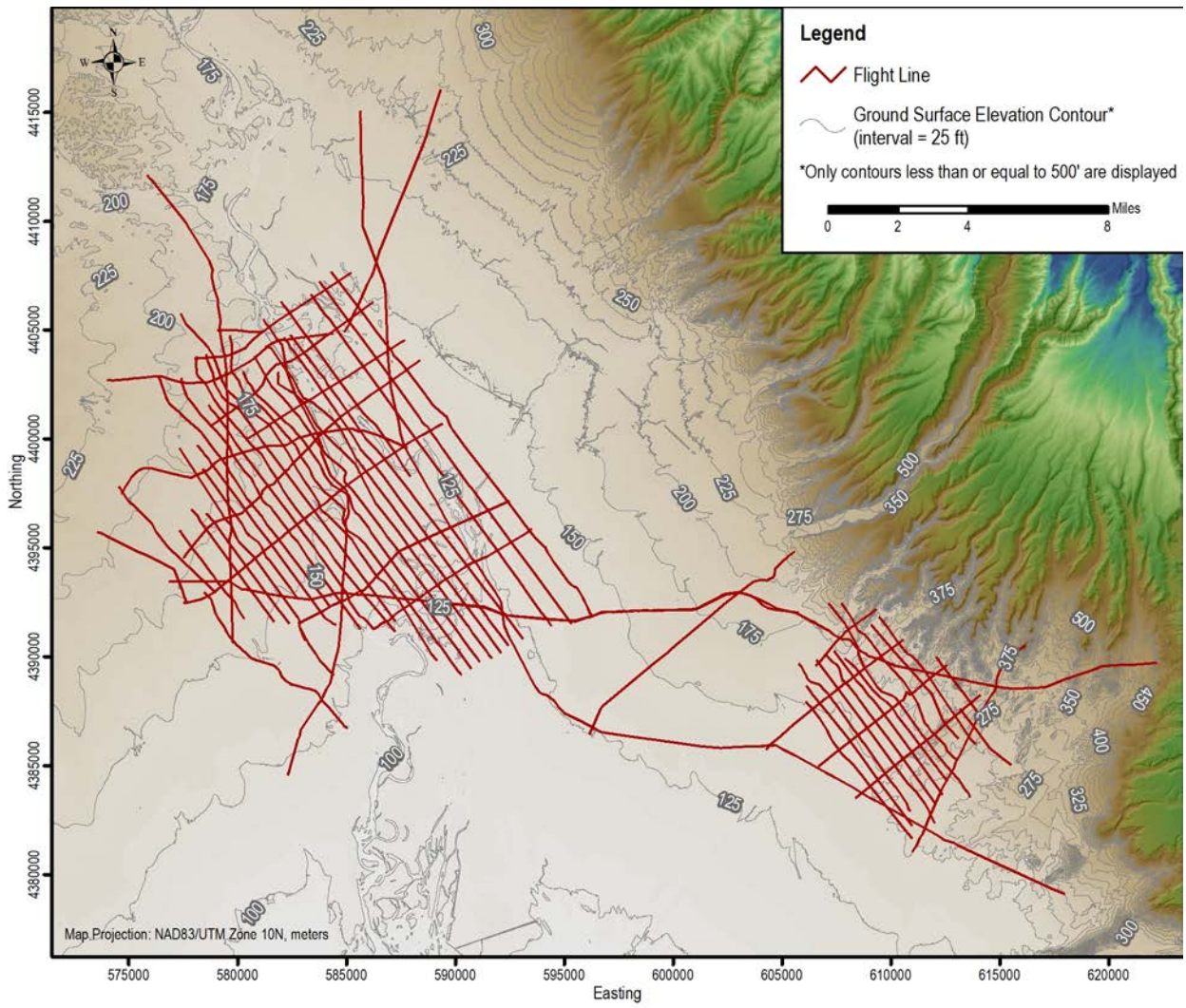

Figure 5-1. Map of the Digital Elevation Model for the Butte AEM survey area. Data source is the one (1) arc-second National Elevation Dataset (U.S. Geological Survey, 2018a). North American Datum of 1983 (NAD 83) meters and the elevation values are referenced to the North American Vertical Datum of 1988 (NAVD 88) feet.

5.2 Create Interpretative 2D Profiles

After final combination of the AEM data, characterization of the subsurface was performed in cross-section format using Datamine Discover Profile Analyst (DatamineDiscover, 2018). During interpretation, the horizontal and vertical scale of the profiles were adjusted to facilitate viewing. The color scale of the resistivity data was also adjusted to illuminate subtle differences in the resistivity structure within the inverted AEM resistivity model related to the area being interpreted. The first step in the interpretation process was reviewing the previous work that was completed in the area as referenced in Section 2.0. The CA-DWR report entitled "Geology of the Northern Sacramento Valley" (CA-DWR, 2014) provided descriptions of the geological units including their ages, lithologies, and their sources as well as their relationships and CA-DWR's interpretation of the spatial distribution of the different units based on available borehole information. In addition to the description of the geological units, the CA-DWR (2014) included a geological map (Figure 2-2 in Section 2.1.5) and several geological cross-sections on plates 2 and 3 presenting the interpreted stratigraphy. Portions of cross-sections B-B', E-E', and F-F' are included in Section 2.1.5 of this report as Figure 2-4, Figure 2-5, and Figure 2-6, respectively. These cross-sections were used to develop an understanding of the nature of the subsurface geology imaged by the AEM survey.

The locations of B-B', E-E', and F-F' are presented in Figure 2-3. Cross-section B-B' starts in the foothills and proceeds west through the middle of the 312 AEM Block flight area. Along the way B-B' intersects section E-E' just to the east of Chico and the 312 AEM Block area and then intersects section F-F' just to the west of the 312 AEM Block area.

Cross-section E-E' starts north of the start of section B-B' in Figure 2-3 and then proceeds south just east of Chico and crosses three of the 304 Reconnaissance AEM flight lines and one 312 Reconnaissance AEM flight line. It may appear as if three lines are crossed, but L730300 and L710610 overlap right where cross-section E-E' crosses over them.

An important observation about cross-section F-F' is not that it doesn't actually cross over any of the AEM flight lines, as it is subparallel to and west of the 312 AEM Block flight lines. Rather, what is interesting is that F-F' presents the Tuscan FM (***Tt***) as being discontinuous in nature (Figure 2-6)in the vicinity of western side of the 312 AEM Block flight lines. This will come into play during interpretation of the western side of the 312 AEM flight area.

With the analysis of cross-section B-B', E-E', and F-F' in mind, the next step in the interpretative process was to begin digitizing the interpreted contacts between all the different geologic units indicated in the CA-DWR (2014) cross-sections in the investigation area including: Quaternary (***Q***), Tertiary Tehama FM (***Tte***), Tertiary Tuscan FM (***Tt***), Tertiary Upper Princeton Valley Fill FM (***Tupvf***), Tertiary Lovejoy Basalt FM (***Tl***), Tertiary Ione FM (***Ti***), and the Jurassic-Cretaceous Great Valley Sequence (***JKgvs***).

The interpretative process began with selecting an AEM flight line to start the geologic contact digitization. It came to mind that the best place to start would be on a line that begins in the foothills and proceeds out into the Valley, similar to what is presented on the east end of cross-section B-B'. This line turned out to be L730300, acquired by the 304M. Since the geological units are shallow on the east

end of section B-B', they should similarly be shallow on the east end of line L730300. Then as the line proceeds westerly into the Valley, the deeper units that are shallow in the foothills will go to depth and so become harder to image from AEM. The east end of section B-B' and 304 flight line L730300 are presented in Figure 5-2.

The next step was to study the available geophysical and lithological logs provided by Dr. Todd Greene of CSU-Chico (Section 3) and then overlay them on the profiles if they are within 1,640 ft (500 m) of a flight line (Figure 5-3). On the profiles geophysical electrical resistivity logs are labeled in black and lithological logs are labeled in brown. The lithology color legend is in the upper right corner of the image. On the geophysical logs of interest were locations and depths of resistive and conductive zones. Then lithology logs were studied to correlate lithologies of volcanic origin found in the ***Tte*** and ***Tt*** formations (clay, sandy clay, silty sand, sand, sand and gravel, lava rock, lahar material) with the observed resistivities.

Part of the AEM inversion analysis is also an analysis of the borehole logs. As noted in Section 3 there were 362 lithological logs made available. Of these, the mean bottom depth of the lithology logs was 339 ft with a standard deviation of 289 ft and maximum bottom depth of 1,520 ft. Of the 183 resistivity logs made available, the average bottom of borehole depth of the resistivity logs was 1,790 ft with a standard deviation of 489 ft and a maximum bottom depth was 2,279 ft, much deeper than the AEM is imaging. The bottom line is that the majority of lithology logs will be located in the ***Tte*** and the resistivity logs will be in both the ***Tte*** and the ***Tt*** formations. There is more discussion coming below on the comparison of the borehole resistivity logs and the AEM inversion results in Section 5.1.4.

Despite the shallow extent of the lithology logs, they did provide information on the nature of the material in the near-surface along L730300. Lahar material is identified in the logs near the surface on the east side of the profile, similar to the geologic map in CA-DWR (2014) which indicates ***Tt*** outcrops in this area. The resistivities of the materials identified by the lithology logs and by the CA-DWR (2014) geologic map present very high resistivities in the resistivity section that end on the surface about half-way along the profile towards the west and more conventional sediment is indicated, likely ***Q*** on the surface. The L730300 resistivity profile indicates that the ***Tt*** material proceeds below the surface at about that location.

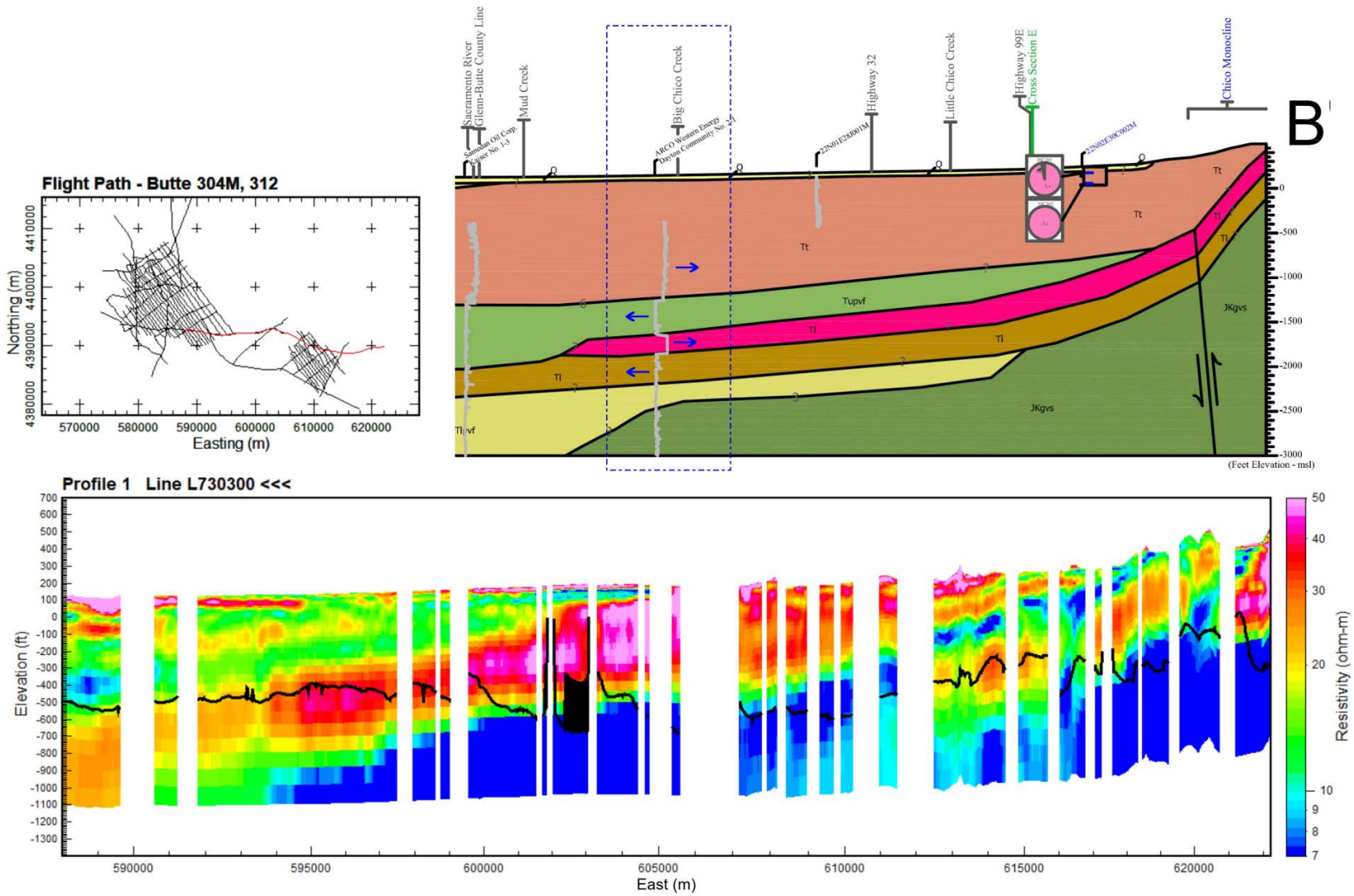

Figure 5-2. 2D profile of resistivity data from Butte 304M flight line L730300 and the east end of cross-section B-B'. Note the dashed blue box around the location where cross-section B-B' crosses Big Chico Creek and the borehole log printed in grey under the Big Chico Creek label. The blue arrows indicate the general direction of the resistivity log. The solid black line is an approximate measure of the Depth of Investigation (DOI).

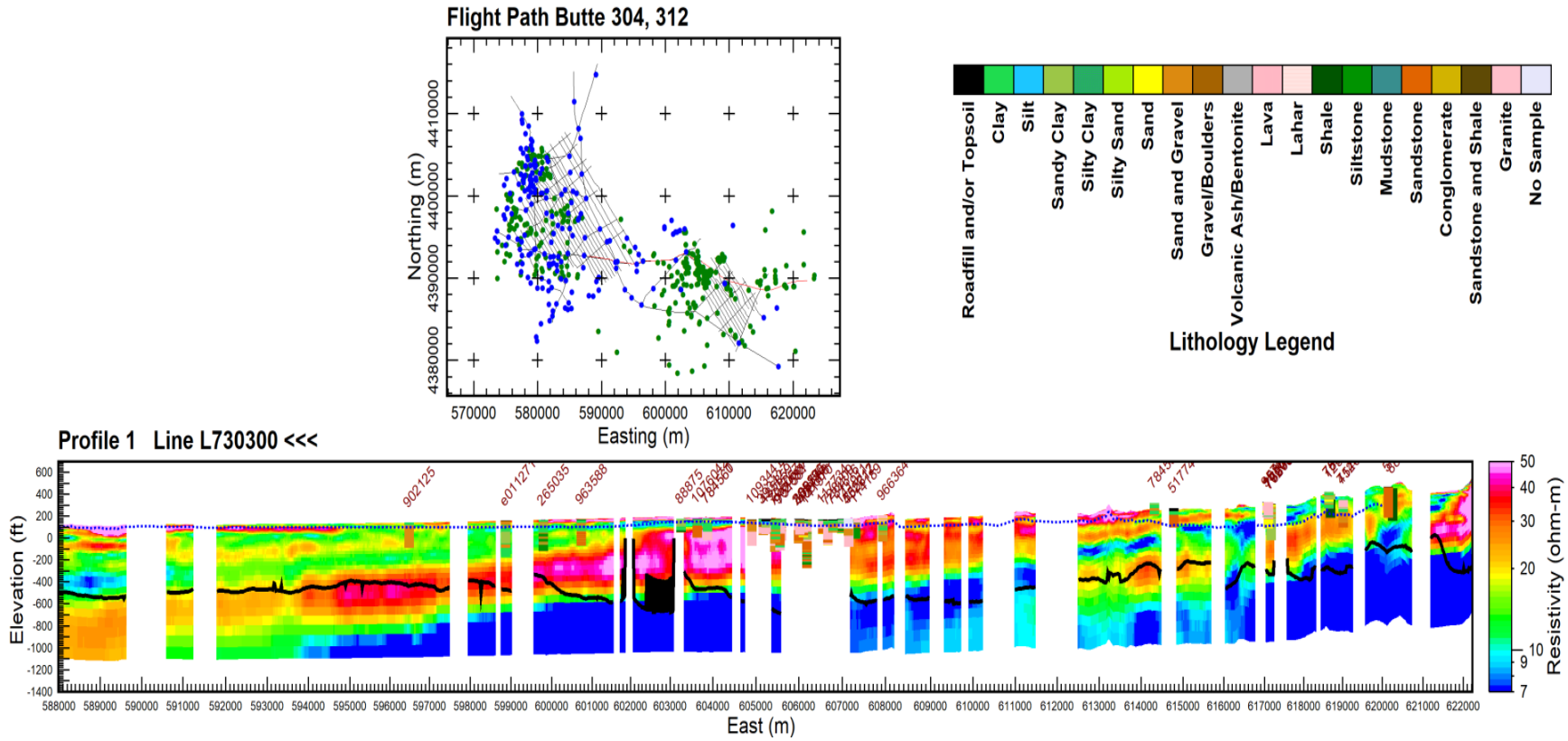

Figure 5-3. 2D profile of resistivity data from Butte 304M flight line L730300 with geophysical and lithological borehole data projected if within 1,640 ft (500 m). On the flight map green dots are locations of boreholes with lithology data and blue dots represent locations of boreholes with geophysical data. On the profile boreholes with names in black are geophysical logs and boreholes with names in brown are lithological logs. The geophysical logs use the same resistivity scale as the profile. The lithology color legend is in the upper right corner. The black block of DOI lines at easting 603000 is due to the projection of the curvature of the profile.

Examination of the right side of the resistivity profile in Figure 5-2, leads one to observe alternating bands of red and blue colored zones indicating bands of more resistive and more conductive material. Next, closer examination of the portion of cross-section B-B' presented in Figure 5-2 shows that just under the location where cross-section B-B' crosses Big Chico Creek (surrounded by a blue dashed box) there is what appears to be a resistivity log overlaid on the cross-section. Of interest is that the resistivity log moves right in the ***Tt***, left in the ***Tupvf***, right again in the ***Tl***, and then left again in the ***Ti***, the ***Tlpvf***, and the ***JKgvs***. The resistivity log moving to the right usually indicates more resistive material and moving to the left, more conductive material. This became a good guide on how to examine the AEM resistivity data on the right side of L730300 in Figure 5-2. We could now correlate the more resistive material with the ***Tt*** and the ***Tl*** and the more conductive material with the ***Tupvf***, ***Ti***, and the ***JKgvs***.

Next item of interest is what is below the thin resistive surface material on the western side of L730300. On the surface on the far-left side of Figure 5-3 we see a thick resistive zone which turns out to be the location of the Sacramento River and its flood plain (Figure 1-2). The portion of cross-section B-B' in Figure 2-4 indicates that right at the location of the Sacramento River on B-B' the ***Tte*** thins out. However, there are question marks, "?", on the indicated contacts on the section indicating that the location may not be accurate. Now the resistivities under the Sacramento River in Figure 5-3 indicate interbedded more resistive (red), moderately resistive (green), and conductive (blue) materials continue east from under the Sacramento River until they thin out right about at the location where the ***Tt*** proceeds below the surface. This suggests that it is permissible that the ***Tte*** could actually continue farther east than what is indicated in cross-section B-B' and that what we see spreading out to the west on top of the resistive ***Tt*** along L730300 is likely ***Tte***. The alternating resistive and conductive zones likely indicate sands and gravels, sands, and clay.

With this interpretational basis, digitization of geological contacts on L730300 could proceed.

The results of the stratigraphic analysis of AEM flight line L730300 is presented in Figure 5-4. The top profile is the resistivity data on which digitization occurred and the bottom profile is the stratigraphic interpretation. There is a good basis for the locations and depths of the interpreted contacts presented on the right side of the profile based on the examination of cross-section B-B' and because there is an easily observable electrical resistivity contrast between these units on this part of the profile. We see ***Tt*** on top of ***Tupvf*** on top of ***Tl*** on top of ***Ti*** on top of ***JKgvs*** material.

However, as one moves west past the end of the electrically resistive ***Tl*** at depth, it becomes clear that no observable resistivity contrast is apparent between the ***Tupvf***, the ***Ti***, and the ***Jkgvs*** material. They are all electrically conductive (less than 5-7 ohm-m).

Next, note the black line in Figure 5-2. This line represents an approximation of the Depth of Investigation (DOI) (Asch, 2015). This is the approximate depth at which resolution of the true resistivity turns to detection of some representation of the true resistivity.

Next, note the bright red zone on the east end of L730300. This has been interpreted to be granitic material of the pre-Cretaceous metamorphic and igneous rocks (***pKmi***). It is just to the east of the end of

cross-section B-B' where we see the formations trending upwards but not what is causing the upward trend. In Figure 5-2 the resistive material representing the granite doesn't go to depth as we expect granitic material would. This is because of the DOI. The granitic material is there, but we are not able to fully image it.

Next, note the relation of the DOI in Figure 5-2 to the conductive material in the ***Tupvf***, ***Ti***, and ***JKgvs***. We are not getting good resolution of the resistivity for this conductive material, just that it is conductive. Thus, because there is no resistivity contrast, and the material is generally below the DOI, there becomes no solid foundation for distinguishing between the different conductive units. Therefore, in all the stratigraphic interpretations presented here on in this report, the ***Tupvf*** and ***Ti*** and the JKgvs are all grouped together into one undivided stratigraphic unit, even when there is a contrast between units such as the eastern end of L730300.

Figure 5-5 presents the updated stratigraphic interpretation along L730300 using the new undivided stratigraphic designation for the grouped conductive units. Also, in Figure 5-5, at the top, is a Public Land Survey System (PLSS) map showing the location of the AEM flight line presented on the profile in terms of section, township, and ranges The color legend for the stratigraphic units is highlighted in Figure 5-6, along with the legend for the lithology boreholes. The interpreted stratigraphic contacts are now also overlaid on the resistivity profile so that an easy comparison could be made between the resistivity and interpreted stratigraphy profiles.

The interpretative 2D profiles presented here are also located in Appendix 1 – 2D Profiles.

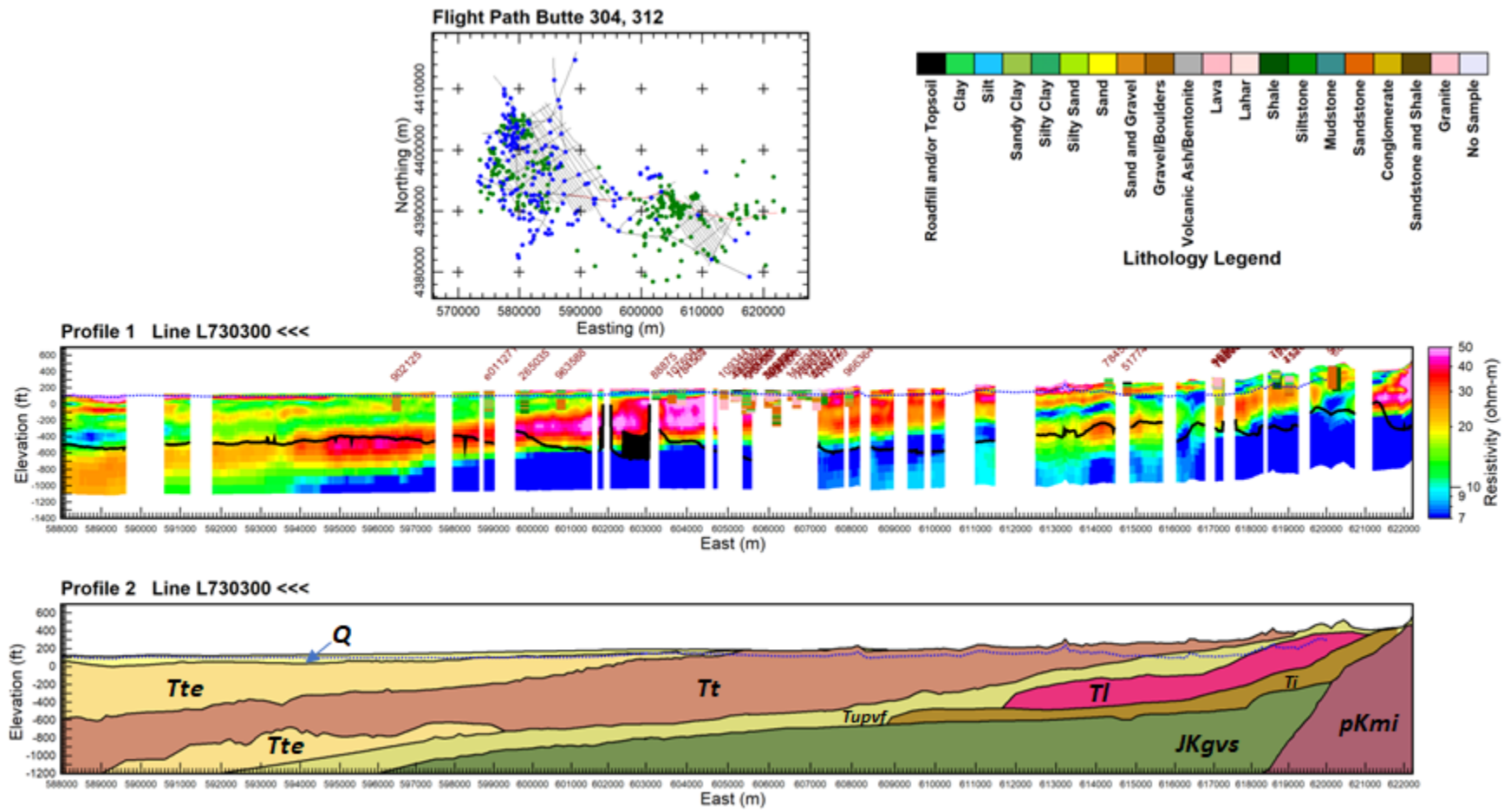

Figure 5-4. Example digitization of stratigraphic contacts for AEM flight line L730300.Stratigraphic units indicated: Quaternary (*Q*), Tehama FM (*Tte*), Tuscan FM (*Tt*), Upper Princeton Valley Fill (*Tupvf*), Lovejoy Basalt (*Tl*), Ione FM (*Ti*), Great Valley Sequence (JKgvs), and Granite (*pKmi*).

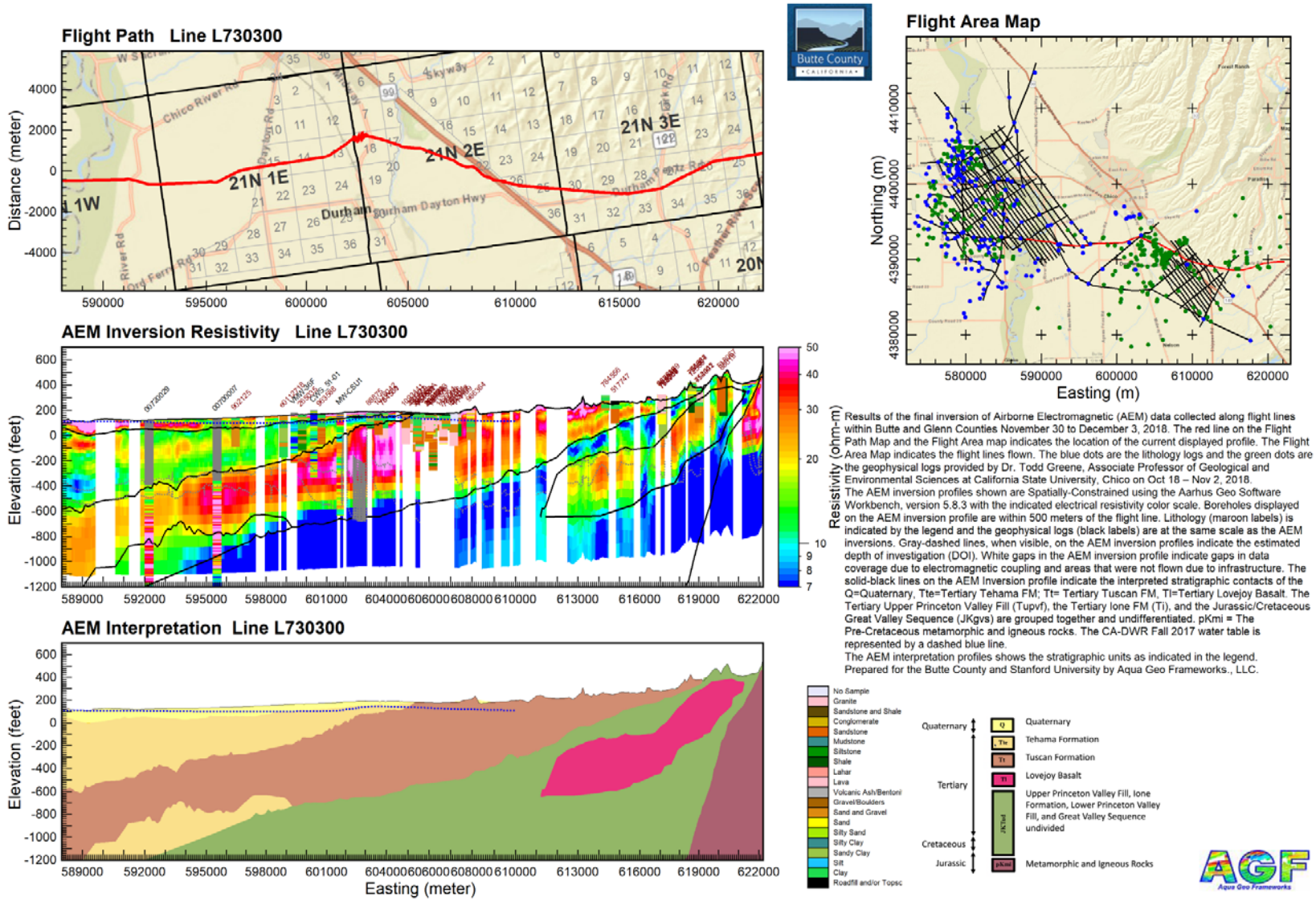

Figure 5-5. Same digitization as in Figure 5-4, except all conductive stratigraphic units at depth below the Tuscan, which cannot be distinguished because of a lack of electrical resistivity contrast between them, are now grouped into one conductive basement stratigraphic unit.

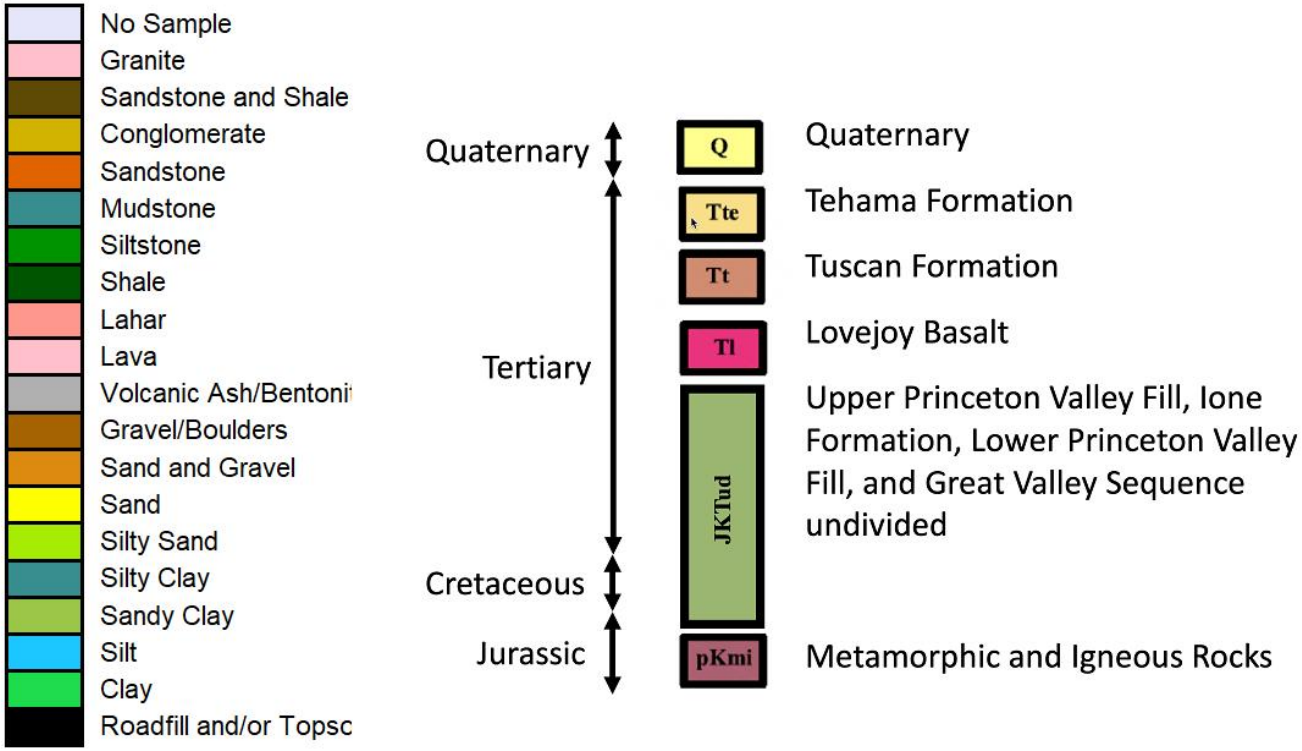

Figure 5-6. Lithology borehole color legend and grouped stratigraphic color scale.

.

A few examples of the stratigraphic interpretation of the Butte AEM resistivity earth models along both the Reconnaissance AEM flight lines and the Block AEM flight lines for both the western and eastern investigation areas are now presented. Borehole logs are projected onto the profiles if they are 1,640 ft (500 m) of the flight lines.

304M AEM flight line L730100 (Figure 5-7) is an approximately 15-mile long southeast-northwest reconnaissance line on the south side of the 304M AEM Block flight area. This flight line shows a similar stratigraphy to that for L730300 in Figure 5-5 as it is also coming out of the Sierra Nevada foothills and is sub-parallel to L730300. One difference is that the Lovejoy Basalt has a little more topography on its surface. Another item of interest is that the dotted line representing the 2017 water table (CA-DWR, 2018) does not progress all the way across the profile, stopping at an Easting of 613000, consistent with the water table surface presented in Figure5-47.

312 AEM flight line L710201, presented in Figure 5-8, is an approximately 14-mile long north-south reconnaissance line that begins south of the 312 AEM Block flight area and then proceeds to traverse across the 312 AEM Block flight area. There are two items of interest along this line. One is that the Tuscan FM (***Tt***) terminates on its south end in the Valley at a Northing of about 4387400.

The other item of interest on L710201 in Figure 5-8 is that the ***Tt*** here shows what appears to be a notched pattern in places along its top and bottom edges. This could be evidence of fractures. This can be checked by a slight variation of the scale on the resistivity profile from its current range of 7 – 50 ohm-m to 9 – 50 ohm-m; Just a slight change of two ohm-m. The result of this slight change is presented in Figure 5-9. Note the vertical light blue zones that were not apparent in Figure 5-8 but are now present in the Tuscan FM at Northings of 4388000, 4391600, 4392200, 4401200, and 4403000 along the profile. These indicate more conductive material is located at these positions and the pyramid-like shapes located underneath these likely fractures suggest a piling up of conductive material such as sandy clay or possibly poor-quality water as well.

What suggested the possibility of the ***Tt*** becoming fractured at some point are the two fragments of ***Tt*** presented on CA-DWR (2014) cross-section F-F' in Figure 2-6. That kind of geologic presentation can't occur unless the unit was fractured, eroded, and the rock fragments become more isolated over time from the main unit.

Figure 5-10 presents a 304M AEM Block flight line L300801 which is about 6-miles in length and runs northwest-southeast. Of interest on this profile is the apparent fractured nature of the ***Tl***. Even at a scale of 7 – 50 ohm-m, the sub-vertical blue zones observed on 312 Reconnaissance flight line L700201 on Figure 5-9 using a scale of 9 – 50 ohm-m represent, at least, weathering and, possibly, apparent fractures well.

A perpendicular 304M Block flight line to L300801 is L400401 (presented in Figure 5-11) which is approximately 4.5-miles long and trends southwest-northeast. Here the ***Tl*** appears to be more coherent. Of interest is that the dotted line just under the ground surface representing the water table only progresses across about half of the profile before it terminates.

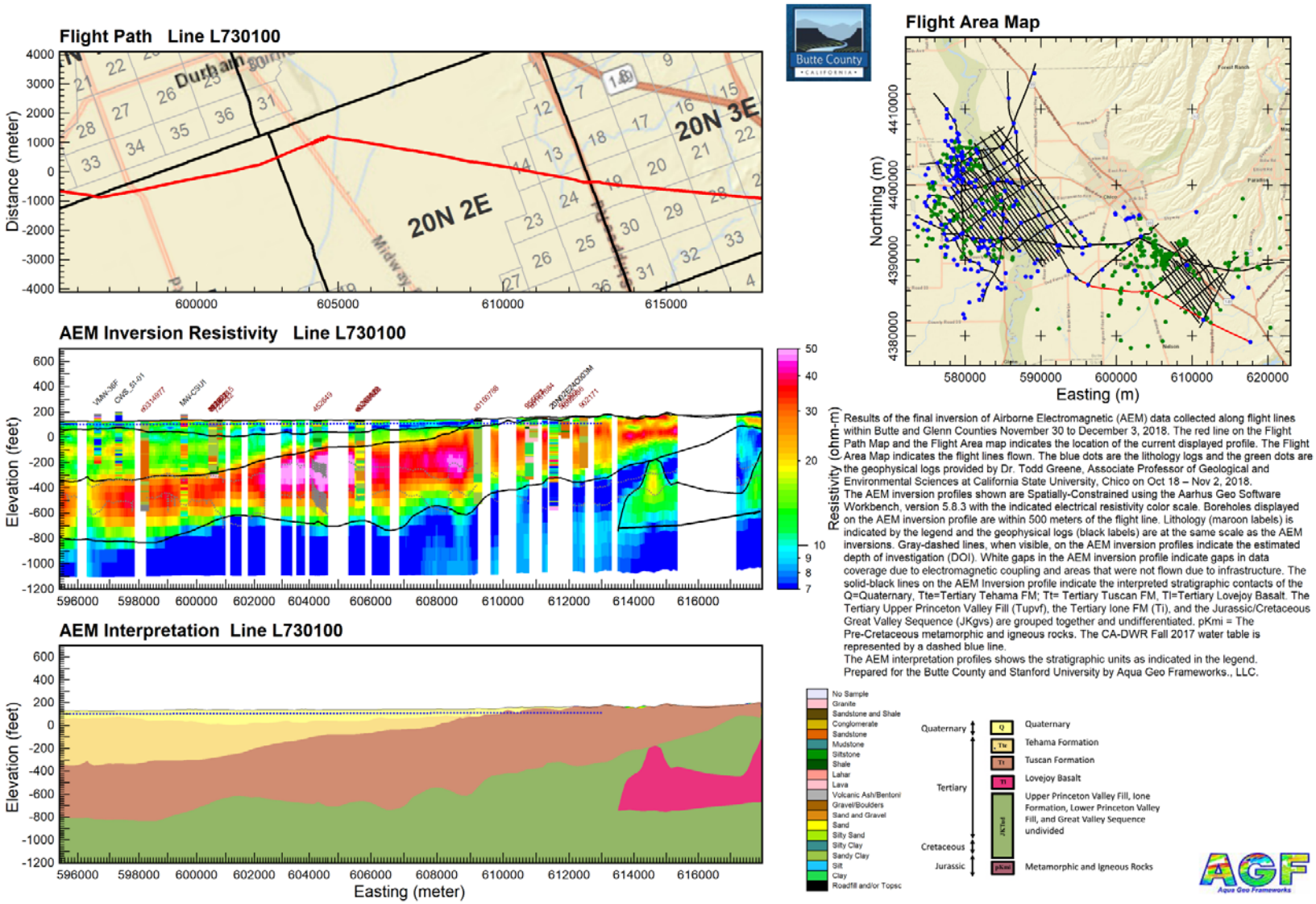

Figure 5-7. 304M AEM Reconnaissance flight line L730100 displaying the flight path (red line) on the USGS 100K topo map (top map), the inverted resistivity section along the flight line (top profile), and interpreted stratigraphy on the bottom profile. White gaps in the resistivity profile indicate areas clipped out due to coupling or not flown due to infrastructure.

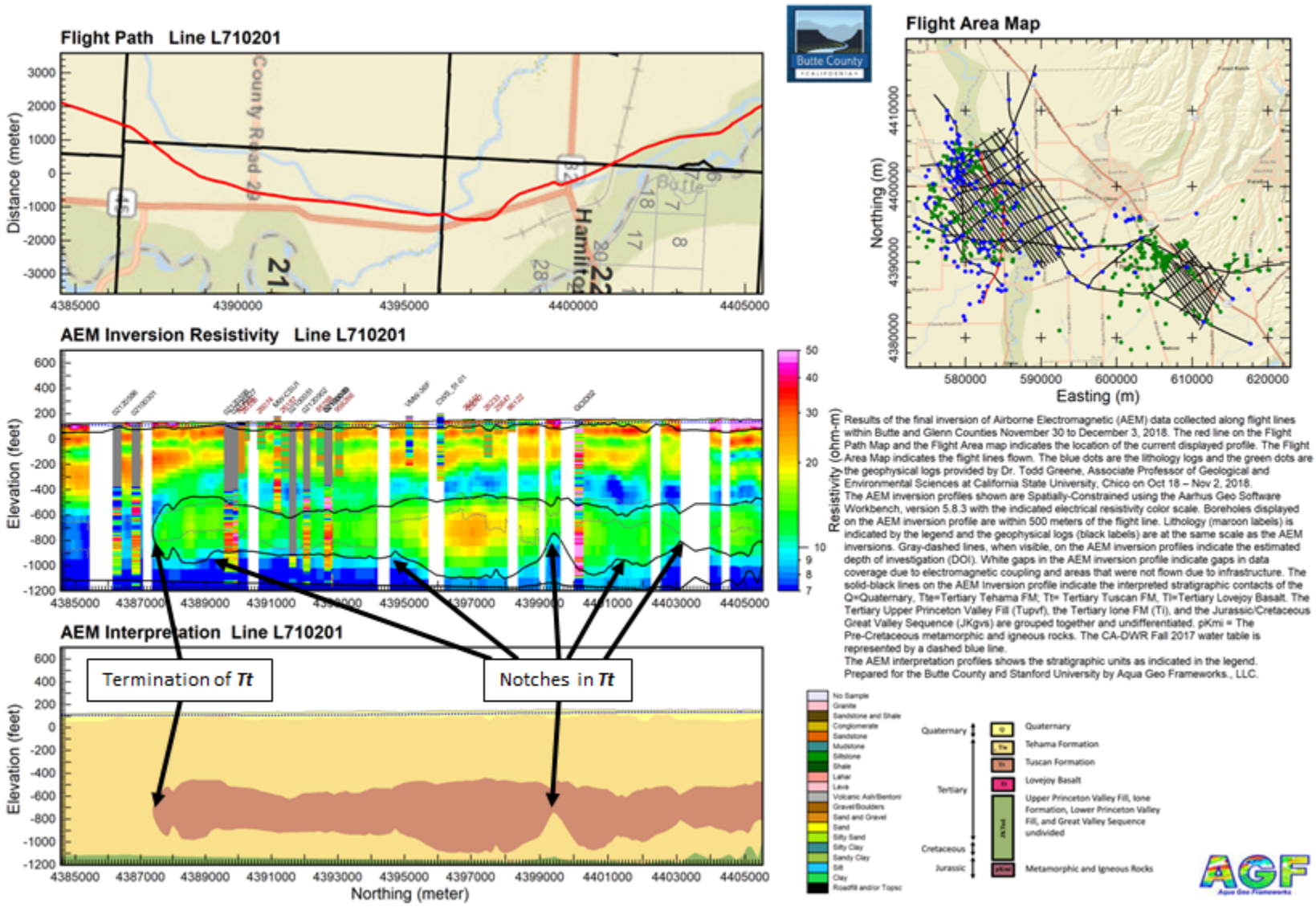

Figure 5-8. 312 AEM Reconnaissance flight line L710201 displaying the flight path (red line) on the USGS 100K topo map (top map), the inverted resistivity section along the flight line (top profile), and interpreted stratigraphy (bottom profile). White gaps in the resistivity profile indicate areas clipped out due to coupling or not flown due to infrastructure.

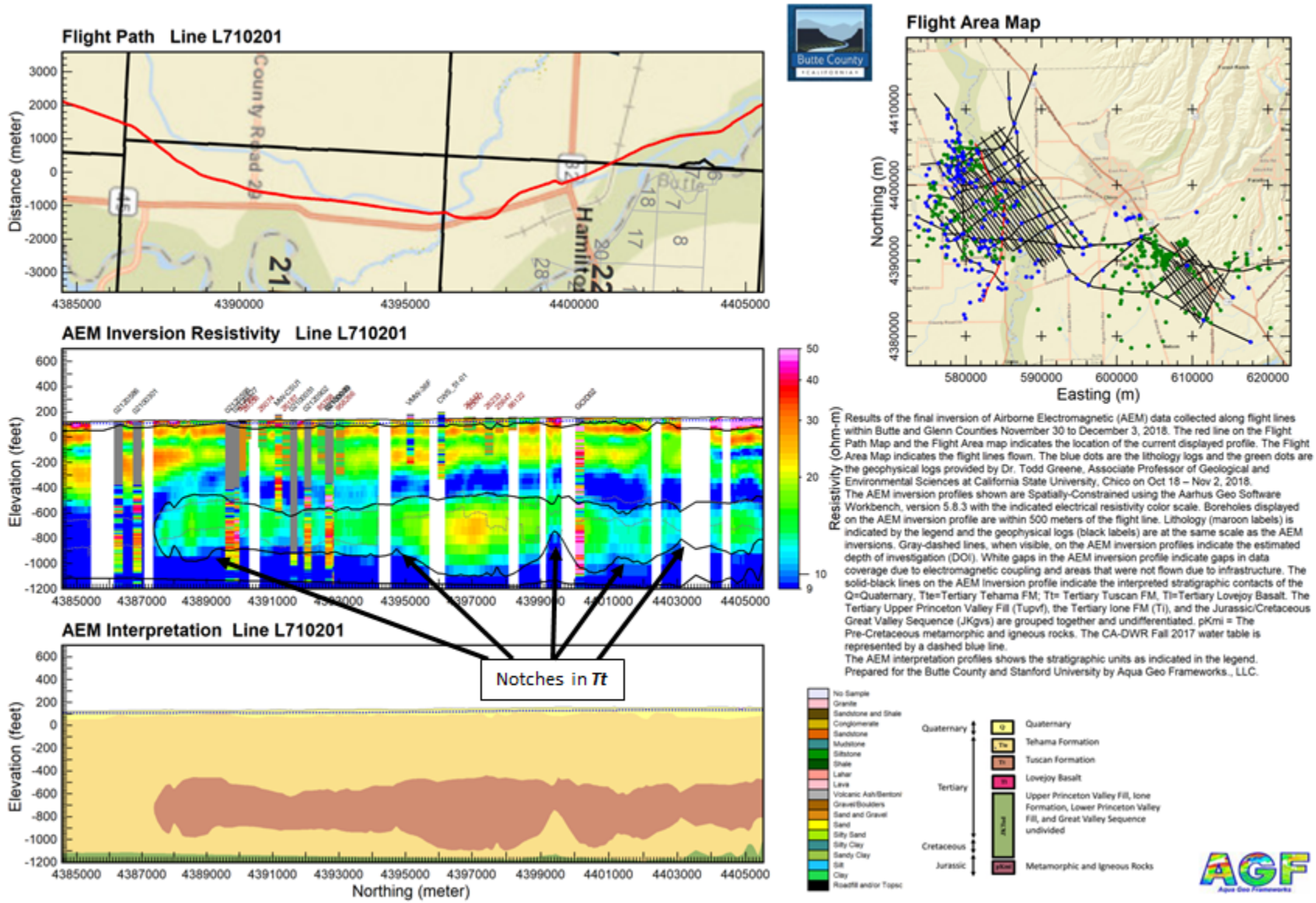

Figure 5-9. 312 AEM Reconnaissance flight line L710201, the same as in Figure 5-8, except that the resistivity color scale now ranges from 9 ohm-m to 50 ohm-m (compared to 7 - 50 ohm-m in Figure 5-8). Note the vertical light blue zones in the Tuscan FM (*Tt*) indicating fractures.

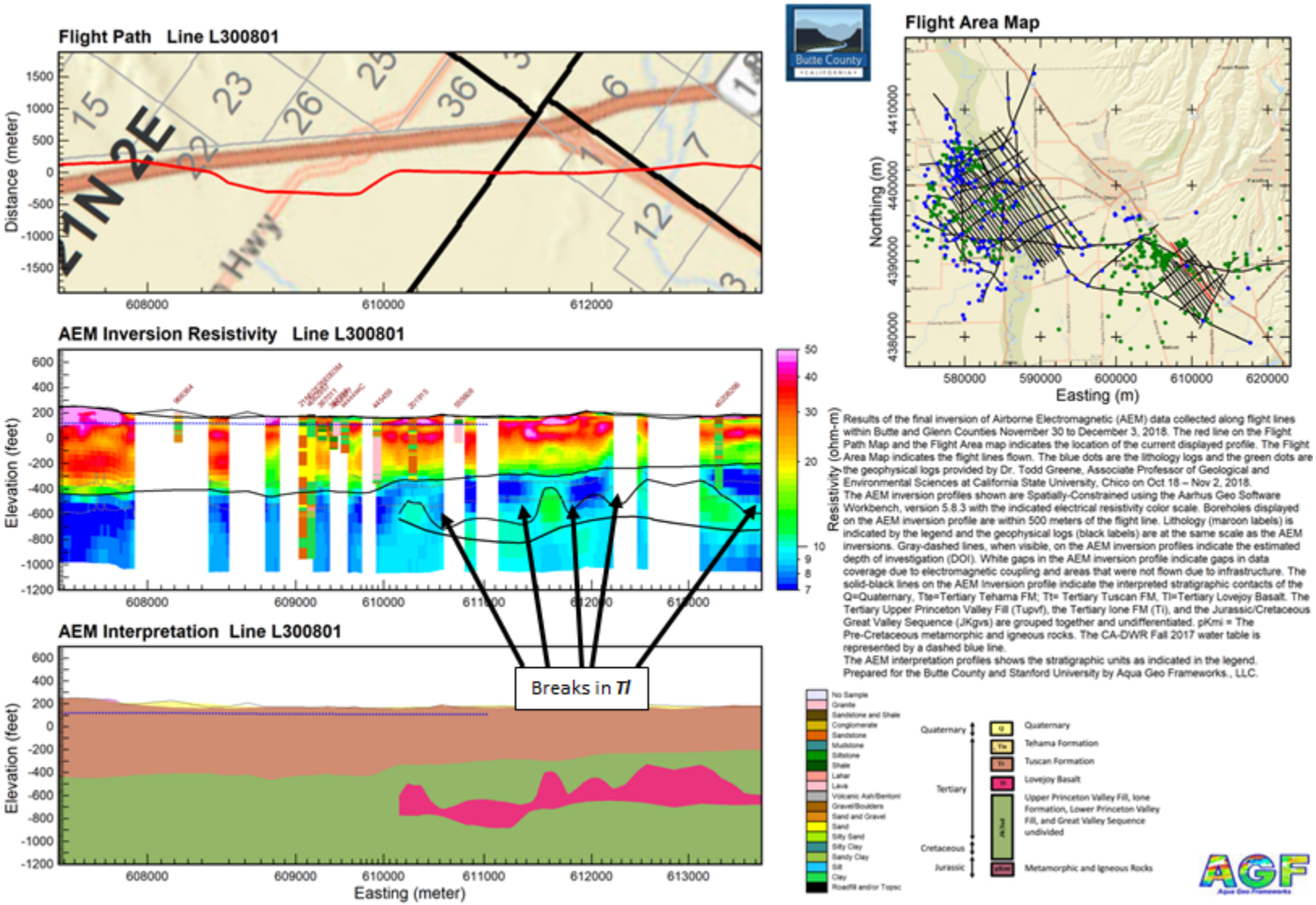

Figure 5-10. 304M AEM Block flight line L300801 displaying the flight path (red line) on the USGS 100K topo map (top map), the inverted resistivity section along the flight line (top profile), and interpreted stratigraphy (bottom profile). White gaps in the resistivity profile indicate areas clipped out due to coupling or not flown due to infrastructure.

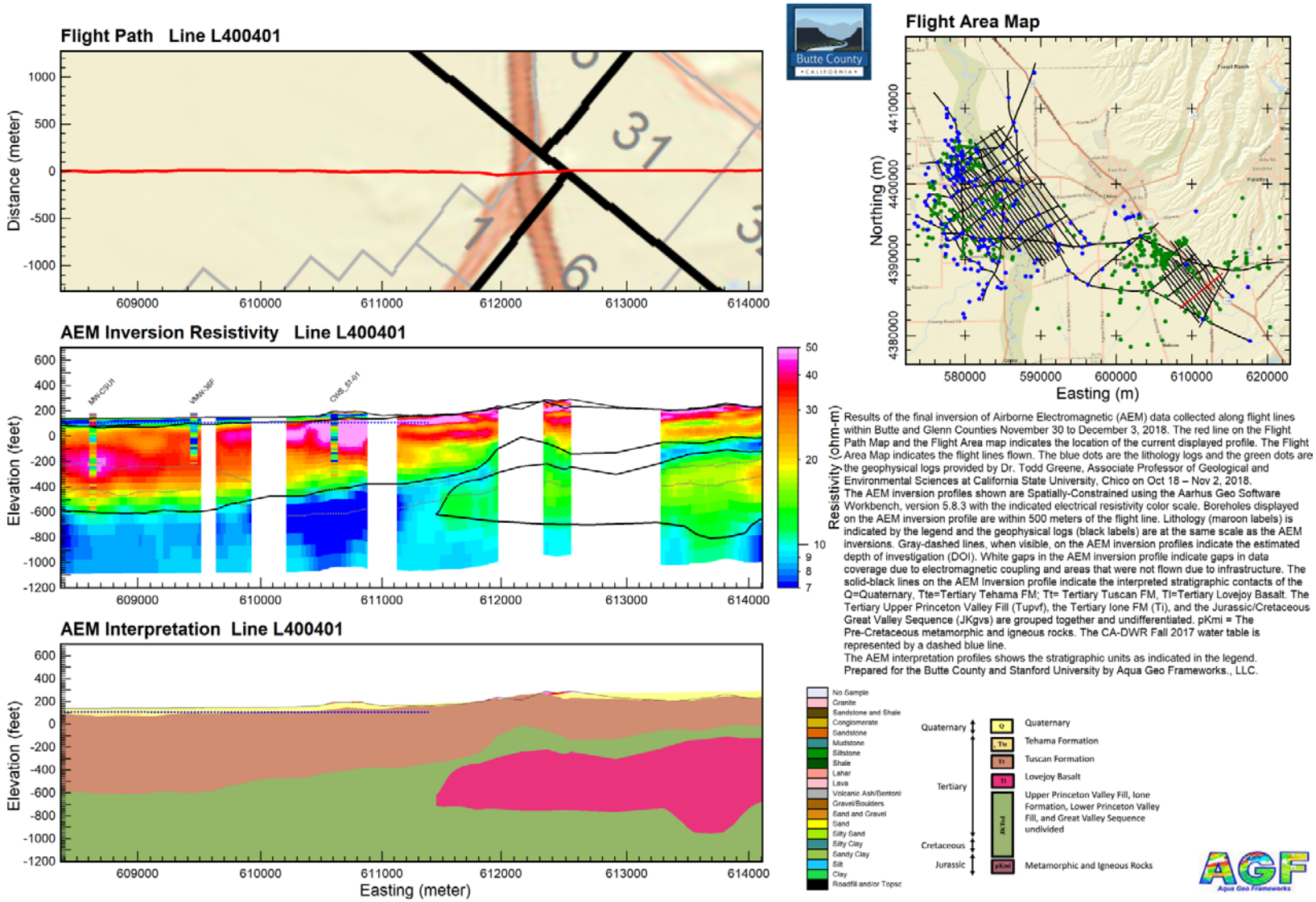

Figure 5-11. 304M AEM Block flight line L400401 displaying the flight path (red line) on the USGS 100K topo map (top map), the inverted resistivity section along the flight line (top profile), and interpreted stratigraphy (bottom profile). White gaps in the resistivity profile indicate areas clipped out due to coupling or not flown due to infrastructure.

312 AEM Block flight line L100700, presented in Figure 5-12, is approximately 16-miles long, trends northwest-southeast, and is located about 3.5 miles (at its center) from CA-DWR (2014) cross-section F-F'. The notch pattern in the top and bottom contact of the ***Tt*** is quite clear, again likely indicating fractures and erosion of the ***Tt*** at these locations. Figure 5-13 presents L100700 again, but with the 9 – 50 ohm-m resistivity scale. Now the sub-vertical light blue zones representing locations of fractures are quite clear as are the pyramid-like shapes of Tehama FM sitting on top of the undivided ***Tupf***/***Ti***/***JKgvs*** unit and likely containing saturated sandy clay.

312 AEM Block flight line L200500, presented in Figure 5-14, is approximately 8-miles long, trends southwest-northeast, and has its southwest located about 3 miles from CA-DWR (2014) cross-section F-F'. What is interesting here is the apparent competent nature of the ***Tt*** at this location even though we know from the just examined 312 flight line L100700 (Figure 5-12, Figure 5-13) that the ***Tt*** is fractured on either side.

Figure 5-15 is a repeat of Figure 5-13 but with the addition of a dashed line indicating the location along L100700 at which L200500 crosses. The location of the blue dashed line indicates a competent ***Tt***.

This last combination of profiles illustrates the application, and importance, if necessary and desired, of applying a dense block flight pattern versus a reconnaissance flight pattern. If mapping the fractured nature of the ***Tt*** was an important and desired AEM investigation goal, then block flight lines are required. If only an indication of the nature of the ***Tt***, whether it is even present at a given location is desired, then maybe the investigation could get by with a reconnaissance flight line design.

Again, all the interpretative 2D profiles presented here are also located in Appendix 1 – 2D Profiles

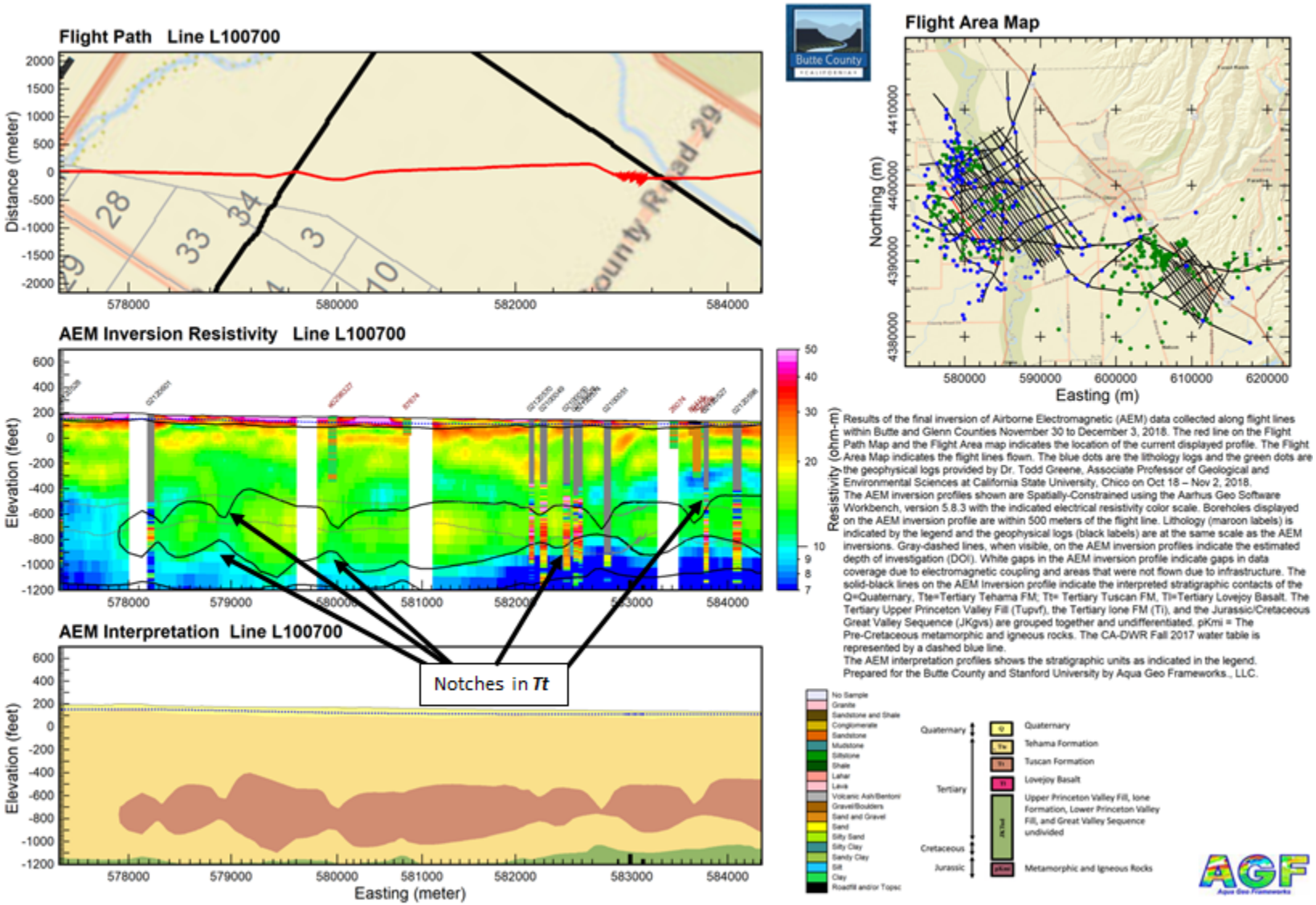

Figure 5-12. 312 AEM Block flight line L100700 displaying the flight path (red line) on the USGS 100K topo map (top map), the inverted resistivity section along the flight line (top profile), and interpreted stratigraphy (bottom profile). White gaps in the resistivity profile indicate areas clipped out due to coupling or not flown due to infrastructure.

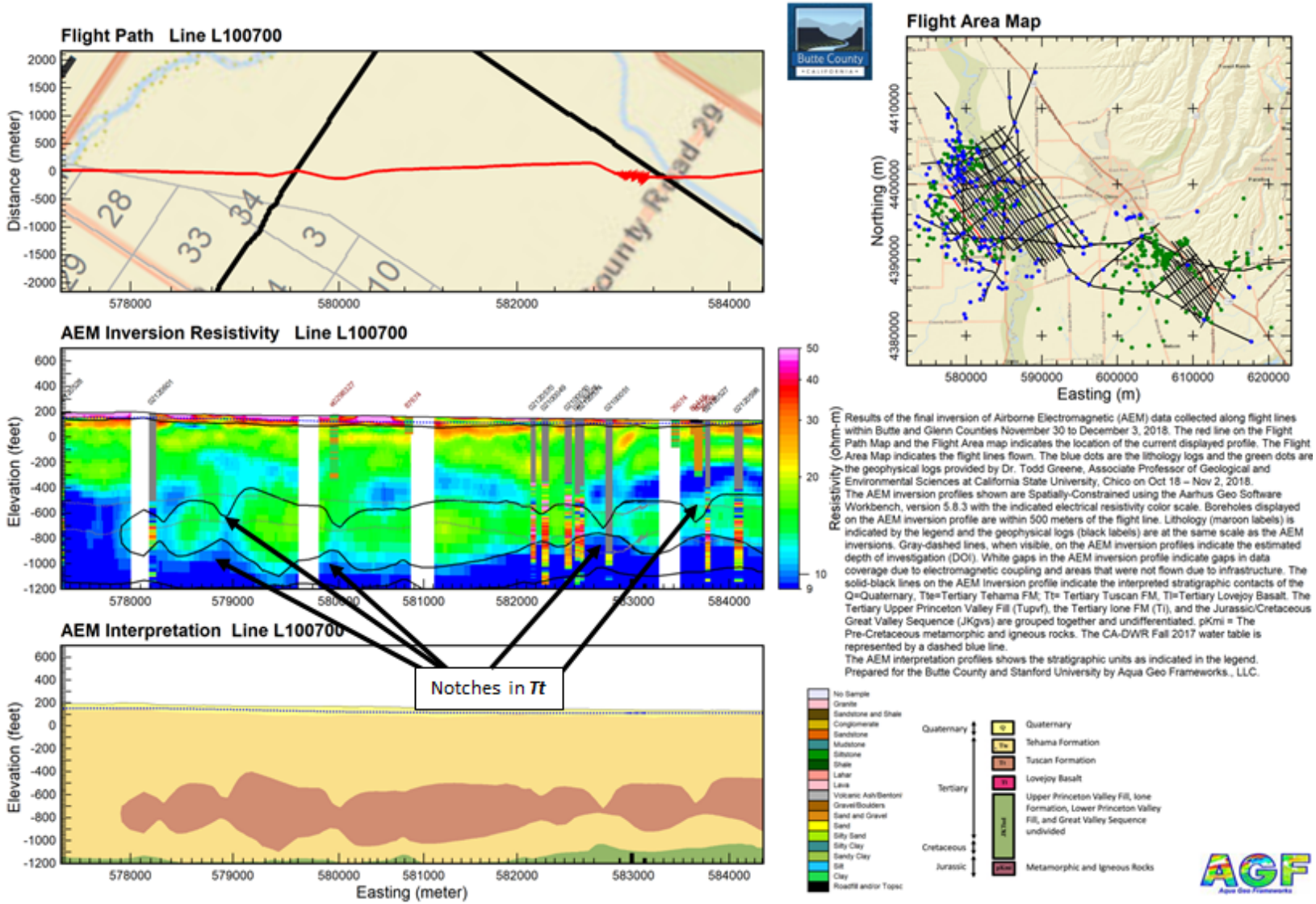

Figure 5-13. 312 AEM Block flight line L100700, the same as in Figure 5-12, except that the resistivity color scale now ranges from 9 - 50 ohm-m (compared to 7 ohm-m to 50 ohm-m in Figure 5-12). Note the vertical light blue zones in the Tuscan FM indicating fractures that were not visible in Figure 5-12 using the 7 – 50 ohm-m scale.

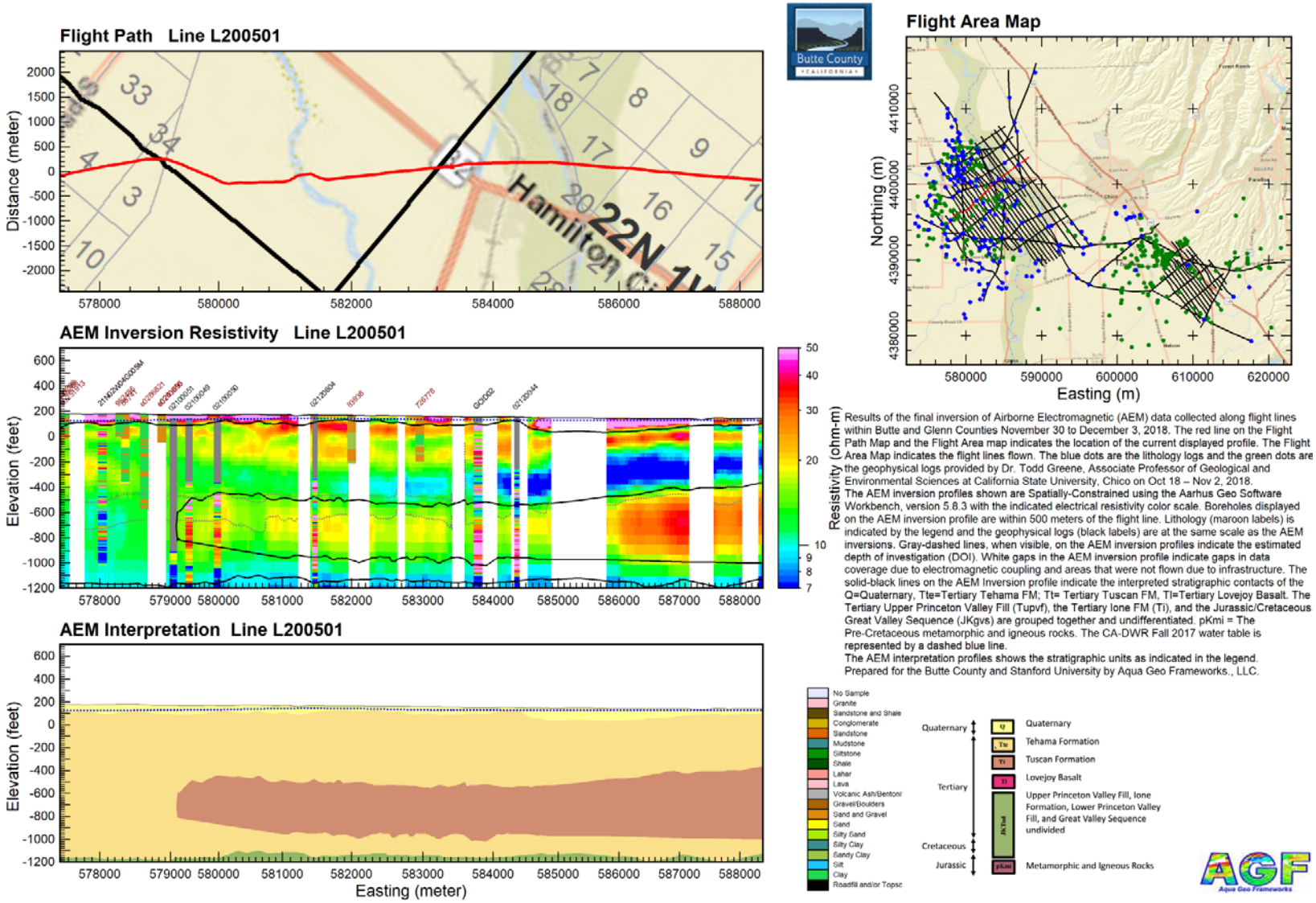

Figure 5-14. 312 AEM Block flight line L200501 displaying the flight path (red line) on the USGS 100K topo map (top map), the inverted resistivity section along the flight line (top profile), and interpreted stratigraphy (bottom profile). White gaps in the resistivity profile indicate areas clipped out due to coupling or not flown due to infrastructure.

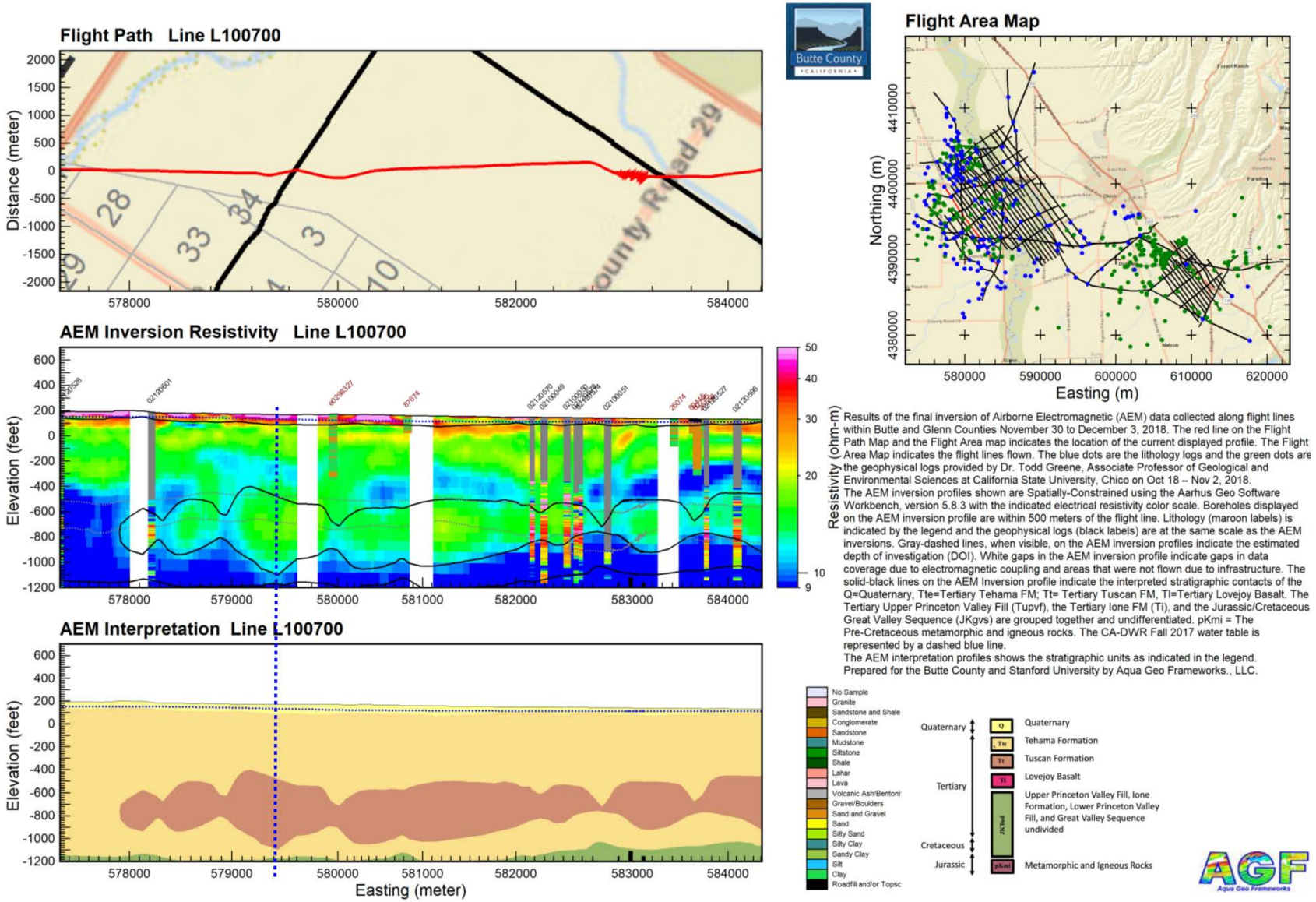

Figure 5-15. 312 AEM Block flight line L100700, the same as in Figure 5-13, with the addition of a line at Easting 579400, the location at which L200501 crosses L100700. Note the nature of the Tuscan FM at this location.

5.3 Comparison of Borehole Logs and the AEM Inversion Results

It is important to compare the AEM earth-model inversion results to the available borehole information. You want to look how the patterns of inverted AEM resistivities match up with the majority of geophysical borehole logs. It is quite often the case that borehole logs are not well calibrated or not operated correctly. This is not to say that when the borehole data was acquired that the tool was perfectly suitable for what was expected from the logging results.

What follows in this section are samples from across the investigation area of the resistivity and stratigraphic interpretation profiles similar to what have been presented, but with an emphasis on comparing the borehole electrical resistivity logs with the inverted AEM earth models.

Note that from the map of geophysical and lithological borehole locations (Figure 3-1), it is clear that there are many more electrical resistivity logs out in the Valley in the vicinity of the 312 AEM flight lines than are near the 304M AEM flight lines. Thus, the majority of images comparing borehole resistivity logs and the AEM inversion results will be from the 312 AEM flight area. The lithology logs that project onto the flight lines within the 1,640 ft (500 m) zone in the 304M AEM flight area are also compared.

Starting with AEM flight line L100700 already introduced above (presented in Figure 5-12, Figure 5-13, and Figure 5-15), most of the borehole resistivity logs match the AEM inversion results very well. On the far-left side of this profile borehole log *02120601* is right about at the location of an identified fracture in the ***Tt***. As does the AEM inversion results, the resistivity log indicates conductive material above the ***Tt***, resistive in the ***Tt***, and conductive material below the ***Tt***.

Figure 5-16 presents the interpretative profile for AEM flight line L200401. There is a good lithology match AEM inversion results and lithology log *24957* on the left side of the profile as well as resistivity log *720027* towards the center of the profile. Log *24957* also shows up on 312 Block flight line L101501 below (Figure 5-21).

A comparison between AEM flight line L101201 and borehole resistivity and lithology logs is presented in Figure 5-17. The resistive zones on the borehole logs line up with the resistive AEM inversion results in the Tuscan FM. There are also several logs on the far left indicating that possibly the ***Tt*** continues further to the northwest. However, a slight change in the resistivity scale from 7 – 50 ohm-m to 9 – 50 ohm-m (Figure 5-18) shows that there is slightly more conductive material (more blue) in the vicinity of the resistivity logs that are indicating the ***Tt*** continuous beyond the interpreted contact. There is also a good lithology match between log e0251916 and the AEM earth-model in the upper ***Tte*** in the center of the profile.

The next flight line to the northeast from L101201, L101301 (Figure 5-19), also shows those same boreholes as on L101201 in Figure 5-17 indicating that the ***Tt*** continues, but are now a little more centered on the profile. Again, changing the resistivity color scale to 9 – 50 ohm-m (Figure 5-20), shows that the area off to left is more conductive than it appears at a scale of 7 – 50 ohm-m.

Figure 5-21 presents AEM flight line L101501 and also shows a good match between the AEM inversion results and the borehole resistivity logs as well as with lithology logs *24957* (also on line L200401) and *86122*.

AEM flight line L101700 is compared with borehole logs in Figure 5-22. The resistivity logs match well except for log *22N01W29N001-4M* which appears to indicate much more conductive material than the AEM results and neighboring resistivity logs and so is likely poorly calibrated. This is not that unusual and interpreters should be wary of logs, both resistivity and lithology, until verified against other logs or other geophysical data.

There are also several lithology logs along flight line L101700 (Figure 5-22) that match the AEM earth model very well including *24955*, *82097*, *e0225919*, *726778*, *26440*, *25647*, and *26687*.

Both lithology and resistivity logs match the AEM inversion results along flight line L200301 (Figure 5-23) except for one log on the far-left side of the profile. Possibly a calibration issue.

Figure 5-24 presents AEM flight line L300301 which is located in the 304M AEM flight area. There is a very good match between the AEM inversion results and lithology log e0160820 on the right side of the profile.

A comparison of the AEM inversion results and the logs along AEM flight line L30081 in the 304M AEM flight area (Figure 5-25) shows a very good match with lithology log e062957 and a very poor match with log 21N02E26E003M. It is not clear why this should be the case since lithology would be logged by a person but there is a very big difference between the two logs.

Additional comparisons between the AEM inversion results and borehole resistivity and lithology logs along AEM Reconnaissance flight lines L710101 in the 312-flight area and L730201 in the 304M-flight area (Figure 5-26 and Figure 5-27, respectively). On L730201 note the very good match between resistivity log MW-CSU1 in the center of the profile and the AEM inversion results. Resistivity log VMW-36 agrees very well with the AEM-interpreted contacts between the ***Tt***, ***Tupvf***, and the ***Tl***.

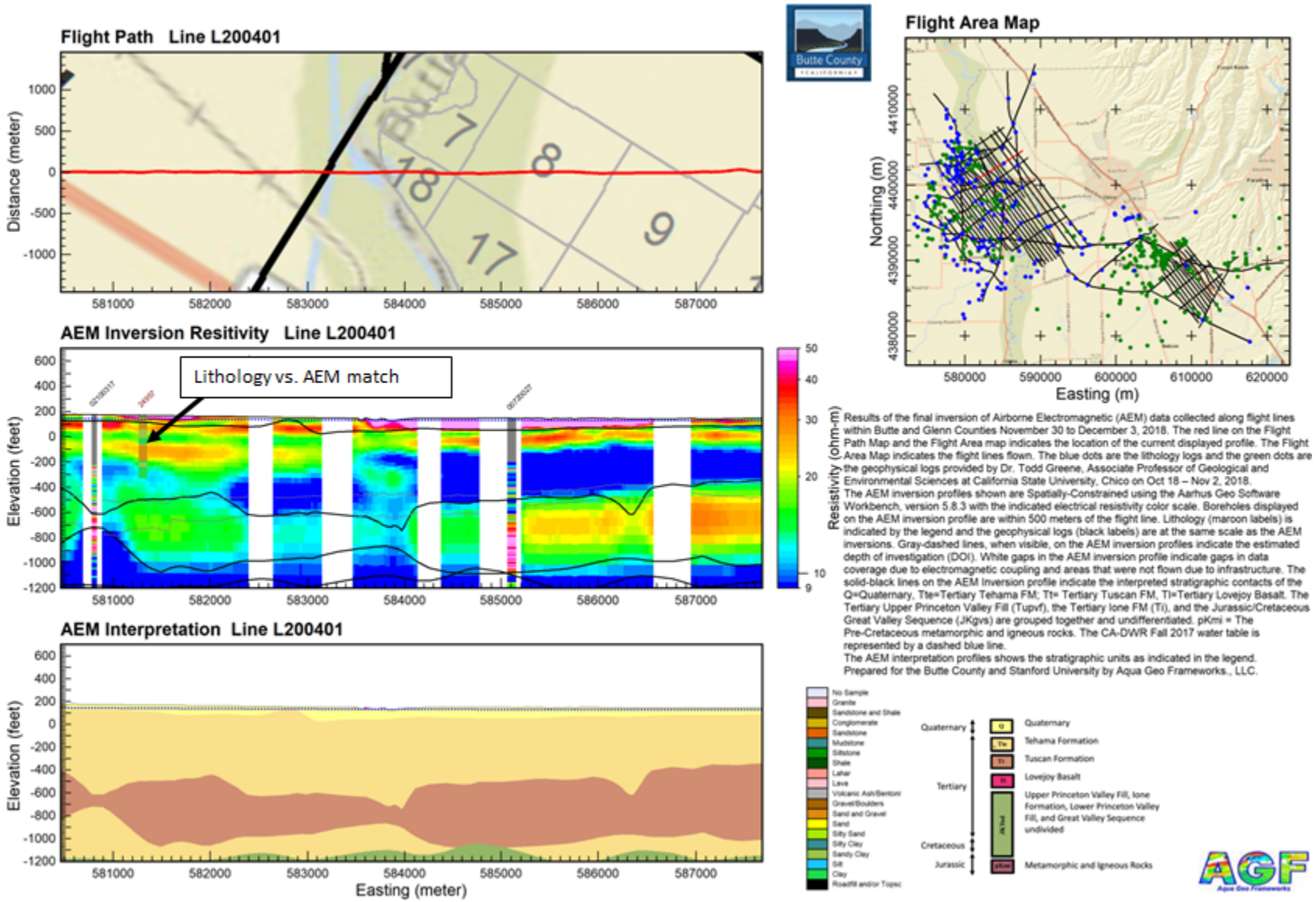

Figure 5-16. Comparison of borehole resistivity and lithology logs and AEM flight line L200401. Note the good lithology match of lithology log *24957* and the AEM inversion results on the left side of the profile as well as resistivity log *720027* towards the center of the profile.

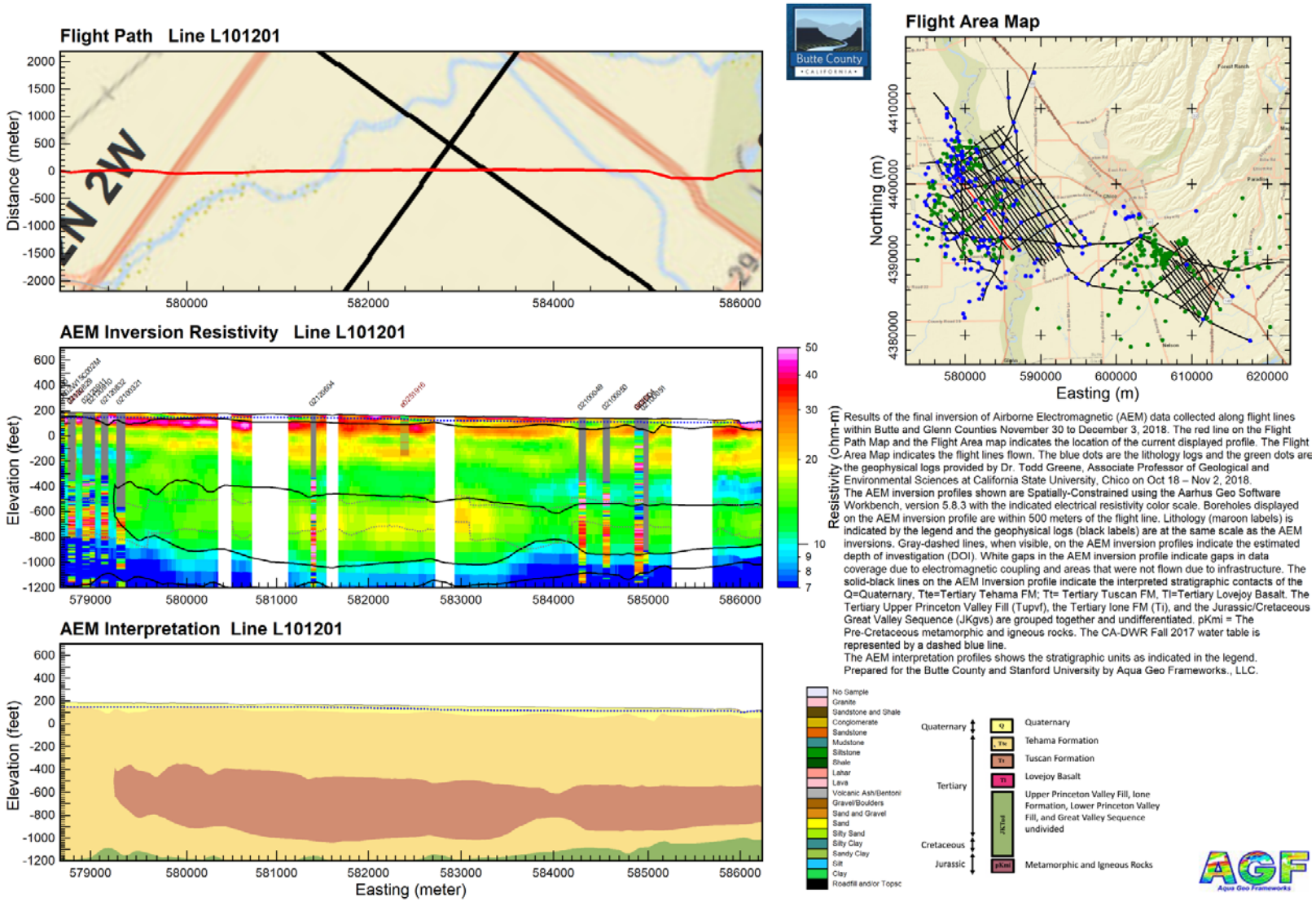

Figure 5-17. Comparison of borehole resistivity and lithology logs and AEM flight line L101201. The resistive zones on the borehole logs line up nicely with the resistive AEM inversion results in what's been interpreted as the Tuscan FM. However, some are outside the contact on the left side. Also note the good lithology match of log *e0251916* with the AEM in the upper Tehama FM in the center of the profile.

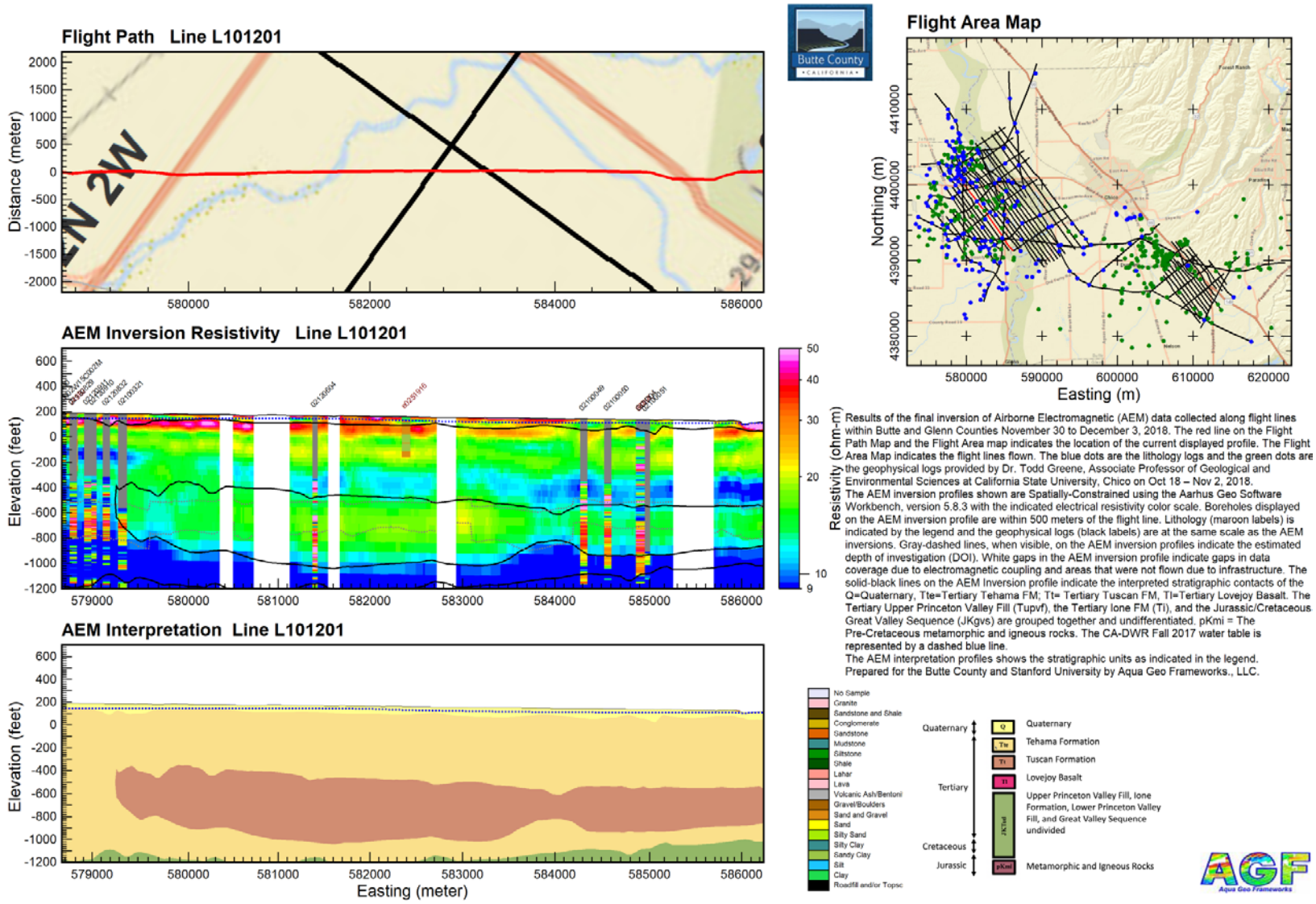

Figure 5-18. This is the same interpreted profile as in Figure 5-17 for L101201 except that the resistivity scale has been changed from 7 – 50 ohm-m to 9 – 50 ohm-m. Note that this scale the AEM results indicate more conductive material where the logs are saying it is resistive.

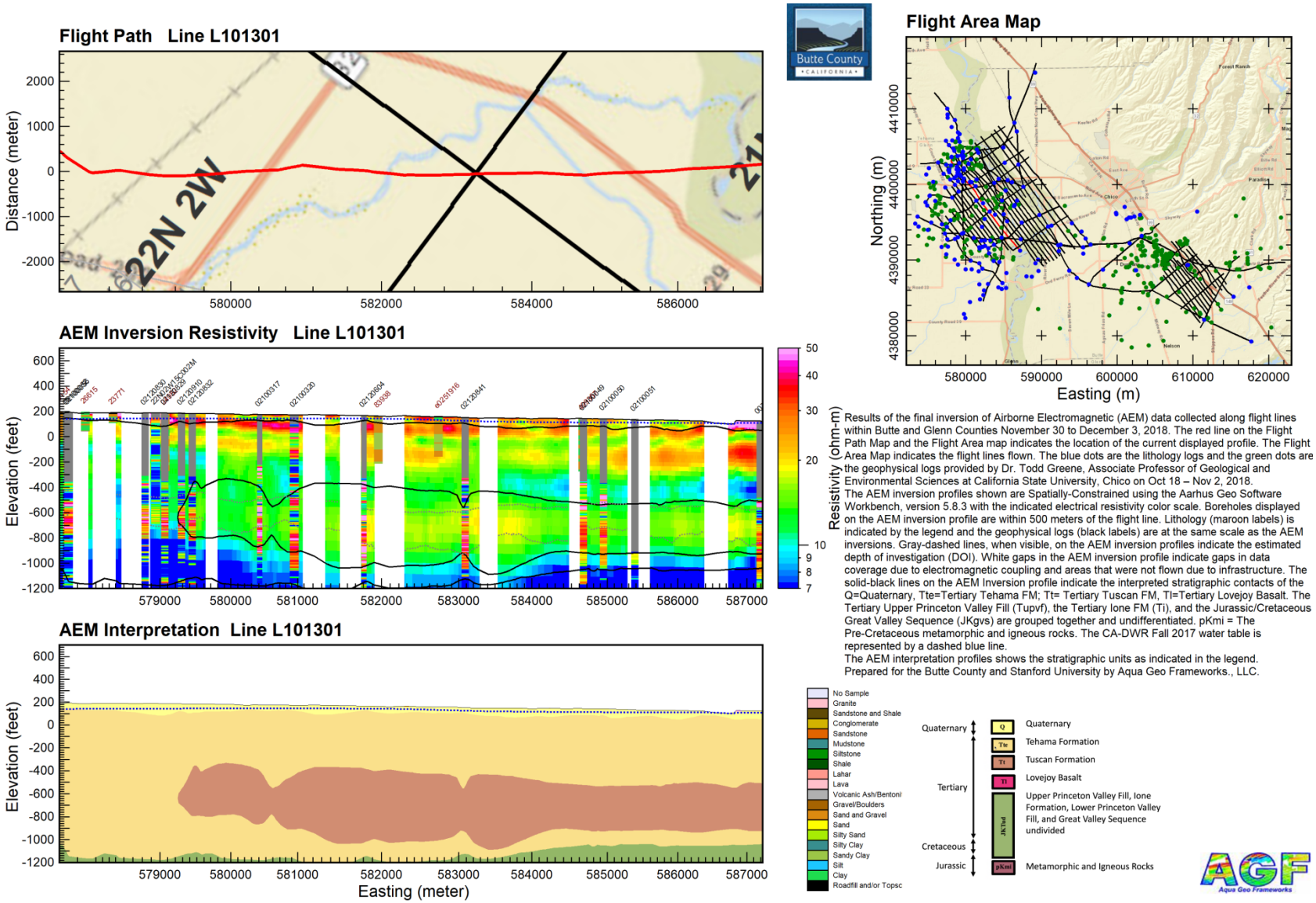

Figure 5-19. This is the next line to the northeast from L101201 in Figure 5-18, L101301. Note again the resistive zone in the borehole logs just outside the interpreted Tuscan FM contact.

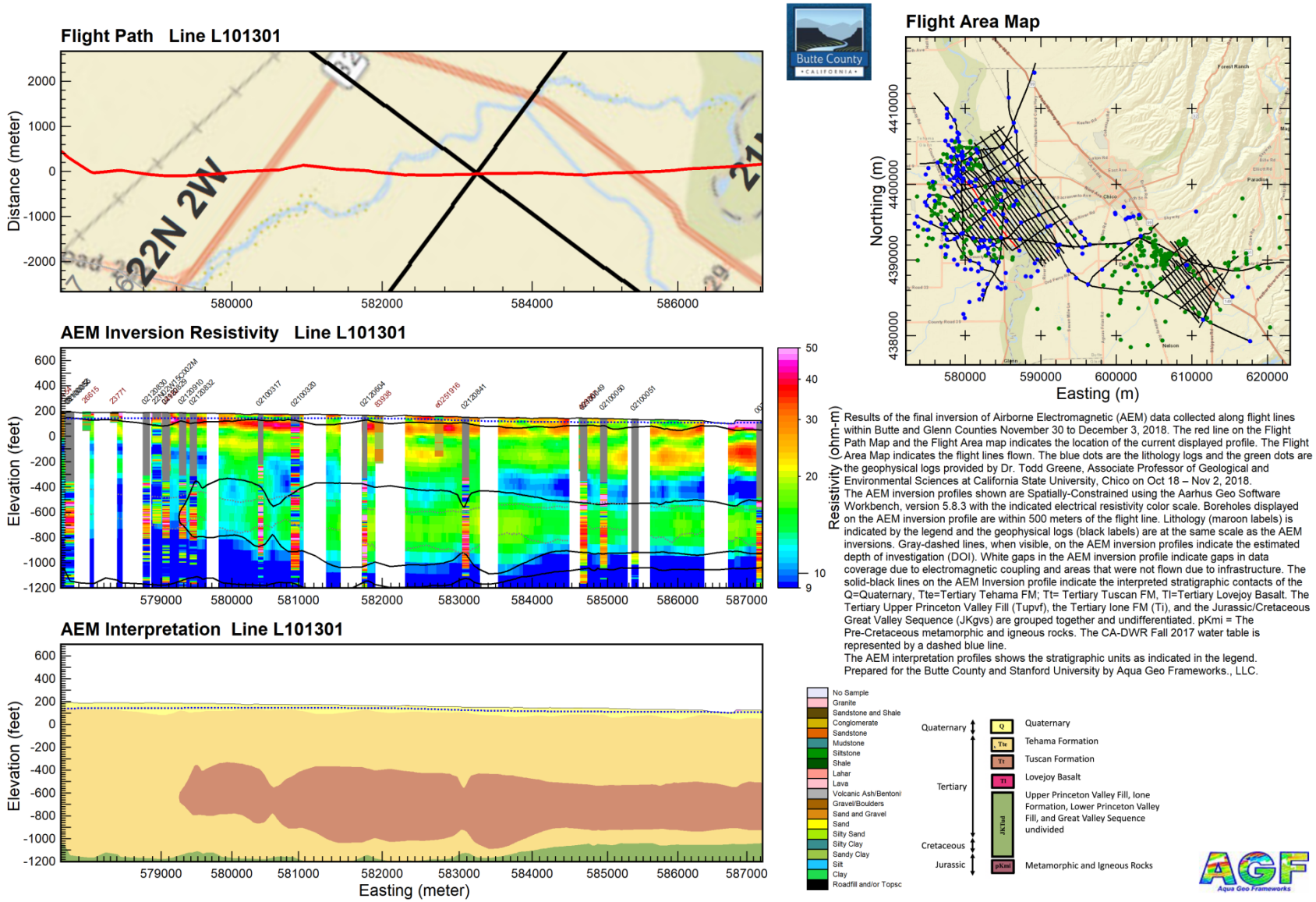

Figure 5-20. This is the same profile, L101301, as in Figure 5-19 except that the resistivity scale has changed from 7 – 50 ohm-m to 9 – 50 ohm-m. The area behind the resistive zone in the borehole logs has become bluer, indicating more conductive material.

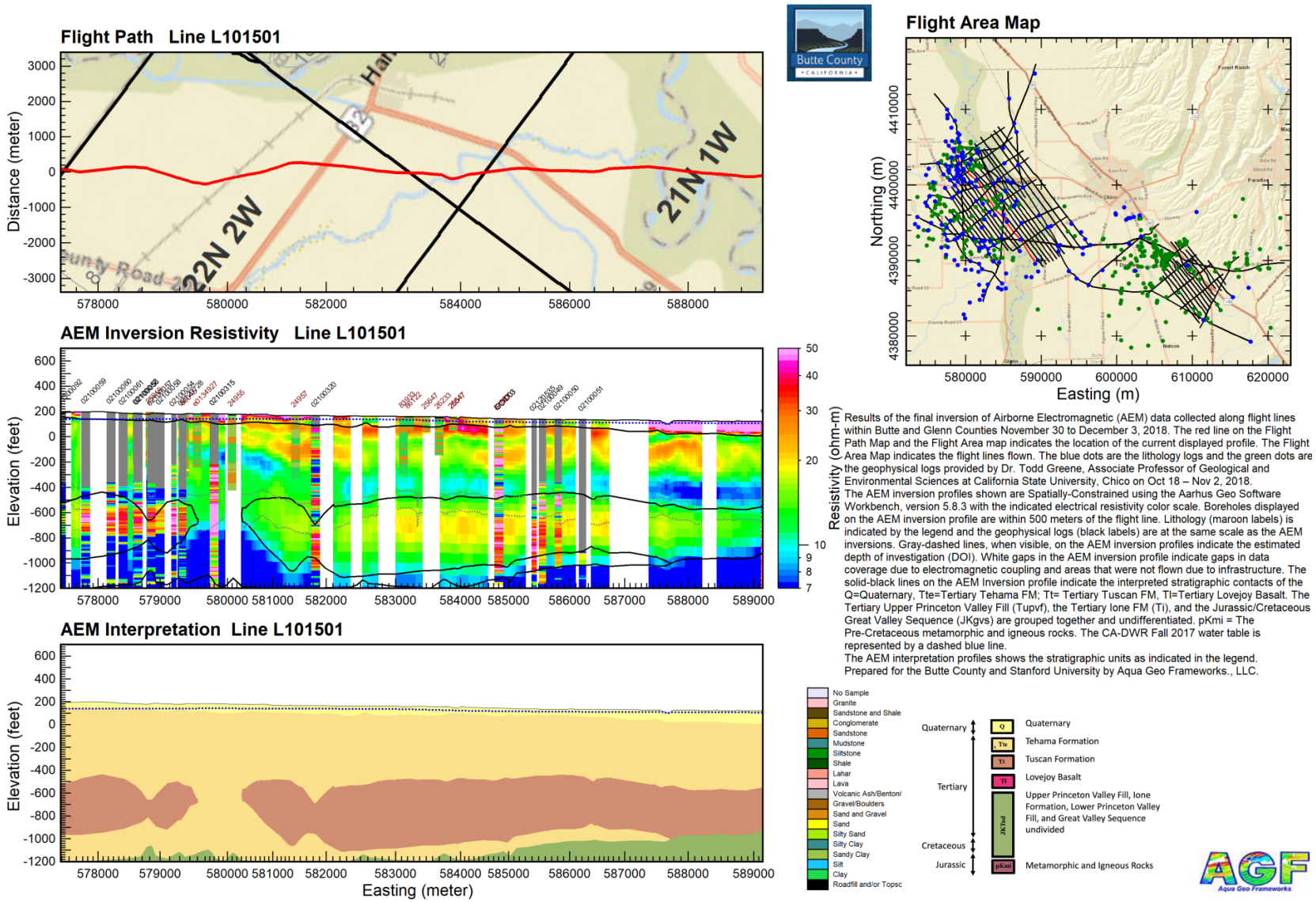

Figure 5-21. Comparison of borehole resistivity and lithology logs and AEM flight line L101501. Note the good match of the resistivity logs with the AEM in the Tuscan FM as well as the good correlation of the AEM with lithology logs *24957* (also on L200401) and *86122*.

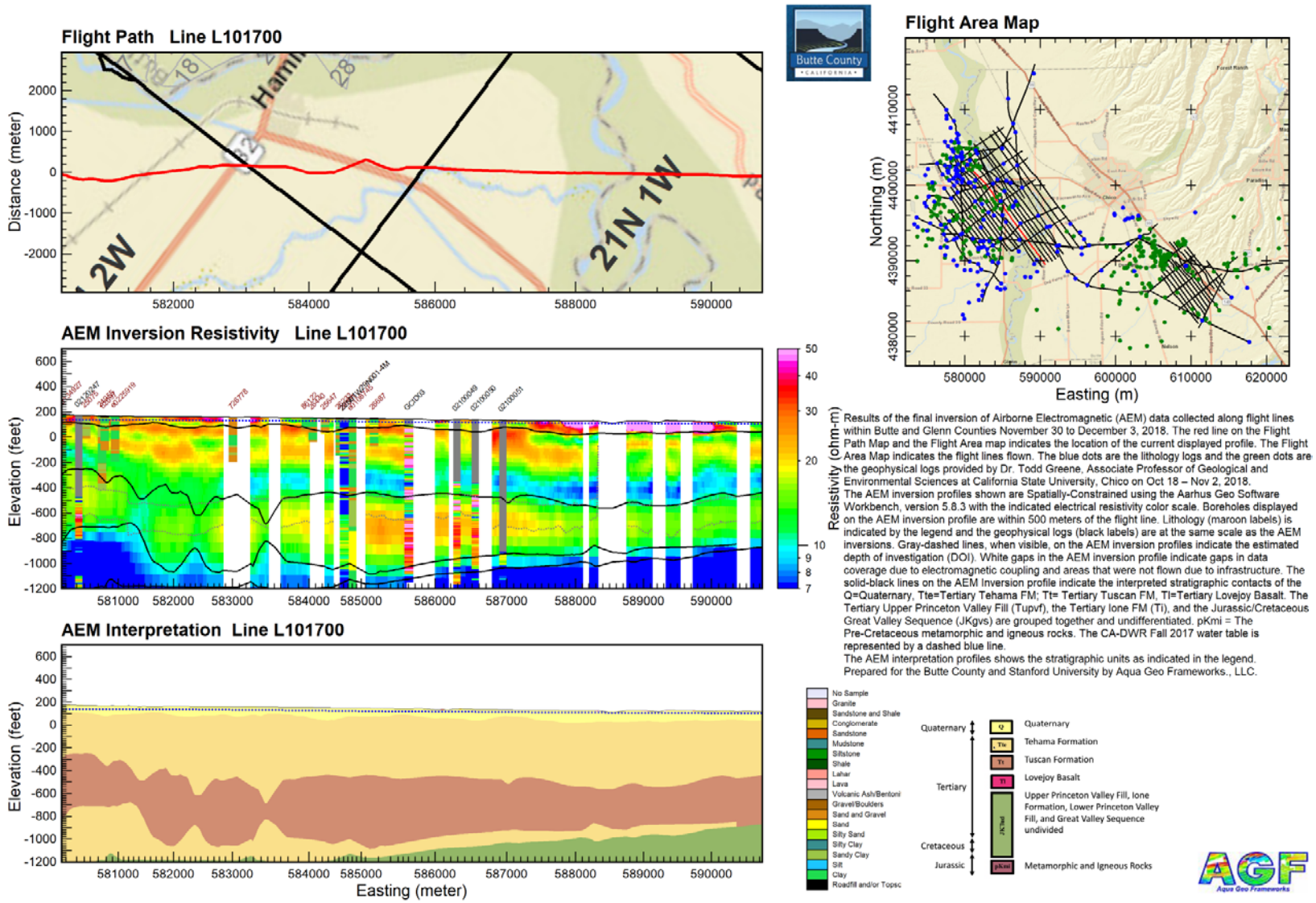

Figure 5-22. Comparison of borehole resistivity and lithology logs with AEM flight line L101700. The resistivity logs match well except for log *22N01W29N001-4M* which appears to be poorly calibrated. Lithology logs 24955, 82097, e0225919, 726778, 26440, 25647, and 26687 all match the AEM very well.

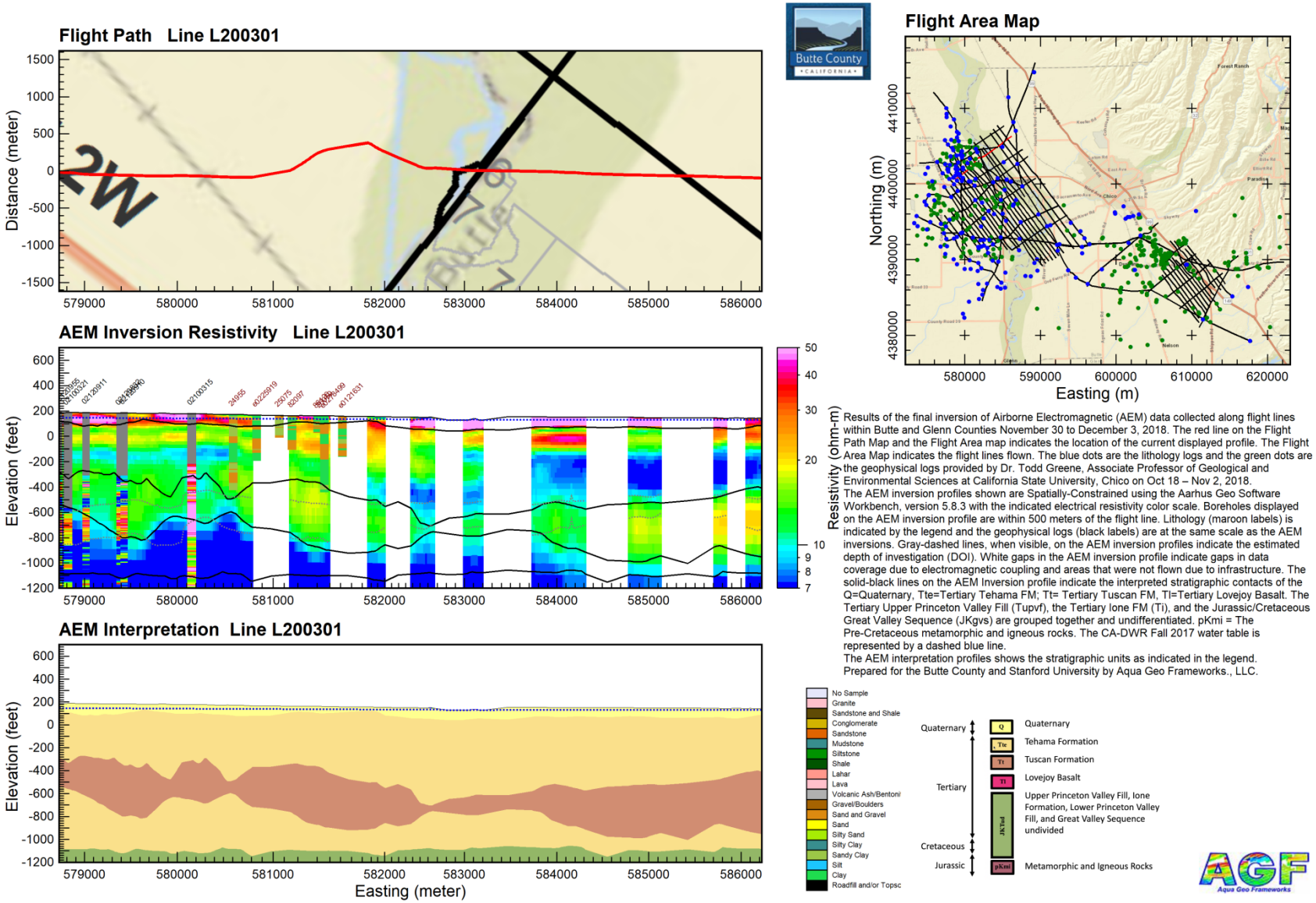

Figure 5-23. Both lithology and resistivity logs match the AEM inversion results for L200301 very well except on the very far left.

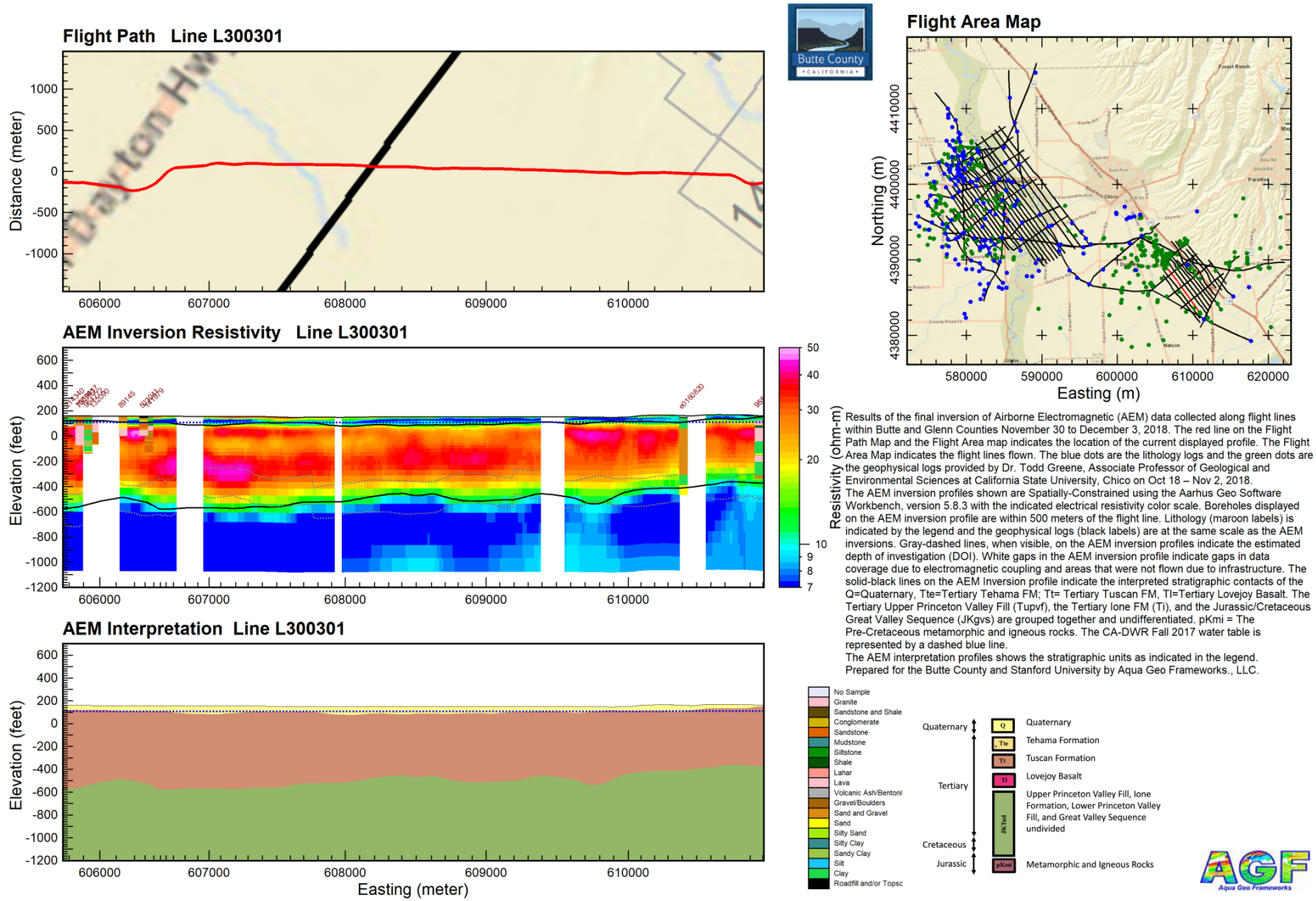

Figure 5-24. AEM flight line L300301 in the 304M AEM flight area. Note the very good match between lithology log *e0160820* on the right side of the profile and the AEM inversion results.

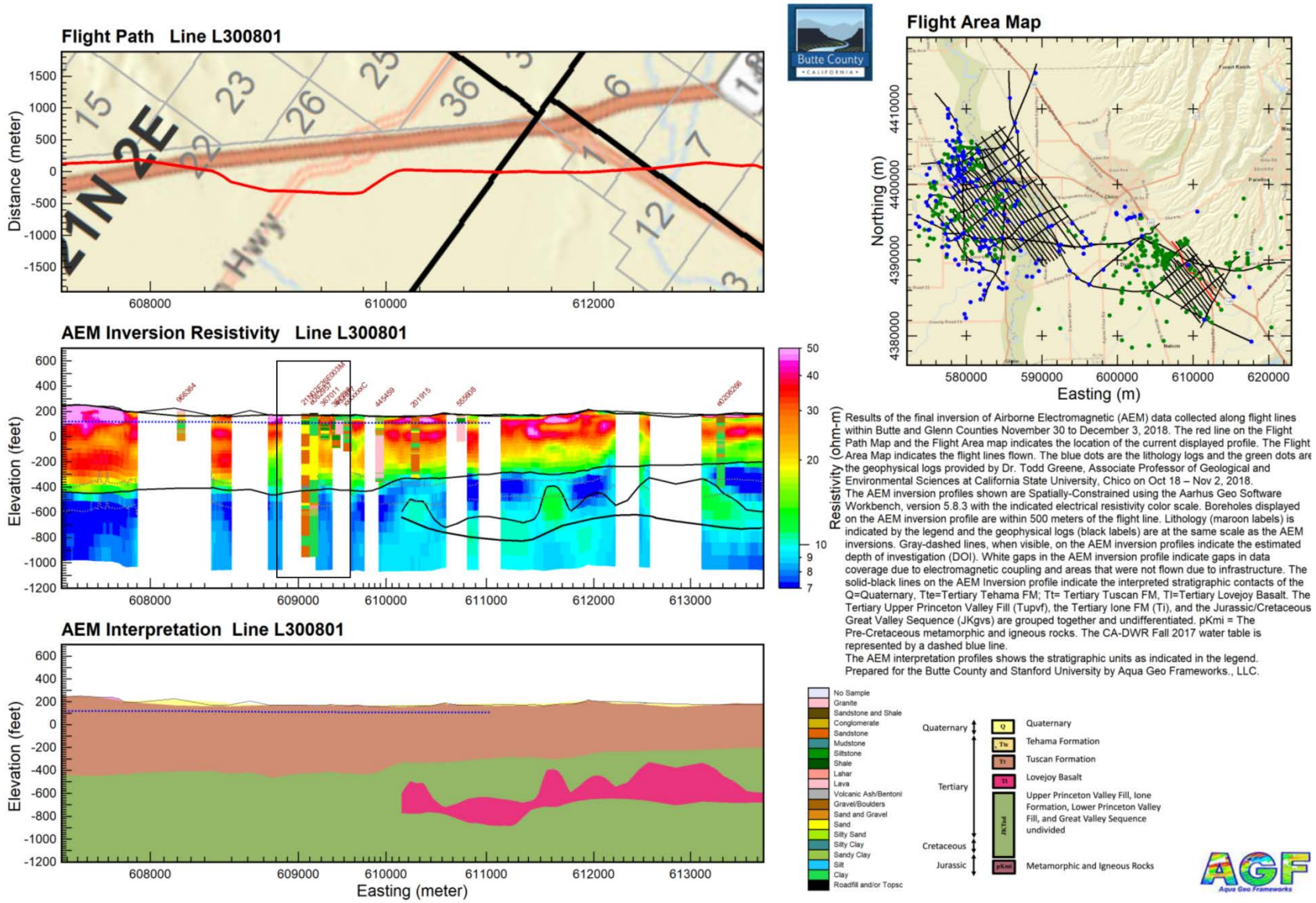

Figure 5-25. AEM flight line L300801 in the 304M AEM flight area. Note the very good match between lithology log *e062957* and the very poor match with log 21N02E26E003M.

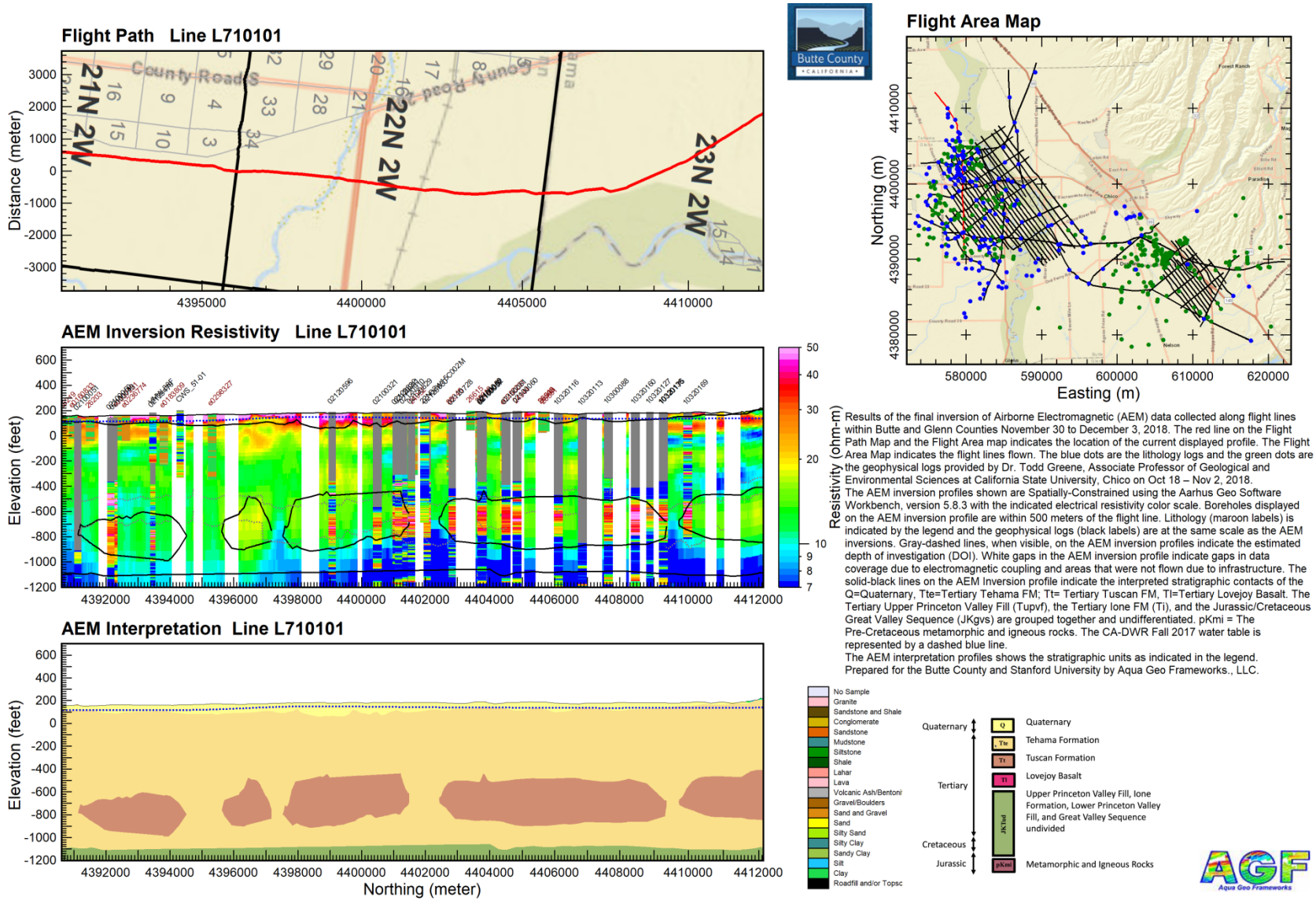

Figure 5-26. AEM Reconnaissance flight line L710101 in the 312 AEM flight area. There is a very good match with the resistivity logs along this profile.

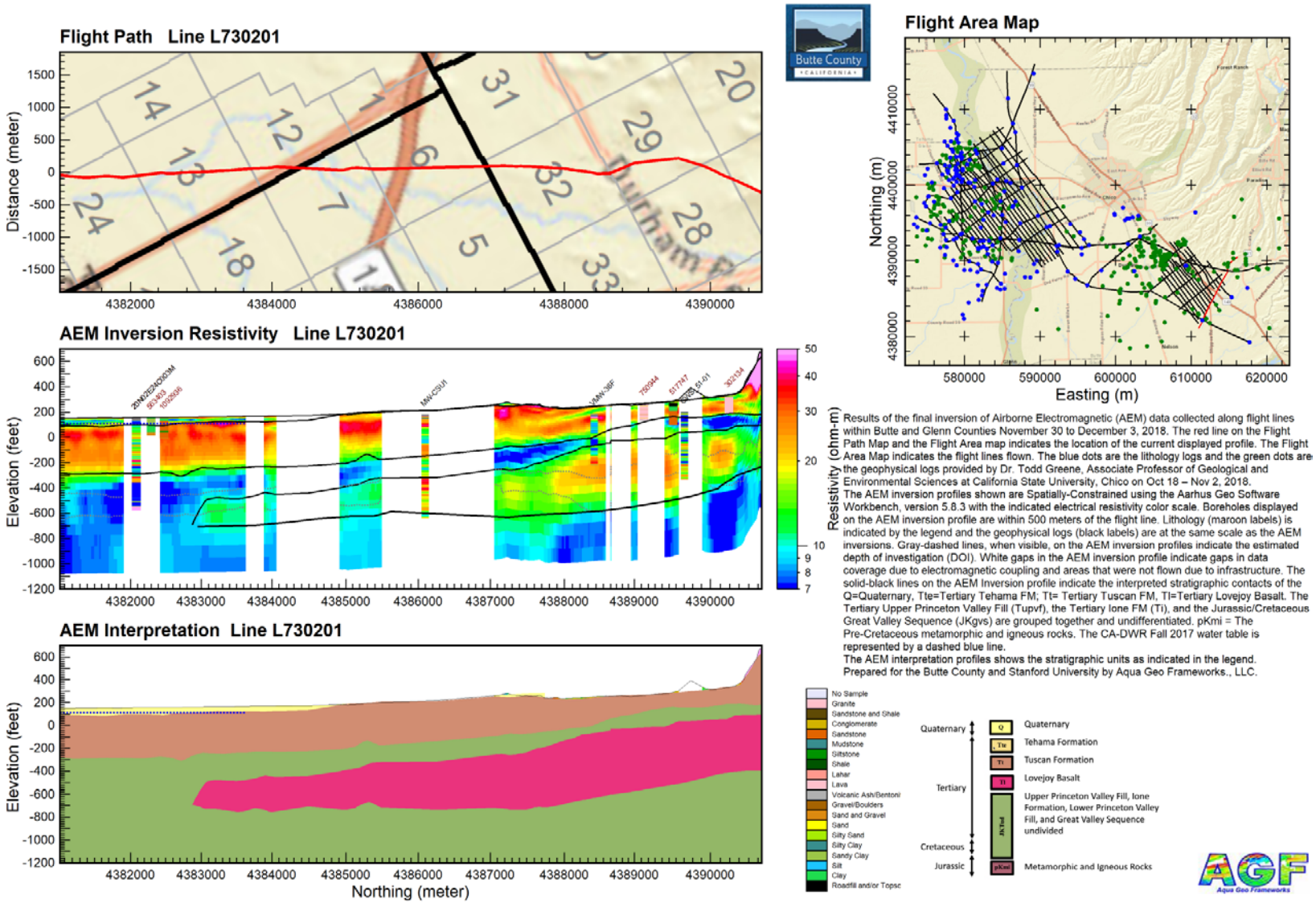

Figure 5-27. AEM Reconnaissance flight line L730201 in the 304 AEM flight area. Note the very good match between resistivity logs MW-CSU1 in the center of the profile with the AEM inversion results and resistivity log VMW-36F located across the Tuscan, Upper Princeton Valley Fill, and Lovejoy Basalt contacts.

5.4 Comparison of CA-DWR (2014) Cross-Sections and the AEM Inversion Results

Part of the analysis of the Butte AEM investigation was a comparison between the AEM earth-model inversion results and the cross-sections that were published as part of a report (CA-DWR, 2014) on the geology of the northern Sacramento Valley. Portions of those cross-sections (B-B', E-E', and F-F') are included in Section 2 and were discussed earlier. The CA-DWR (2014) cross-sections present interpretations of the stratigraphy in the vicinity of the AEM investigation area based on surface geologic mapping and available borehole information.

After some thought it was decided that the best way to compare the CA-DWR (2014) cross-sections to the AEM inversion results is to examine them together in the stratigraphic realm in three dimensions (3D) as a fence diagram. Initially, the AEM inversion results represented as interpreted stratigraphy will be presented and then the CA-DWR (2014) cross-sections will be added into the view and then discussed.

A 3D fence diagram of the stratigraphic interpretation of the Butte AEM flight lines, including both Reconnaissance and Block flight lines and looking to the north, is presented in Figure 5-28. The color scale for the AEM stratigraphy is in Figure 5-6. Just the western (312) and eastern (304M) area Block flights are presented in Figure 5-29, looking north-northeast and looking to the southwest in Figure 5-30. Figure 5-31 presents a 3D fence diagram of all the AEM Reconnaissance flight lines with their stratigraphic interpretation, looking to the northeast. An alternate view of the Butte AEM interpreted Reconnaissance flight lines as a 3D fence diagram is presented in Figure 5-32, looking to the southwest.

CA-DWR (2014) cross-sections B-B' and E-E' are introduced to the view of the AEM Reconnaissance flight lines in Figure 5-33. The view is looking south along cross-section E-E' and so the details on cross-section E-E' are not visible. In comparing the AEM stratigraphic interpretation with CA-DWR (2014) cross-section B-B' several observations stand out. The first is that the general stratigraphy is similar for both the AEM earth-model and the cross-section B-B' as the lines proceed out from the Sierra Nevada foothills.

The next thing are the differences between the two. Especially in the middle of the view where one AEM flight line crosses B-B' at the level of the ***Tt*** in B-B'. What we see are two different colored units (AEM ***Tt*** and ***Tte*** formations yellow over brown) crossing into one colored unit (the thick brown ***Tt*** on B-B'). The AEM interpretation at that location is that there is both ***Tte*** and ***Tt*** at that location but that the ***Tte*** is thinning out towards the east, i.e. towards the left. This is the location discussed earlier in Section 5.1.3 about the uncertainty in the location of the ***Tte*** contact along cross-section B-B'. The discussion was on whether the ***Tte*** thinned out under the Sacramento River or continued east a little further and then thinned out. What is observed in Figure 5-33 is the result of this difference in interpretation. On the Reconnaissance flight lines behind cross-section B-B' in Figure 5-33 the ***Tte*** can be observed to be thinning to the east.

A second view of the combined cross-sections B-B' and E-E' and the AEM interpreted stratigraphy is presented in Figure 5-34. The view is now to the northwest and the side of cross-section E-E' is visible. It can be observed that 304M Reconnaissance lines L730100 and L730300 are crossing E-E'. What is observed at the intersection of these lines is that E-E' shows ***Tt*** and the AEM shows ***Tt*** and a shallower

depth to the top of the undivided ***Tupvf-Ti-JKgvs*** material. Going back to cross-section E-E' in CA-DWR (2014), it can be observed that there are questions marks "?" also on the ***Tupvf*** contact implying that the depth to the contact is not certain and so it could be higher if there were other information available (such as AEM).

A third view of the AEM inversion results and cross-sections B-B' and E-E' is presented in Figure 5-35. The view is to the northeast. Cross-section B-B' is in the foreground and E-E' runs along the view in the back. There are seven items of interest in this view that really boil down to just two. The first six deal with how the AEM lines cross into B-B' and E-E' in terms of which units and which depths are the contacts at the crossing. What is interesting is that at the location of where the first AEM Reconnaissance line in the foreground (L710101) crosses into B-B', the size of the piece of ***Tt*** on the AEM line is small and the ***Tt*** layer on the cross-section is thin. Whereas on the second line, L710201, both are thicker. There is some congruence in that. The discussion on the location and thinning of the ***Tte*** as it progresses east describes the other five AEM Reconnaissance line intersections with B-B' and E-E' in Figure 5-35.

The other main item of interest in Figure 5-35 is that the Lovejoy Basalt, or at least what appears to be the ***Tl*** on both B-B' and E-E', goes under the AEM Reconnaissance lines. That is, the depth to the top of the ***Tl*** at these locations is greater than the Depth of Investigation (DOI, Section 4.5) of the SkyTEM 304M used in area of the investigation. An alternate view of this situation is presented in Figure 5-36 where the ***Tl*** out in the Valley is deeper than the bottoms of the AEM profiles acquired by the 304M.

A third view of the "too deep" ***Tl*** is presented in Figure 5-37.

Now it may be that the view of the ***Tl*** on B-B' in Figure 5-38 could be indicating that the lava flow may not have extended out far enough into the Valley to possibly be imaged by the 312 system. But, again, the top of the ***Tl*** appears to also be below the DOI for the 312, based on the acquired data from this investigation.

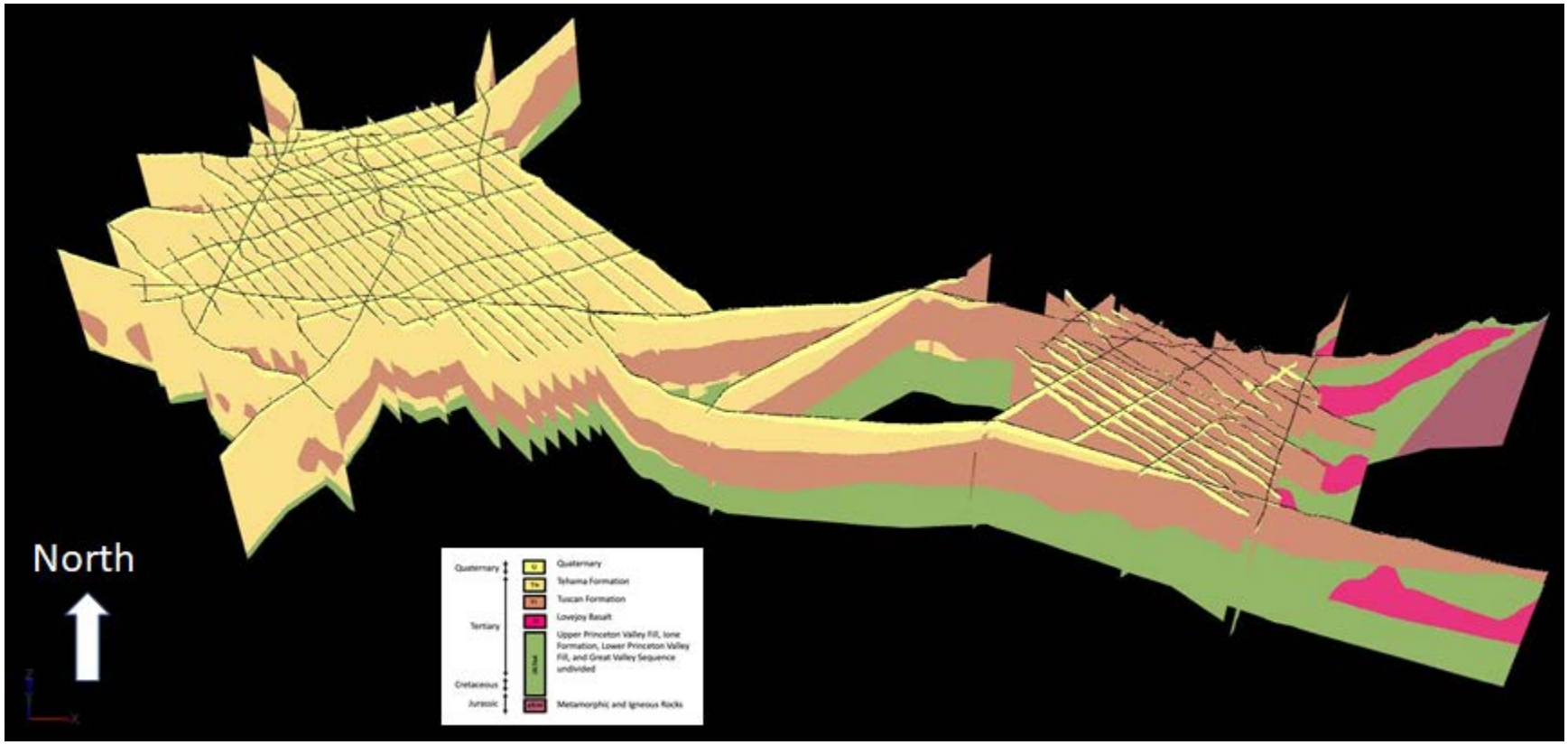

Figure 5-28. 3D fence diagram of the stratigraphic interpretation of the Butte AEM flight lines, including both Reconnaissance and Block flight lines, looking to the north. The color scale for the AEM stratigraphy is in Figure 5-6.

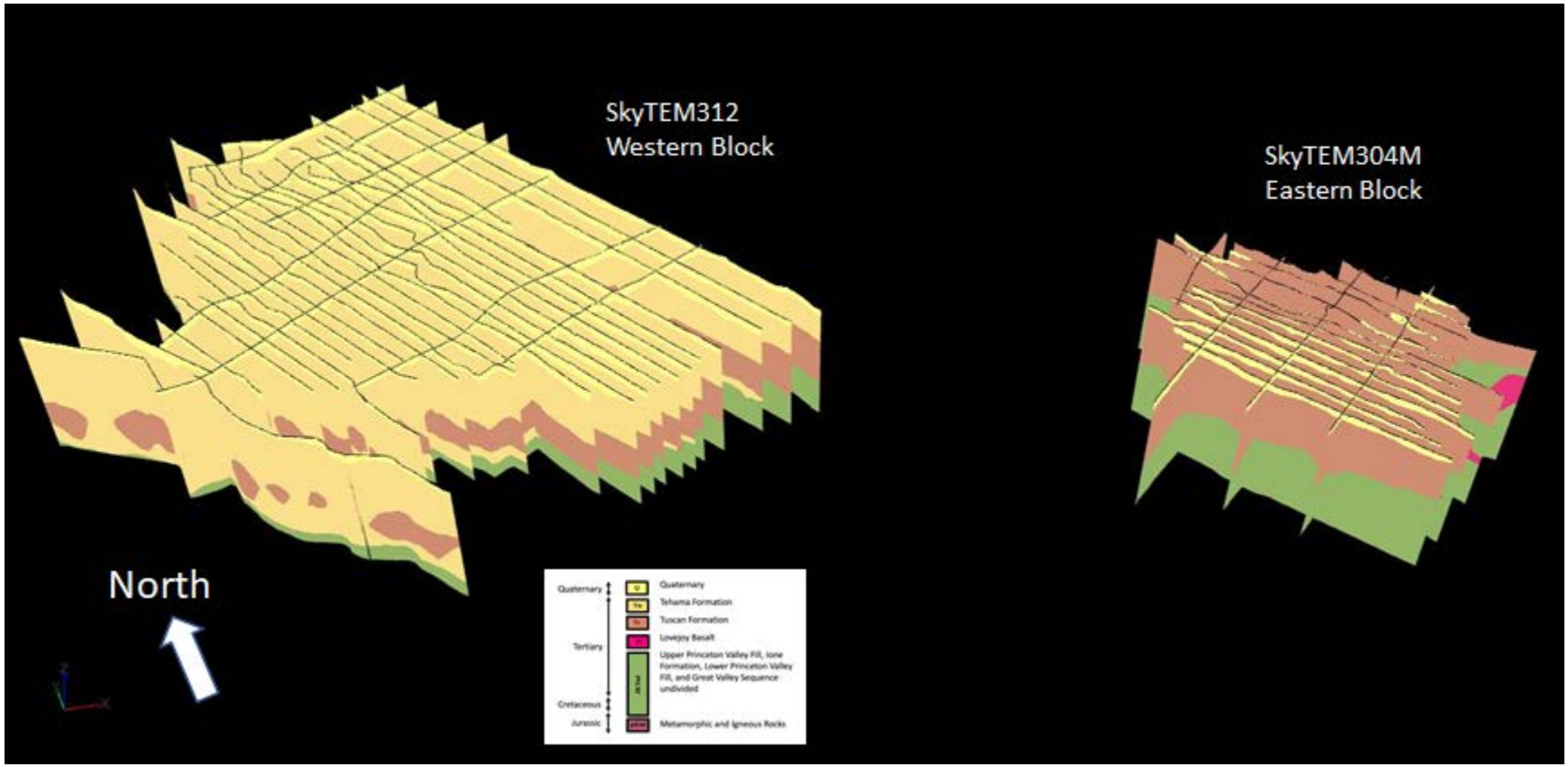

Figure 5-29. 3D fence diagram of the stratigraphic interpretation of the Butte AEM Block flight lines, looking to the north-northeast. The western (312) area is to the left and the eastern (304M) area is on the right. The color scale for the AEM stratigraphy is in Figure 5-6.

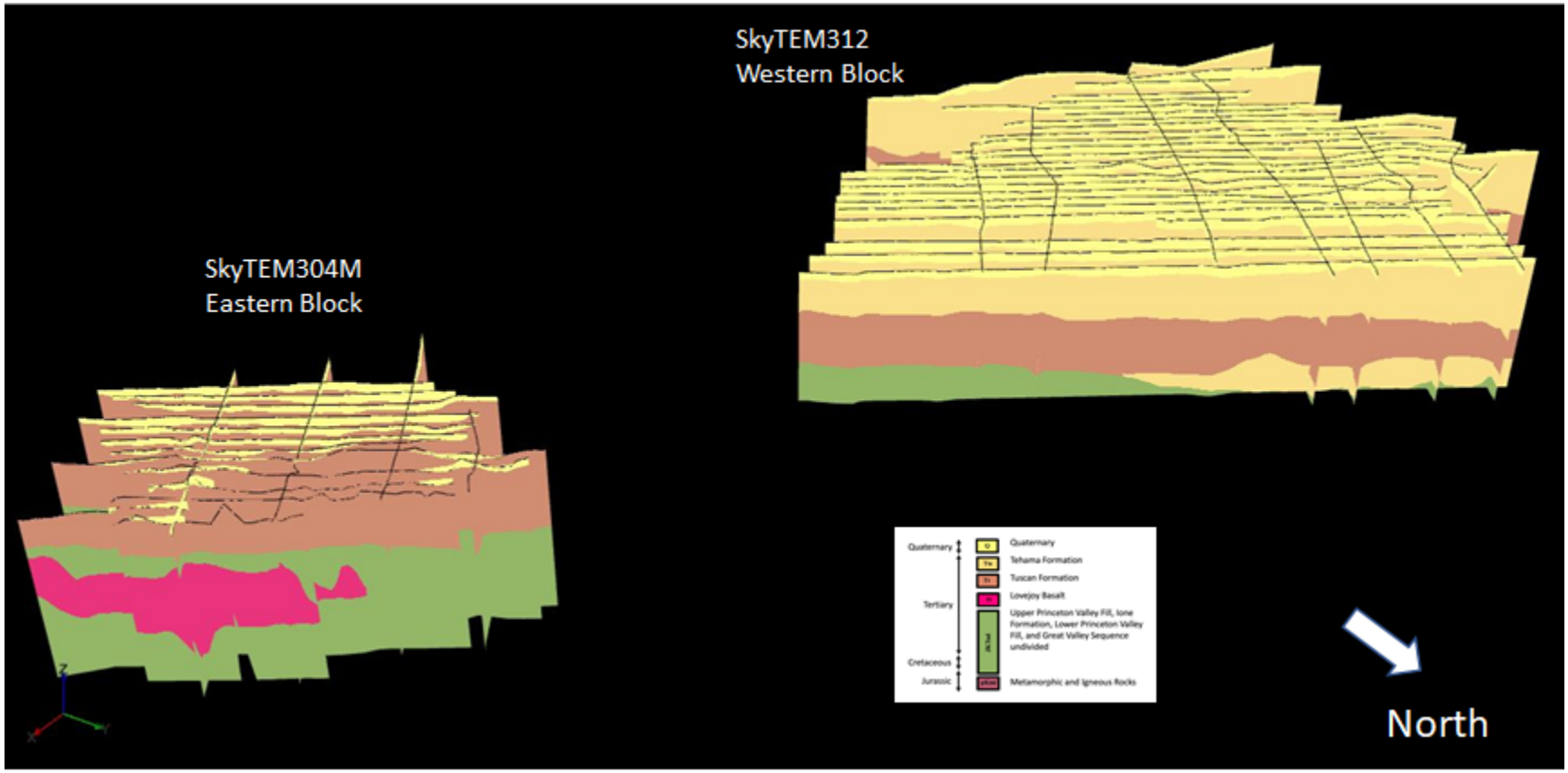

Figure 5-30. 3D fence diagram of the stratigraphic interpretation of the Butte AEM Block flight lines, looking to the southwest. The western (312) area is to the left and the eastern (304M) area is on the right. The color scale for the AEM stratigraphy is in Figure 5-6.

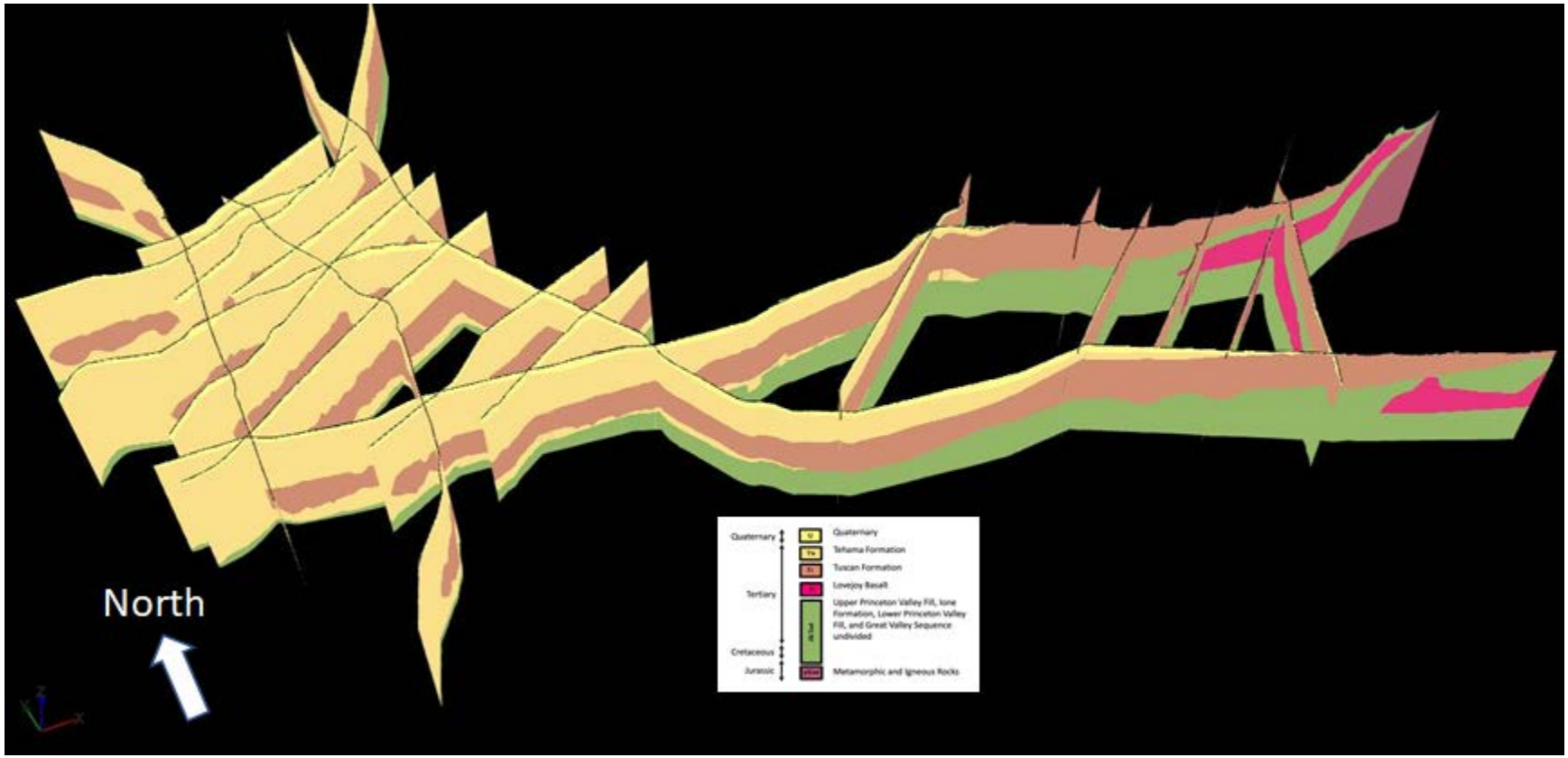

Figure 5-31. 3D fence diagram of the stratigraphic interpretation of the Butte AEM Reconnaissance flight lines looking to the northeast. The color scale for the AEM stratigraphy is in Figure 5-6.

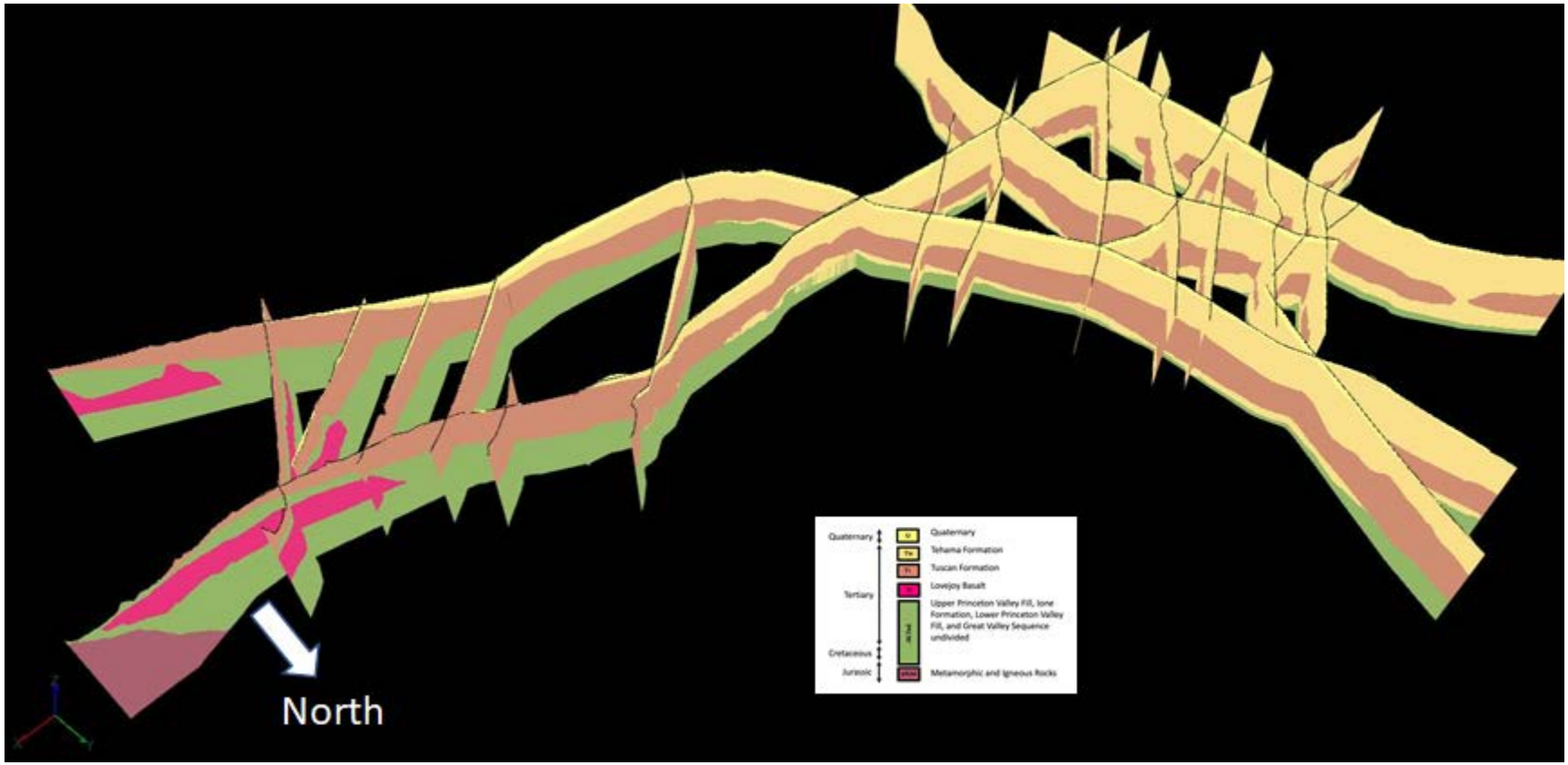

Figure 5-32. 3D fence diagram of the stratigraphic interpretation of the Butte AEM Reconnaissance flight lines looking to the southwest. The color scale for the AEM stratigraphy is in Figure 5-6.

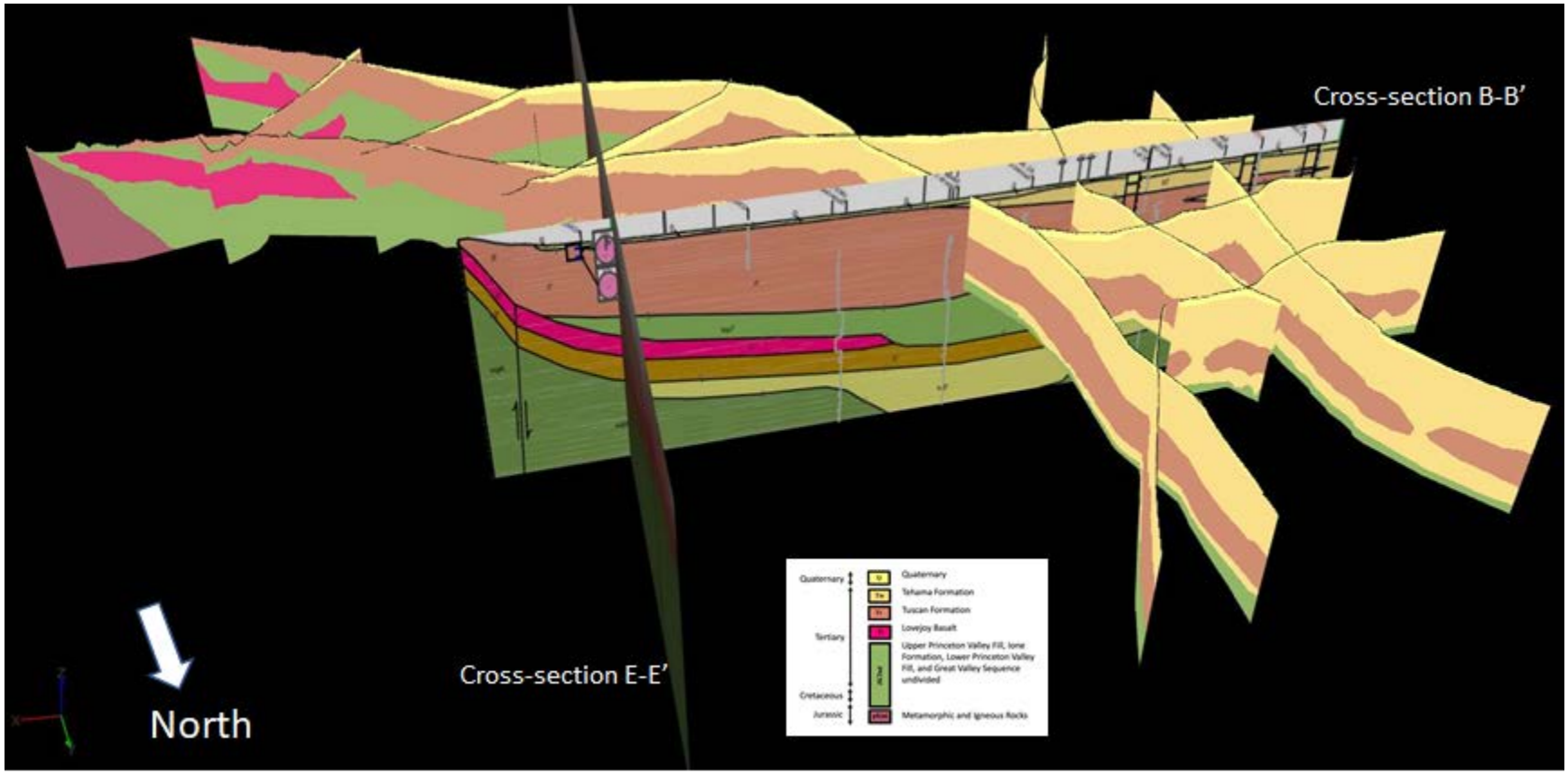

Figure 5-33. 3D fence diagram of the stratigraphically-interpreted Butte AEM Reconnaissance flight lines with CA-DWR (2014) cross-sections B-B' and E-E'. The view is looking south along cross-section E-E'. The color scale for the AEM stratigraphy is in Figure 5-6.

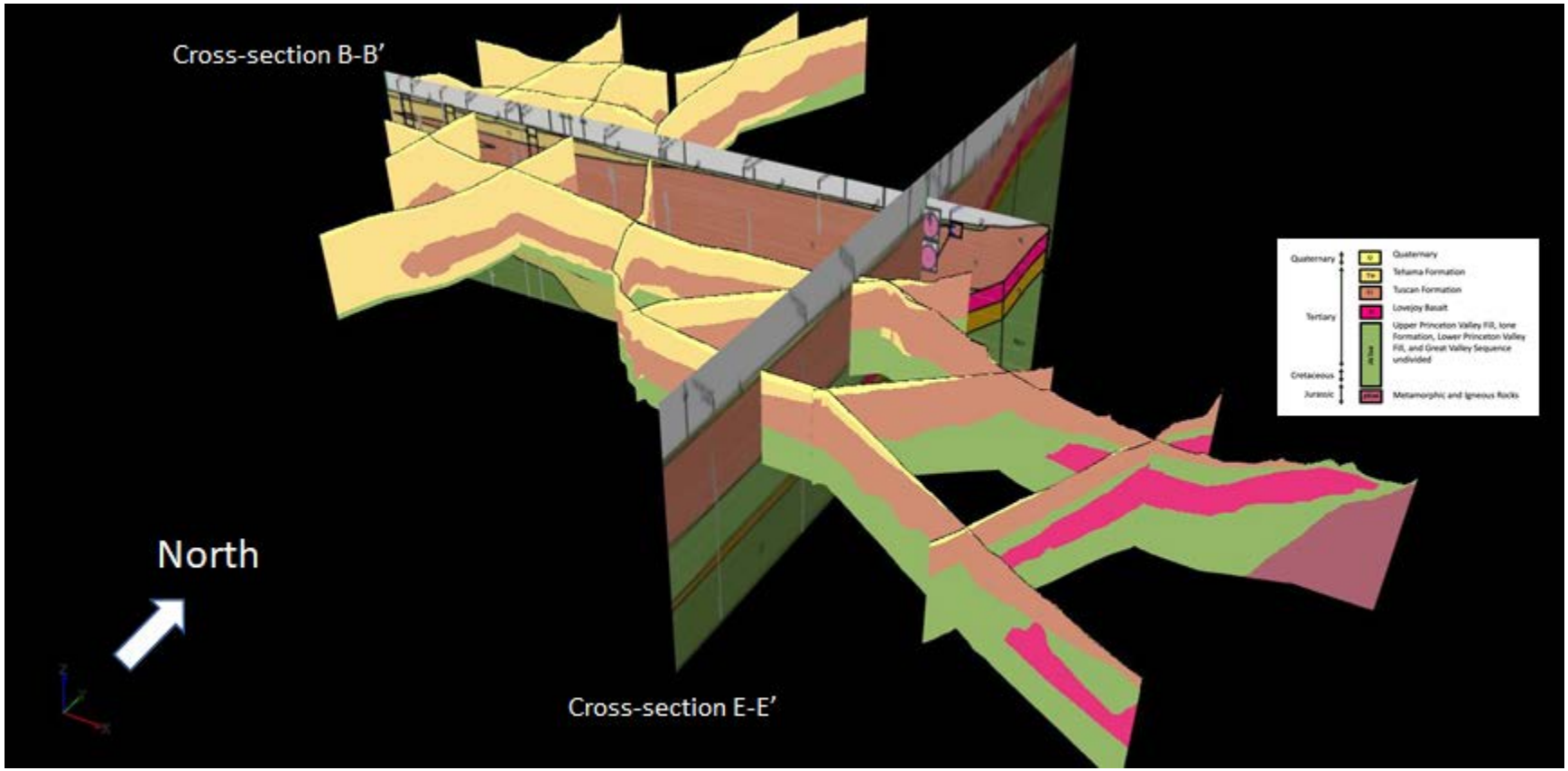

Figure 5-34. 3D fence diagram of the stratigraphically-interpreted Butte AEM Reconnaissance flight lines with CA-DWR (2014) cross-sections B-B' and E-E'. The view is looking northwest. The color scale for the AEM stratigraphy is in Figure 5-6.

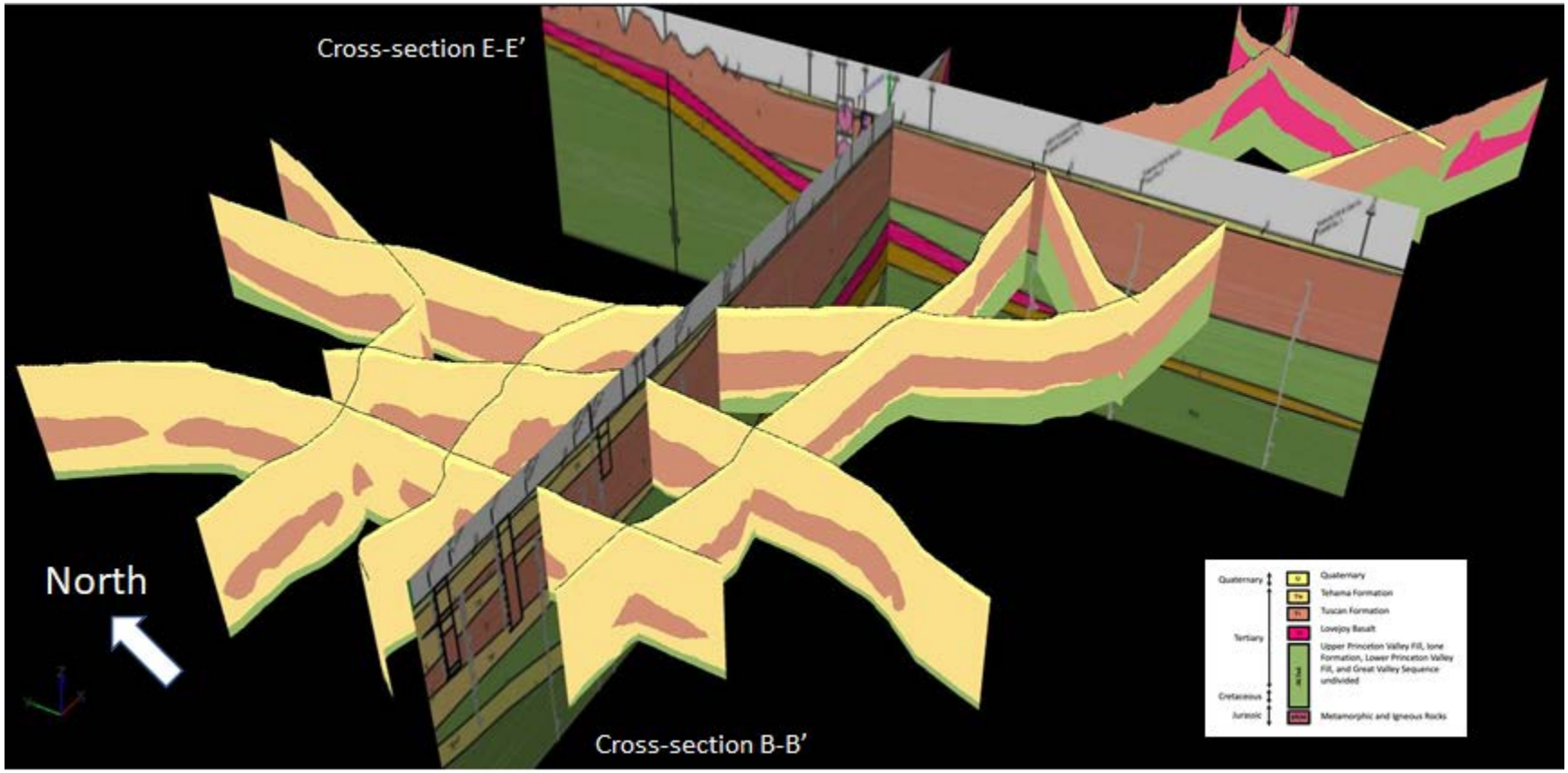

Figure 35. 3D fence diagram of the stratigraphically-interpreted Butte AEM Reconnaissance flight lines with CA-DWR (2014) cross-sections B-B' and E-E'. The view is looking northeast. The color scale for the AEM stratigraphy is in Figure 5-6.

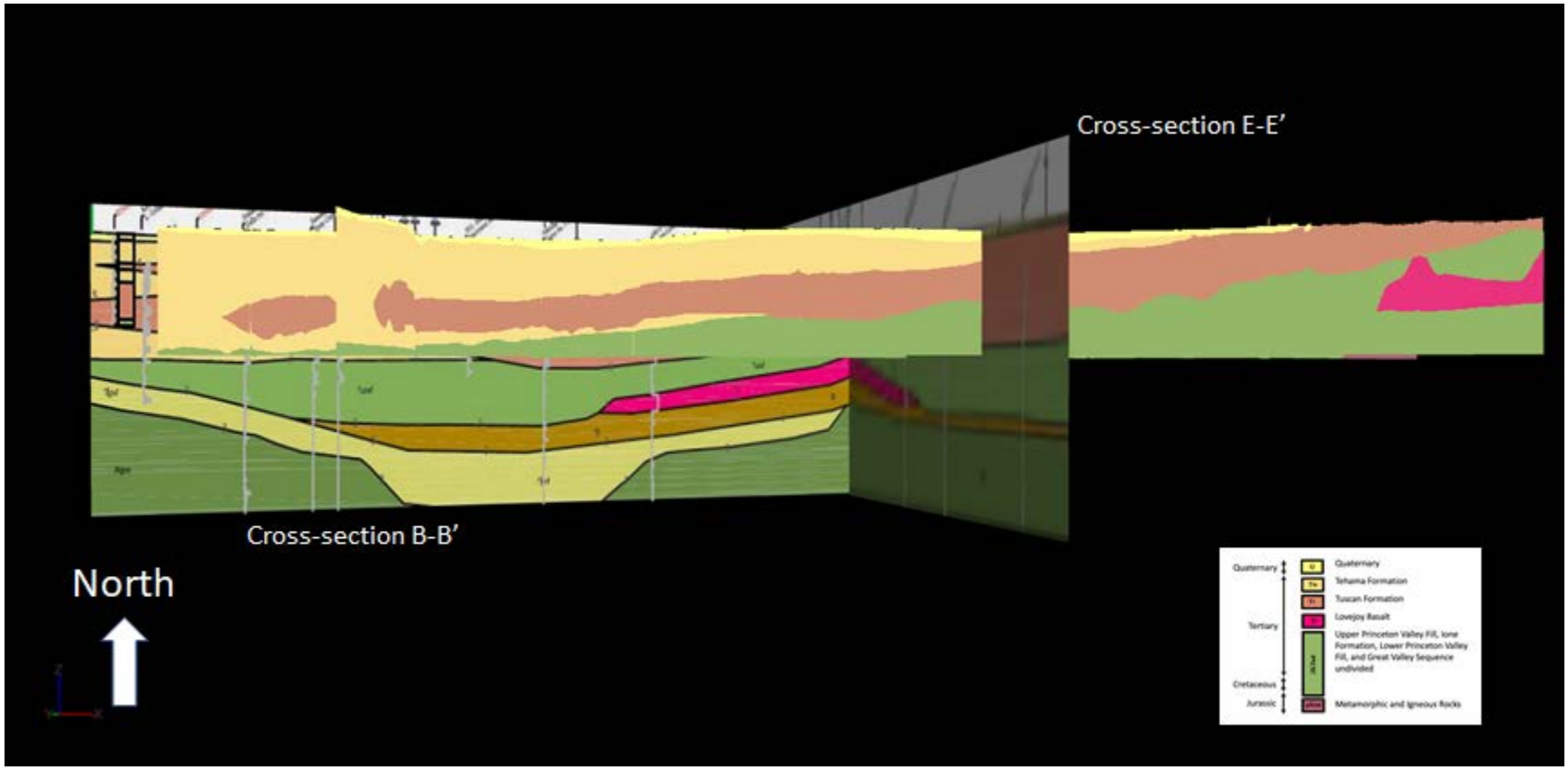

Figure 5-36. An alternate view of the Lovejoy Basalt being "too deep" out in the Valley and below the Depth of Investigation of the SkyTEM304M.

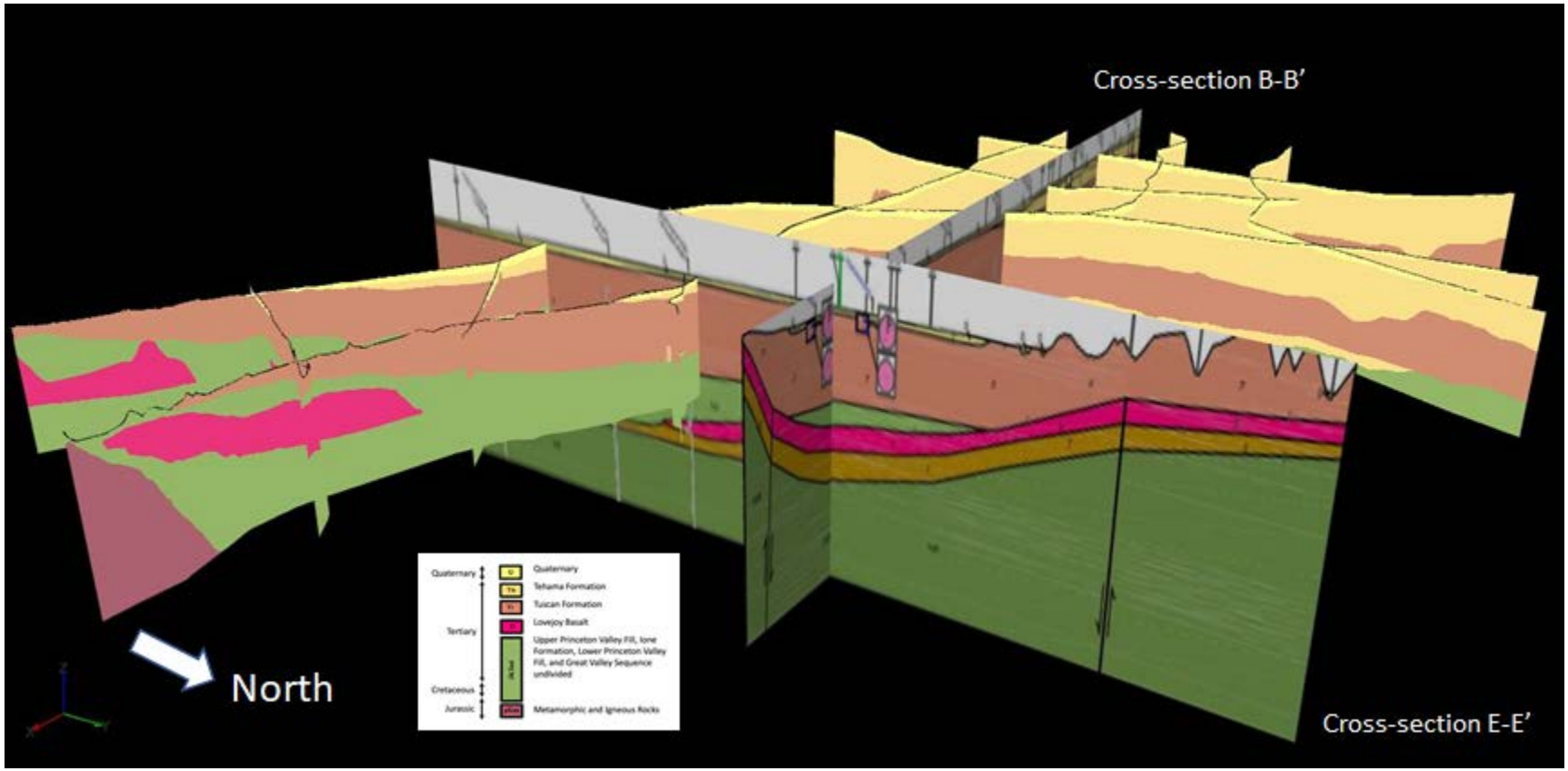

Figure 5-37. A third view of the "too deep" Lovejoy Basalt below the Depth of Investigation (DOI) of the SkyTEM304M.

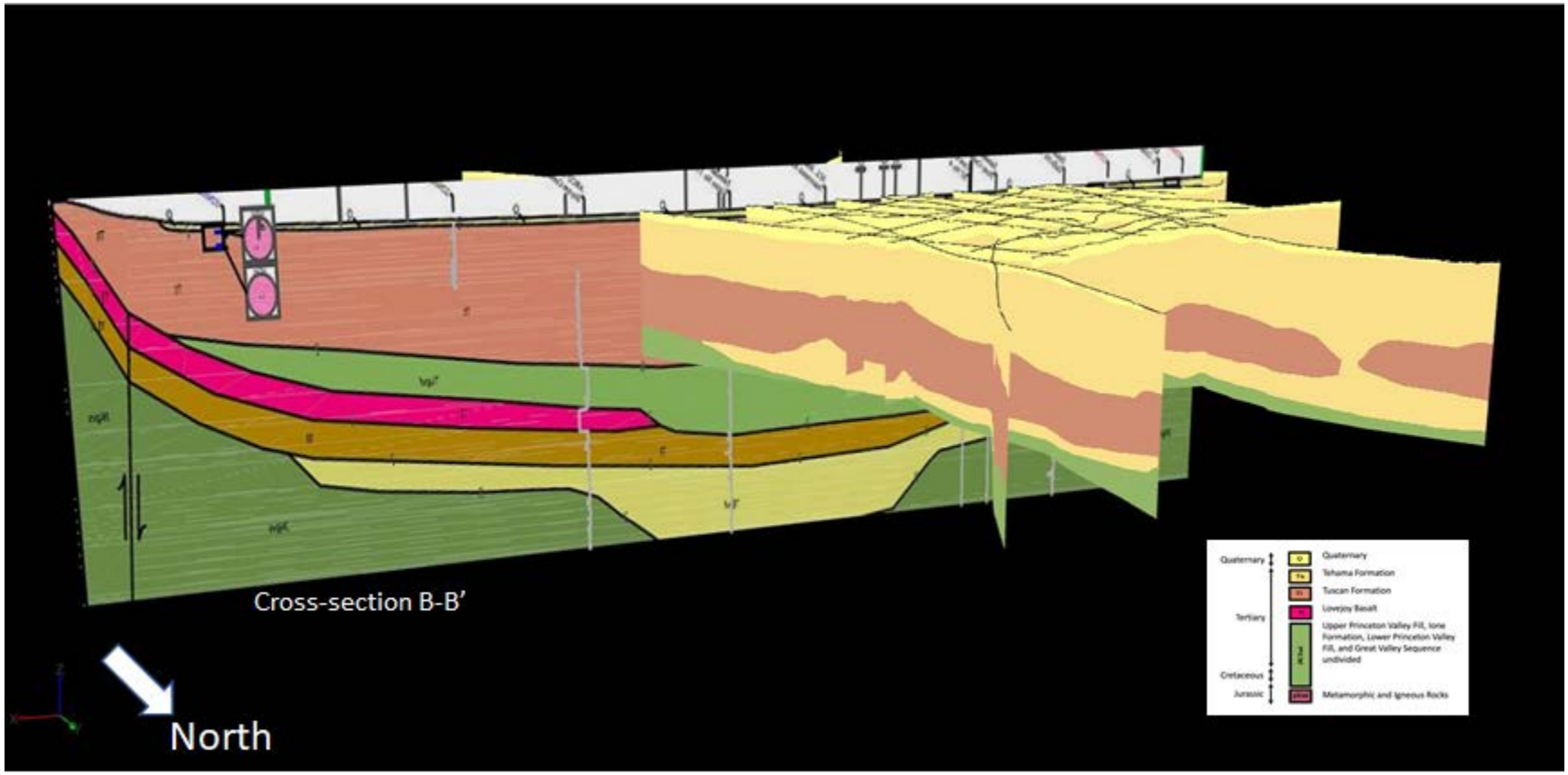

Figure 5-38. View of the Lovejoy Basalt not quite extending to a location beneath the SkyTEM312 AEM flight lines. This could relate to the unit not being detected by the AEM as well as being beyond the systems' Depth of Investigation.

5.5 Comparison of 304M and 312 Systems

As discussed earlier, two airborne electromagnetic TEM systems were operated during the Butte AEM investigation. One was the SkyTEM304M (304M) and the other was the SkyTEM312 (312). In order to compare the systems, part of a traverse was flown twice, once by the 312 as part of flight line L710601 and a second time by the 304M as part of flight line L730300. This section compares the AEM inversions results of the two systems.

A map of the flight line with the overlap section is presented in Figure 5-39. The dark blue line is the full length of the combined flight lines, about 30 miles (48.6 km). The light blue line in Figure 5-39 is the section over which both systems acquired data and imaged the same ground, about 11.5 miles (18.6 km). The overlap region is between eastings of 588000 and 606000.

The AEM inversion results for 304M line L730300 and 312 line L710601 are presented in Figure 40 and Figure 41, respectively. Although already presented earlier in previous sections, they are presented here again for convenience. Figure 5-42 presents the results for these two lines again but arranged so that where the lines overlap, is where the profiles in the image overlap. Remember, the overlap is between eastings of 588000 and 606000. The 312 L710601 line is on top and the 304 L730300 is on the bottom.

The circled areas on the profiles in Figure 5-42 is where they are different. The 312 inversion result shows much better resolution at depth than does the 304M. Especially for eastings less than 596000 down to the 588000 end of line easting. At about an elevation of about -800 ft, the 304M loses its ability to accurately resolve the deeper resistivities. At about -900 ft to -1000 ft elevation, the bottom has dropped out of the 304M's ability to resolve the resistivities of the conductive material. The 312 shows no issues with the DOI until about elevations -1100 ft to -1200 ft.

3D fence diagram versions of how these lines appear are presented from two different views, first looking south and then from the other side looking north. Figure 5-43 shows L730300 as a fence diagram by itself and then Figure 5-44 shows what happens when L710601 is added to the view. Similarly, Figure 5-45 shows L730300 by itself looking to the north and then Figure 5-46 shows how the two lines look together when L710601 is added. What you see is that contact at depth in the overlap zone is much more highly resolved with the 312 than what was achieved by the 304M alone.

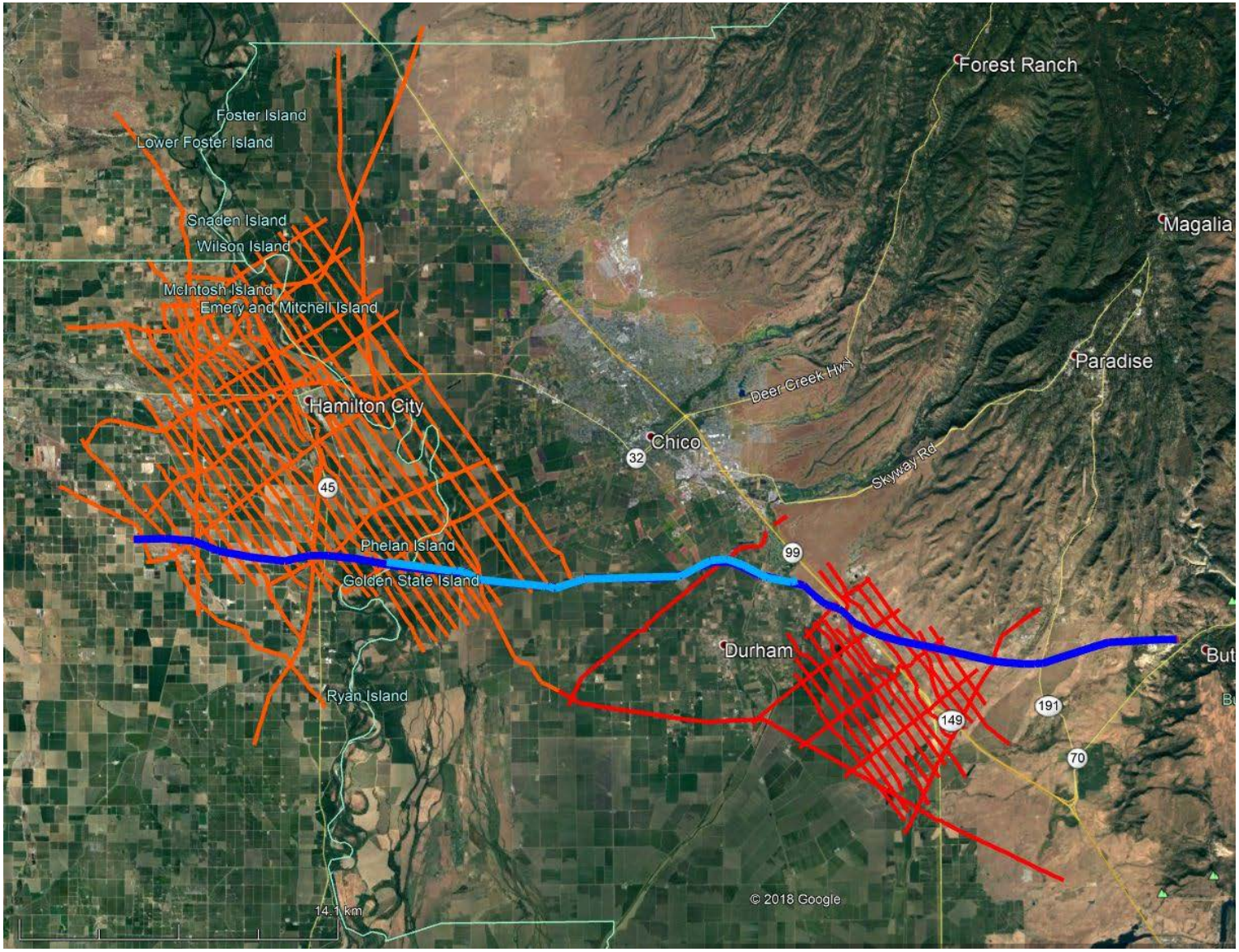

Figure 5-39. AEM flight line over part of which both the 304M and the 312 acquired data. 312 AEM flight lines are in orange. 304 AEM flight lines are in red. Dark blue line is the full length of combined flight lines. Light blue line is the section over which both systems acquired data.

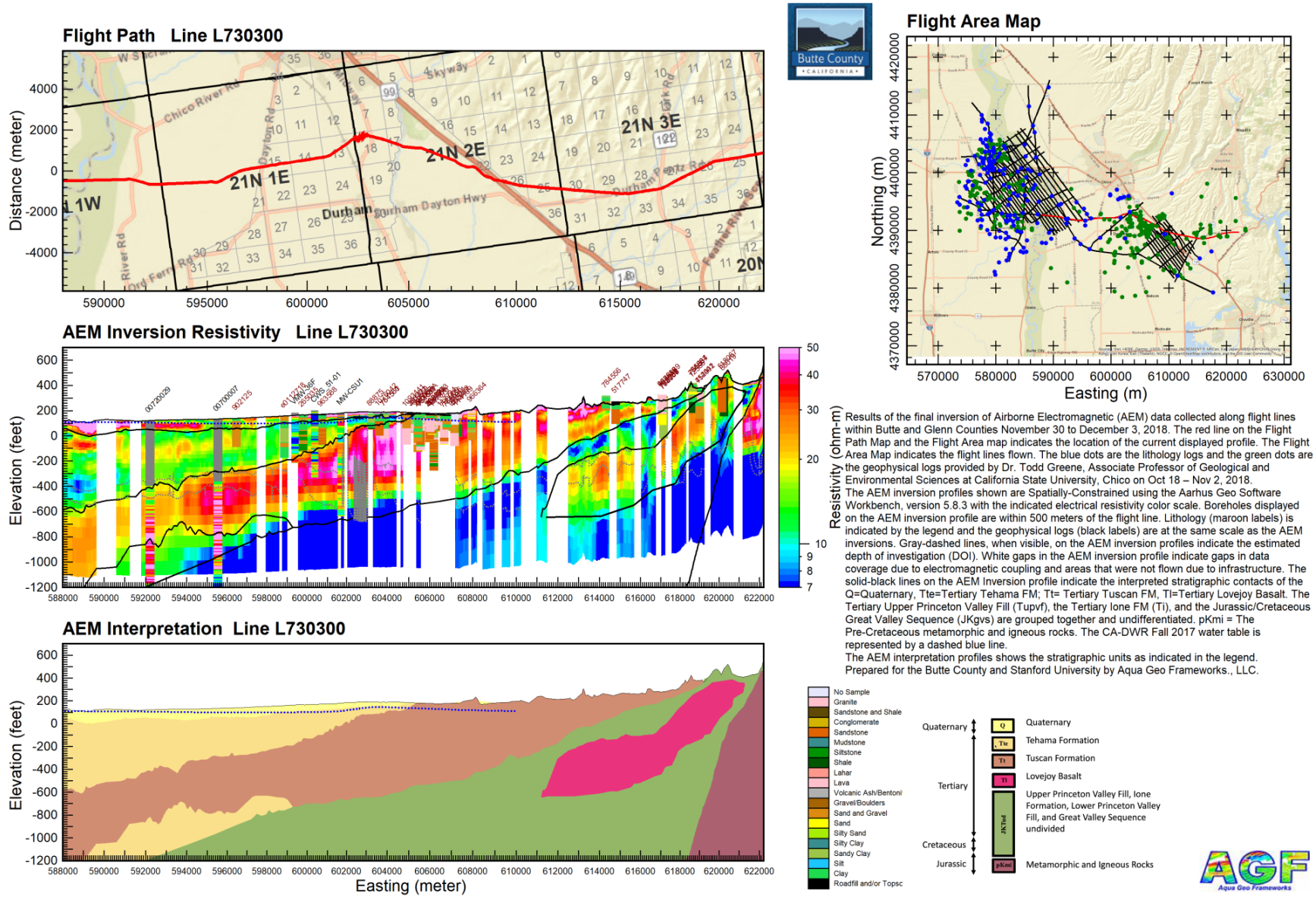

Results of the final inversion of Airborne Electromagnetic (AEM) data collected along flight lines within Butte and Glenn Counties November 30 to December 3, 2018. The red line on the Flight Path Map and the Flight Area map indicates the location of the current displayed profile. The Flight Area Map indicates the flight lines flown. The blue dots are the lithology logs and the green dots are the geophysical logs provided by Dr. Todd Greene, Associate Professor of Geological and Environmental Sciences at California State University, Chico on Oct 18 – Nov 2, 2018.

The AEM inversion profiles shown are Spatially-Constrained using the Aarhus Geo Software Workbench, version 5.8.3 with the indicated electrical resistivity color scale. Boreholes displayed on the AEM inversion profile are within 500 meters of the flight line. Lithology (maroon labels) is indicated by the legend and the geophysical logs (black labels) are at the same scale as the AEM inversions. Gray-dashed lines, when visible, on the AEM inversion profiles indicate the estimated depth of investigation (DOI). White gaps in the AEM inversion profile indicate gaps in data coverage due to electromagnetic coupling and areas that were not flown due to infrastructure. The solid-black lines on the AEM Inversion profile indicate the interpreted stratigraphic contacts of the Q=Quaternary, Tte=Tertiary Tehama FM; Tt= Tertiary Tuscan FM, Tl=Tertiary Lovejoy Basalt. The Tertiary Upper Princeton Valley Fill (Tupvf), the Tertiary Ione FM (Ti), and the Jurassic/Cretaceous Great Valley Sequence (JKgvs) are grouped together and undifferentiated. pKmi = The Pre-Cretaceous metamorphic and igneous rocks. The CA-DWR Fall 2017 water table is represented by a dashed blue line.

The AEM interpretation profiles shows the stratigraphic units as indicated in the legend.

Prepared for the Butte County and Stanford University by Aqua Geo Frameworks., LLC.

Figure 5-40. Inversion results for 304M AEM flight line L730300.

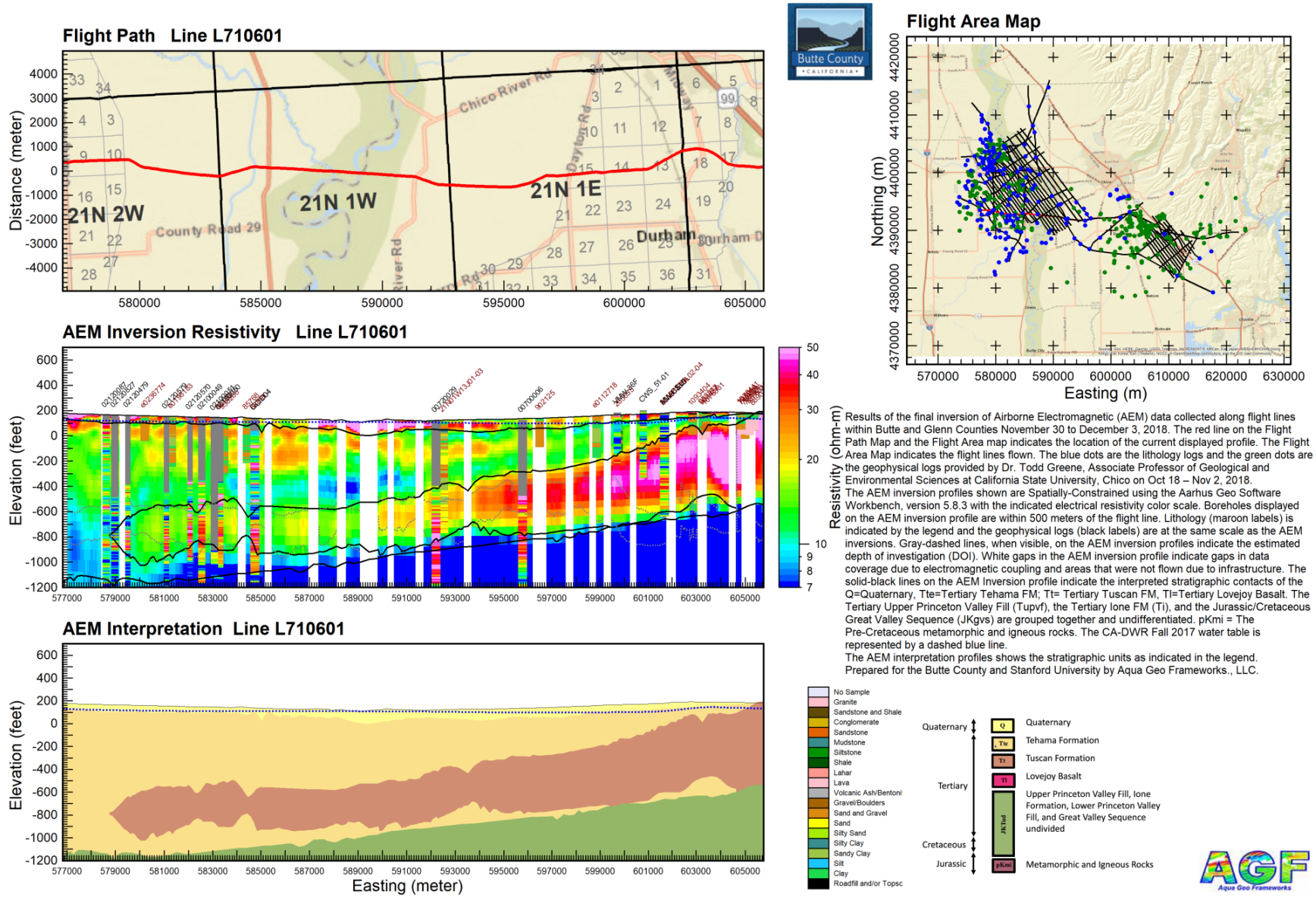

Results of the final inversion of Airborne Electromagnetic (AEM) data collected along flight lines within Butte and Glenn Counties November 30 to December 3, 2018. The red line on the Flight Path Map and the Flight Area map indicates the location of the current displayed profile. The Flight Area Map indicates the flight lines flown. The blue dots are the lithology logs and the green dots are the geophysical logs provided by Dr. Todd Greene, Associate Professor of Geological and Environmental Sciences at California State University, Chico on Oct 18 – Nov 2, 2018.
The AEM inversion profiles shown are Spatially-Constrained using the Aarhus Geo Software Workbench, version 5.8.3 with the indicated electrical resistivity color scale. Boreholes displayed on the AEM inversion profile are within 500 meters of the flight line. Lithology (maroon labels) is indicated by the legend and the geophysical logs (black labels) are at the same scale as the AEM inversions. Gray-dashed lines, when visible, on the AEM inversion profiles indicate the estimated depth of investigation (DOI). White gaps in the AEM inversion profile indicate gaps in data coverage due to electromagnetic coupling and areas that were not flown due to infrastructure. The solid-black lines on the AEM Inversion profile indicate the interpreted stratigraphic contacts of the Q=Quaternary, Tte=Tertiary Tehama FM; Tt= Tertiary Tuscan FM, Tl=Tertiary Lovejoy Basalt. The Tertiary Upper Princeton Valley Fill (Tupvf), the Tertiary Ione FM (Ti), and the Jurassic/Cretaceous Great Valley Sequence (JKgvs) are grouped together and undifferentiated. pKmi = The Pre-Cretaceous metamorphic and igneous rocks. The CA-DWR Fall 2017 water table is represented by a dashed blue line.
The AEM interpretation profiles shows the stratigraphic units as indicated in the legend.
Prepared for the Butte County and Stanford University by Aqua Geo Frameworks., LLC.

Figure 5-41. Inversion results for 312 AEM flight line L710601.

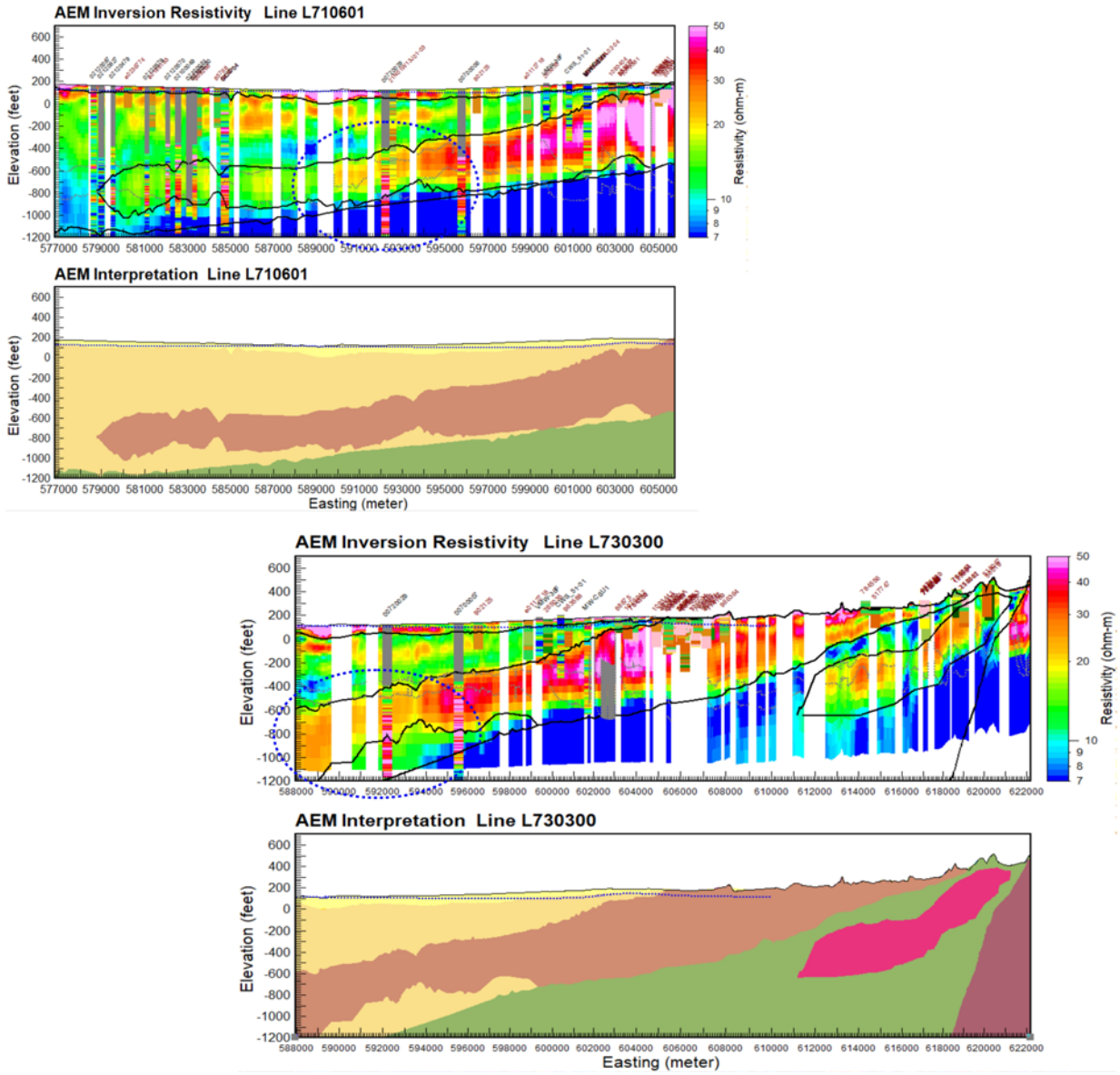

Figure 5-42. Zone of overlap of inversion results for 304M flight line L730300 and 312 flight line L710601. The circled areas are where there are differences due to different Depth of Investigations.

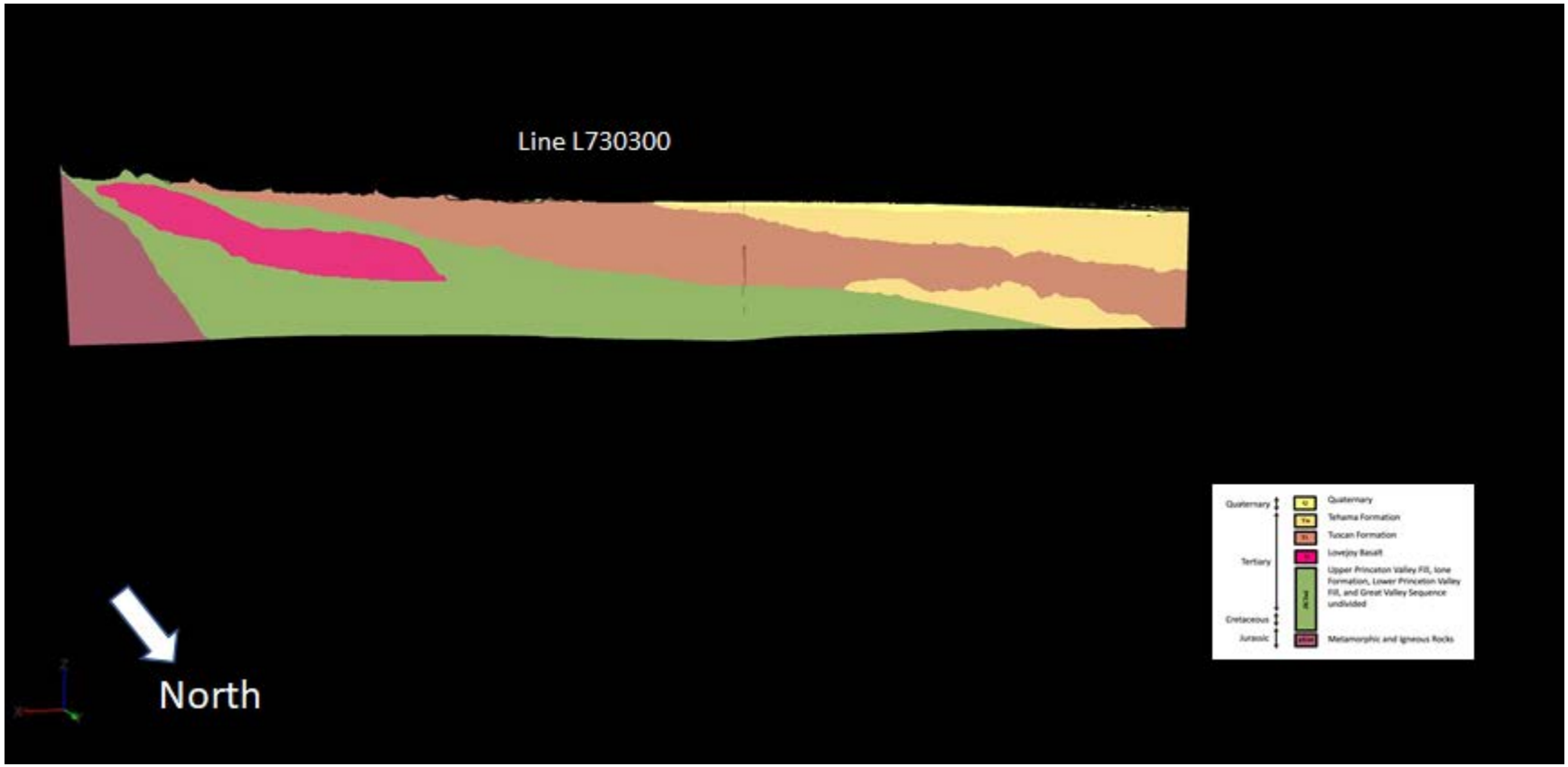

Figure 5-43. 3D fence diagram of stratigraphic interpretation for 304 AEM flight line L730300 inversion results. Looking south. The color scale for the stratigraphy is in Figure 5-6.

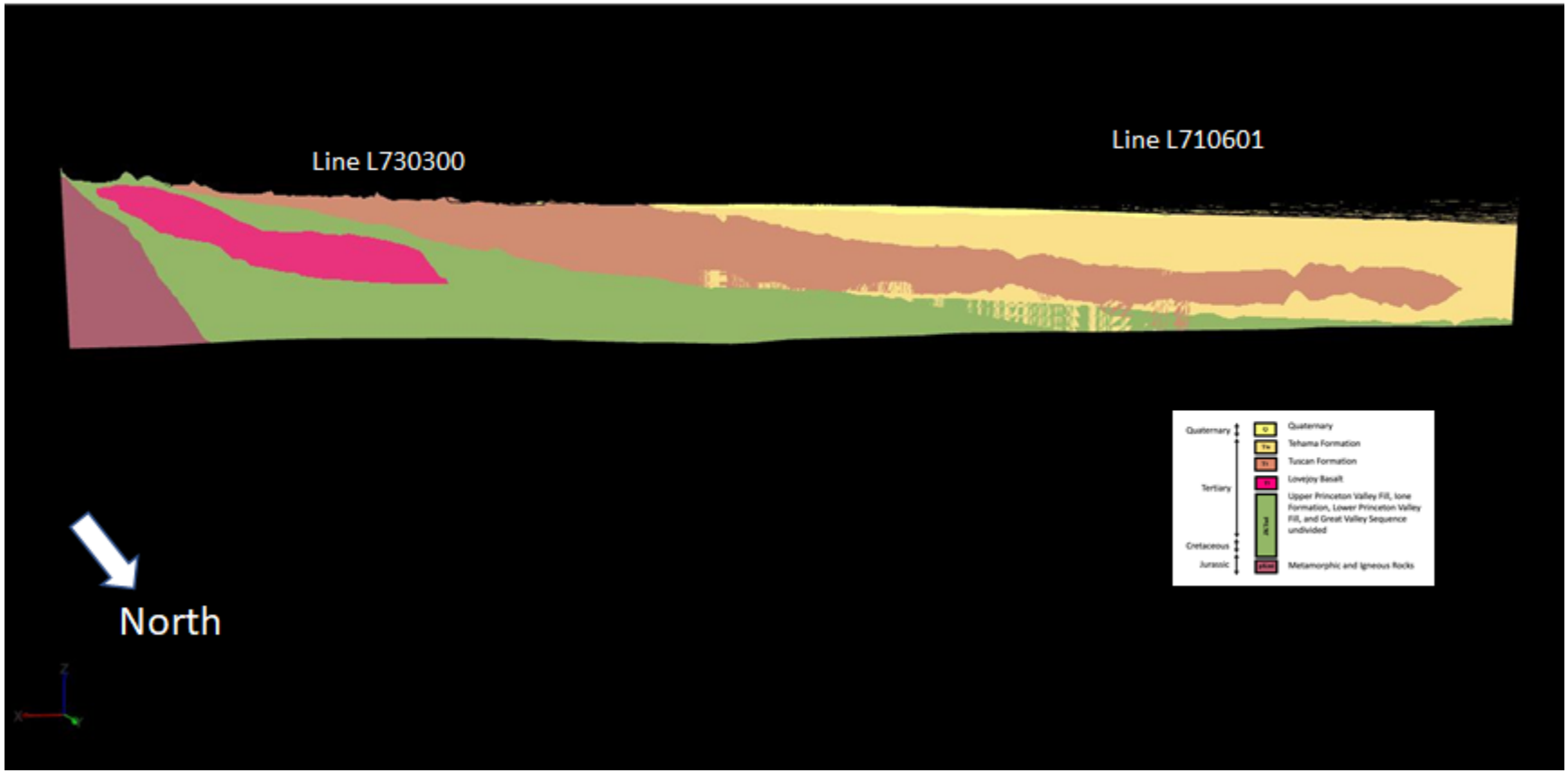

Figure 5-44. 3D fence diagram of stratigraphic interpretation for 304 AEM flight line L730300 inversion results with overlay of overlap area with 312 AEM flight line L710601. Looking south. The color scale for the stratigraphy is in Figure 5-6. The hashing effect at the bottom in the *JKTud* is an artifact of the video card trying to mix the two images.

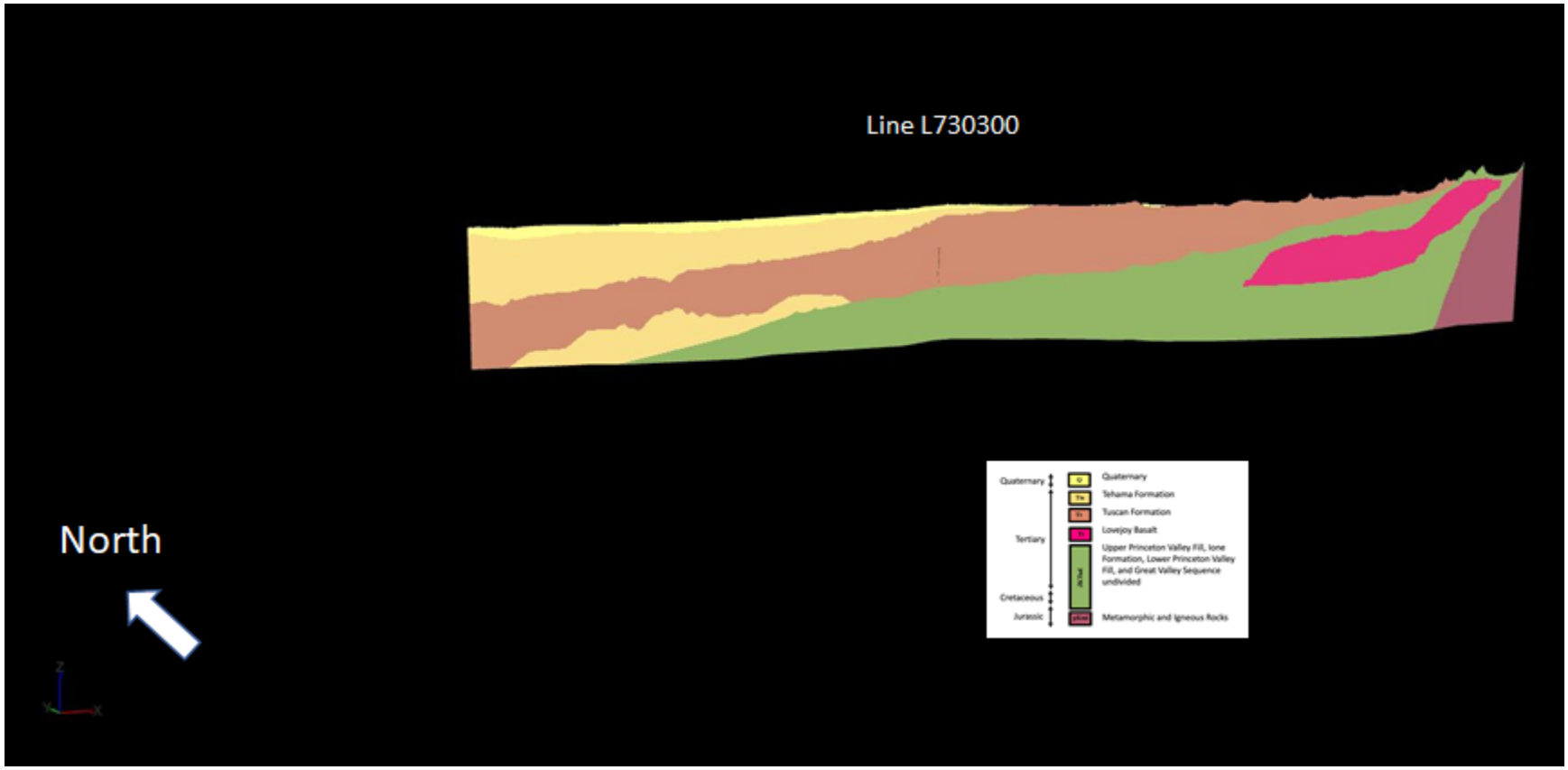

Figure 5-45. 3D fence diagram of stratigraphic interpretation for 304 AEM flight line L730300 inversion results. Looking north. The color scale for the stratigraphy is in Figure 5-6.

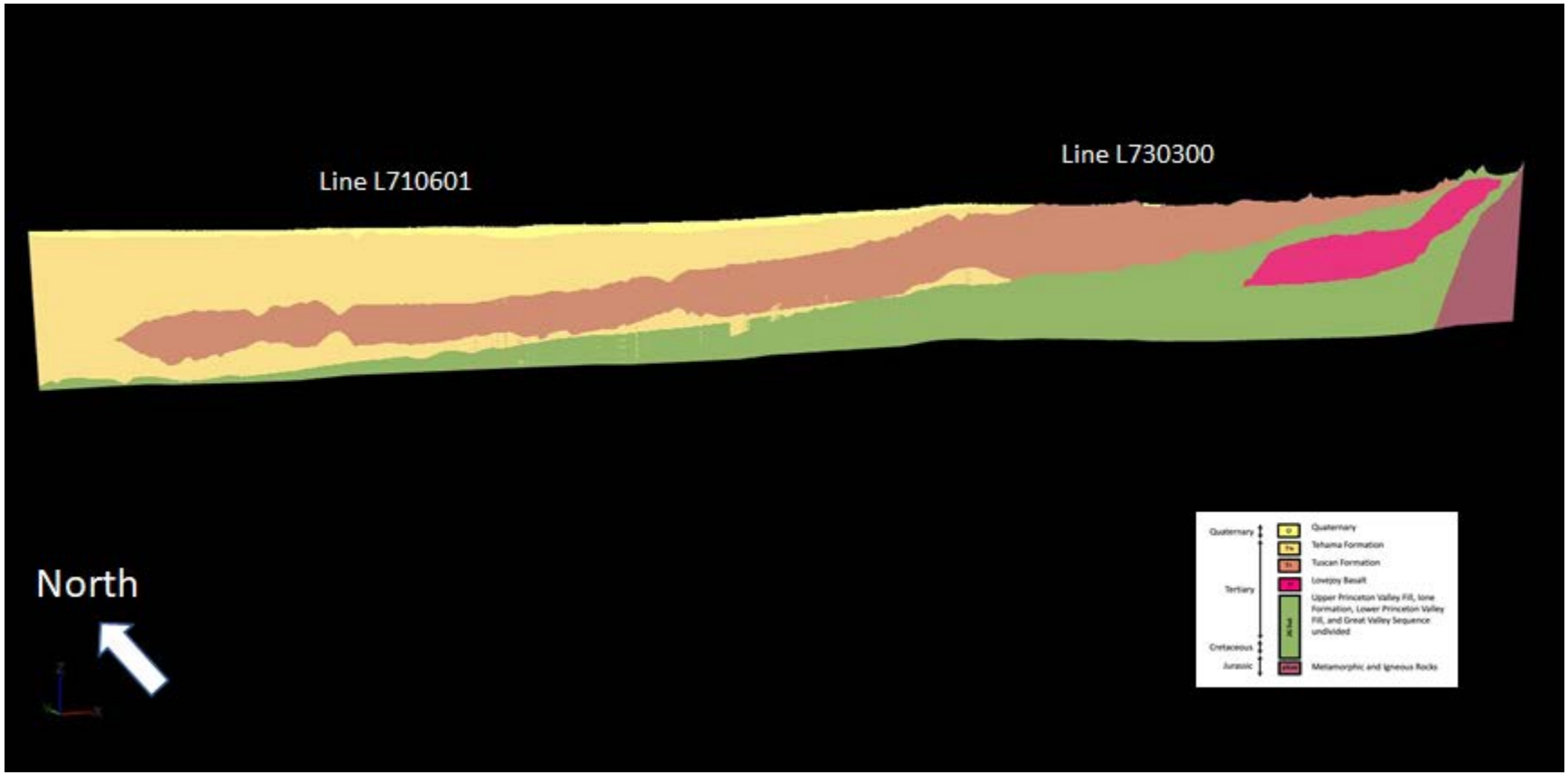

Figure 5-46. 3D fence diagram of stratigraphic interpretation for 304 AEM flight line L730300 inversion results with overlay of overlap area with 312 AEM flight line L710601. Looking north. The color scale for the stratigraphy is in Figure 5-6. The hashing effect at the bottom in the *JKTud* is an artifact of the video card trying to mix the two images.

5.6 Create Interpretative Surface Grids

Butte survey area surface elevation and thickness grids were produced. To create these grids, data such as a ground surface digital elevation model (DEM), water table (WT) elevations, and AEM interpreted point data of the survey area were imported into ESRI's ArcMap. Point data were interpolated to continuous raster surfaces using the kriging method in conjunction with a focal statistics smoothing factor. These data were processed in ArcMap along with the Spatial and Geostatistical Analyst extensions.

For the water table surface, elevation contours representing the water table elevation during the fall of 2017 were downloaded from the CA-DWR (2018) Groundwater Information Center Interactive Map Application. The contours were converted to a 200-meter resolution raster dataset with the 'Topo to Raster' tool available in ArcMap's Spatial Analyst extension. The raster was clipped to the extent of the available contours. Figure 5-47 is a map of the water table elevation within and surrounding the Butte AEM survey area.

For the top of the ***Tte*** elevation grid, almost 22,000 data points extracted from the AEM interpretation were input into ArcMap. The elevation data points with NULL values for ***Tte*** elevation, either indicating that ***Tte*** does not exist or that no data was collected due to obstructions such as power lines, were compared against the subsurface material profiles created in Datamine Discover Profile Analyst (Datamine Discover, 2019). Those points where ***Tte*** did not actually exist (indicating that the NULL value represents a zero thickness) were set to zero and retained and all other NULL values were removed from the point dataset. The remaining points were interpolated into a continuous grid using the ordinary kriging, circular model and the grid was processed with a focal statistic smoothing factor. The cell size was set to 200 m due to the approximate 500 m spacing across line and 25 m down line spatial distribution of the point data. The resultant grid was clipped to the approximate extent of the ***Tte***. Figure 5-48 is a map of the top of ***Tte*** surface elevation within the Butte survey area.

For the top of the ***Tt*** elevation grid, almost 22,000 data points extracted from the AEM interpretation were input into ArcMap. The elevation data points with NULL values, either indicating that ***Tt*** does not exist or that no data was collected due to obstructions such as power lines, were compared against the subsurface material profiles created in Datamine Discover Profile Analyst (Datamine Discover, 2019). Those points where ***Tt*** did not actually exist (indicating that the NULL value represents a zero thickness) were set to zero and retained and all other NULL values were removed from the point dataset. The remaining points were interpolated into a continuous grid using the ordinary kriging, circular model and the grid was processed with a focal statistic smoothing factor. The cell size was set to 200 m due to the approximate 500 m spacing across line and 25 m down line spatial distribution of the point data. The resultant grid was clipped to the approximate extent of ***Tt***, which was determined with the AEM interpreted data points (i.e. zero thickness data points were excluded from the extent of the ***Tt***). Figure 5-49 is a map of the top of ***Tt*** surface elevation within the Butte survey area.

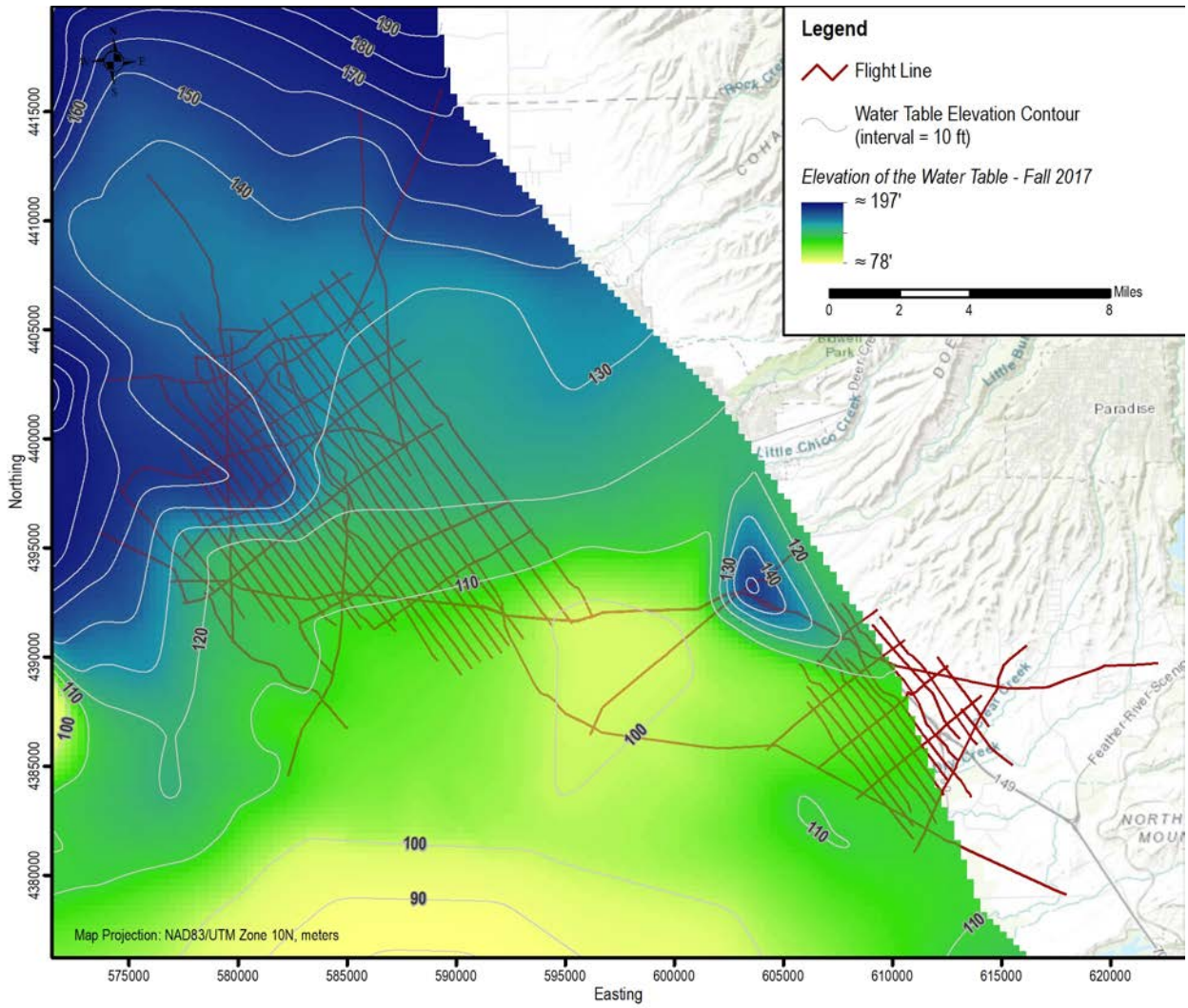

Figure 5-47. Map of the water table elevation during the fall of 2017 within and surrounding the Butte AEM survey area. The projection is NAD83 UTM Zone 10N (meters) and the elevation values are referenced to NAVD 88 (feet).

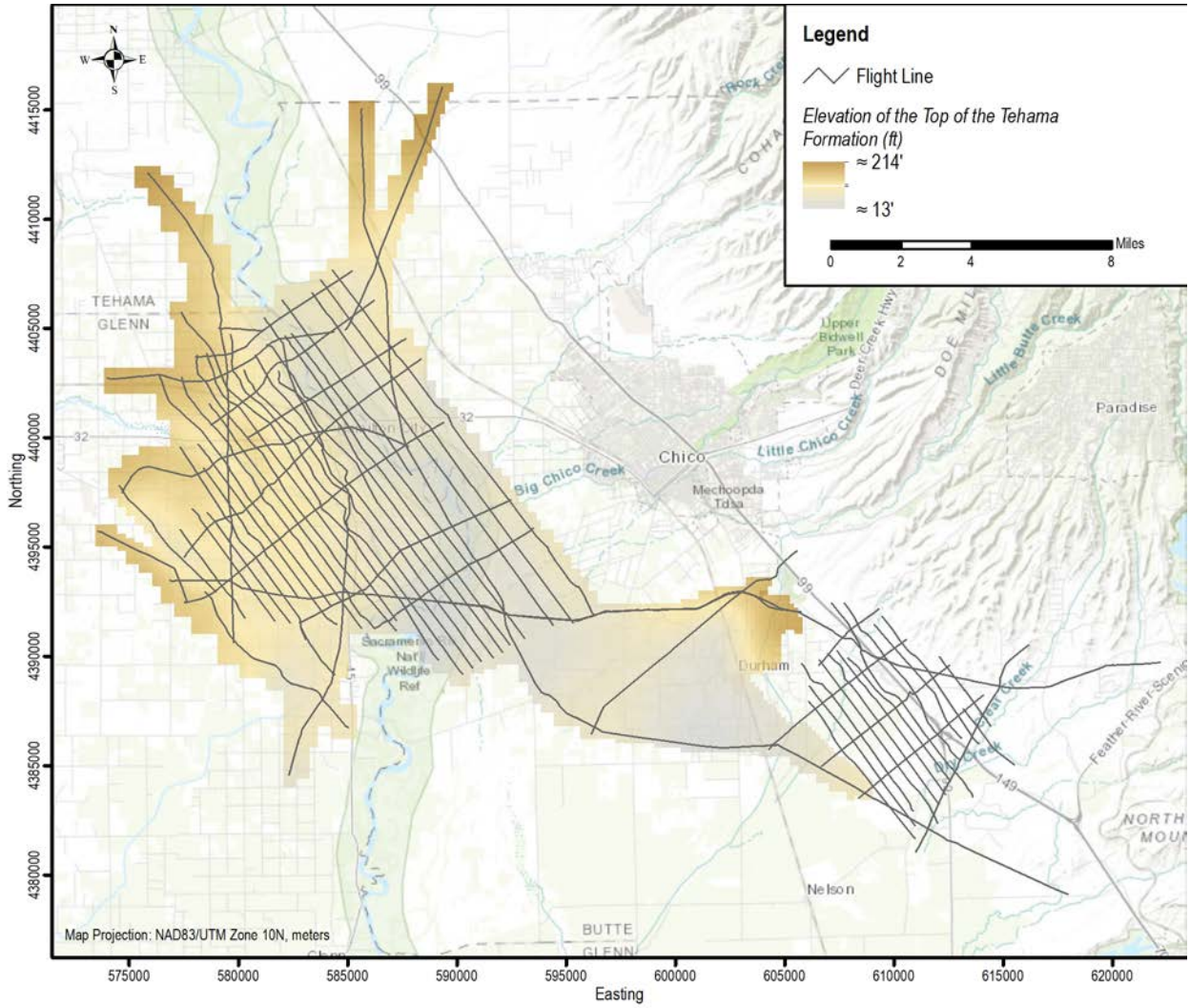

Figure 5-48. Map of the elevation of the top of the Tehama FM within the Butte AEM survey area. The projection is NAD83 UTM Zone 10N (meters) and the elevation values are referenced to NAVD 88 (feet).

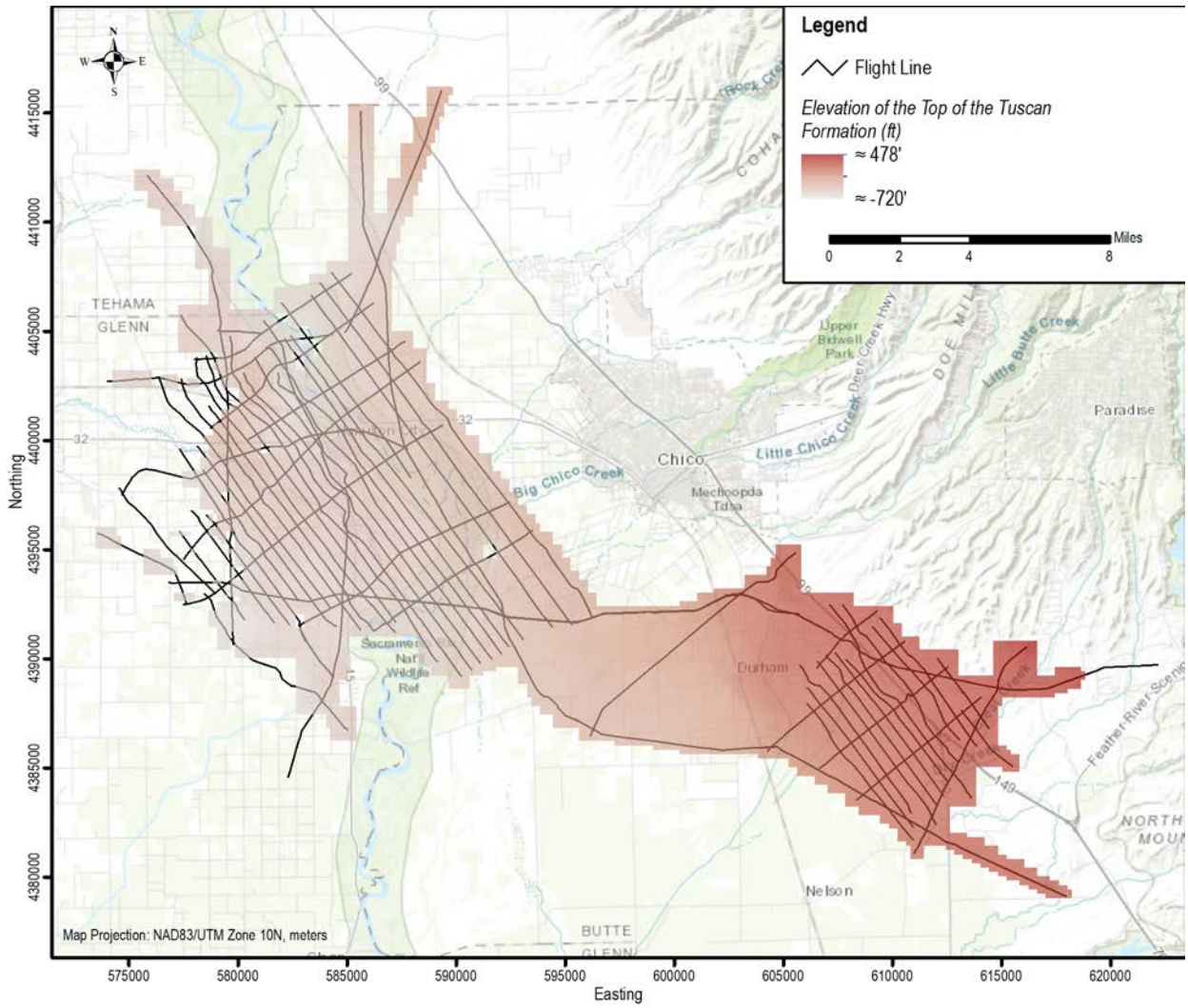

Figure 5-49. Map of the elevation of the top of the Tuscan FM within the Butte AEM survey area. The projection is NAD83 UTM Zone 10N (meters) and the elevation values are referenced to NAVD 88 (feet).

For the of top of the ***Tl*** elevation grid, almost 22,000 data points extracted from the AEM interpretation were input into ArcMap. The elevation data points with NULL values, either indicating that ***Tl*** does not exist or that no data was collected due to obstructions such as power lines, were compared against the subsurface material profiles created in Datamine Discover Profile Analyst (Datamine Discover, 2019). Those points where ***Tl*** did not actually exist (indicating that the NULL value represents a zero thickness) were set to zero and retained and all other NULL values were removed from the point dataset. The remaining points were interpolated into a continuous grid using the ordinary kriging, circular model and the grid was processed with a focal statistic smoothing factor. The cell size was set to 200 m due to the approximate 500 m spacing across line and 25 m down line spatial distribution of the point data. The resultant grid was clipped to the approximate extent of ***Tl***, which was determined with the AEM interpreted data points (i.e. zero thickness data points were excluded from the extent of the Tl). Figure 5-50 is a map of the top of ***Tl*** surface elevation within the Butte survey area.

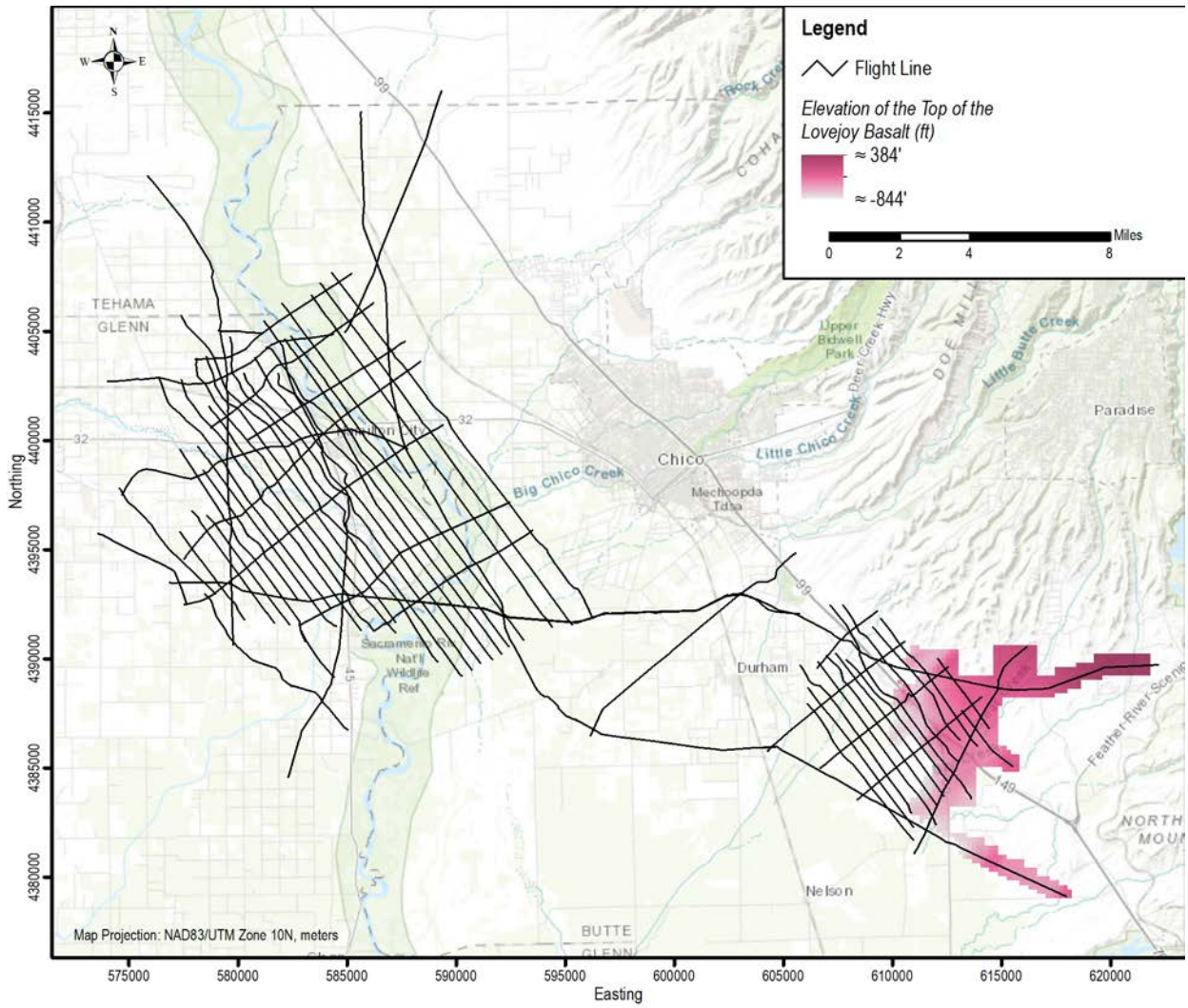

Figure 5-50. Map of the elevation of the top of the Lovejoy Basalt within the Butte AEM survey area. The projection is NAD83 UTM Zone 10N (meters) and the elevation values are referenced to NAVD 88 (feet).

For the of top of ***Tupvf*** elevation grid, over 22,000 data points extracted from the AEM interpretation were input into ArcMap. The elevation data points with NULL values, either indicating that ***Tupvf*** does not exist or that no data was collected due to obstructions such as power lines, were compared against the subsurface material profiles created in Datamine Discover Profile Analyst (Datamine Discover, 2019). Those points where ***Tupvf*** did not actually exist (indicating that the NULL value represents a zero thickness) were set to zero and retained and all other NULL values were removed from the point dataset. The remaining points were interpolated into a continuous grid using the ordinary kriging, circular model and the grid was processed with a focal statistic smoothing factor. The cell size was set to 200 m due to the approximate 500 m spacing across line and 25 m down line spatial distribution of the point data. The resultant grid was clipped to the approximate extent of ***Tupvf***. Figure 5-51 is a map of the top of ***Tupvf*** surface elevation within the Butte survey area.

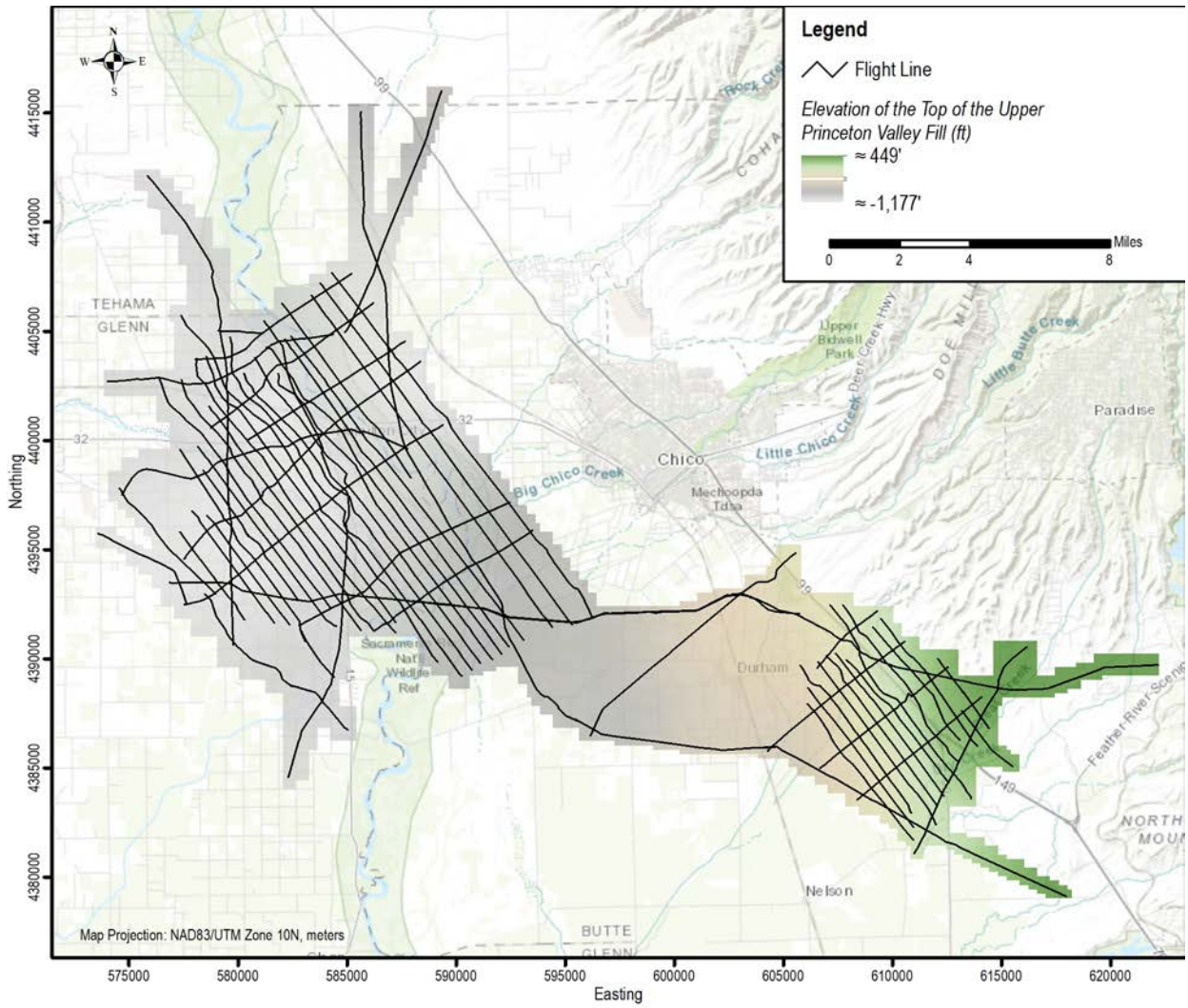

Figure 5-51. Map of the elevation of the top of the Upper Princeton Valley Fill within the Butte AEM survey area. The projection is NAD83 UTM Zone 10N (meters) and the elevation values are referenced to NAVD 88 (feet).

For the unconsolidated ***Q*** thickness grid, almost 22,000 data points extracted from the AEM interpretation were input into ArcMap. The ***Q*** thickness data points with NULL values, either indicating that ***Q*** does not exist or that no data was collected due to obstructions such as power lines, were compared against the subsurface material profiles created in Datamine Discover Profile Analyst (Datamine Discover, 2019). Those points where ***Q*** did not actually exist (indicating that the NULL value represents a zero thickness) were set to zero and retained and all other NULL values were removed from the point dataset. The remaining points were interpolated into a continuous grid using the ordinary kriging, circular model and the grid was processed with a focal statistic smoothing factor. The cell size was set to 200 m due to the approximate 500 m spacing across line and 25 m down line spatial distribution of the point data. The resultant grid was clipped to the approximate extent of ***Q***. Figure 5-52 is a map of the total thickness of unconsolidated ***Q*** deposits within the Butte AEM survey area.

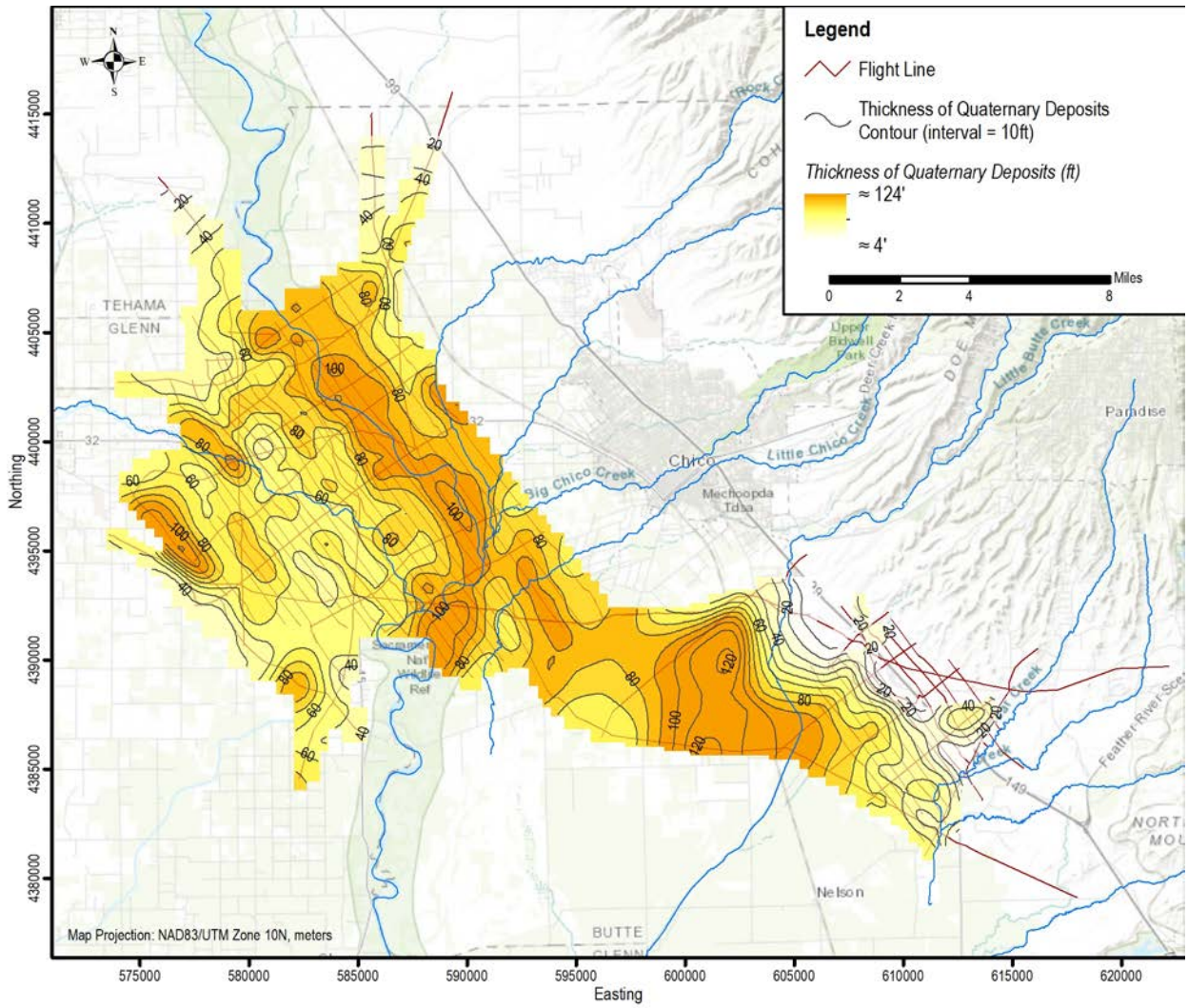

Figure 5-52. Map of the total thickness of Quaternary deposits within the Butte survey area. The projection is NAD83 UTM Zone 10N (meters) and the elevation values are referenced to NAVD 88 (feet).

For the ***Tte*** thickness grid, the data points retained to interpolate the top elevation grid (as described above) were interpolated into a continuous grid using the ***Tte*** thickness values and the ordinary kriging, circular model. After interpolation the grid was processed with a focal statistic smoothing factor. The cell size was set to 200 m due to the approximate 500 m spacing across line and 25 m down line spatial distribution of the point data. The resultant grid was clipped to the approximate extent of ***Tte***. Figure 5-53 is a map of ***Tte*** total thickness within the Butte AEM survey area.

For the ***Tt*** thickness grid, the data points retained to interpolate the top elevation grid (as described above) were interpolated into a continuous grid using the ***Tt*** thickness values and the ordinary kriging, circular model. After interpolation the grid was processed with a focal statistic smoothing factor. The cell size was set to 200 m due to the approximate 500 m spacing across line and 25 m down line spatial distribution of the point data. The resultant grid was clipped to the approximate extent of ***Tt***. Figure 5-54 is a map of ***Tt*** total thickness within the Butte survey area.

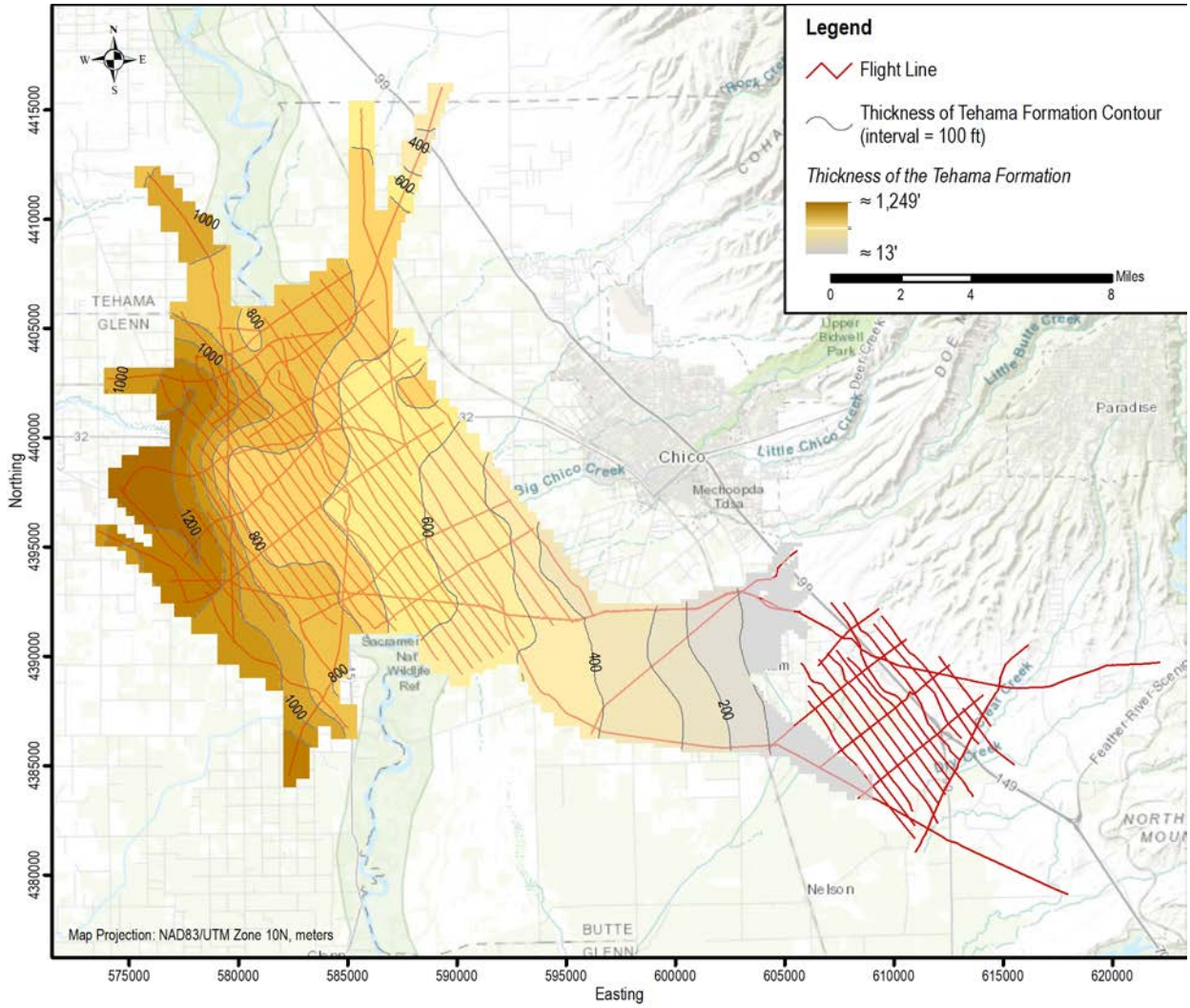

Figure 5-53. Map of the total thickness of the Tehama FM within the Butte AEM survey area. The projection is NAD83 UTM Zone 10N (meters) and the elevation values are referenced to NAVD 88 (feet).

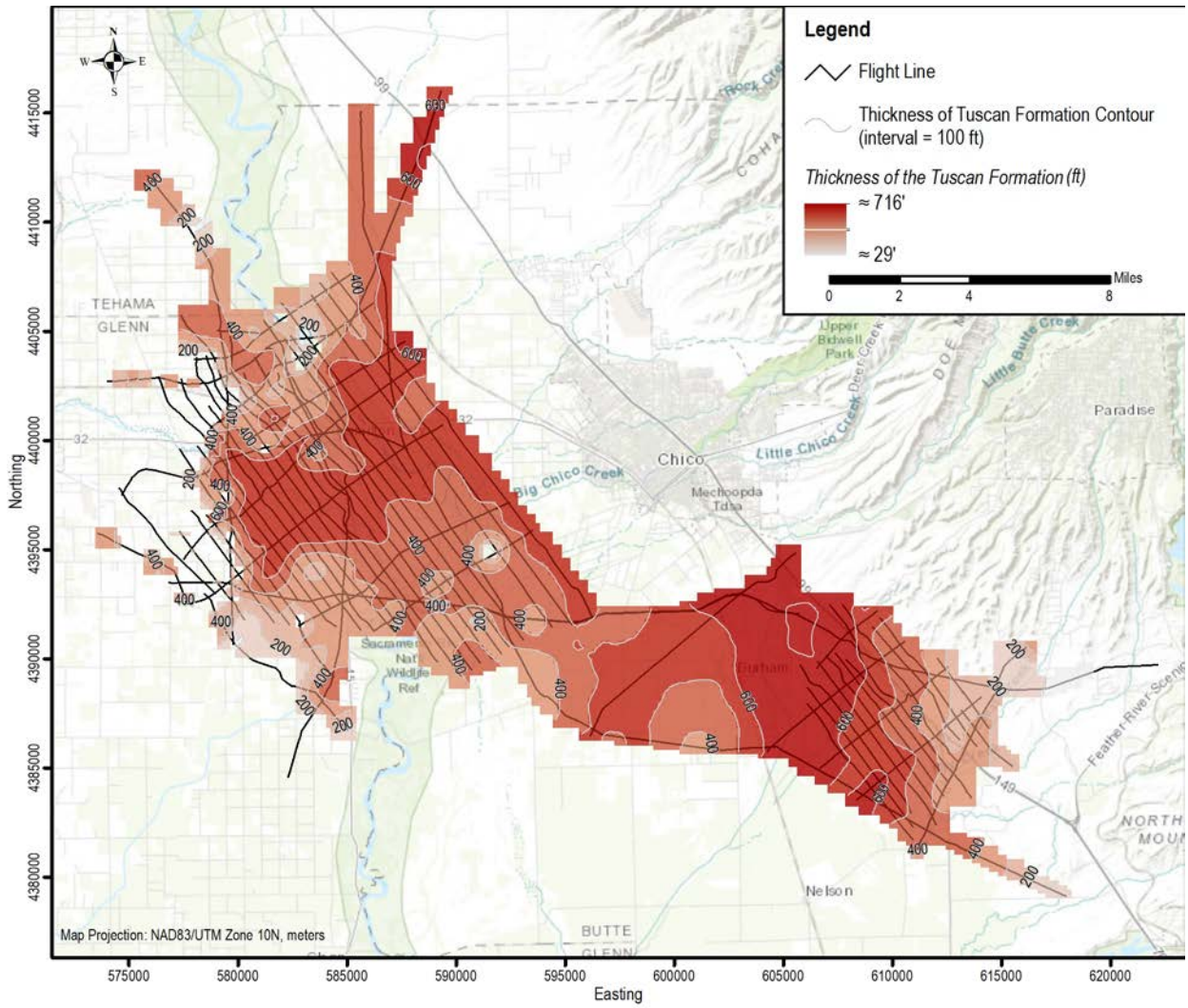

Figure 5-54. Map of the total thickness of the Tuscan FM within the Butte AEM survey area. The projection is NAD83 UTM Zone 10N (meters) and the elevation values are referenced to NAVD 88 (feet).

For the ***Tl*** thickness grid, the data points retained to interpolate the top elevation grid (as described above) were interpolated into a continuous grid using the ***Tl*** thickness values and the ordinary kriging, circular model. After interpolation the grid was processed with a focal statistic smoothing factor. The cell size was set to 200 m due to the approximate 500 m spacing across line and 25 m down line spatial distribution of the point data. The resultant grid was clipped to the approximate extent of ***Tl***. Figure 5-55 is a map of ***Tl*** total thickness within the Butte AEM survey area. Figure 5-56 is a map of total thickness of ***Tte*** sand and gravel within the Butte AEM survey area. This data was derived from the resistivity voxel model using the AEM-derived stratigraphic boundaries.

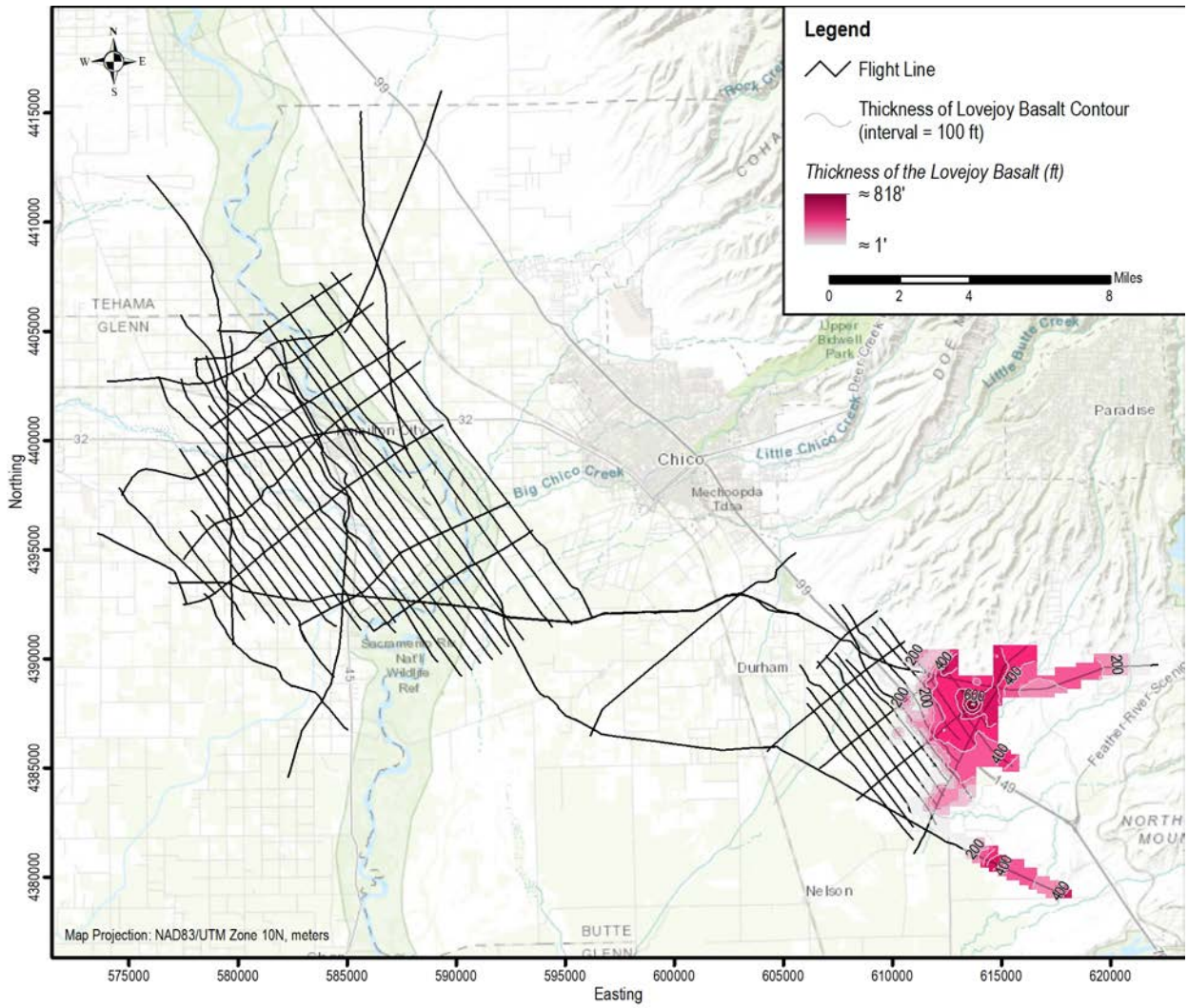

Figure 5-55. Map of the total thickness of the Lovejoy Basalt within the Butte survey area. The projection is NAD83 UTM Zone 10N (meters) and the elevation values are referenced to NAVD 88 (feet).

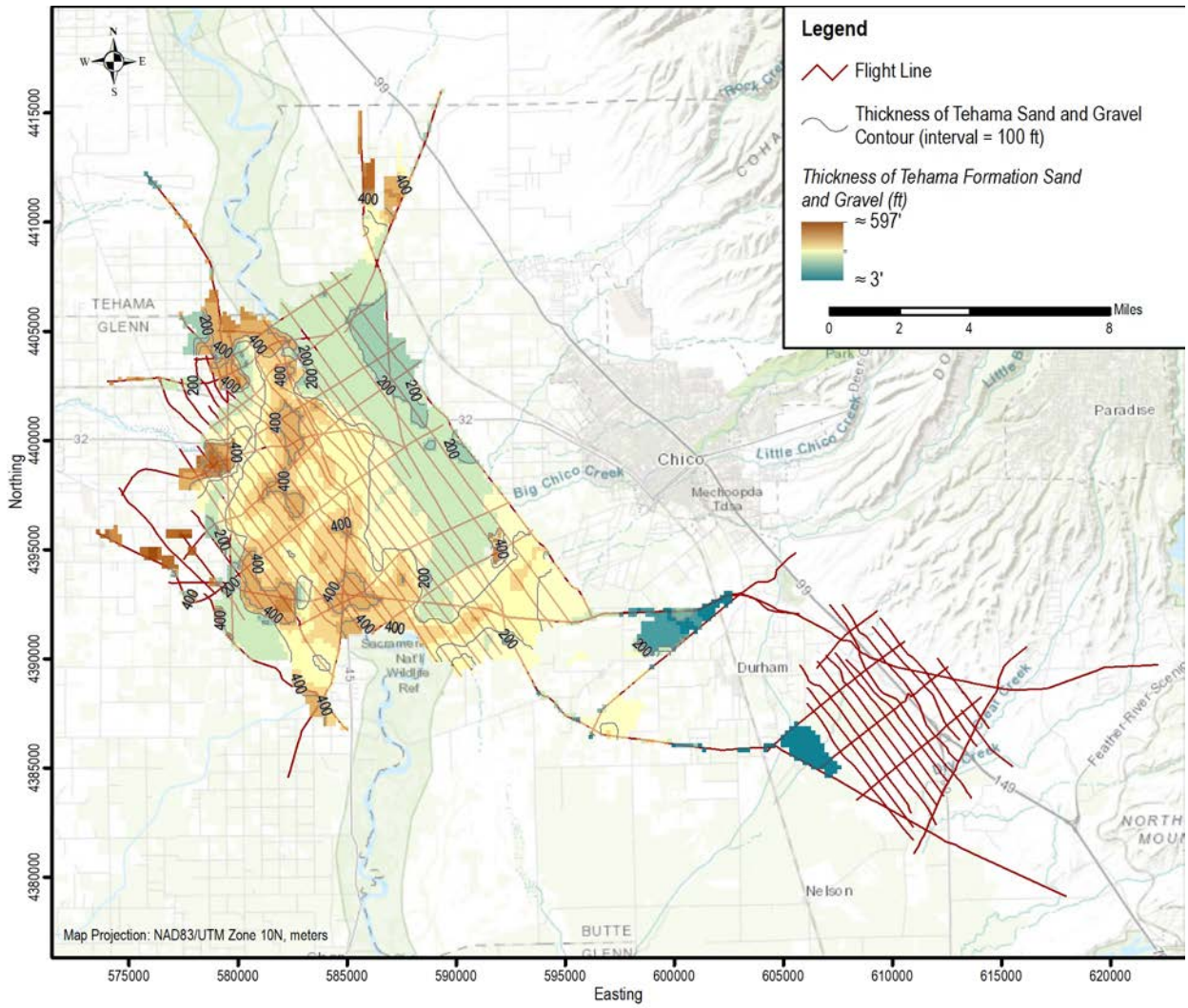

Figure 5-56. Map of the thickness of sand and gravel within the Tehama FM within the Butte AEM survey area. The projection is NAD83 UTM Zone 10N (meters) and the elevation values are referenced to NAVD 88 (feet).

5.7 Resistivity-Lithology Relationship

A critical aspect of a geophysical survey, for whatever purpose, is assessing the nature of the material detected by the geophysical method applied in the investigation. In regard to the Butte AEM survey, an assessment of the lithologic character of the Tehama (***Tte***) and Tuscan (***Tt***) formations was conducted to determine the overall composition of the major categories used to define aquifer and aquitard material. As noted above, there was, generally, very good agreement between the lithological logs and AEM inversion results in the Butte AEM survey area. Where the lithology logs indicated sand, the AEM said the ground was resistive; where the logs indicated clay, the AEM showed a conductor; and where the logs showed lahar, the AEM showed that the material was very resistive. So, after careful study of the lithology logs in conjunction with the AEM inversion results, the resistivity ranges for the Butte AEM survey area, as presented in Figure 5-57, were determined. This color scale was been applied to the AEM inversion results and an AEM lithological interpretation was developed. Several examples are presented below. The rest of the flight line profiles are located in Appendix 1 – 2D Profiles.

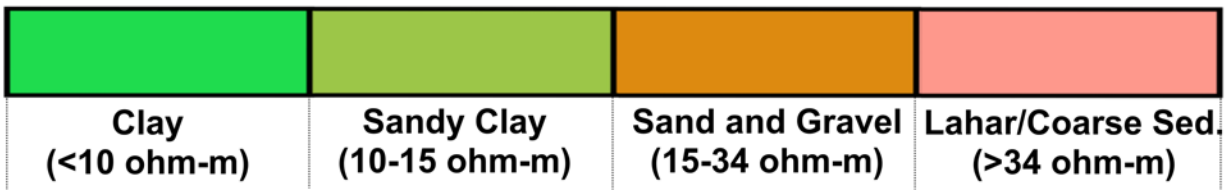

Figure 5-57. Plot displaying the resistivities by major lithological material color categories (green – clay, yellowish green – sandy clay, orange – sand and gravel, pink – lahar/coarse sediments).

The group with resistivities greater than 34 ohm-m is labeled as being both Lahar mudflows and Coarse Sediments. Lahars are very well known as being very hard and competent rock. So it is now surprise that they are also very resistive. The coarse sediments moniker refers to resistive coarse sand and gravel, in particular, in the vicinity of the Sacramento River and its flood plain and beneath the River in the shallower regions of the ***Tte***.

Note that on the images that follow, this color scheme is only applied to the ***Tte*** and ***Tt*** formations and not the ***Q*** sediments. Since the ***Q*** sediments are generally very thin in the Butte AEM survey area (less than 50 ft-100 ft), their quality in terms of aquifer material has not been delineated. There is, however, discussion below in the Recharge section (Section 5.9) on the ***Q*** sediments.

AEM Reconnaissance flight line L730300 is again presented in Figure 5-58. This time the figure is showing the application of the color ranges in Figure 5-57 to the AEM earth model. Note the interbeds of Sand and Gravel, Sandy Clay, and Clay in the ***Tte*** on the left and the very resistive Lahar material within the ***Tt*** as well as Sand and Gravel on the western end of the profile.

The lithological interpretation of AEM Reconnaissance flight line L710701 is presented in Figure 5-59. The ***Tt*** shows Lahar on the northern end (right side) of the profile and Sand and Gravel to the south towards the Valley. The ***Tte*** shows some near-surface Coarse Sediments along most of the profile and a very thick Clay zone on the south end (left side) of the profile.

The lithological interpretation of AEM Reconnaissance flight line L710501 is presented in Figure 5-60. The ***Tt*** shows Sand and Gravel on the eastern end of the profile, closer to the foothills, and more Sandy Clay on the western end of the profile. The ***Tte*** shows Coarse Sediments in the center of the profile under the creek coming out of Black Butte Lake as well as under the Sacramento River.

The lithological interpretation of AEM Reconnaissance flight line L710301 is presented in Figure 5-61. This long flight line starts at the foot of the foothills, proceeds and skirts just east of the Sacramento River, and ends up in the Valley on its southern end. The ***Tt*** shows mostly Sand and Gravel across this profile. The ***Tte*** shows Coarse Sediments on the far right going up towards the foothills and near the surface along the Sacramento River but also a very thick Clay zone (up to 300 ft thick) along the length of the profile away from the foothills.

The lithological interpretation of AEM Reconnaissance flight line L710101 is presented in Figure 5-62. The Tuscan FM here is mostly Sandy Clay with some Sand and Gravel in spots. The Tehama FM has a thick Sand and Gravel zone (about 200 ft thick) near the surface and is underlain by interbeds of Clay and Sand and Gravel.

As mentioned above, the rest of the lithological interpretations of the AEM inversion results are located in Appendix 3/2D Profiles.

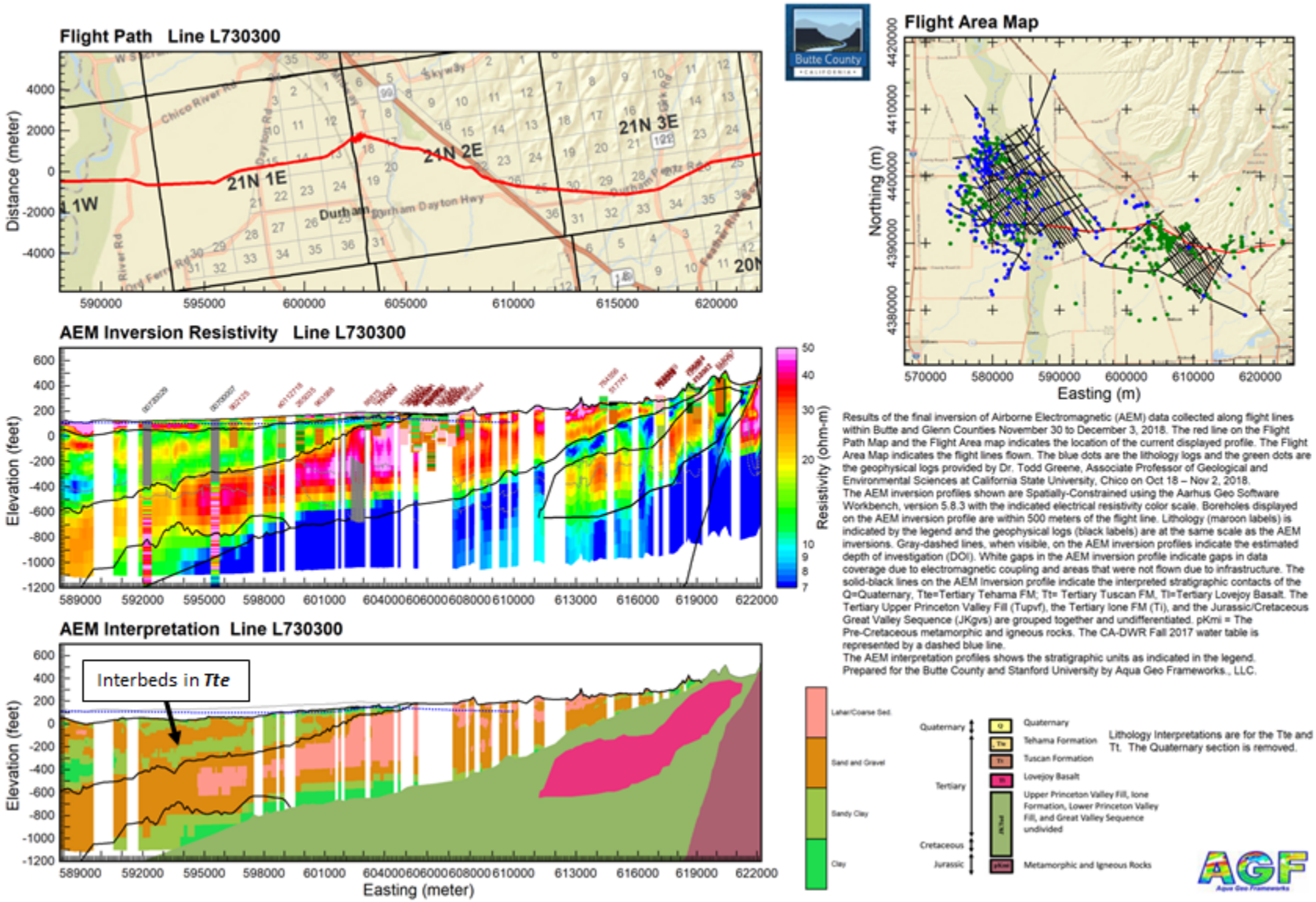

Figure 5-58. Lithological interpretation of AEM Reconnaissance flight line L730300 in the bottom profile. Scale to the right. Note that the Quaternary unit has been left off the interpreted profile.

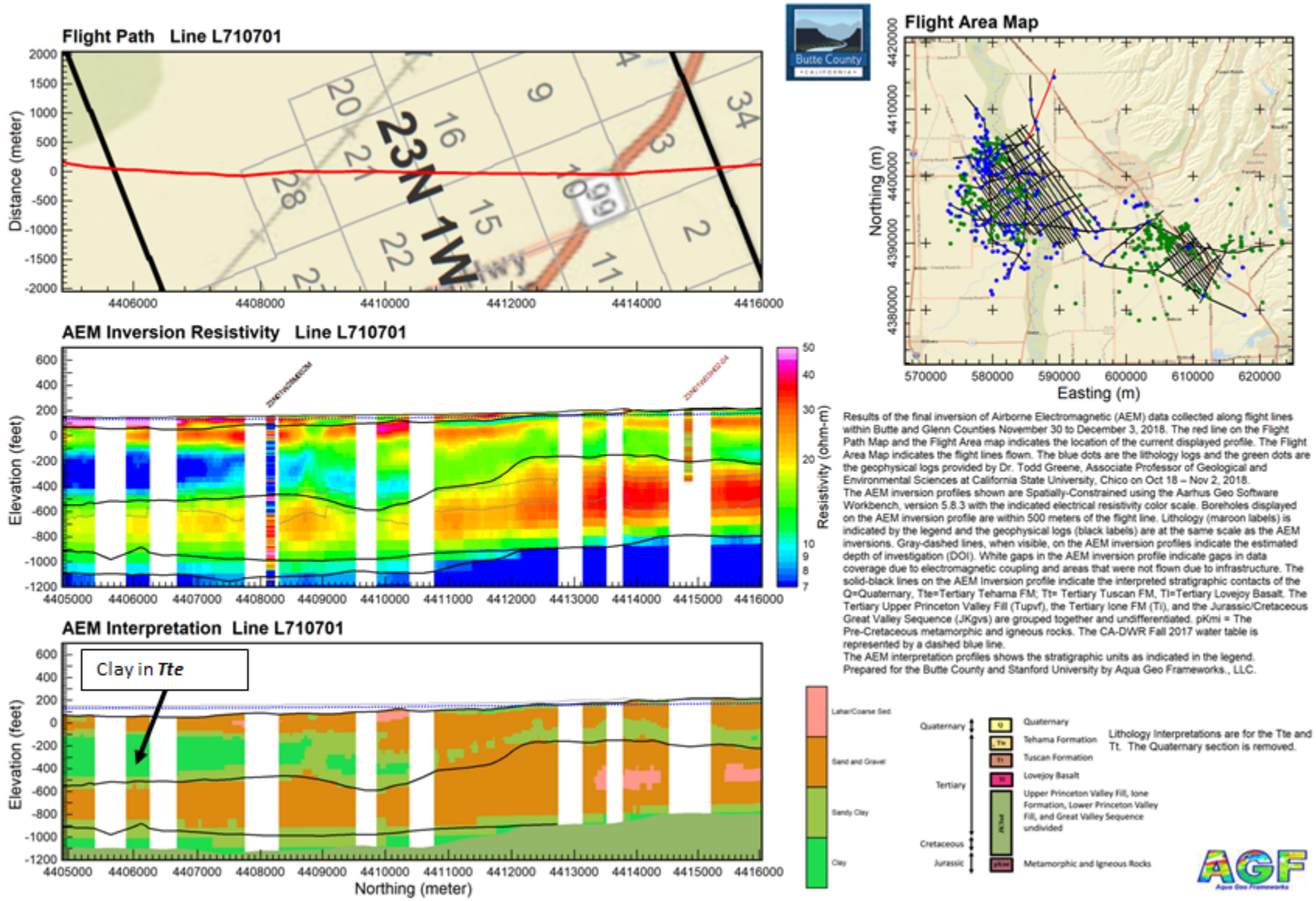

Figure 5-59. Lithological interpretation of AEM Reconnaissance flight line L710701 in the bottom profile. Scale to the right. Note that the Quaternary unit has been left off the interpreted profile.

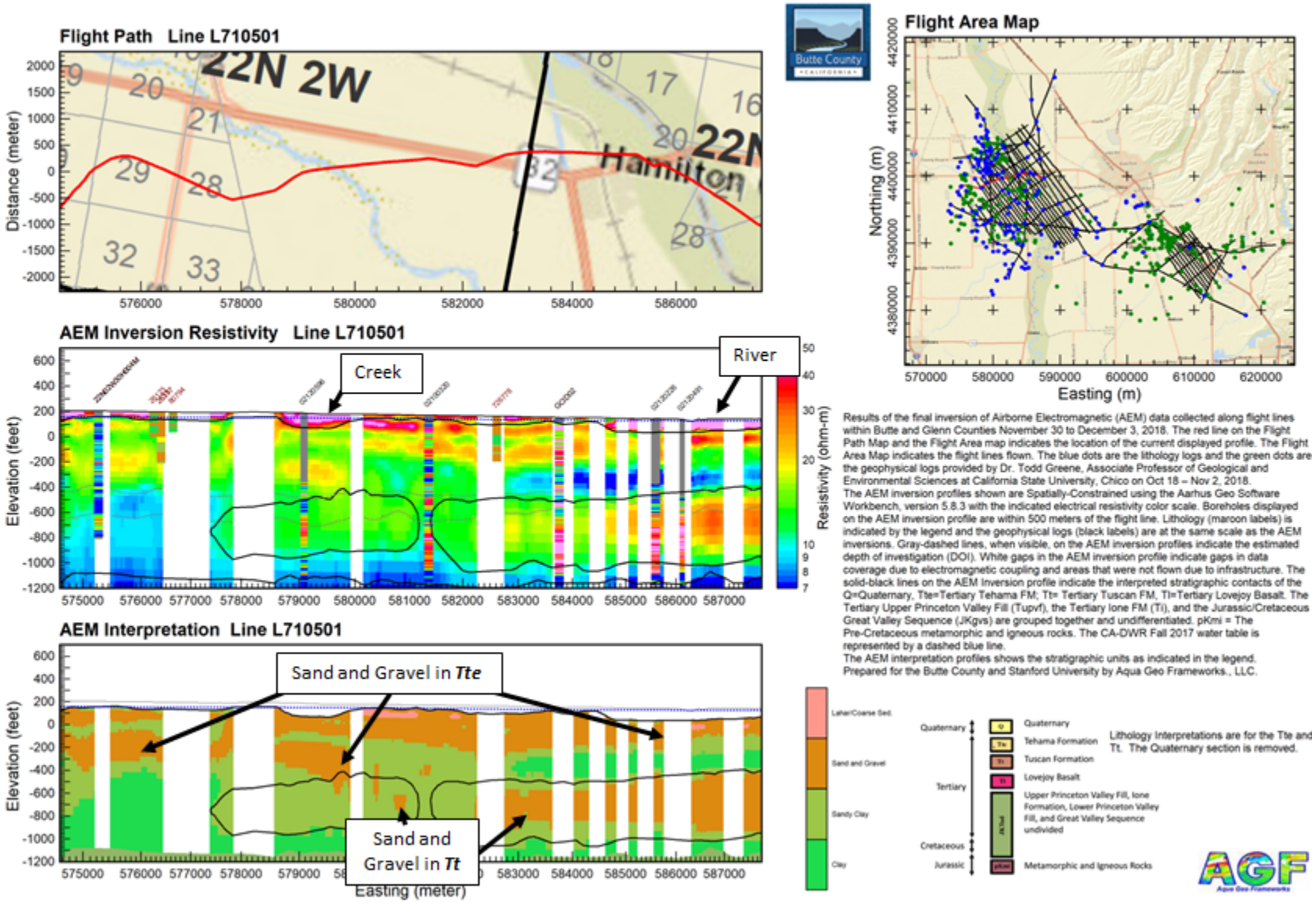

Figure 5-60. Lithological interpretation of AEM Reconnaissance flight line L710501 in the bottom profile. Scale to the right. Note that the Quaternary unit has been left off the interpreted profile.

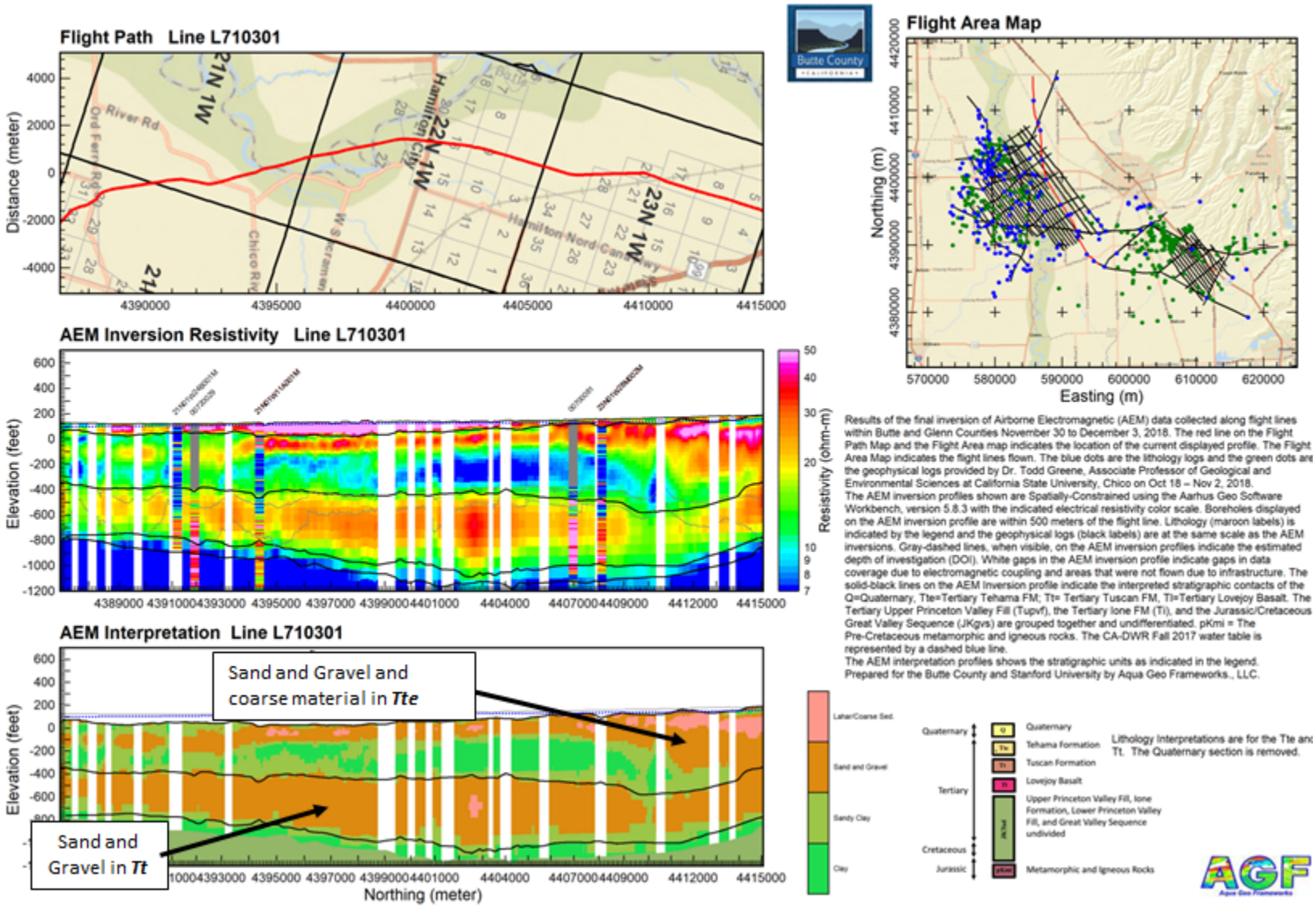

Figure 5-61. Lithological interpretation of AEM Reconnaissance flight line L710301 in the bottom profile. Scale to the right. Note that the Quaternary unit has been left off the interpreted profile. Note that the resistive material at the top of the Tehama FM in the center of the profile are coarse sediments as are the material on the far right.

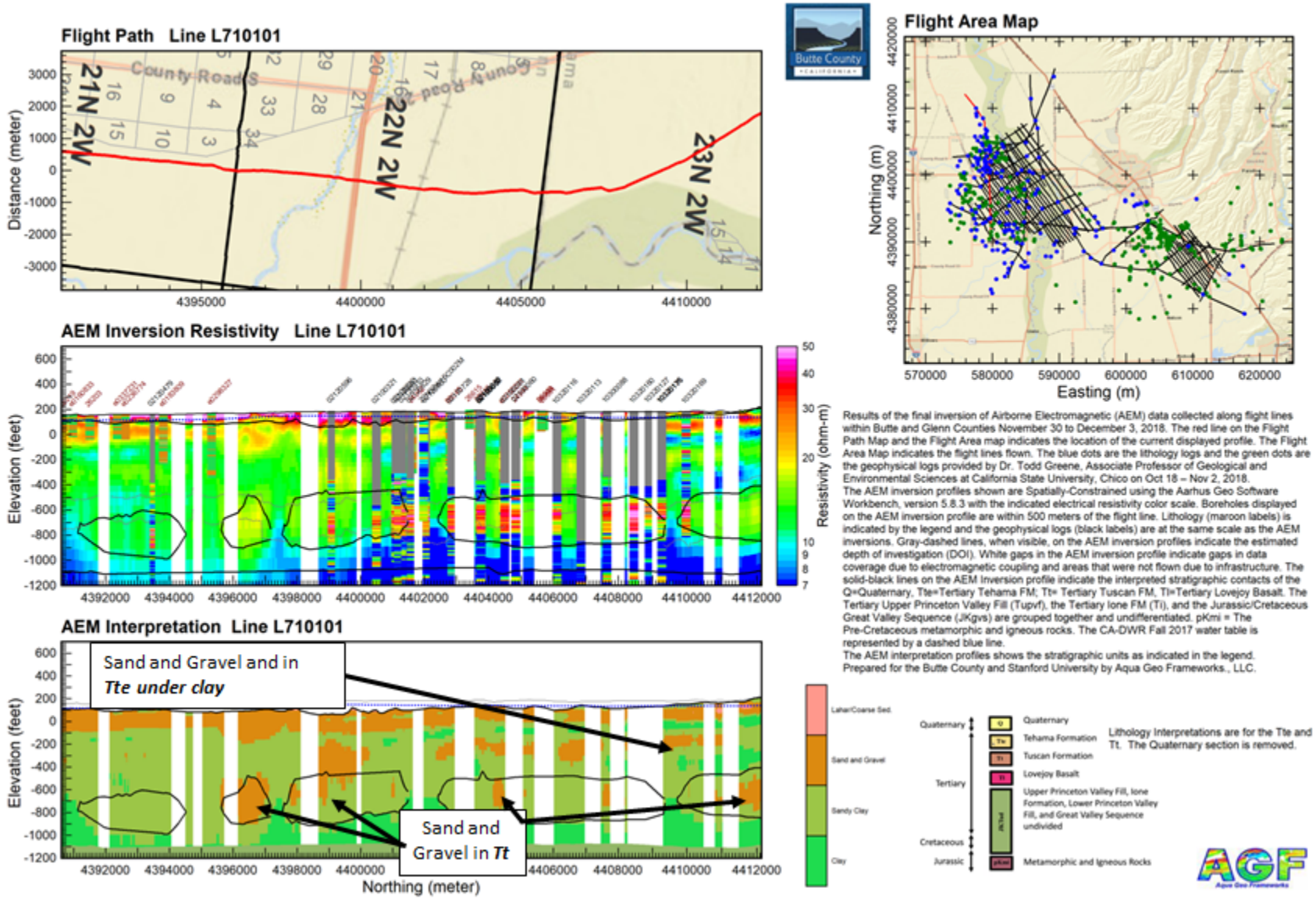

Figure 5-62. Lithological interpretation of AEM Reconnaissance flight line L710101 in the bottom profile. Scale to the right. Note that the Quaternary unit has been left off the interpreted profile.

5.8 Hydrogeological Framework of the Butte AEM Survey Area

The 2018 Butte AEM investigation provides high resolution data of the subsurface along the flight paths within the survey area. These AEM-derived results provide new and updated information on the geology and hydrogeology in areas that were previously unknown or were only known to a limited extent from just the borehole information. The AEM profiles provide for greater understanding of the heterogeneity within and between all geologic formations in the survey area. This heterogeneity will be shown to be an important control to groundwater flow, storage, and quality. This investigation, completed in 2018 by AGF, provides the basis for this hydrogeologic discussion.

The 2018 AEM survey reveals variability in the ***Q*** deposits across the Butte AEM investigation AEM survey area and this unit is not subdivided into geologic materials for purposes of this report. The ***Q*** materials make up the aquifer materials overlying the ***Tte*** and ***Tt*** bedrock units. Figure 5-63, looking north, is a 3D Fence diagram of the Butte AEM investigation flight lines. The ***Q*** aquifer materials are indicated by the legend. The thin layer of ***Q*** sediments can be seen throughout most of the survey area except where the Tuscan FM outcrops up against the foothills. Figure 5-64 is a 3D Fence diagram of the Butte AEM investigation area looking south showing how the geologic formations are heterogeneous across the survey area. The ***Q*** alluvial deposits of the area are in good agreement with the AEM results which are providing more detail on the character of the ***Q***. However, though the ***Q*** are extensive throughout the area, except along the foothills, they are thin (<100 ft) which makes them difficult to break out into distinct sediment packages.

The undifferentiated ***Q*** aquifer materials are considered to be unconsolidated aquifer material and are saturated below the water table throughout the study area. These materials are predominantly composed of alluvial deposits related to the current drainages. These sediments originate from the Coast Range and the Sierra Nevada Mountains. They come from their respective ranges and were deposited towards the center of the valley often intermixing with each other and being reworked at the same time. The similarity of the sediments from each source make them somewhat difficult to separate by the AEM method. As noted above, the dominant hydrogeologic features in the Butte AEM survey area are the Sacramento River and its tributaries. These alluvial deposits have been identified in previous studies by the CA-DWR (2014) and others.

Figure 5-65 again presents AEM flight line L730300. It is one of the longest west-east flight lines in the survey. The profile is oblique to the dip of the ***Tt*** deposits coming off the slope of the Sierra Nevada Mountains to the east. These deposits lie on the Tertiary Upper Princeton Valley Fill which also dips to the west. The ***Tupvf*** is made up of clay and silty clay and is not only not an aquifer but can be considered to be a boundary condition to groundwater flow. The ***Tt*** lies upon the ***Tupvf*** in this area and is an aquifer where it has coarse grained materials like sand and gravel in its makeup. As can be seen, the ***Tt*** subcrops/outcrops to the east spanning an area over 9.3 miles (about 15 km) along the flight line making it an excellent place to recharge the formation from the near surface down gradient. It also will provide a hydraulic head difference to create a potentiometric surface for groundwater where confined and semi-confined conditions exist. This area is one of the important parts of the hydrogeologic framework of the survey area.

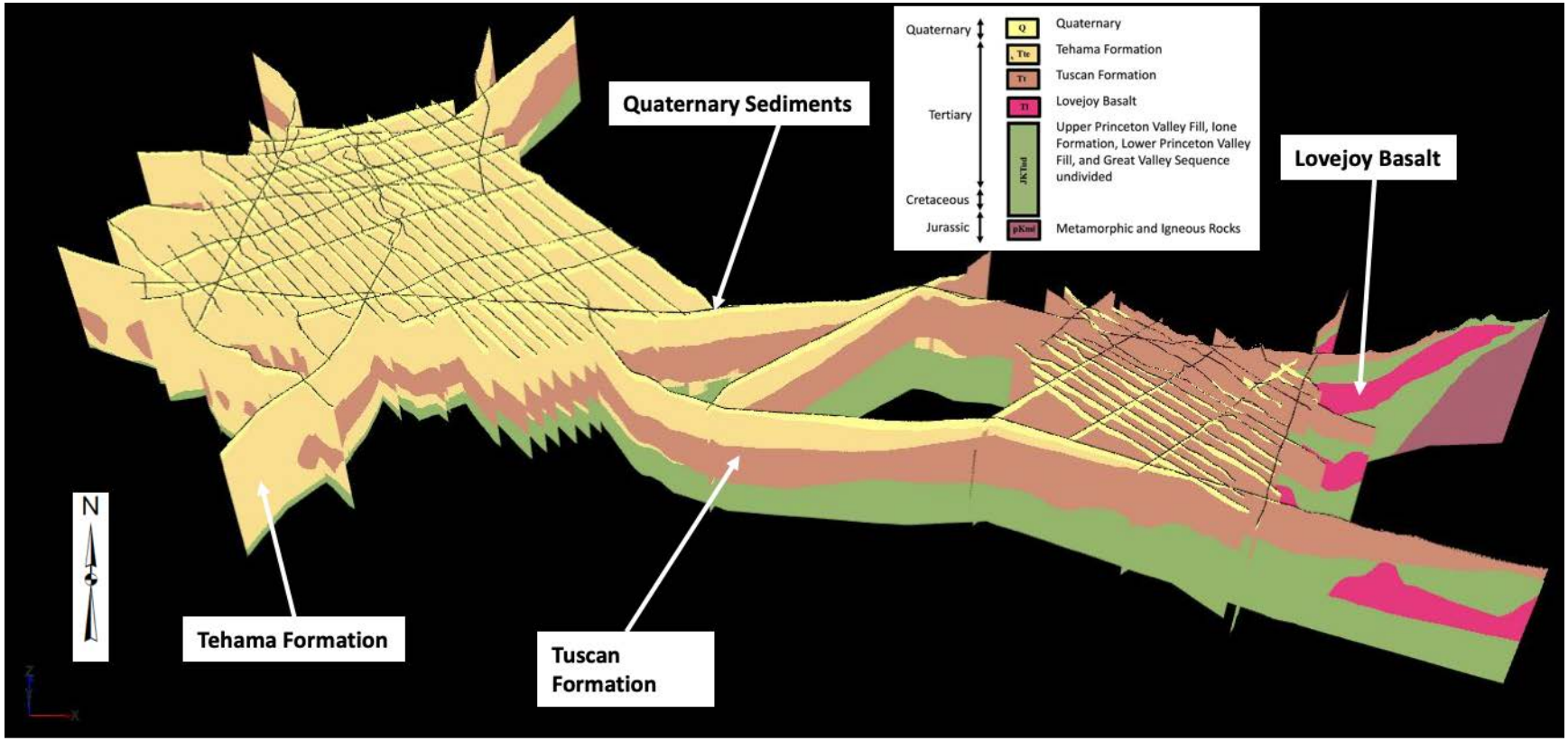

Figure 5-63. 3D fence diagram, looking north, of the interpreted geologic formations within the AEM survey area. Note the thin Quaternary sediments in the near surface and also the thinning of the Quaternary sediments to the east side of the area.

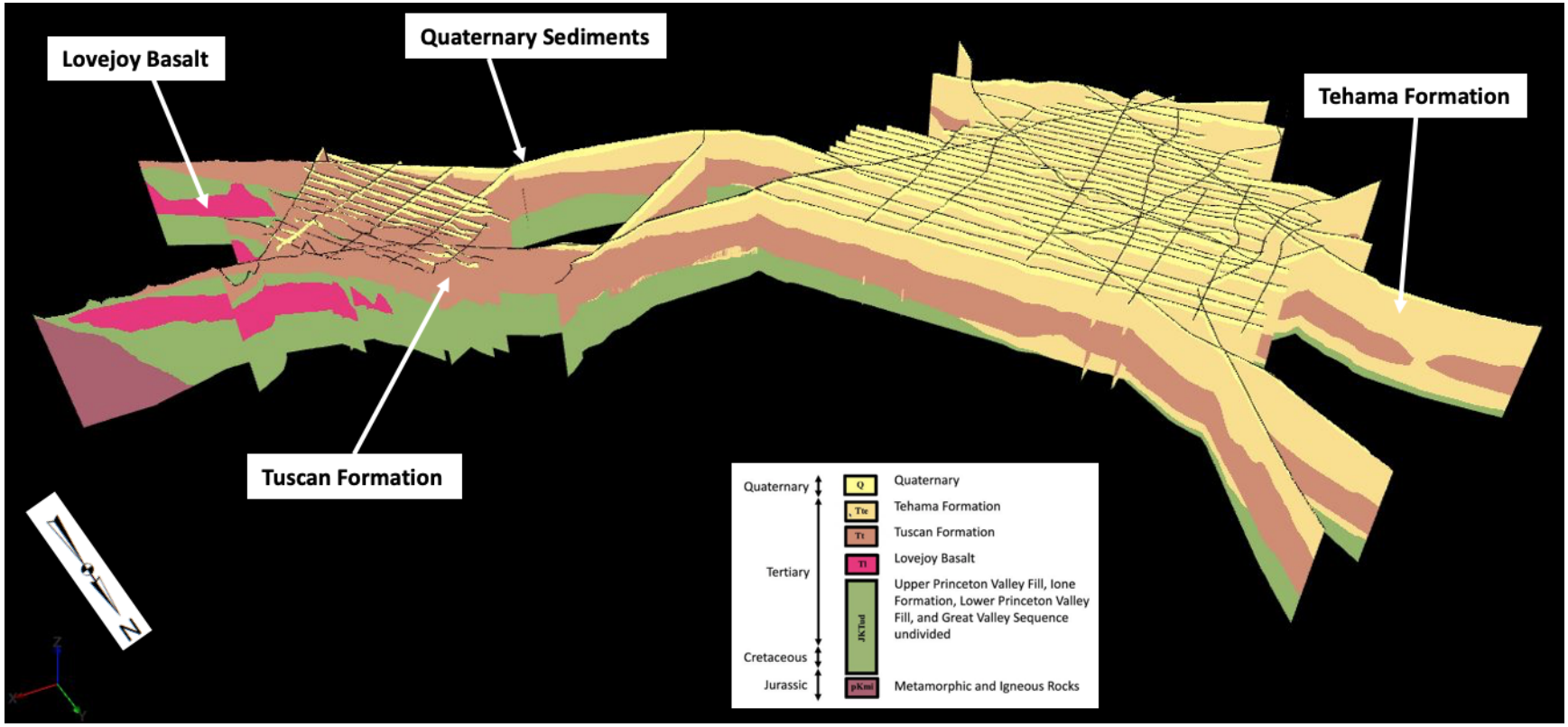

Figure 5-64. 3D fence diagram, looking south, of the interpreted geologic formations within the AEM survey area. Note the thin Quaternary sediments in the near surface and also the thickening of the Tehama deposits along the west side of the area.

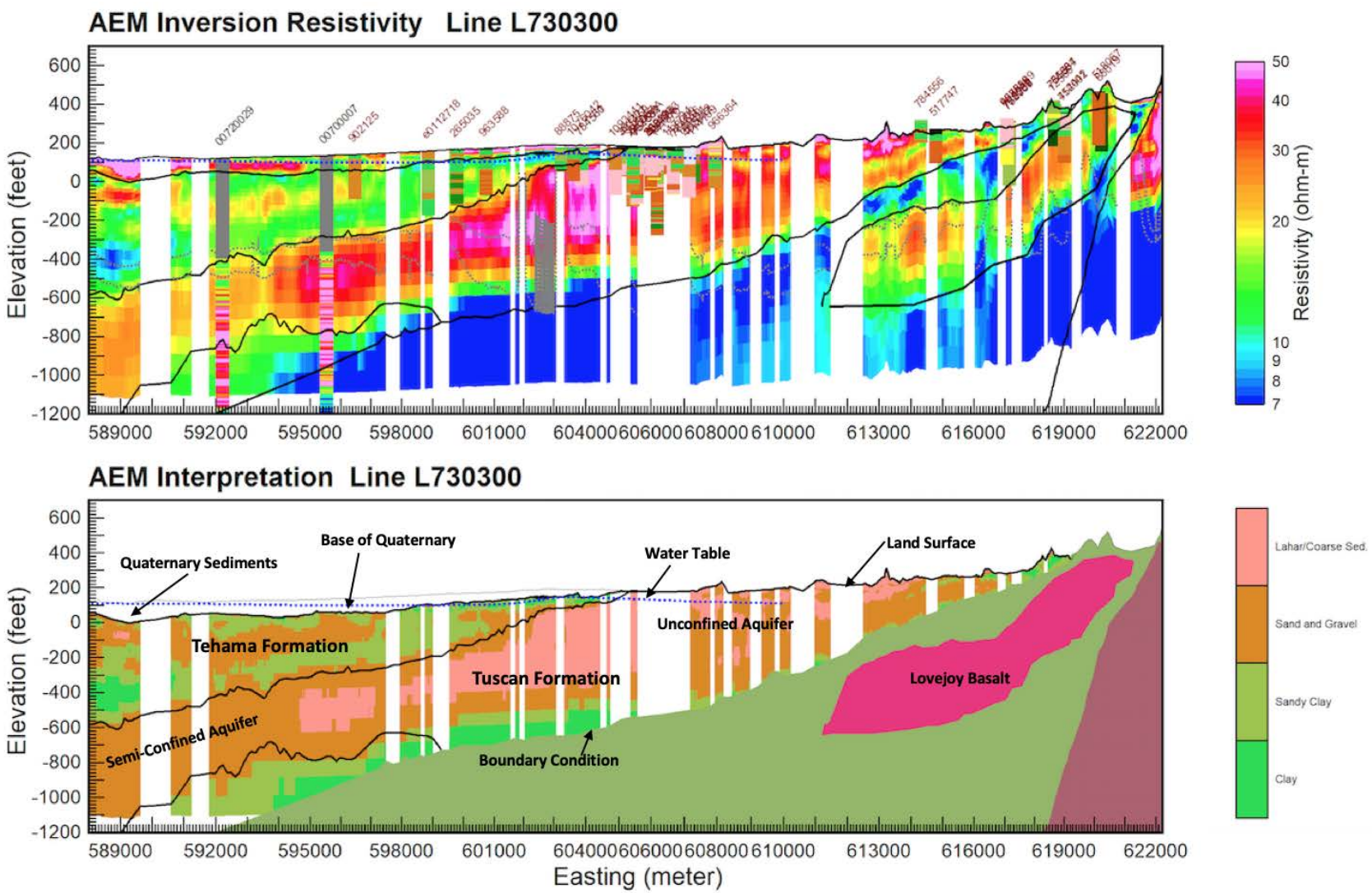

Figure 5-65. Interpreted AEM profile L730300 which is a west to east flight line. Note the dipping beds to the west. The top of the Upper Princeton Valley Fill (*Tupvf)* is considered a boundary condition in this report. Tuscan and Tehama formations are considered aquifers and receive recharge, generally, across the survey area.

In some areas of the survey there are profiles that show many of the objectives of this project. Northwest-southeast line L101501 (Figure 5-66) is in the center of the 312 AEM flight area and crosses the Sacramento River on the flight line's southern end. The profile shows many of the features of the sedimentary deposits that make up the hydrogeologic framework. The resistivity profile shows the great amount of detail that is contained in the flight line. In particular, the heterogeneity of the ***Q***. materials with the Sacramento River floodplain on the right end of the profile and sparse and thin material elsewhere. In the interpretation profile, areas of unconfined and semi-confined to confined areas are indicated. Most of the ***Tte*** is unconfined and hydrologically connected to the ***Q***. Between the ***Tte*** and the ***Tt***, layers of clay and sandy clay act as confining to semi-confining layers that rest upon the sand and gravel deposits. The clay and sandy clay act as boundaries because of their lower hydraulic transmissivity characteristics compared to sand and gravel. The detailed geometry provided by the AEM allows for high definition, within the aquifer systems, of where these sharp flow boundaries are.

Southwest-northeast AEM flight line L200701 (Figure 5-67), south center of the Western area, also displays similar features as Figure 5-65 in both the resistivity and interpreted profile. The sand and gravel in the ***Tte*** are a continuous single feature at depth and are predominantly unconfined. There is, however, a thicker clay seam (100 ft to 200 ft) between the ***Tte*** and ***Tt*** for a good length of this profile. Note the thinning of the coarse sediments of the ***Tte*** as you move from west to east, in agreement with the other AEM profiles and the CA-DWR (2014) report.

Using the interpretive surfaces and grids that were produced as described above in Section 5.6, an enhanced understanding of the hydrogeological framework of the Butte AEM investigation area can be achieved. Figure 5-52 is the total thickness of the ***Q*** deposits which make up the near surface aquifer where saturated. There are well defined channels near the Sacramento River and Little Butte Creek that have thicknesses up to 120 feet. These channel deposits make good aquifers where saturated and the sediment packages are made up of sand and gravel. Note that the flight lines that are on the slope of the hills southeast of Chico have limited to no ***Q*** materials where the ***Tt*** outcrops.

Figure 5-53 is the thickness map of the ***Tte***. The ***Tte*** is an aquifer where it is saturated and has sufficient thickness and permeable sedimentary packages to provide water to wells. The overall shape and geometry of the ***Tte*** in the survey area shows thinning of the unit towards the east with a change in thickness from 0 to over 1200 feet. This is consistent with the deposition of sediment in the ***Tte*** which originates in the Coast Range. The ***Tte*** sitting underneath the permeable ***Q*** materials (Figure 5-65) allows for recharge to move into the formation from above. The ***Tte*** is in contact with the ***Q*** everywhere in the survey area.

Figure 5-54 is a thickness map of the ***Tt***. The ***Tt*** is an aquifer where it is saturated and has sufficient thickness and permeable sedimentary packages to provide water to wells. Within the ***Tt*** the lahar deposits are treated as non-aquifer materials except for where they are fractured. The overall shape and geometry of the ***Tt*** in the survey area shows thinning of the unit from east to west with a change in thickness from 0 to over 700 feet which is consistent with the origin of the sediments coming out of the Sierra Nevada Mountains to the east. There appears what may be channel deposits in the ***Tt*** just west of the Sacramento River west of Chico (Figure 5-68). The ***Tt*** subcrops to outcrops in the east (Figure 5-65)

and the thick section of ***Tt*** to the southeast of Chico in Figure 5-68 is partly made up of lahar mudstone closest to the foothills and coarse sand and gravel further out which allows for recharge to move into the formation from the ***Q*** and ***Tte*** sediments above.

Figure 5-51 shows the elevation of the top of the ***Tupvf***, a generally smooth sloping surface from east to west. The surface changes in elevation from ~449 feet in the east to ~-1,177 in the west. The ***Tupvf*** is considered a base of the aquifer units in the AEM survey area as it is electrically conductive and so is primarily composed of fine sediments in this area and should be considered a boundary condition. The ***Tupvf*** can receive fresh water on the eastern side of the survey area.

The ***Tl*** can be treated as a non-aquifer and is a boundary condition. It can potentially provide water wells where it is fractured and has hydraulic connection to permeable sediments surrounding it. Figure 5-65 shows the location of the ***Tl*** underneath the ***Tupvf.***

The CA-DWR (2014) report states that the base of the ***Tte*** and the base of the ***Tt*** are considered to be the base of fresh water in the northern Sacramento Valley. In corroboration of this statement, examination of the AEM resistivity inversion results indicate that water quality at depth compared to the resistivity in the profile L710201 (Figure 5-8 or Figure 5-72 below) shows that a potential change can be seen along the base of the ***Tt*** that possibly indicates an upwelling of poor quality water near easting 4400000 and at the western end of the profile between easting 438500-4387000. A test-hole/water quality monitoring well installation would conclude whether the water quality is high in TDS and thus the contributes to the conductive signature in that area.

Well yields in the survey area are dependent on the aquifer materials present, the geometry of the aquifer, surface water hydrologic connection, hydrologic connection between the aquifers, heterogeneity of the geologic formations, the transmissivity of the aquifer materials, screen length, and well development among other things. Section 2 of this report gives a list of public aquifer test results near the project area (Table 2-3). These tests are point source in nature and should not be used at a regional level but used locally. CA-DWR (2014) lists borehole lithology, geophysical logs, well completion records, and screened intervals related to the formations. The information on well yield is qualitative in these well reports and listed as only good or fair. The best potential well yield can be best seen in the 2D profiles like Figure 5-68 which shows the thickness of the sand and gravel deposits in the ***Tt***.

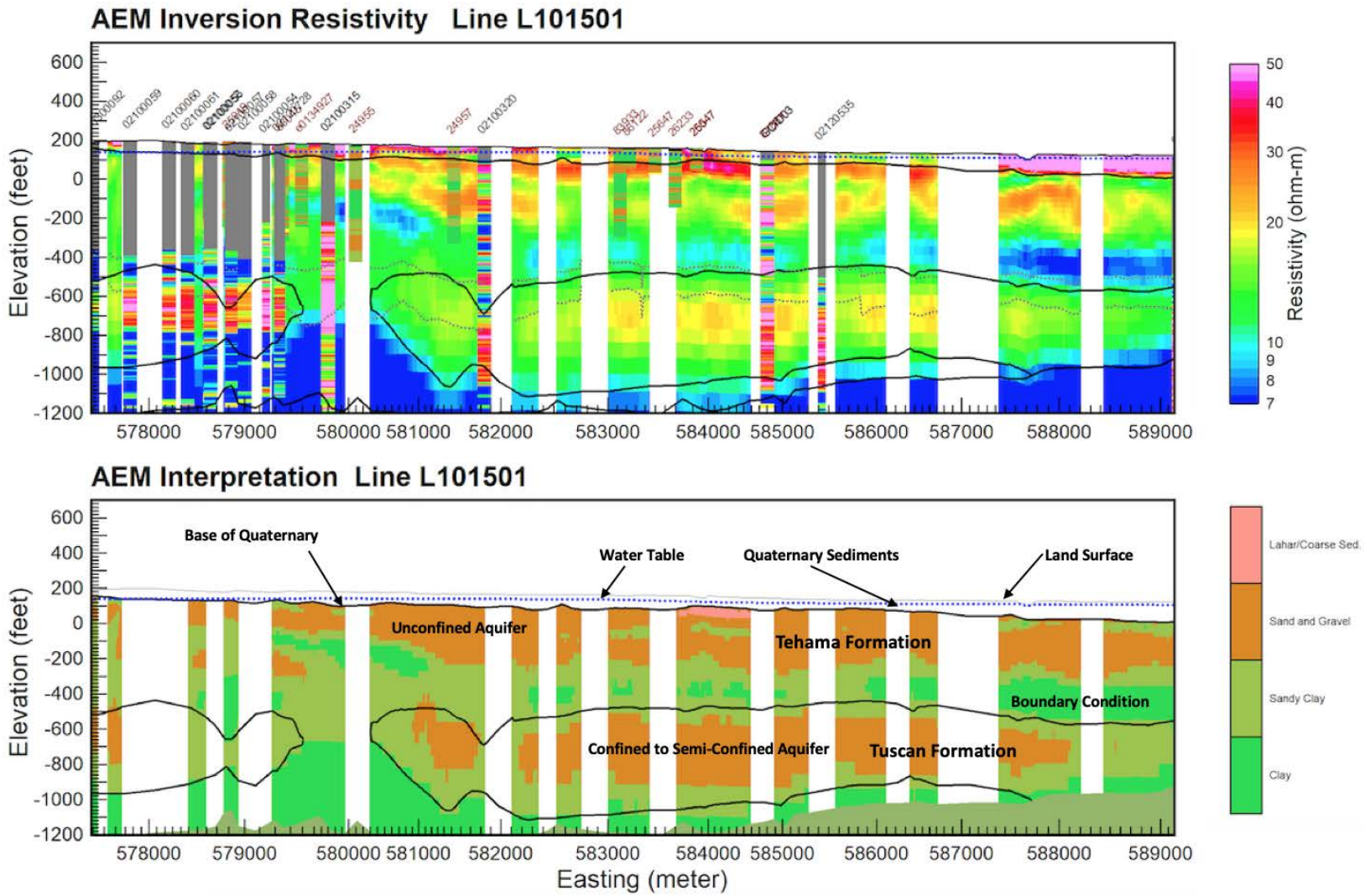

Figure 5-66. Interpreted AEM profile L101501 which is a northwest to southeast flight line. Note the heterogeneity within the Tuscan (*Tt*) and Tehama (*Tte*) formations. Where these formations have enough permeable material, they are good aquifers.

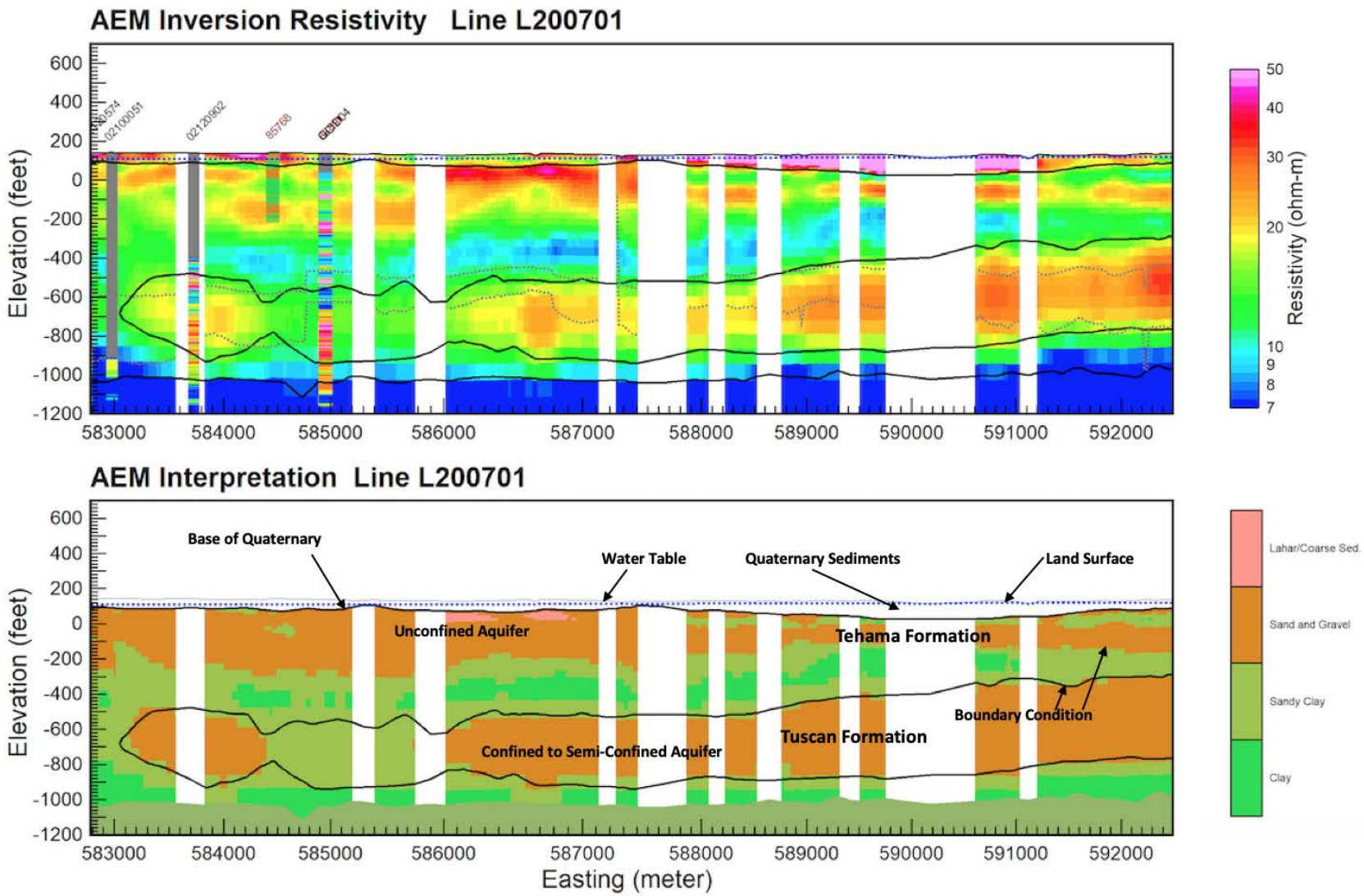

Figure 5-67. Interpreted AEM profile L200701 which is a southwest to northeast flight line. Note the heterogeneity within the Tuscan (*Tt*) and Tehama (*Tte*) formations which are considered aquifers. The *Tte* is in in contact with the Quaternary sediments throughout the area. Where these formations have enough permeable material, they are good aquifers.

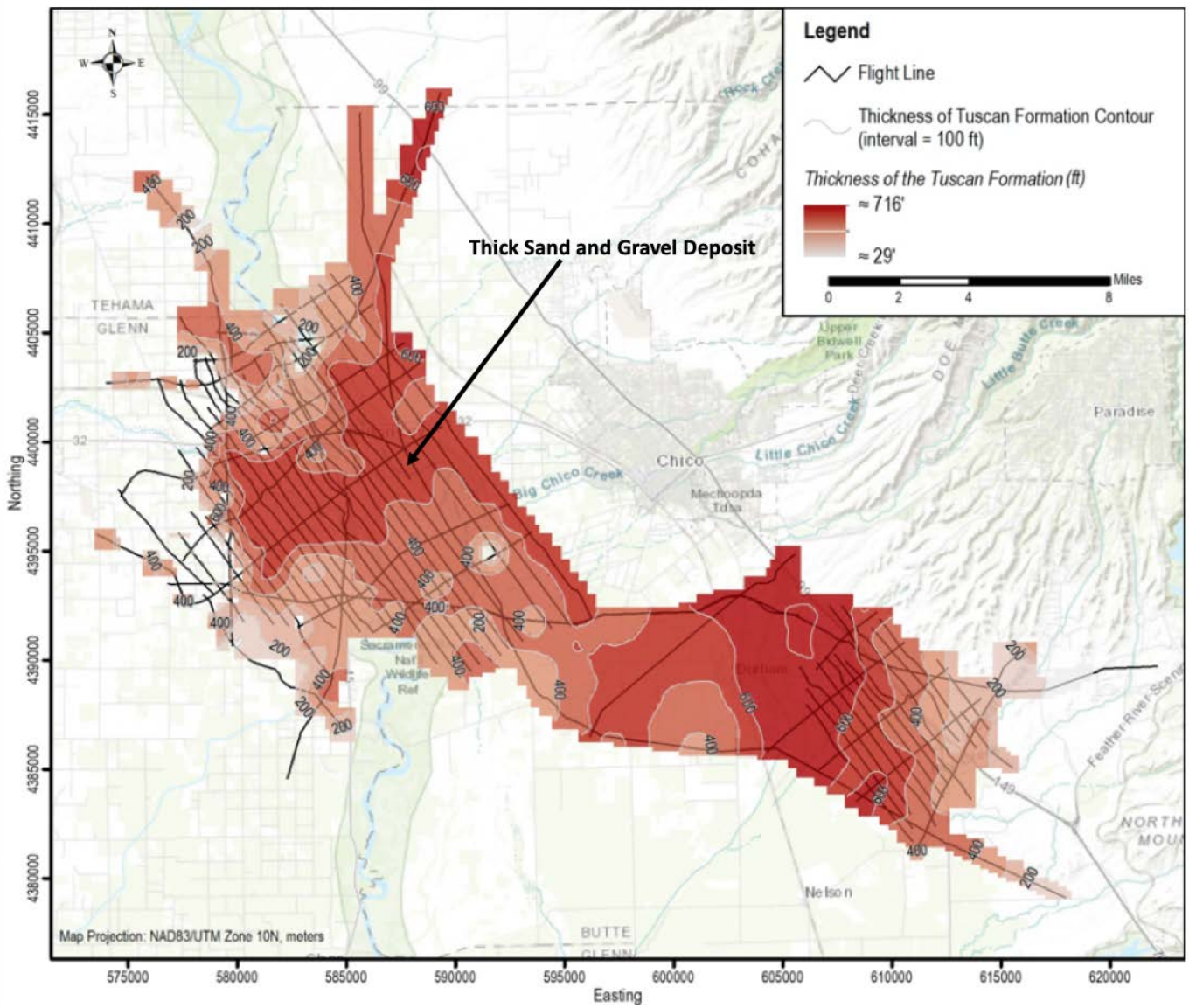

Figure 5-68. Map of the total thickness of the Tuscan FM within the Butte AEM survey area showing areas of thick sand and gravel deposits as well as lahar in some places. The projection is NAD83 UTM Zone 10N (meters) and the elevation values are referenced to NAVD 88 (feet).

5.9 Recharge Areas within the Butte AEM Survey Area

3D representations of the subsurface resulting from AEM investigations illustrate areas of aquifer materials from the DOI and/or bedrock up to the land surface. From these interpretations a series of near-surface maps were constructed that include the intervals from 0 to 3 ft, 3 ft to 7 ft, and 7 to 11 ft. The three intervals listed are noteworthy because they cover the first 3 layers from the land surface downward of the inverted AEM earth model. Remember from the discussion around Table 4-5, that each model layer represents an average of the earth's resistivities within those layers, based on the physics of the electromagnetic exploration technique. The first layer through the third layer maps (Figure 5-69, Figure 5-70, and Figure 5-71) show the changes in resistivity as a color ramp from blue, the most transmissive, to dark yellow the least transmissive. These maps are only showing those resistivities greater than 20 ohm-m. These would include the Coarse Sediments and Sand and Gravel lithological groupings. These maps indicate the areas near the land surface that can potentially transmit water to the aquifers in the area. By viewing layers 1 through 3, in order, an understanding of subtle changes in the heterogeneity of the geologic materials and their distribution can be achieved. There is not always a direct path downwards to the geologic from the land surface. Often there is no path available for the water to move through. A KMZ of all the layers can be viewed in Google Earth and are in the Appendix 3\KMZ\Recharge.

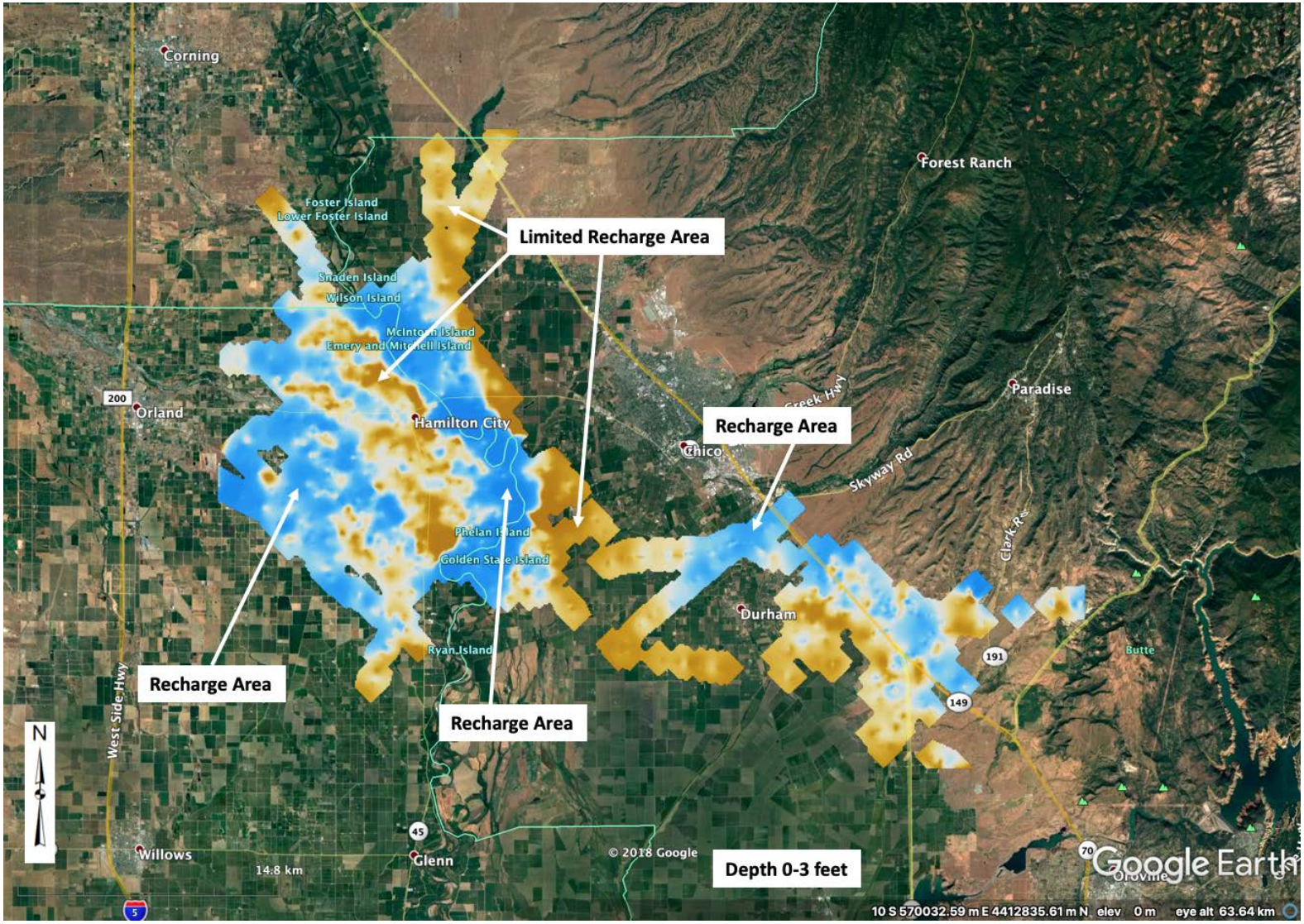

Figure 5-69. Map of the inverted AEM resistivities (>20 ohm-m) related to the geologic materials from 0' to 3' below the ground surface within the 2018 Butte AEM survey area. Blue areas indicate higher rates of recharge.

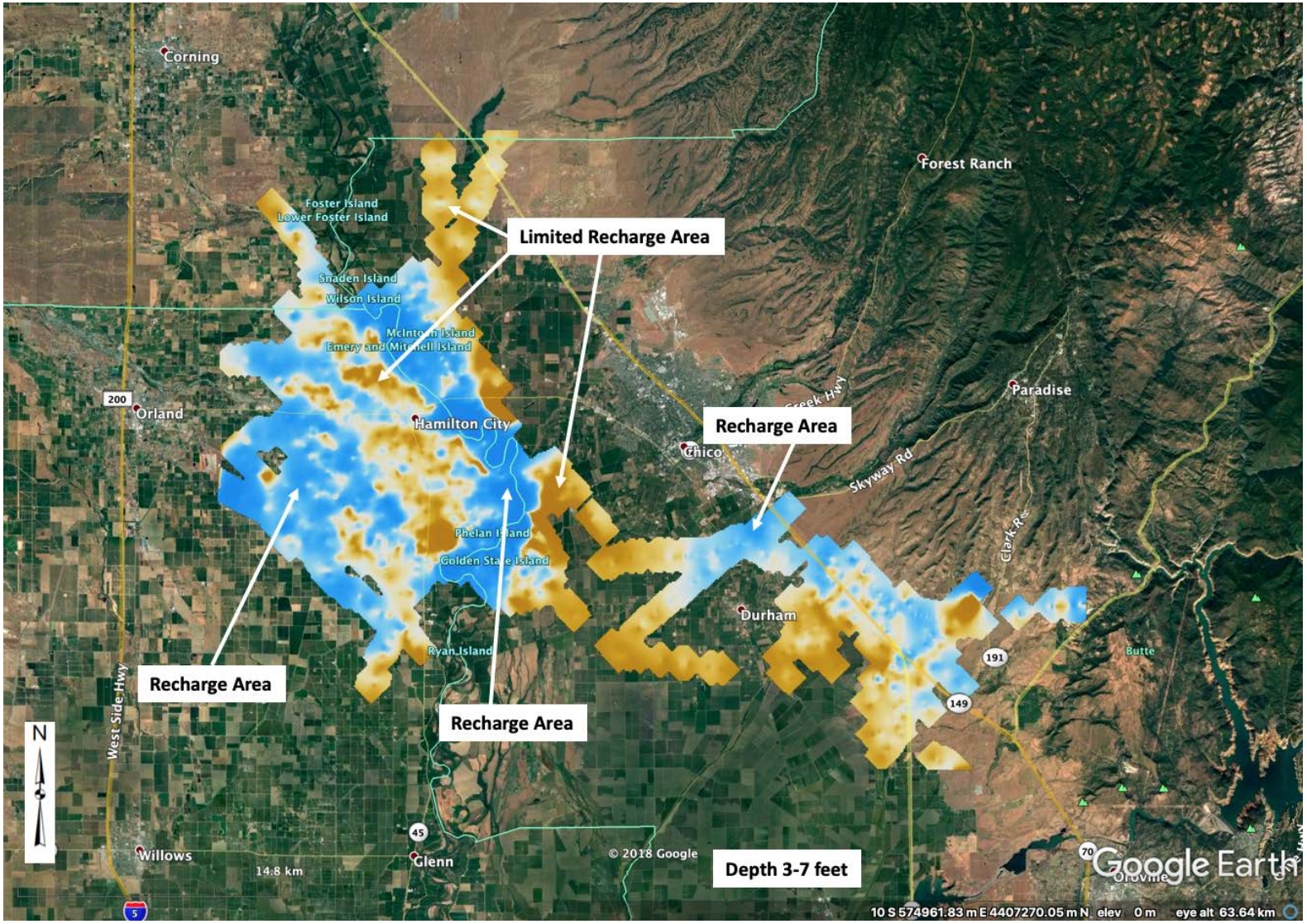

Figure 5-70. Map of the inverted AEM resistivities (>20 ohm-m) related to the geologic materials from 3' to 7' below the ground surface within the 2018 Butte AEM survey area. Blue areas indicate higher rates of recharge.

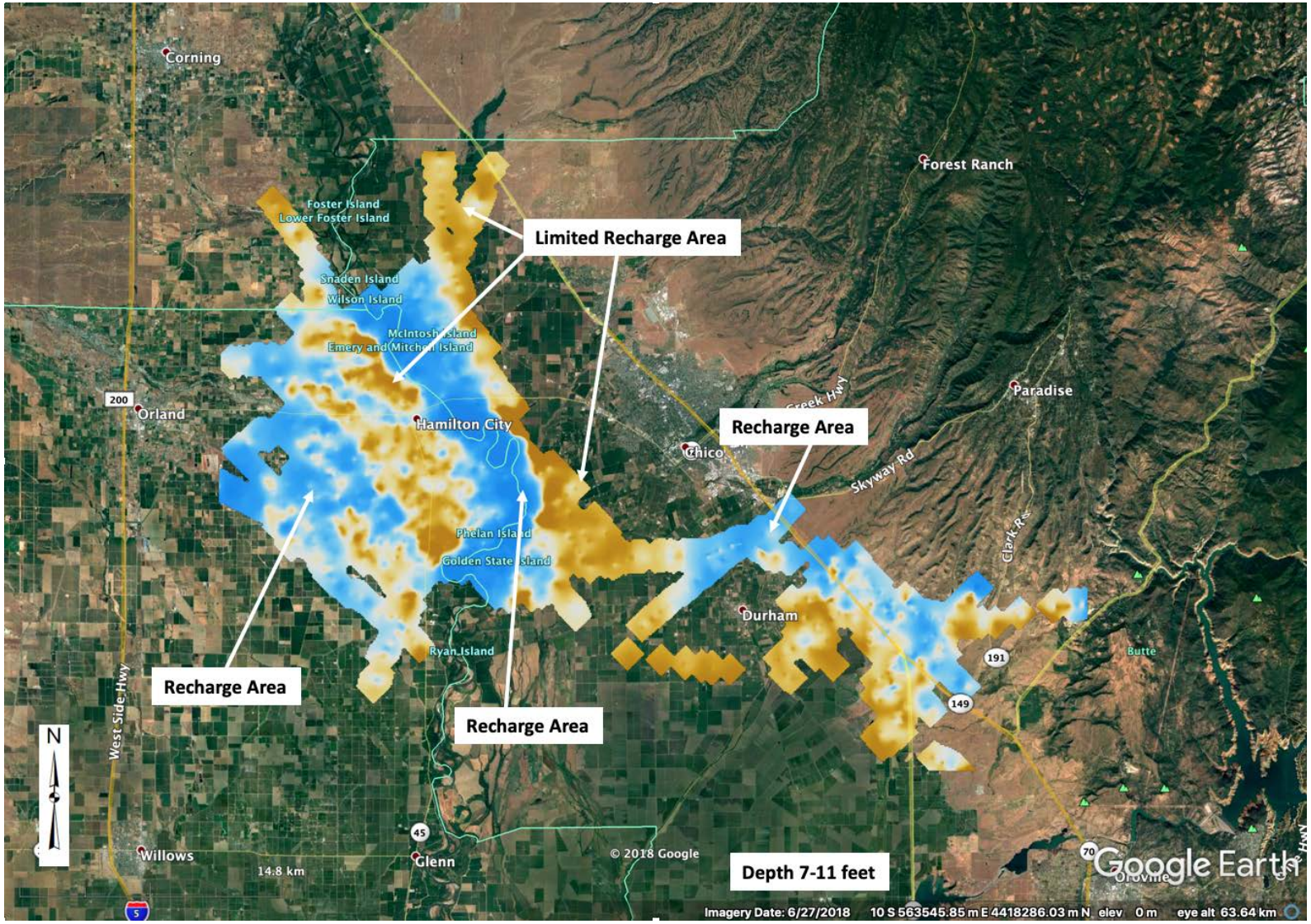

Figure 5-71. Map of the inverted AEM resistivities (>20 ohm-m) related to the geologic materials from 7' to 11' below the ground surface within the 2018 Butte AEM survey area. Blue areas indicate higher rates of recharge.

However, since the amount of slope of the land surface plays a large role in the amount of residence time that water will spend in an area, the greater the length of time spent at a location, the greater the amount of infiltration potential. The greatest possibility for recharge in the Butte investigation AEM survey area is the alluvial valley floor and the creek beds that have geologic materials that conduct water easily and are near the land surface. On the valley side slopes and valley, the best possible location for recharge would be where there is a combination of geologic materials at the land surface on the uplands with little relief in elevation with a pathway of similar materials down to the saturated aquifer at depth. AEM profile L710201 (Figure 5-72) provides an example of this with the flight path paralleling the Sacramento River from south to north. Note that while the ***Q*** geologic materials are thin, they are in direct contact with the underlying ***Tte*** and there is a good pathway to the underlying aquifer materials.

AEM profile L200801 (Figure 5-73) provides a different perspective. This flight path is perpendicular to the Sacramento River from west to east. Note the ***Q*** geologic materials are thin, are mostly sand and gravel, and are in direct contact with the underlying Tehama FM. However, the upper ***Tte*** materials contain low transmissivity geologic materials due to the presence of clay and sandy clay just underlying the ***Q*** materials. Note that there are windows of transmissive geologic materials along the flight lines to the aquifer below.

Figure 5-74 is a voxel model cut across the Sacramento River in order to show the inverted AEM resistivities of the geologic materials, greater than 15 ohm-m, from the ground surface to depth. The voxel model represents the changes in resistivity by color from low-green to high-pink as a color ramp, which is related to geologic materials from Sand to Sand and Gravel. The continuous nature of the data in the form of the voxel model allows the reader to see the connections between similar geologic materials in 3D. This figure shows the pathways for water to get from the land surface downward under the River and the boundary conditions that exist from the slightly less transmissive geologic materials.

Analysis of the recharge potential of the area shows that there are many areas that are recharging the aquifers of the survey area. Using these maps, cross-sections, and voxels will allow for a greater understanding of the pathways the recharge takes for management purposes. Water quality management can be improved by tailoring the management practices for the recharge in an area. An example is that you would want limit fertilizer application over areas of good recharge versus areas of low recharge. For water quantity management an example is to site managed aquifer recharge areas to locations that have the greatest recharge potential, greatest unsaturated thickness, and the ability to move water to the site. The use of AEM data along with other sources of information like soils maps will be beneficial for many hydrogeologic decisions in the survey area.

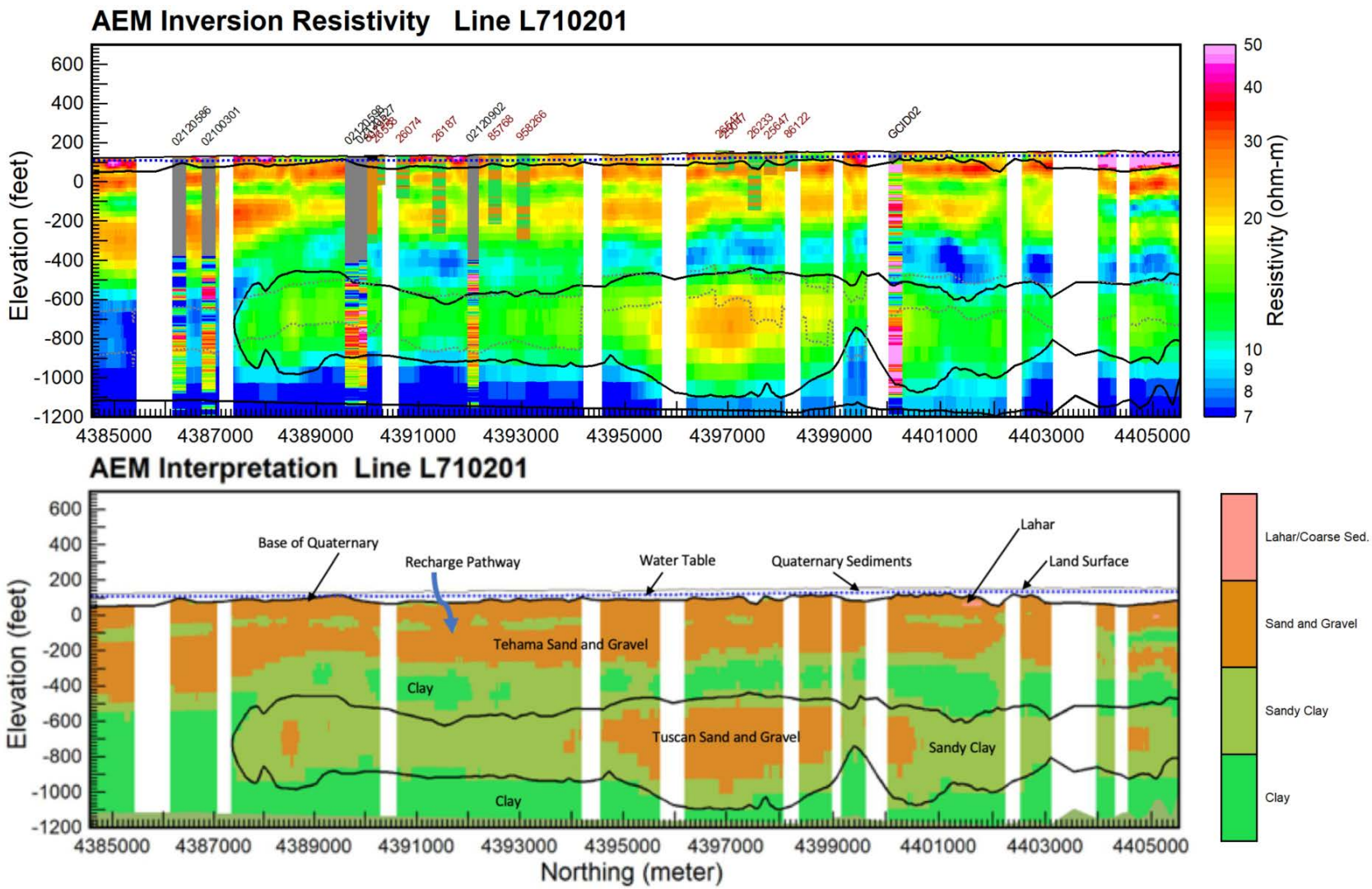

Figure 5-72. Profile L710201 provides interpretation of the geologic materials along a flight path paralleling the Sacramento River from south to north. Note the Quaternary (*Q*) geologic materials are thin and are in direct contact with the underlying Tehama Formation and have a high transmissivity.

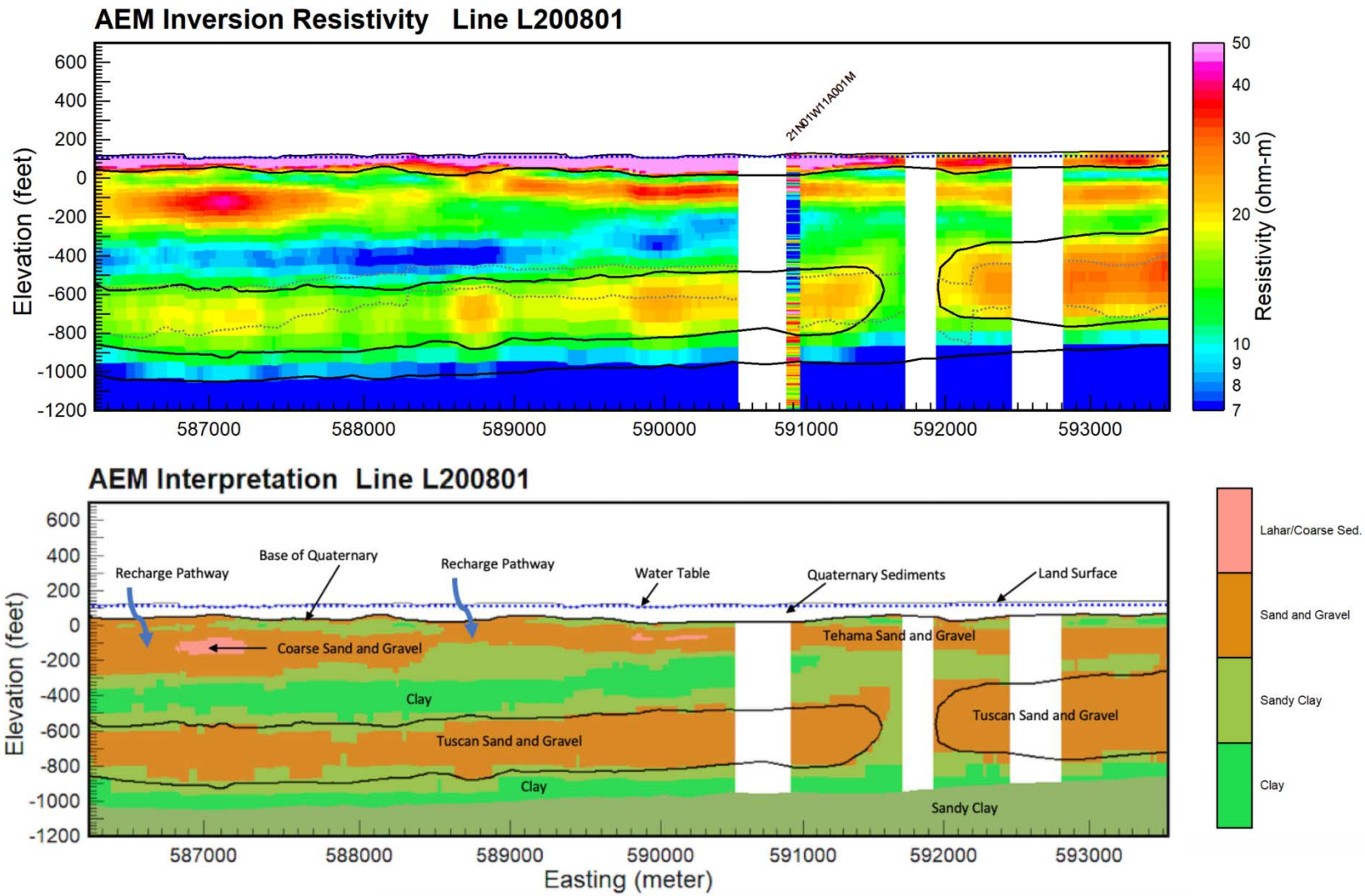

Figure 5-73. Profile L200801 provides interpretation of the geologic materials along a flight path perpendicular to the Sacramento River from west to east. While the Quaternary (Q) geologic materials along this profile are made of coarse material, the unit is thin. The top of the underlying Tehama Formation is made of a mix of less transmissive geologic materials (clay and sandy clay) but does have windows of transmissive geologic materials along the flight path.

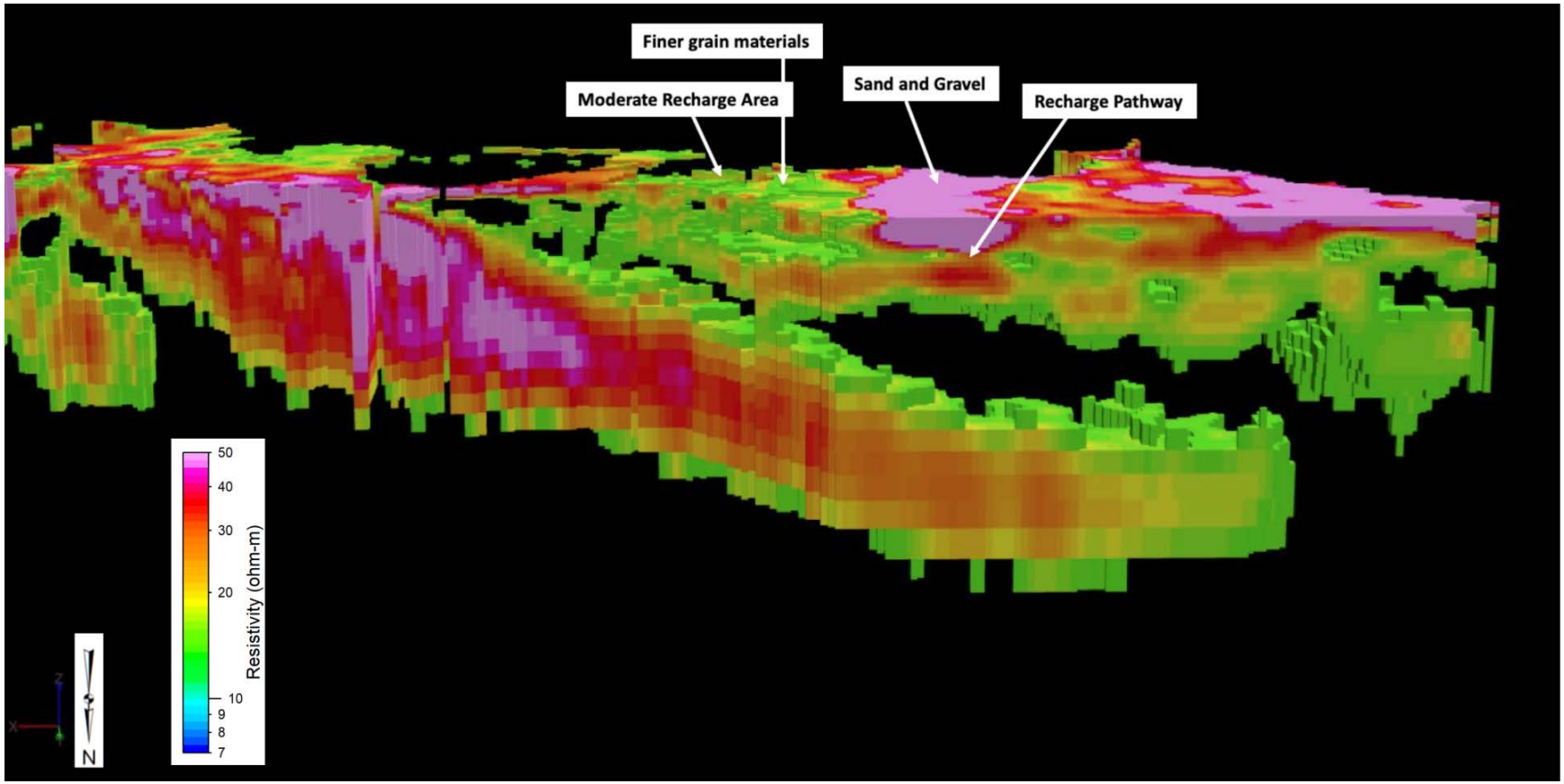

Figure 5-74. A cut voxel model showing the resistivity of the geologic materials greater than 15 ohm-m from the ground surface to the top of the undivided Upper Princeton Valley Fill/Ione FM/Great Valley Sequence. The voxel model represents the changes in resistivity by color from low-green to high-pink as a color ramp, which is related to geologic materials Sand-green to Sand and Gravel-pink. View is to the south.

5.10 Key AEM Findings

5.10.1 Boreholes

Information from boreholes was used to analyze the Butte AEM inversion results. A total of 362 holes contained lithology information and 183 holes contained geophysical information within the Butte AEM survey area. These boreholes were provided by Dr. Todd Greene, Associate Professor of Geological and Environmental Sciences at California State University, Chico under separate contract. The AEM inversion results matched up well with most of the both the geophysical logs and also the lithological logs.

5.10.2 Digitizing Interpreted Geological Contacts

Characterization and interpretation of the subsurface was performed in cross-section and derived surface grid formats. Contacts between the geologic units were digitized in 2D including: Quaternary (***Q***), Tertiary Tehama FM (***Tte***), Tertiary Tuscan FM (***Tt***), Tertiary Upper Princeton Valley Fill (***Tupvf***), Tertiary Lovejoy Basalt (***Tl***), Tertiary Ione FM (***Ti***), and the Jurassic-Cretaceous Great Valley Sequence (***JKgvs***). However, because the ***Tupvf***, ***Ti***, and ***JKgvs*** are all very electrically conductive, and could not be distinguished from each other at depth, they were grouped into one unit, ***JKTud*** – Undivided Upper Princeton/Ione/Great Valley Sequence. The interpretive process greatly benefited from the use of the borehole logs. Surface grids of the interpreted geologic formations were produced as well as interpretative profiles. Each flight line profile with interpretation is included in the appendices as well as the interpretative surface grids.

5.10.3 Comparing the AEM Results with the CA-DWR (2014) Cross-Sections

The stratigraphic interpretation of the Butte AEM inversion results compared very well with cross-sections B-B', E-E', and F-F' from the CA-DWR (2014) report on the geology of the northern Sacramento Valley. There were two main difference between the AEM and the CA-DWR cross-sections. One was that the AEM shows the Tehama FM continuing further east than what is shown on cross-section B-B' before it thins out up against the foothills of the Sierra Nevada Mountains. The second difference was that the 312 did not image an extension of the Lovejoy Basalt because the flow was apparently too deep. Although it is also not clear if the Lovejoy actually extends out as far as the 312 AEM flight lines so that it could be imaged.

5.10.4 Comparing Results From the 304M and 312 Systems on the Overlap Line

Two airborne electromagnetic TEM systems were operated during the Butte AEM investigation. One was the SkyTEM304M (304M) and the other was the SkyTEM312 (312). In order to compare the systems, part of a traverse was flown twice, once by the 312 as part of flight line L710601 and a second time by the 304M as part of flight line L730300. While the 304M imaged the very near surface (<16 ft (<5 m)) better than the 312, below about 82 ft (25 m) depth, both systems imaged the subsurface equally well until an elevation of about -950 ft (-290 m). After that depth, the 312 system showed much better resolution than did the 304M.

5.10.5 Resistivity/Lithology Relationship

An assessment of the lithologic character of the Tehama and Tuscan formations was conducted to determine the overall composition of the major categories used to define aquifer and aquitard material. The lithological log-AEM inversion match up information was used to develop the resistivity-lithology relationship. They are: Clay (<10 ohm-m), Sandy Clay (10-15 ohm-m), Sand and Gravel (15-34ohm-m) and Lahar/Coarse Sediments (>34 ohm-m). This allowed for the characterization of the ranges of resistivities present in the major geologic units described in this report which were then used in understanding the hydrogeological framework.

5.10.6 Hydrogeological Framework of the Butte AEM Survey Area

The Quaternary aquifer system was too thin and heterogeneous to subdivide into sediment packages. The water table is present in the Quaternary and is close to the land surface in most of the area. Thus, Quaternary alluvial material provides the pathway for recharge into the underlying Tertiary Tehama and Tuscan formations. The Tertiary Tehama Formation is heterogeneous and in direct contact with the Quaternary across the AEM survey area providing a good hydrologic connection. The Tertiary Tuscan Formation is in direct contact with the Tertiary Tehama formation across most of the AEM survey area and has a good hydrologic connection in many areas but is also limited in some areas due to thick clay zones above the Tuscan FM in the lower Tehama FM. The Great Valley Sequence Undivided formational package is considered the base of aquifer for this study. The Tertiary Lovejoy Basalt is considered a non-aquifer in this report. The lahar deposits are considered non-aquifers in this report as they are competent rock units, except where fractured. The eastern section of the survey area has near surface sub-crops and outcrops of the Tuscan FM and, in places, is nine miles wide providing an excellent recharge area for groundwater. Water quality at depth compared to some of the resistivity profiles shows that a potential change can be seen along the base of the Tuscan FM that possibly indicates an upwelling of poor-quality water in certain locations. A test-hole/water quality monitoring well installation would conclude whether the water quality is high in TDS and thus the contributes to the conductive signature in that area.

5.10.7 Estimation of Aquifer Volume and Water in Storage in the Butte AEM Survey Area

Estimation of aquifer volume and yield were not calculated for the Butte AEM survey area because the units are a complex mix of lahar, sandstone, sand and gravel, sand, silty clay, and clay. The Tuscan FM, breaking down and discontinuous on its western extremum, is difficult to properly characterize without good aquifer production information such as porosity and specific yield to break down water availability in the different lithologies. If such information becomes available, an add-on project could be proposed to make the aquifer and volume estimations using the lithological-resistivity relationships developed during this investigation.

5.10.8 Potential Recharge Zones within Butte AEM Survey Area

The Quaternary deposits are hydrologically connected to the streams and rivers of the AEM survey area. This hydrologic connection can be strong in many areas due to the coarse nature of a large percentage of the sediments present. Where the Tehama, and underneath it, the Tuscan, are in direct contact with the Quaternary sediments, there is a direct hydrologic connection between them in many places. Recharge can be good between the surface, Quaternary sediments and Tehama and Tuscan Formations along favorable sand and gravel sediments in

contact with each other. Where there is subcrop and outcrop of the Tuscan FM along the east side of the 304M survey area, recharge can go directly from the surface to the groundwater system increasing the potentiometric surface downgradient from this area.

5.11 Recommendations

Recommendations provided to the Butte/Glenn Counties in this section are based on the interpretation and understanding gained from the addition of the AEM data to existing information and from discussions with the Butte/Glenn Counties about their management challenges. There are additional recommendations based on the results related to the pilot project experience.

5.11.1 Additional AEM Mapping

The aquifer maps provided in this report represent the detailed framework developed for the western and eastern block-flights and the reconnaissance level flight lines. The detail provided in the hydrogeological interpretations of the western and eastern block-flights allowed for confident development of hydrogeologic framework. The interpretations match well with the boreholes. No additional high resolution AEM information is needed within the Western and Eastern block-flights areas to resolve questions of resource management. Thus, it is recommended that additional areas of closely spaced lines or “block-flights” be collected to develop detailed frameworks in other areas. The 1640 ft (500 m) spacing between flight lines could be reduced to a 984 ft (300 m) spacing for greater detail and fidelity to the natural system.

Reconnaissance flight lines and the surrounding area should be mapped in detail by block flights to provide information on the hydrogeologic framework and the recharge areas. This would potentially be done in cooperation with the neighboring counties to get details to the continuous aquifer system that is shared in the area. The line spacing for the block flights should be on the order of 984 ft (300 m).

It is recommended that additional closely spaced block flight lines for collection of AEM data and interpretation be considered in critical areas of eastern Butte/Glenn Counties. This will supply the Butte/Glenn Counties with information at greater detail on groundwater flow, aquifer sustainability, and depletion to streams, well interference, groundwater withdrawal, and other management considerations.

5.11.2 Update the Water Table map

The groundwater data used in the analyses presented in this report used the Fall 2017 water table map. Additional water level measurement locations would improve the water table map. In particular, up in the foothills.

5.11.3 Siting new test holes and production wells

The AEM framework maps and profiles provided in this report provide insight in 3D on the relationship between current test holes and production groundwater wells. At the time of this report, the currently available lithology and geophysical log data for the Butte/Glenn Counties area were used in building the framework maps and profiles. It is recommended that the results from this report be used to site new

test holes and monitoring wells. Often test holes are sited based on previous work that is regional in nature or for local projects of small size. By utilizing the maps in this report new drilling locations can be sited in optimal locations. Consideration for the areas that have been identified as confined to semi-confined aquifers is a good place to start doing this work. These wells need to be screened in discreet zones in order to understand the potentiometric surfaces from each zone. These wells should also be spaced geographically for water level/potentiometric head measurements as well as water quality sampling. Small screened intervals would allow for age dating the water for improved understanding of recharge, time of travel along flow paths and groundwater-surface water interaction.

The location of new water supply wells for communities can also use the AEM results in this report to guide development of new water supply wells. Planners should locate wells in areas of greatest saturated thickness with the least potential for non-point source pollution.

5.11.4 Aquifer testing and borehole logging

Aquifer tests are recommended to improve estimates of aquifer characteristics. A robust aquifer characterization program is highly recommended at the state, county, and smaller municipal levels. Aquifer tests can be designed based on the results of AEM surveys and existing production wells could be used in conjunction with three or more installed water level observation wells (which can be used as monitoring wells for levels and water quality sampling after the test).

Additional test holes with detailed, functional, and well calibrated geophysical logging for aquifer characteristics are highly recommended. Most of the borehole geophysical logs provided for this investigation were well calibrated. However, there were also quite a few that demonstrate that additional calibrated and verified geophysical logs would be useful in the Butte/Glenn Counties.

Examples of additional logging would be flow meter logs and geophysical logs including gamma, neutron, electrical, and induction logs. Detailed aquifer characteristics can be accomplished with nuclear magnetic resonance logging (NMR). This is a quick and effective way to characterize porosity and water content, estimates of permeability, mobile/bound water fraction, and pore-size distributions with depth. NMR logs compare well with the aquifer tests in our experience and are very cost effective when compared to traditional aquifer tests.

5.11.5 Recharge Zones

The Butte/Glenn Counties hydrogeologic framework in this report provides areas of recharge from the ground surface to the groundwater aquifers. The block flights of AEM data acquisition provide the most detailed information for understanding recharge throughout the block flight areas. It is recommended that additional AEM data be collected and interpreted utilizing closely-spaced flight lines using an AEM system that has near-surface resolution in the reconnaissance line flight areas. It is further recommended that future work integrate new soils maps with the results of this study to provide details on soil permeability, slope, and water retention to provide a more complete understanding of the transport of water from the land surface to the groundwater aquifers.

5.11.6 Managed Aquifer Recharge

There are areas which may have potential for managed aquifer recharge (MAR) or aquifer storage and recovery (ASR) facilities. Detailed analysis for this purpose would need to be done to determine if this is a viable opportunity for the Butte/Glenn Counties. Additional AEM mapping along the streams in the Butte/Glenn Counties would also locate similar locations. A detailed plan for locating and developing Managed Aquifer Recharge sites would be beneficial to the Butte/Glenn Counties for providing storage and release of water for stream flow and other uses. During times of high surface water flow a prebuilt system of moving water from the rivers and streams to MAR or ASR facilities would be recommended to easily take advantage of this opportunity.

6 Description of Data Delivered

6.1 Tables Describing Included Data Files

Table 6-1 describes the raw data files included in Appendix 3_Deliverables \Raw_Data. As discussed above, five (5) 312 flights and two (2) 304 flights were required to acquire the Butte AEM data (Figure 4-5). Grouped by flight date, there are four (4) data flies included in Appendix 3\Raw_Data for each flight. These files have extensions of "*.sps" and "*.skb". The "*.sps" files include navigation and DGPS location data and the "*.skb" files include the raw AEM data that have been PFC-corrections (discussed in section 4.4.1). Two additional sets of files are used for all the flights. These are the system description and specifications file (with the extension "*.gex") in the GEO subdirectory and the 'mask' file (with the extension "*.lin"), in the MASK subdirectory, which correlates the flight dates, flight numbers, and assigned line numbers.

Table 6-2 describes the data columns in the ASCII *.xyz files Butte_EM304_MAG.xyz and Butte_EM312_MAG.xyz. This file contains the electromagnetic data, plus the magnetic and navigational data, as supplied directly from SkyTEM.

The result of the SCI is included in Butte_304_312_AEM_SCI_Inv_v1.xyz and the data columns of these databases are described in Table 6-3.

The borehole data used to assist in the interpretation of the SCI inversion results are included in the files listed in Table 6-4. Each type of borehole information has both a collar file containing the location of each of the wells, and a second file containing the borehole data for the individual wells. The data column descriptions for the collar files are listed in Table 6-5. Table 6-6 describes the channels in the lithology borehole data files and Table 6-7 describes the channels in the geophysical borehole data files.

The various interpretation results are included in the data file Butte_InterpSurfaces_v1 in ASCII xyz format. Table 6-8 describes the data columns of those files.

ESRI Arc View Binary Grids of the surfaces that were used in the interpretation (DEM, water table) and derived from the interpretation (top of geological units) of the AEM and borehole are listed in Table 6-9 and stored in Appendix 3_Deliverables\Grids.

Two voxel grids (converted to ASCII) were completed for the AEM inversion results within the Butte AEM survey area. The voxel grids were made using a 200 m grid cell size and the 304M model layer thickness (Table 4-5). One voxel grid has all the inverted resistivities (Butte_AEM_ALLRho_voxel.xyz) and the other has had a 15 ohm-m threshold applied (Butte_AEM_gt15_voxel.xyz). The columns of these files are described in Table 6-10 and stored in Appendix 3_Deliverables\Voxel.

In summary, the following are included as deliverables:

- Raw EM Mag data as ASCII *.xyz
- SCI inversion as ASCII *.xyz
- Borehole databases as ASCII *.xyz
- Interpretations as ASCII *.xyz
- Raw Data Files - SkyTEM files *.geo, *skb, *.lin
- ESRI ArcView grid files – surface, topo, etc
- 3D fence diagrams of the Stratigraphic interpretation
- 3D voxel models as ASCII *.xyz for the Butte AEM data

KMZs for AsFlown, Retained, Recharge, and Interpretation results (Discussed in Section 6.2)

Table 6-1. Raw SkyTEM data files

Folder	File Name	Description
Data	..NavSys.sps, …PaPc.sps, ...RawData_PFC.skb, …DPGS.sps	Raw data files included for each flight used in importing to Aarhus Workbench
Geo	20181217_304_Butte_DualWaveform_60Hz_skb.gex 20181217_304_Butte_DualWaveform_60Hz_skb_SR2.gex 20181217_304_Butte_DualWaveform_60Hz_skb_SR2.sr2	304M System Description
Geo	20181211_312_Butte_DualWaveform_60Hz_skb.gex 20181211_312_Butte_DualWaveform_60Hz_skb_SR2.gex 20181211_312_Butte_DualWaveform_60Hz_skb_SR2.sr2	312 System Description
Mask	455_USA_Butte_County_Prod.lin	Production file listing dates, flights, and assigned line numbers

Table 6-2 Channel name, description, and units for Butte_EM304_MAG.xyz and Butte_EM312_MAG.xyz with EM, magnetic, DGPS, Inclinometer, altitude, and associated data.

Parameter	Description	Unit
Fid	Unique Fiducial Number	
Line	Line Number	
Flight	Name of Flight	yyyymmdd.ff
DateTime	DateTime Format	Decimal days
Date	DateTime Format	yyyymmdd
Time	Time UTC	hhmmss.sss
AngleX	Angle (in flight direction)	Degrees
AngleY	Angle (perpendicular to flight direction)	Degrees
Height	Filtered Height Measurement	Meters [m]
Lon	Longitude, WGS84	Decimal Degrees
Lat	Latitude, WGS84	Decimal Degrees
E_UTM10N_m	Easting, NAD83 UTM Zone 10N	Meters [m]
N_UTM10N m	Northing, NAD83 UTM Zone 10N	Meters [m]
DEM	Digital Elevation	Meters [m]
Alt	DGPS Altitude above sea level	Meters [m]
GDSpeedL	Ground Speed	Kilometers/hour [km/h]
Curr_LM	Current, Low Moment	Amps [A]
Curr_HM	Current, High Moment	Amps [A]
LMZ_G01	Normalized (PFC-Corrected) Low Moment Z-RxCoil values array	$pV/(m^4*A)$
HMZ_G01	Normalized (PFC-Corrected) High Moment Z-RxCoil values array	$pV/(m^4*A)$
HMX_G01	Normalized (PFC-Corrected) High Moment X-RxCoil values array	$pV/(m^4*A)$
PLNI	Power Line Noise Intensity monitor	V/m^2
Bmag	Raw Base Station Mag Data filtered	nanoTesla [nT]
MAG_Raw	Raw Mag Data	nanoTesla [nT]
Mag_ED	Mag filtered	nanoTesla [nT]
Diurnal	Diurnal Mag Data	nanoTesla [nT]
Mag_Cor	Mag Data Corrected for Diurnal Drift	nanoTesla [nT]

RMF	Residual Magnetic Field	nanoTesla [nT]
TMI	Total Magnetic Intensity	nanoTesla [nT]

Table 6-3. Channel name, description, and units for Butte_304_312_AEM_SCI_Inv_v1.xyz with EM inversion results.

Parameter	Description	Unit
LINE	Line Number	
East_M	Easting NAD83, UTM Zone 10	Meters [m]
North_M	Northing NAD83, UTM Zone 10	Meters [m]
DEM_M	DEM from survey	Meters [m]
DEM_FT	DEM from 100 ft grid NED NAVD88	Feet [ft]
FID	Unique Fiducial Number	
TIME	Date Time Format	Decimal days
ALT_M	Altitude of system above ground	Meters [m]
INVALT	Inverted Altitude of system above ground	Meters [m]
INVALTSTD	Inverted Altitude Standard Deviation of system above ground	Meters [m]
DELTAALT	Change in Altitude of system above ground	Meters [m]
RESDATA	Residual of individual sounding	
RESTOTAL	Total residual for inverted section	
DOI_CONSERVATIVE_FT	More conservative estimate of DOI	Feet [ft]
DOI_STANDARD_FT	Less conservative estimate of DOI	Feet [ft]
RHO_0 THROUGH RHO_38	Inverted resistivity of each later	Ohm-m
RHO_STD	Inverted resistivity error per layer	
SIGMA_I_0 THROUGH SIGMA_I_39	Conductivity	S/m
DEP_TOP_304_0_FT THRU DEP_TOP_304_38_FT	Depth to the top of individual layers	Feet [ft]
DEP_BOT_304_0_FT THRU DEP_BOT_304_38_FT	Depth to the bottom of individual layers	Feet [ft]
THK_304_0_FT THROUGH THK_304_38_FT	Thickness of individual layers	Feet [ft]
DEP_TOP_312_0_FT THRU DEP_TOP_312_38_FT	Depth to the top of individual layers	Feet [ft]
DEP_BOT_312_0_FT THRU DEP_BOT_312_38_FT	Depth to the bottom of individual layers	Feet [ft]
THK_312_0_FT THROUGH THK_312_38_FT	Thickness of individual layers	Feet [ft]

Table 6-4. Files containing borehole information.

Database (*.xyz)	Description
Butte_ELogs_Final_Collar.xyz	ELogs logs with original data received from Todd Greene, CSU-Chico
Butte_ELogs_Final_Data.xyz	
Butte_Lith_Final_Collar.xyz	Lithology logs with original data received from Todd Greene, CSU-Chico
Butte_Lith_Final_Data.xyz	

Table 6-5: Channel name, description, and units for collar files.

Parameter	Description	Unit
DH_Hole	Name of individual boreholes	
DH_East	Easting of boreholes, NAD83, UTM Zone 10	Feet [ft]
DH_North	Northing of boreholes, NAD83, UTM Zone 10	Feet [ft]
DH_RL	Elevation of top of borehole	Feet [ft]
DH_Dip	Dip of borehole	Degrees
DH_Azimuth	Azimuth of borehole	Degrees
DH_Top	Depth to top of borehole	Feet [ft]
DH_Bottom	Depth to bottom of borehole	Feet [ft]

Table 6-6: Channel name description and units for Lithology borehole data.

Parameter	Description	Unit
DH_Hole	Name of Borehole	
DH_East	Easting of boreholes, NAD83, UTM Zone 14	Feet [ft]
DH_North	Northing of boreholes, NAD83, UTM Zone 14	Feet [ft]
DH_RL	Elevation of top of borehole	Feet [ft]
DH_From	End of interval	Feet[ft]
DH_To	Start of interval	Feet [ft]
Lithcode	Lithology description associated with 30 categories	
DH_Description	Description of lithology material	

Table 6-7: Channel name description and units for E-Logs borehole data.

Parameter	Description	Unit	Type of Log
DH_Hole	Name of Borehole		
DH_East	Easting of boreholes, NAD83, UTM Zone 10	Meters (m)	All
DH_North	Northing of boreholes, NAD83, UTM Zone 10	Feet [ft]	All
DH_RL	Elevation of top of borehole	Feet [ft]	All
DH_Depth	Depth	Feet [ft]	GP
DH_SP	Self Potential	milliVolt [mV]	GP
DH_SN	Short Normal Resistivity	Ohm-m	GP
DH_SFL	Spherically Focus Log	Ohm-m]	GP
ILD	Induction Log Deep depth	Siemens/m [S/m]	GP
ILM	Induction Log Medium depth	Siemens/m [S/m]	GP
LATERAL	Laterolog Resistivity	Ohm-m	GP
LL8	Laterolog Resistivity	Ohm-m	GP
GR	Natural Gamma	Counts	GP
AM_RES	Type of Resistivity	Ohm-m	GP
SN	Short Normal Resistivity 16in	Ohm-m	GP
LN	Long Normal Resistivity 64in	Ohm-m	GP
LAT20	Laterolog Resistivity 20 in	Ohm-m	GP
LAT18	Laterolog Resistivity 20 in	Ohm-m	GP
SP	Self Potential	milliVolt [mV]	GP
Res_FL	Resistivity of the fluid	Ohm-m	GP
AO	Type of Resistivity Log	Ohm-m	GP
AHT	Type of Resistivity Log	Ohm-m	GP
AHT10	Type of Resistivity Log	Ohm-m	GP
POINT_RHO	Single-Point Resistivity Log	Ohm-m	GP

Table 6-8: Channel name, description, and units for the interpretation results file Butte_InterpSurfaces_v1.xyz.

Parameter	Description	Unit
Easting	Easting NAD83, UTM Zone 10	Meters (m)
Northing	Northing NAD83, UTM Zone 10	Meters (m)
DEM_ft	Topography at 100ft sampling (NAVD 1988)	Feet [ft]
RHO[0] through RHO[38]	Array of Inverted model resistivities of each later	Ohm-m
RESDATA	Inversion model residuals of each individual sounding	
DEP_TOP[0] through DEP_TOP[38]	Depth to the top of individual layers	Feet [ft]
DEP_BOT[0] through DEP_BOT[38]	Depth to the bottom of individual layers	Feet [ft]
DOI_Standard	Less conservative estimate of DOI from Workbench	Feet [ft]
DOI_Conservative	More conservative estimate of DOI from Workbench	Feet [ft]
WaterTable_2017	Elevation of the top of the water table from the 2017 report.	Feet [ft]
Top_Q	Top of Quaternary (***Q***) sediments in the Butte AEM survey area	Feet (ft)
Top_Tte	Top of Tehama FM (***Tte***)	Feet [ft]
Top_Tt	Top of Tuscan FM (***Tt***)	Feet [ft]
Top_TteLower	Top of lower Tehama FM contact (bottom of ***Tt***) (TteLower)	Feet [ft]
Top_Tupvf	Top of Upper Princeton Valley Fill (Tupvf)	Feet [ft]
Top_Tl	Top of Lovejoy Basalt (***Tl***)	Feet [ft]
Top_Ti	Top of Ione FM (***Ti***)	Feet [ft]
Top_JKgvs	Top of Jurassic-Cretaceous Great Valley Sequence (***JKgvs***)	Feet [ft]
Top_Granite	Top of Granite which only occurs on L730300	Feet [ft]

Table 6-9. Files containing ESRI ArcView Binary Grids *.flt (NAD 83 UTM 10 North)

Grid File Name	Description	Grid Cell Size (meters)
Butte_DEM	Digital Elevation Model (ground surface elevation) (NAVD88 feet) of the 2018 Butte survey area, NAD83/UTM Zone 10N meters	10
Butte_WT_F2017	Elevation (NAVD88 feet) of the water table (Fall 2017) for the 2018 Butte Survey area, NAD83/UTM Zone 10N meters	10
Butte_Q_Thickness	Total thickness (feet) of the unconsolidated Quaternary deposits for the 2018 Butte Survey area, NAD83/UTM Zone 10N meters	200
Butte_Tte_Thickness	Total thickness (feet) of the Tehama Formation for the 2018 Butte Survey area, NAD83/UTM Zone 10N meters	200
Butte_Tt_Thickness	Total thickness (feet) of the Tuscan Formation for the 2018 Butte Survey area, NAD83/UTM Zone 10N meters	200
Butte_Tl_Thickness	Total thickness (feet) of the Lovejoy Basalt for the 2018 Butte Survey area, NAD83/UTM Zone 10N meters	200
Butte_Tte_Ele	Elevation (NAVD88 feet) of the top of the Tehama Formation for the 2018 Butte Survey area, NAD83/UTM Zone 10N meters	200
Butte_Tt_Ele	Elevation (NAVD88 feet) of the top of the Tuscan Formation for the 2018 Butte Survey area, NAD83/UTM Zone 10N meters	200
Butte_Tupvf_ele	Elevation (NAVD88 feet) of the top of the Upper Princeton Valley Fill for the 2018 Butte Survey area, NAD83/UTM Zone 10N meters	200
Butte_Tl_ele	Elevation (NAVD88 feet) of the top of the Lovejoy Basalt for the 2018 Butte Survey area, NAD83/UTM Zone 10N meters	200
Butte_TTeSandGravel_Thickness	Tehama Formation total sand and gravel thickness (feet) for the 2018 Butte Survey area, NAD83/UTM Zone 10N meters	200

Table 6-10. Channel name, description, and units for Butte_AEM_gt15_voxel.xyz and Butte_AEM_ALLRho_voxel.xyz

Parameter	Description	Unit
X	Easting NAD83, UTM 10N	Meters (m)
Y	Northing NAD83, UTM 10N	Meters (m)
Z	Depth of Voxel Node	feet [ft]
Elevation	Surface Elevation of Voxel Node	NAVD88 [ft]
Resistivity	Voxel cell resistivity value	Ohm-m

6.2 Description of Included Google Earth KMZ Data and Profiles

In addition to the data delivered in .xyz format, a Google Earth .KMZ file was generated to view the geophysical AEM flight line locations and interpreted geologic data. KMZ files for all "*As-Flown*" flight lines and data "*Retained*" for inversion after editing are included in the folder "*Appendix_3_Deliverables\KMZ\FlightLines*".

KMZ files of the potential recharge zones in the Butte AEM investigation area are included in the folder "*Appendix_3_Deliverables\KMZ\Recharge*"

Unique KMZ files were created for each individual flight line. Within this specialized KMZ file, the AEM flight line is shown as well as place marks at each location where there are interpreted geologic results. The attribute data for each unique place mark contains location information plus the elevations of tops of the interpreted stratigraphy as well as the 2017 water table. This KMZ file is located within the "*Appendix_3_Deliverables\KMZ\Interpretation\Butte_Profiles*" folder. Also, in this folder is a "*GoogleE_Readme.pdf*" file that provides instructions in regard to the "*Settings*" changes that need to be made in Google Earth, and how to use the KMZ files in Google Earth including a legend of what attributes are displayed when an AEM sounding location is clicked. This file is repeated below as a convenience. An example of the Butte AEM Interpretation KMZ is presented in Figure 6-1.

6.2.1 Included README for the Butte AEM Interpretation KMZ

README for:

Butte_AEM_Interpretation.kmz

Data Files - Please copy the folder *Butte_Profiles* to your C:\ drive. Do not rename any of the images within the folder.

Google Earth Instructions:

STEP 1: In Google Earth, click "*Tools*", then "*Options*".

STEP 2: In the Google Earth Options box, click the "*General*" tab.

STEP 3: Under "*Placemark balloons*", make sure the box is checked to allow access to local files (the profiles).

STEP 4: Under "*Display*", make sure the box is checked to show web results in external browser.

STEP 5: The *Butte_AEM_Interpretation.kmz* file within the folder named *Butte_Profiles* can now be opened and viewed in Google Earth.

Data:

East (m) – Easting coordinate in NAD83, UTM 10N, in meters

North (m) – Northing coordinate in NAD83, UTM 10N, in meters

Elev (ft) – Digital Elevation Model (DEM) elevation in feet

WaterTable2017 Elev (ft) – 2017 Water Table elevation, in feet

Top_Q (ft) – Top of Quaternary sediments (usually the same as the Elev (ft)), in feet

Top_Tte (ft) – Top of the Tehama FM, in feet

Top_Tt (ft) – Top of the Tuscan FM, in feet

Top_TteLower – Lower contact of Tuscan FM, when Tuscan FM is present, in feet

Top_Tupvf – Top of Upper Princeton Valley Fill, in feet

Top_Tl – Top of Lovejoy Basalt, in feet

Top_Ti – Top of Ione FM, in feet

Top_JKgvs – Top of Jurassic-Cretaceous Great Valley Sequence, in feet

Top_Granite – Top of Granite on L730300, in feet

ProfileS – Link to AEM Interpreted Stratigraphy profile images

ProfileL – Link to AEM Interpreted Lithology profile images

Legend – Link to this write-up describing data channels listed here

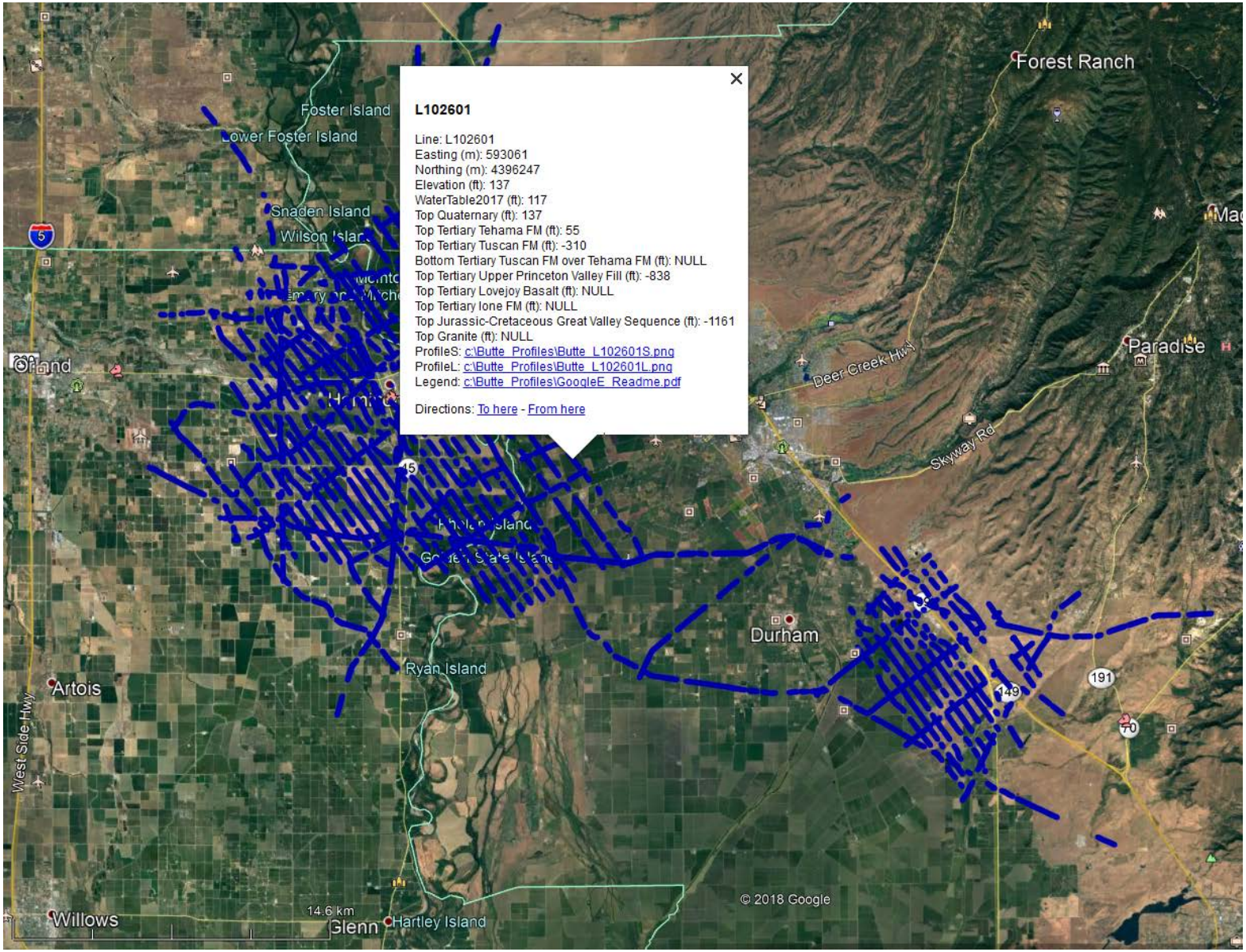

Figure 6-1. Example Google Earth image for the Butte AEM Interpretation kmz.

7 References

Asch, T.H., Abraham, J.D., and Irons, T., 2015, A discussion on depth of investigation in geophysics and AEM inversion results, Presented at the Society of Exploration Geophysicists Annual Meeting, New Orleans.

Asch, T.H., Abraham, J.D., Cannia, J.C., 2017, AEM-based hydrogeological frameworks in the Owens and Central valleys of California: Fast Times, v.22, no.3, p.47-57.

Asch, T.H., Gottschalk, I., Knight, R., Abraham, J.D., Cannia, J.C., Van Der Maaten, K., 2018, An airborne electromagnetic investigation of the Marina, CA hydrogeologic framework: presented at the Symposium on the Application of Geophysics to Environmental and Engineering Problems, Nashville, Tennessee, 27 March 2018.

Bear, J., 1979, Hydraulics of groundwater: McGraw-Hill, New York, 569 p.

Blair, T.C., Baker, F.G., and Turner, J.B., 1991, Cenozoic Fluvial-Facies Architecture and Aquifer Heterogeneity, Oroville, California, Superfund Site and Vicinity, in A.D. Miall and N. Tyler, eds., The Three-Dimensional Facies Architecture of Terrigenous Clastic Sediments and Its Implications for Hydrocarbon Discovery and Recovery, SEPM, Concepts in Sedimentology and Paleontology, vol 3, 1991.

Blake, M.S., Helley, E.J., Jayko, A.S., Jones, D.L., and Ohlin, H.N., 1992, Geologic map of the Willows 1:100,000 quadrangle, California: U.S. Geological Survey, Open-File Report 92-271, scale 1:100,000

Brown and Caldwell, 2013, Aquifer performance test report Lower Tuscan aquifer monitoring, recharge and data management project: Brown and Caldwell, for Butte County Department of Water and Resource Conservation, April 26, 2013, 6 sections, various pagination.

Burnett, J.L., Ford, R.S., and Scott, R.G., 1969, Geology of the Richardson Springs quadrangle, California: California Division of Mines and Geology, Map Sheet 13, scale 1:62,500

California Department of Water Resources, 1996, M&T Chico Ranch conjunctive use investigation: Phase III, Memorandum Report; December 1996 [reference from Brown and Caldwell, 2013]

California Department of Water Resources, 2003a, Sacramento Valley Groundwater Basin, Corning Subbasin (5-21.51): State of California Department of Water Resources, Bulletin 118 Groundwater Basin Descriptions, accessed March 29, 2019 at: https://water.ca.gov/Programs/Groundwater-Management/Bulletin-118

California Department of Water Resources, 2003b, Sacramento Valley Groundwater Basin, Colusa Subbasin (5-21.52): State of California Department of Water Resources, Bulletin 118 Groundwater Basin Descriptions, accessed March 29, 2019 at: https://water.ca.gov/Programs/Groundwater-Management/Bulletin-118

California Department of Water Resources, 2003c, Sacramento Valley Groundwater Basin, Vina Subbasin (5-21.57): State of California Department of Water Resources, Bulletin 118 Groundwater Basin Descriptions, accessed March 29, 2019 at: https://water.ca.gov/Programs/Groundwater-Management/Bulletin-118

California Department of Water Resources, 2009, Glenn-Colusa Irrigation District test-production well installation and aquifer testing, March 2009, Appendix A-2, accessed March 29, 2019 at: http://www.buttecounty.net/waterresourceconservation/taifinalreport

California Department of Water Resources, 2014, Geology of the Northern Sacramento Valley, California: State of California, California Natural Resources Agency, California Department of Water Resources Northern Region Office, 213 p., 4 pl., at https://cawaterlibrary.net/wp-content/uploads/2017/05/Geology-of-the-Northern-Sacramento-Valley.pdf

California Department of Water Resources, 2018, Groundwater information center groundwater interactive map application: State of California, California Natural Resources Agency, California Department of Water Resources, accessed online March 29, 2019 at: https://gis.water.ca.gov/app/gicima/

California Department of Water Resources, 2019, Groundwater Information Center Interactive Map Application, (https://gis.water.ca.gov/app/gicima/#bookmark_GroundwaterElevation; (accessed March 10, 2019).

Carney, C.P., Abraham, J.D., Cannia, J.C., and Steele, G.V., 2015, Airborne Electromagnetic Geophysical Surveys and Hydrogeologic Framework Development for Selected Sites in the Lower Elkhorn Natural Resources District: prepared for the Lower Elkhorn Natural Resources District by Exploration Resources International Geophysics LLC, Vicksburg, MS. .http://www.enwra.org/LENRD2014AEMDataDownload.html (accessed December 31, 2018)

Christensen, N. B., J. E. Reid, and M. Halkjaer, 2009, "Fast, laterally smooth inversion of airborne time-domain elecromagnetic data." *Near Surface Geophysics* 599-612.

Christiansen, A. V. and E. Auken, 2012, "A global measure for depth of investigation." *Geophysics,Vol. 77, No. 4* WB171-177.

City of Chico, 2010, Geology and soils: City of Chico, California, General Plan Documents, Section 4.8 of Draft Environmental Impact Report – Geology and Soils, accessed online December 17, 2018 at: www.chico.ca.us/document_library/general_plan/documents/4.8GeologyandSoils.pdf

Crystal Geyser, 2009, Application for site plan review, October 5, 2009 [reference from Brown and Caldwell, 2013]

Dames & Moore, 1993, Extraction well field report, initial phase off-property groundwater remedial action: Koppers Company, Incorporated Superfund Site (Feather River Plant), July 1993 [reference from Brown and Caldwell, 2013]

DatamineDiscover, 2018, Datamine Discover Profile Analyst, available on the world-wide web at: https://www.dataminesoftware.com/discover/.(accessed December 31, 2018)

Davis, S.N. and Hall, F.R., 1959, Riverbank Formation description: Stanford University, Pub. Geol. Sci., v. 5 no 1, p. 6, 12, 16-20, pl 2, 3.

Driscoll, F.G, 1987, “Groundwater and Wells”, Published by Johnson Division, St. Paul, MN.

Foged, N., Auken, E., Christiansen, A.V., and Sorensen, K.I., 2013, Test-site calibration and validation of airborne and ground based TEM systems: Geophysics, V.78, No.2, E95-E106.

Freeze, R.A. and J.A. Cherry, 1979, Groundwater: Published by Prentice Hall, New Jersey, ISBN 0-13-365312-9.

French, J.J., Page, R.W., Bertoldi, G.L., and Fogelman, R.P., 1983, Data for ground-water test hole near Butte City, Central Valley Aquifer Project, California: U.S. Geological Survey Open-File Report 83-697, 54 p.

Greene, T.J. and Hoover, K., 2014, Hydrostratigraphy and pump-test analysis of the Lower Tuscan/Tehama Aquifer, Northern Sacramento Valley, CA: California State University – Chico Department of Geological and Environmental Sciences, Final Report, 105 p.

Heath, R.C., 1983. Basic ground-water hydrology, U.S. Geological Survey Water-Supply Paper 2220, 86p, http://pubs.er.usgs.gov/publication/wsp2220 (accessed Jan 8, 2017)

HydroGeophysics Group, Aarhus University, 2010, "Validation of the SkyTEM system at the extended TEM test site." Aarhus, Denmark.

HydroGeophysics Group, Aarhus University, 2011, "Guide for processing and inversion of SkyTEM data in Aarhus Workbench", Version 2.0."

Ingersoll, R.V. and Dickinson, W.R., 1981, "Great Valley Group (Sequence), Sacramento Valley, California," in V Frizzell, ed., *Upper Mesozoic Franciscan rocks and Great Valley Sequence, Central Coast ranges, California*: Society of Economic Paleontologists and Mineralogists, Pacific Section, Los Angeles, CA: p. 1-33.

Knight, R., Smith, R., Asch, T., Abraham, J., Cannia, J., Viezzoli, A., and Fogg, G., 2018, Mapping aquifer systems with airborne electromagnetics in the Central Valley of California: Groundwater, v.55, no.6, p.893-908.

Ley-Cooper, Y. and Davis, A., 2010. Can a borehole conductivity log discredit a whole AEM survey?: *in* Extended abstracts of the Australian Society of Exploration Geophysicists Annual meeting Aug 20-24, Sydney, Australia.

Marchand, D.E. and Allwardt, Alan, 1971, Late Cenozoic stratigraphic units, northeastern San Joaquin Valley, California: US Geological Survey, Geological Survey Bulletin 1470, 71pp.

National Water Quality Monitoring Council, 2017, Water Quality Portal: National Water Quality Monitoring Council, accessed March 29, 2019, at: https://www.waterqualitydata.us

Page, R.W., 1986, Geology of the fresh ground-water basin of the Central Valley, California, with texture maps and sections; Regional Aquifer System Analysis: U.S. Geological Survey Professional Paper 1401-C, 54 p., 6 pl.

Planert, M. and Williams, J.S., 1995, Ground Water Atlas of the United States, Segment 1, California, Nevada: U.S. Geological Survey Hydrologic Investigations Atlas, 730-B, 28 p.

Saucedo, G.J., and Wagner, D.L., 1992, Geologic map of the Chico quadrangle: California Division of Mines and geology, Regional geologic Map 7A, scale 1:250,000

Schamper, C., Auken, E., and Sorensen, K., 2014, Coil response inversion for very early time modelling of helicopter-borne time-domain electromagnetic data and mapping of near-surface Geologic Layers. European Association of Geoscientistis & Engineers, Geophysical Prospecting.

SkyTem Airborne Surveys Worldwide, 2019, SkyTEM304M, https://skytem.com/tem-systems/ (accessed March 28, 2019)

Steele, W.C., 1980, Quaternary stream terraces in the northwestern Sacramento Valley, Glenn, Tehama, and Shasta Counties, California: U.S. Geological Survey Open-File Report 80-472, 157 p.

U.S. Census Bureau, 2018, Census 2010 total population: U.S. Census Bureau, accessed November 5, 2018, at: https://factfinder.census.gov/faces/nav/jsf/pages/index.xhtml#none

U.S. Geological Survey (USGS). Water. https://water.usgs.gov/edu/earthgwaquifer.html (accessed January 9, 2017)

U.S. Geological Survey (USGS), 2018a, The National Map, 2018, 3DEP products and services: The National Map, 3D Elevation Program Web page, http://nationalmap.gov/3DEP/3dep_prodserv.html (accessed March 29, 2019)

U.S. Geological Survey, 2018b, USGS stream stage water watch: U.S. Geological Survey National Water Information System, accessed March 29, 2019 at: https://waterwatch.usgs.gov/index.php?id=real&sid=w__gmap&r=ca

U.S. Geological Survey, 2018c, USGS Groundwater Data for California: U.S. Geological Survey National Water Information System, accessed March 29, 2019, at: https://waterdata.usgs.gov/ca/nwis/gw

Viezzoli, A., A. V. Christiansen, E. Auken, and K. Sorensen, 2008, "Quasi-3D modeling of airborne TEM data by spatially constrainted inversion." *Geophysics Vol. 73 No. 3* F105-F11